**SANDIA REPORT**
SAND2002-3101
Unlimited Release
Printed October 2002

# Blade Manufacturing Improvement Project: Final Report

Kent Sherwood, Principal Investigator

Prepared by
Sandia National Laboratories
Albuquerque, New Mexico 87185 and Livermore, California 94550

Sandia is a multiprogram laboratory operated by Sandia Corporation, a Lockheed Martin Company, for the United States Department of Energy under Contract DE-AC04-94AL85000.



Issued by Sandia National Laboratories, operated for the United States Department of Energy by Sandia Corporation.



Available to DOE and DOE contractors from
U.S. Department of Energy
Office of Scientific and Technical Information
P.O. Box 62
Oak Ridge, TN 37831

Telephone: (865)576-8401
Facsimile: (865)576-5728
E-Mail: reports@adonis.osti.gov
Online ordering: http://www.doe.gov/bridge

Available to the public from
U.S. Department of Commerce
National Technical Information Service
5285 Port Royal Rd
Springfield, VA 22161

Telephone: (800)553-6847
Facsimile: (703)605-6900
E-Mail: orders@ntis.fedworld.gov
Online order: http://www.ntis.gov/ordering.htm

**SAND 2002-3101**
**Unlimited Release**
**Printed October 2002**

# Blade Manufacturing Improvement Project

## Final Report

**Kent Sherwood**

President and Principal Investigator

**Foam Matrix, Inc.**

1123 East Redondo Boulevard
Inglewood, CA 90302

### Abstract

The Blade Manufacturing Improvement Project explores new, unique and improved materials integrated with innovative manufacturing techniques that promise substantial economic enhancements for the fabrication of wind turbine blades. The primary objectives promote the development of advanced wind turbine blade manufacturing in ways that lower blade costs, cut rotor weight, reduce turbine maintenance costs, improve overall turbine quality and increase ongoing production reliability. Foam Matrix (FMI) has developed a wind turbine blade with an engineered foam core, incorporating advanced composite materials and using Resin Transfer Molding (RTM) processes to form a monolithic blade structure incorporating a single molding tool. Patented techniques are employed to increase blade load bearing capability and insure the uniform quality of the manufactured blade. In production quantities, FMI manufacturing innovations may return a sizable per blade cost reduction when compared to the cost of producing comparable blades with conventional methods.

## Acknowledgements

| | | |
|---|---|---|
| Dale E. Berg | Principal Member of Technical Staff<br>Wind Energy Technology Department | Sandia National Laboratories<br>Albuquerque, NM |
| Tom Ashwill | Principal Member of Technical Staff<br>Wind Energy Technology Department | Sandia National Laboratories<br>Albuquerque, NM |
| Henry M. Dodd | Manager<br>Wind Energy Technology Department | Sandia National Laboratories<br>Albuquerque, NM |
| Kent Sherwood | President and Principle Investigator | Foam Matrix, Inc<br>Inglewood, CA |
| Michael Kramer | Project Manager | Foam Matrix, Inc.<br>Inglewood, CA |
| Michael S. Selig | Professor of Aerodynamics | Department of Aeronautical and Astronautically Engineering<br>University of Illinois at Urbana-Champaign, Urbana, IL 61801 |
| Charles A. Richey | Principal | Mechanical & Composite Engineering<br>Montrose, CO |
| Clare Lees | Principal | BCL & Associates<br>Desert Hot Springs, CA |
| Walter Musial | Certification Test Manager | National Renewable Energy Laboratory<br>Golden, CO |
| Scott Hughes | Test Engineer, Qualification Testing | National Renewable Energy Laboratory<br>Golden, CO |
| Curt Cohee | Contract Manager/Technical Writer | Foam Matrix, Inc.<br>Palm Desert, CA |
| Steve Turek | General Manager | Wind Turbine Industries<br>Prior Lake, MN |
| Svend Duus | Principal | SD Solutions<br>Palm Springs, CA |
| Arnie Neilsen | President | Wind Engineers, Inc.<br>Palm Springs, CA |
| Willard Dill | Field Manager | Lalamilo Wind Farm<br>Hawaii County, HI |

## Foam Matrix Contacts

Foam Matrix, Inc.
1123 E. Redondo Blvd.
Inglewood, CA 90302
Telephone: 310-680-0777
Fax 310-680-6876
www.foammatrix.com
Kent Sherwood, President k.sherwood@foammatrix.com
Michael Kramer m.kramer@foammatrix.com
Curt Cohee, Wind Energy Representative: c.cohee@foammatrix.com

## Supporting Documentation

STATIC TESTING OF THE FOAM MATRIX BMI BLADE

Final Report: NWTC-ST-FMI-STA-01-1000-FR July 9, 2001

FATIGUE TESTING OF THE FOAM MATRIX BMI BLADE

Final Report: NWTC-ST-FMI-02-0201-FR August 20, 2001

National Renewal Energy Laboratory
National Wind Technology Center
1617 Cole Blvd.
Golden, CO 84041

This is a Contractor Report for Sandia National Laboratories that partially fulfills the deliverables required under Contract #AX-2111B

# Table of Contents

## Table of Figures

## Table of Tables

## Executive Summary

Sandia National Laboratories (Sandia) awarded this contract to Foam Matrix in July 1998. The project, titled "Blade Manufacturing Improvements" (BMI), mandated the development of an improved manufacturing process for the construction of wind turbine blades. FMI, a foam core and composite manufacturing company, gathered a design team of experts in both composite engineering and wind blade design. Using a 4.3-meter baseline blade specific to the Jacobs 20-29 turbine, the task was to first design a blade within the allowable parameters of composite materials, then to design and construct a tool for blade fabrication. The last tasks entailed fabrication of prototype blades for qualification and field-testing.

This report documents the various tasks as prescribed by the Sandia AX-2111 Statement of Work (SOW) from project planning through static and field tests. The overall scope of this project focused on the concept of advancing the fabrication of wind turbine blades in ways to lower blade costs and improve their quality and reliability. Innovative processes that overcome current blade deficiencies were encouraged.

The FMI approach employed an innovative proprietary technology that produced a molded foam core (MFC) with all internal hard structures molded in. Adhering to a predetermined engineered lamination schedule, the fabrication steps bonded the foam core and composite skin using a resin transfer molding (RTM) process. The result was a monolithic structure with a bonded core and skin. The underlying core supported the loads and stresses on the skin at any point on the structure and thus minimized skin wrinkling, skin separation, skin failure and core decomposition.

The finished blade exhibited a number of advantages over blades fabricated using wood lamination, hand layup fiberglass or pultrusion molding. A principal advantage is the ability to create blades that are identical in dimension, weight and performance characteristics across any number of production blades over any manufacturing cycle.

Seven BMI prototype, 4.3-meter blades were manufactured under the contract. Three blades have undergone static, fatigue, and modal testing and another three, modified for attachment to a Jacobs 29-20 turbine, went the Lalamilo Wind Farm, Hawaii for field tests.

## Baseline Turbine and Blade Description

The requirements for a baseline turbine as stated in the Statement of Work (SOW) were not limited to any manufacturer, turbine design or turbine power capacity. The only conditions were that the selected baseline turbine have a power output capacity greater than 5kW and that the contractor own or have access to an operational turbine capable of field-testing the prototype BMI blades.

After exploring available turbine options, FMI determined that our established relationship with Wind Turbine Industries (WTI) of Prior Lake, MN, best served the interests, goals and ambition of the AX-2111 SOW. To that end, FMI secured permission and the cooperation of WTI to prototype their copyrighted 4.3-meter blade for this project. WTI provided FMI with an installation quality 4.3 meter wind turbine blade specific to the WTI "Jacobs" 29-20 wind turbine. WTI also provided other information related to the blade design, construction, internal fittings and root structure. WTI also assisted FMI in arranging for the field test site.

Sandia National Laboratories amended the FMI Statement of Work to add the redesign of the airfoil for power enhancement. The new prototype blade design incorporated the root structure of the baseline blade for field tests.

## Summary of Findings

At the conclusion of this project, FMI identified several significant improvements in the blade design and manufacturing process. The most significant findings were:

- Implanting internal heating and cooling fittings in the molding tool to control cure time and reduce cycle time increases both the quality of the product and the number of production turns.
- This iteration of this manufacturing approach delivered a long-lived small wind blade capable of withstanding a Class II wind event.
- As a conservative estimate, it seems likely that FMI wind blades could be economically scaled from as small as 3 meters to perhaps 12-16 meters in length without manufacturing or weight penalties.
- Our field test experience indicates that the BMI Prototype blade cannot be characterized as a replacement blade for the current Jacobs 29-20 turbine. The blade could be a key component of a Jacobs 29-20 turbine reconfiguration or upgrade when certain structural changes and control changes are incorporated to support the increased power produced by the prototype blade. This reconfiguration may, or may not, be economically justified.

## Cost Reductions Identified

This project identified several elements of cost reduction attributed to the FMI blade fabrication process.

Low touch labor, fast cycle production time, a limited number of raw materials, an environmentally friendly manufacturing technique, good surface finish and the incorporation of lean manufacturing techniques contribute to lower costs.

Near perfect blade replication from one part to the next reduces on-site installation costs. Production blades will be within a few grams of the same weight and within a few millimeters of balance.

Additional cost reduction contributions are expected as a result of reduced blade maintenance costs and extended blade useful life.

## Conclusions and Recommendations

The FMI manufacturing process replicates the exact blade design. The blade can be fabricated to meet a variety of loading conditions and with add-on features such as operational tip brakes, imbedded de-icing materials or other fittings, as may be required. It is lightweight and durable.

Once a tool with a specific outer mold line (OML) is created, it is possible to modify certain characteristics of the blade to accommodate different site, climatic or environmental conditions. Such changes might include an anti-icing surface coating or imbedded lightning bleed wiring. Within certain limitations, blade weight and/or blade stiffness can also be modified.

The FMI manufacturing process may have direct application to production of utility grade rotors, rotors in the greater than 80 meter rotor range. Additional research and testing may mandate how FMI technology could be applied.

## Feature Summary of the Foam Matrix BMI Prototype Blade

Features attributed to this design include:

- 4.42 meter root to tip blade length
- SG6050 Airfoil
- Linear Taper Planform
- Soft Stall Regulation
- Blade Weight, 27.2 kilogram
- Low noise tip design
- Low blade tip displacement, (9.17 inches in Hurricane Class II wind)
- 8.5 x 4.626 x 14.69 inch flat surface root section

# 1.0 Introduction and Background

## 1.1 Background

Foam Matrix, Inc. (FMI), using a molded foam core, produces composite products as a subcontractor or original equipment manufacturer (OEM) vendor for a number of manufacturing and marketing concerns. Current contracts, other than wind turbine blades, are with several major aerospace contractors for military and civilian flight vehicle control surfaces. Our success in these divergent products is attributed to experience in reinforced composite products designed to function in extreme environments under high structural loads.

Kent Sherwood, FMI president and CEO, holds various patents that enhance the usability of polyurethane foam to mold rigid structure articles. Common to all FMI products, the molded foam core is the backbone of our finished product.

For wind turbine blades, the FMI process uses a patented technology to create a molded foam core within which all internal hard structures are molded. A resin transfer molding (RTM) process is employed to bond structural woven glass or other composite materials to the foam core. The result is a monolithic structure with a bonded core and skin. Loads and stresses at any point on the structure are distributed across the skin area, which is supported by the underlying core. Skin wrinkling, skin separation, skin failure and core decomposition are minimized.

The finished blade has a number of advantages over blades using a more conventional manufacturing process such as wood lamination, hand layup fiberglass or pultrusion. The principal attribute is the ability to produce blades that are identical in dimension, weight and performance characteristics. Among other advantages are:

- *Fast part production when RTM mold techniques are compared to sprayup or layup,*
- *Encapsulation of ribs, spars, and other internal fixtures in the molded foam core,*
- *Both sides of the part will reflect the finish of the corresponding RTM mold,*
- *Both sides of the part can be gel-coated,*
- *Proper clamping or mold closures maintain close dimensional tolerance. Resin transfer is metered which allows precise control of the resin "richness," or weight,*
- *Manufacturing techniques are environmentally sensitive.*

## 1.2 Project Purpose

Since 1994 the Department of Energy (DOE) and Sandia National Laboratories (SNL) have initiated blade

manufacturing projects intended to make blade manufacturing improvements targeting utility grade (>250kW) turbines. This project, termed the Blade Manufacturing Improvements (BMI) project, funded improvements to blade manufacturing for turbines of any size greater than 5kW. This project is part of the Turbine Research Program managed by the National Renewable Energy Laboratory (NREL).

The goal of the BMI project is to assist the U.S. wind industry in the development of new and improved blade manufacturing processes. The primary objective of the BMI project is to develop advances in the manufacturing of wind turbine blades in ways that lower blade costs and improve their quality and reliability. Innovative processes and materials that have the potential to solve current blade problems are encouraged.

## 1.3 Project Scope

The project scope included the following steps:

- Develop a work plan and schedule.
- Perform trade-off studies for different process variations such as considering some number of lamination schedules and/or composite materials
- Design and build a new or improved blade manufacturing process.
- Design and fabricate several blade prototypes, built within the proposed manufacturing process, for an existing operational wind turbine.
- Perform qualification tests on the blade prototypes, including the field demonstration of one set of blade prototypes on the existing wind turbine.
- Show cost reductions and improvements in quality and reliability in relationship to the baseline blade. The baseline blade is defined as an existing blade on the existing turbine that will be used to test the BMI prototype blades.

## 1.4 Baseline Turbine and Blade Description

After exploring available turbine options FMI determined that our established relationship with Wind Turbine Industries (WTI) of Prior Lake, MN best served the goals of the AX-2111 SOW. FMI secured permission and the cooperation of WTI to prototype their copyrighted 4.3-meter blade for this project. WTI provided FMI with a commercial 4.3 meter wind turbine blade for the WTI Jacobs 29-20 wind turbine. WTI also provided other information related to the blade design, construction, internal fittings and root structure.

The WTI-provided 4.3-meter blade is the blade delivered with new or refurbished WTI 20kW turbines. This blade was designed and put into production in the fall of 1985. The basic Jacobs blade design, with some improvements over time, has been in almost continuous production since 1922.

This project was not intended to develop a new blade for improved or modified aerodynamic performance. However, since the basic Jacobs turbine and rotor specifications remained virtually unchanged from early implementation, some changes seemed advantageous. With all parties to the BMI AX-2111 contract concurring, Sandia National Laboratories amended the FMI Statement of Work to include a newly designed 4.3-meter wind blade airfoil that could be adapted to the WTI Jacobs 29-20 wind turbine.

## 1.5 Blade Design Supplemental Amendment to the AX-2111 BMI Blade Prototype Project

Michael S. Selig, an aerodynamicist from the University of Illinois Urbana-Champaign, IL, agreed to design a 4.3-meter wind turbine blade capable of powering the WTI Jacobs 29-20 turbine. His work is documented in this report. Hereafter, except for baseline blade commentary, the term "BMI prototype blade" will denote the prototype blade of Mr. Selig's design.

The Foam Matrix BMI project team included Charles "Chuck" A. Richey of Mechanical & Composite Engineering, Montrose, CO, as the structural engineer. His role in the project was expanded to work with Mr. Selig to perform various structural trade-off studies on a number of possible airfoils and blade designs. Once a blade design was selected, Mr. Richey was tasked with creating and analyzing a final lamination schedule and blade structure.

## 1.6 Baseline Blade Specifications

Details regarding the Jacobs 29-20 turbine and the Jacobs 29-20 blade provided baseline blade parameters for a FMI prototype blade as a bolt-on Jacobs 29-20 turbine replacement rotor. These specifications are detailed in Appendix A.

Our goal was to establish that the prototype blade would provide an improved operational replacement for the Jacobs 29-20 turbine.

## 1.7 Report Organization

The remained of this report is organized in six major sections;

- BMI Prototype Blade Design, Airfoil Trade-Off Studies,
- BMI Prototype Blade Design, Structure and Lamination,
- Foam Matrix Manufacturing Solution,
- BMI Prototype Blade Qualification and Field Testing,
- Summary of Finding,
- Appendixes

# 2.0 Blade Design/Airfoil Trade-Off Study

## 2.1 Baseline Blade

To study the potential performance improvements over the baseline Jacobs turbine and the resulting difference in blade shape, a trade study was done using five different airfoil "families" along the blade. In addition to data given in Table A.2, the data specific to the trade study is given in Table 2.1. Each airfoil was used on two blade-planform "families" for a total of 10 blades in this study.

**Table 2.1 - Various Parameters Used in the Trade-Off Study**

| | |
|---|---|
| **Blade chord and twist** | **Figures 2.1, 2.2, 2.3, 2.4, 2.5** |
| **Airfoil** | **Table 2.2** |
| **Airfoil performance data** | **Experimental from UIUC wind tunnel (Refs. 5, 8, 9, 10,) and Stuttgart (Ref. 11).** |
| **Blade pitch** | **Note the blade pitch is referenced to the 75% station where the twist is zero. (see Table 2.2)** |

(Also, see Table A.2)

## 2.2 Parameter Selection

### 2.2.1 Airfoils

The airfoils used in the trade-off study are listed in Table 2.2 and shown in Figs. 2.1, 2.2, 2.3, 2.4, and 2.5. First it should be remarked that the airfoils are somewhat thinner than those used on the baseline blade. The selection of thinner airfoils avoids the poor performance of thick airfoils operating at the low Reynolds numbers, which are experienced by the baseline blades.

Briefly, the S822 [Fig. 2.1] is an NREL airfoil. It was intended for use on small stall-regulated wind turbines, but it was nevertheless considered for the current variable-speed application. The S8036 [Fig. 2.2 and [Ref. 9] was designed for use on model aircraft and has subsequently been widely used on scale models because of its very soft and prolonged stall. The price to be paid for this softer stall is a small loss in annual energy production as compared with the S822, which has a sharper stall. Soft stall is desirable to reduce blade fatigue loads. The SG6050 and SG6051 airfoils [Figs. 2.3 and 2.4] are Selig and Giguère designs for use on the WindLite 8-kW variable speed turbine. Finally, the FX 63-137 airfoil [Fig. 2.5], though originally designed by F.X. Wortmann for use on human-power aircraft, was used on many of the small turbines built by World Power Technologies in Duluth, MN (recently acquired by Southwest Windpower, Inc.).

The airfoil performance data was from wind tunnel tests performed at the University of Illinois at Urbana-

Champaign [Refs. 5, 8, 9, 10]. Some additional data for the FX 63-137 came from the low-speed tunnel at Stuttgart, Germany [Ref. 11].

### 2.2.2 Rotor speed and size

In a conversation with Steve Turek of Wind Turbine Industries (WTI) [Ref. 7], it was concluded that, given the nature of the power electronics used on the Jacobs 29-20 turbine, the new rotor should be designed to the same size as the baseline and also that the rated power should remain fixed. This is the conservative approach in the face of uncertainty regarding the balance between the rotor and generator/control circuit. Moreover, experience with alternative configurations has not proven useful [Refs. 3 and 7]. Thus, in this study, a rotor diameter of 29 feet was used, and the rotor was designed to operate at a TSR of 7.

### 2.2.3 Two blade-planform families

Two blade-planform families cases were considered. In the first case, the original planform of the Jacobs turbine was retained. The resulting improvements in performance are therefore due to changes in the blade twist distribution and better airfoil performance. The second case did not include the planform constraint, offering the advantages of changes in both chord and twist.

### 2.2.4 Approach

For all designs, the rotor speed was fixed at a TSR of 7, and the rotor power was limited to 23.53 kW, which yielded an output power of 20 kW assuming a constant drivetrain efficiency of 85%. The power predictions were truncated once the power exceeded 23.53 kW, *i.e.*, imposing a peak power constraint. The feathering/furling action of the blades/rotor was not modeled. For the fully twisted/tapered blades, a desired lift coefficient and axial induction factor distribution were specified at a wind speed of approximately 16 mph. Specifying the lift and axial induction factor in this way resulted in "optimum" blades that could likely only be improved by less than 1% in annual energy production. To achieve these desired aerodynamic characteristics along with the rotor power constraint, the blade chord and twist distributions were determined automatically by PROPID[1]. For the case when the blade planform was fixed to that of the Jacobs blade as described below, only the lift coefficient distribution was prescribed, and the twist was automatically adjusted in PROPID to achieve the prescribed lift coefficient.

PROPID computed the annual energy production using a Rayleigh-Weibull wind speed distribution. Parameters included a generator efficiency of 85% and operating time of 100% to compute the annual energy production (AEP). The cutout wind speed was set at 30 mph for all cases. Although the cutout wind speed might be higher than that in actual operation, beyond 30 mph all of the power curves are identical. Thus, the AEP listed can be used as a basis for comparison.

---

[1] PROPID, a PC computer program for the design and analysis of horizontal axis wind turbines based on the widely-used and validated industry-standard PROP code. In PROPID several additional features have been added, including an inverse design capability as has been well documented in the literature [Ref 6].

### 2.2.5 Discussion

For the cases listed in Table 2.2, Figs. 2.6 - 2.12 show the corresponding airfoils and resulting blade shapes (chord and twist distributions). In studying the gain in AEP[2] vs. the baseline given in the table, some general trends emerged. First, the blades using the thinner airfoils tended to be more efficient (CP4/5 vs CP1/2/3 and NP4/5 vs NP1/2/3). As for the S822 and S8036 blades, which were the same thickness, the S822 had the better performance. Experimental data on these two airfoils showed that the S8036 had a softer, more desirable stall, but this came at the price of lower performance over the usual operating range (used in determining the AEP), hence its lower annual energy production in comparison with the S822 blades. The SG6050 (root) / SG6051 (primary-tip) cases (CP4 and NP4) had slightly better performance than the SG6050 (root-primary-tip) cases (CP3 and NP3) because the SG6051 was thinner and more efficient. Finally, the thinner FX 63-137 / SG6051 cases (CP5 and NP5) were an improvement over all the other cases.

In doing the trade study, the new planforms NP*[*] were considered first with the aim of optimizing the performance (annual energy production). As seen in the plots below, however, the resulting blade planforms [Fig. 2.8] had a broad chord. The chord at any given spanwise location was a strong function of the airfoil lifting capabilities. The low camber airfoils (*e.g.*, S822) had less lift. To obtain the optimum physical load on the blade, the resulting chord had to be broader to compensate for the low lift/camber. The study introduced FX 63-137 (NP5) to reduce the chord. The higher lift/camber required less chord than did the S822 blade. Thus, the taper of the NP5 case proved the more desirable. However, this case also had the lowest physical thickness distribution.

To examine the effects of constraining the chord distribution to something similar to the existing Jacobs turbine, the current planform of the Jacobs (case CP) was used for the same airfoil cases as in NP*. For these cases, the study optimized the blade twist and pitch. The results (based on the CP and power curves presented in Figs. 2.10 - 2.13) showed that the resulting loss in annual energy ranged from approximately 3-8% (see Table 2.2, last column). The range of loss was a function of how close the baseline planform is to the optimized blade. For case CP1 with a relatively broad chord that was far from the optimum, the difference was 8.33% (2.73% vs. 11.28%). For the relatively narrow planform CP5 similar Jacobs turbine, the difference was much smaller — approximately 2.28% (9.87% vs. 12.37%). The insight gained from this first trade study carried over into the second trade study discussed in the following section.

---

[2] Annual Energy Production (AEP) is a subjective calculation of energy production given average wind and rated turbine output on an annual basis.

[*] Denotes all new planforms (case NP)

**Table 2.2 - Rotor Configurations and Resulting Performance Gains for Baseline CP and NP**

| Case | Airfoil (root/primary/tip) | AEP (kW hr/yr) |
|---|---|---|
| *Baseline Jacobs* | | 47949 |

| Case | Airfoil (root/primary-tip) | Pitch (deg) | AEP (kW hr/yr) | Gain in AEP vs baseline |
|---|---|---|---|---|
| *Current planform with new airfoils* | | | | |
| CP1 | S822 (16%) | 3.10 | 49257 | 2.73% |
| CP2 | S8036 (16%) | 1.00 | 48720 | 1.61% |
| CP3 | SG6050 (16%) | 2.51 | 49666 | 3.58% |
| CP4 | SG6050 (16%) / SG6051 (12%) | 2.52 | 50110 | 4.51% |
| CP5 | FX 63-137 (13.7%) / SG6051 (12%) | 2.52 | 52683 | 9.87% |

| Case | Airfoil (root/primary/tip) | Pitch (deg) | AEP (kW hr/yr) | Gain in AEP vs baseline | Gain in AEP vs case CP |
|---|---|---|---|---|---|
| *New planforms with new airfoils* | | | | | |
| NP1 | S822 (16%) | 2.59 | 53359 | 11.28% | 8.33% |
| NP2 | S8036 (16%) | 0.83 | 52631 | 9.76% | 8.03% |
| NP3 | SG6050 (16%) | 2.34 | 53461 | 11.50% | 7.64% |
| NP4 | SG6050 (16%) / SG6051 (12%) | 2.35 | 53812 | 12.23% | 7.39% |
| NP5 | FX 63-137 (13.7%) / SG6051 (12%) | 2.35 | 53882 | 12.37% | 2.28% |

Airfoil families (root/primary/tip)[3],[4]
Note: Number in parentheses is airfoil thickness.

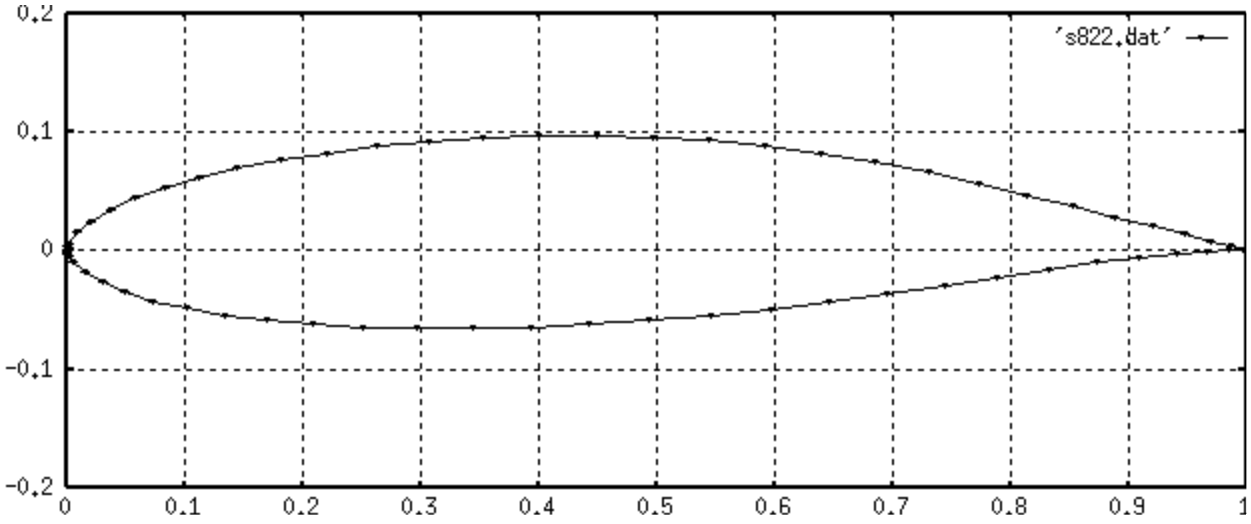

**Fig. 2.1 - S822 airfoil for cases CP1 and NP1**

[3] Airfoil thickness percentage is the maximum thickness ratio over the entire length of the blade (see Fi. 2.6, 2.8).
[4] Pitch in degrees as measured at the 75% spanwise location.

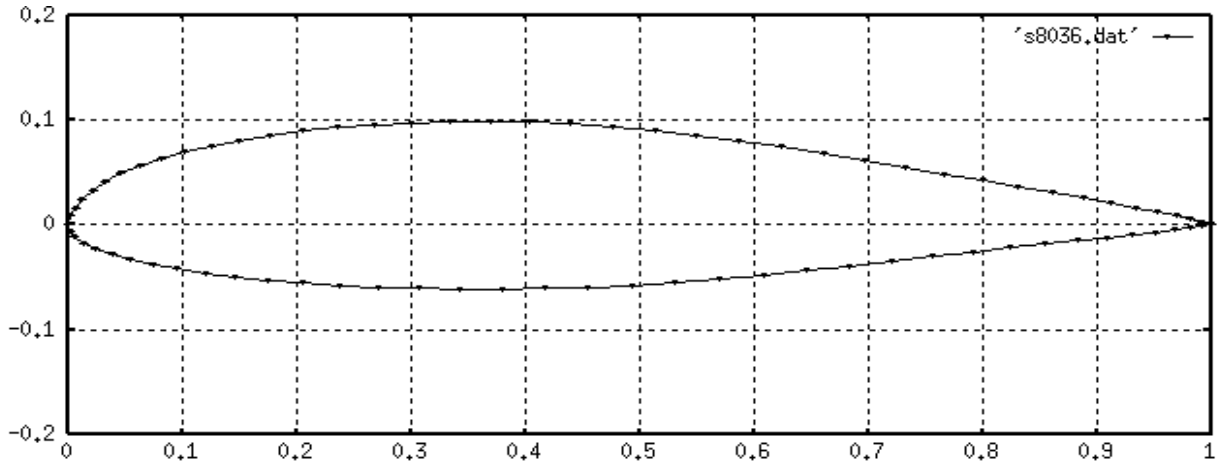


**Fig. 2.2 - S8036 airfoil for cases CP2 and NP2**

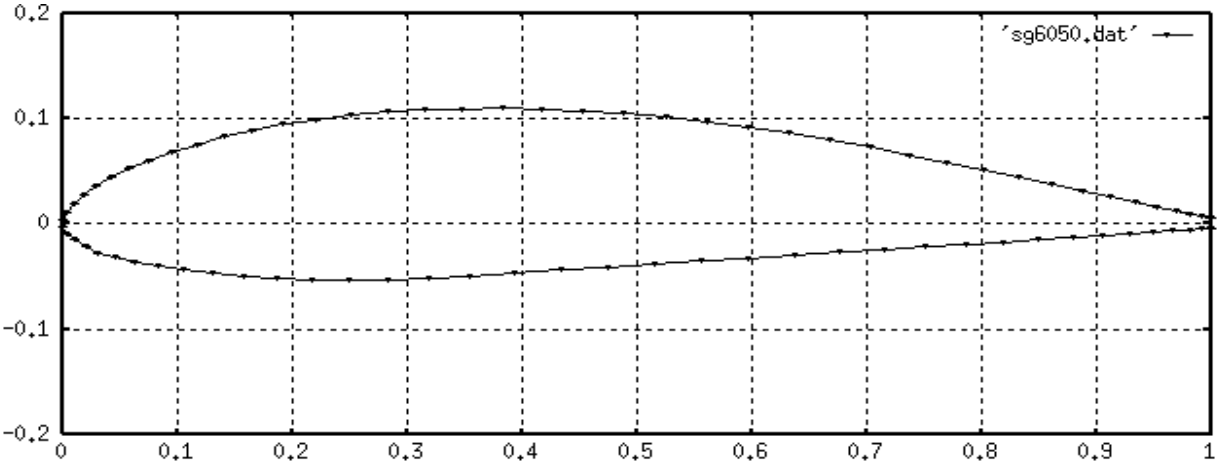


**Fig. 2.3 - SG6050 airfoil for cases CP3 and NP3**

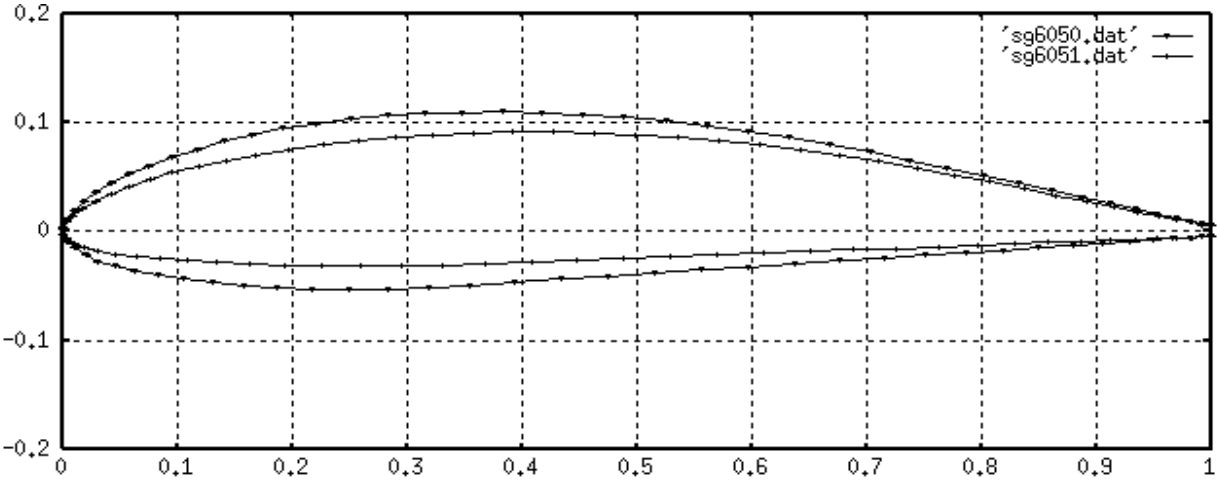


**Fig. 2.4 - SG6050/SG6051 airfoils for cases CP4 and NP4**

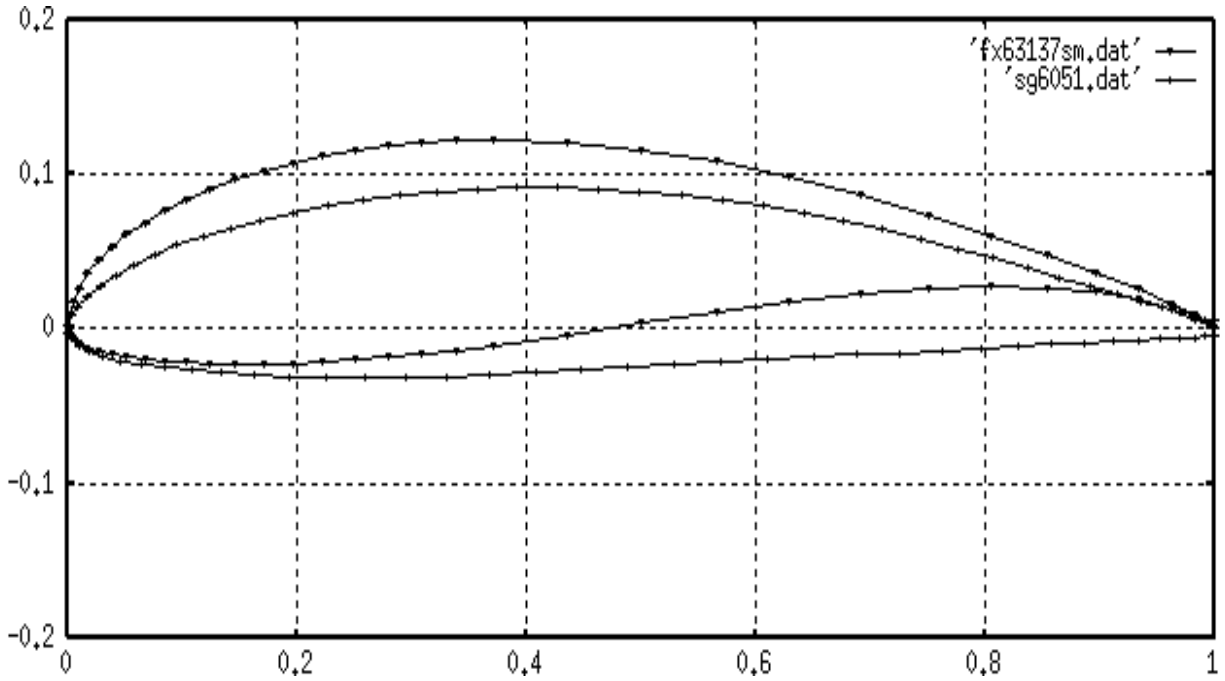


**Fig. 2.5 - FX 63-137/SG6051 airfoils for cases CP5 and NP5**

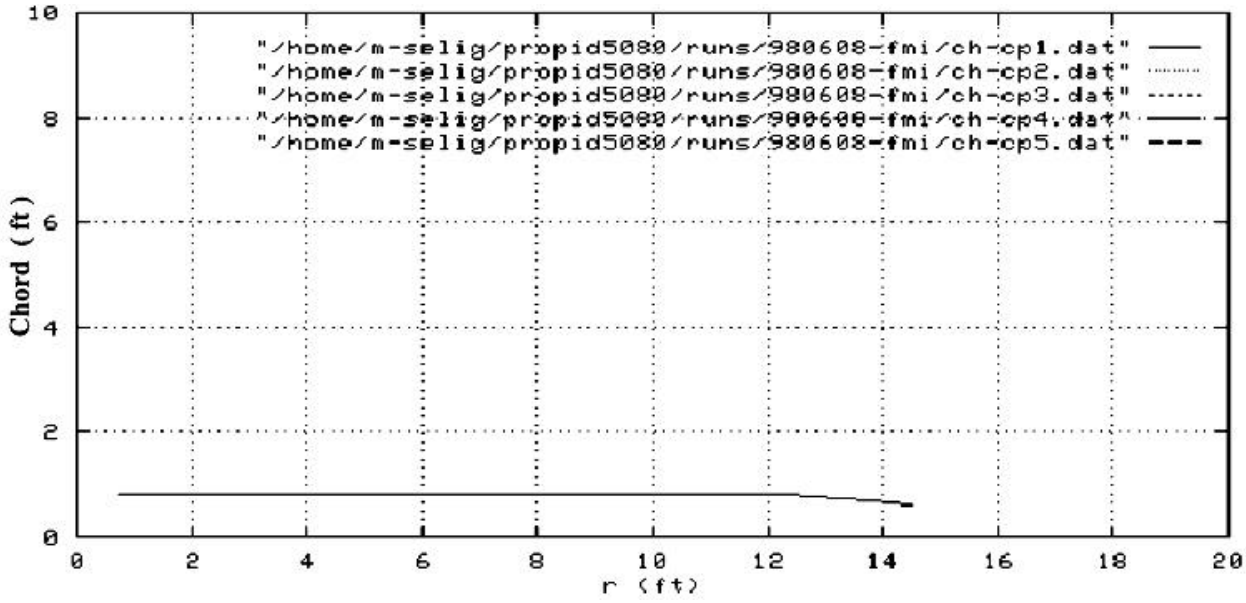


**Fig. 2.6 - Chord distributions for cases CP 1, 2, 3, 4, and 5**
All five plots result with exactly the same data.

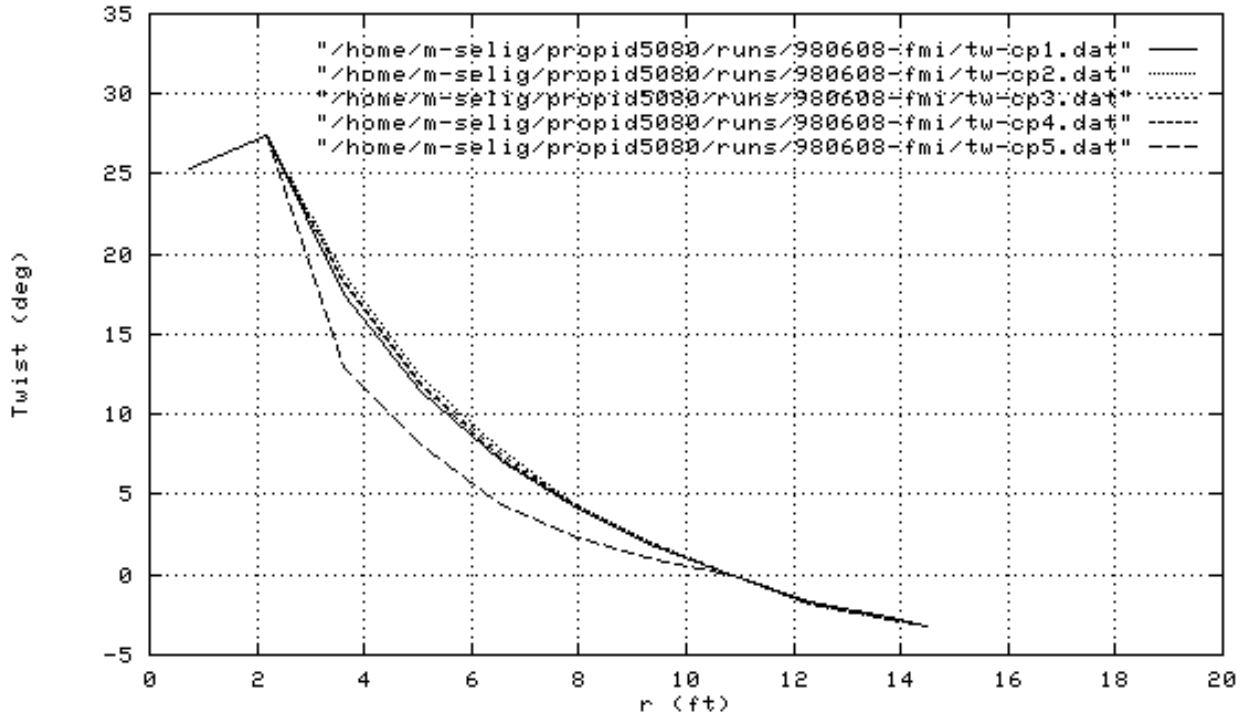


**Fig. 2.7 - Twist distributions for cases CP 1, 2, 3, 4, and 5**

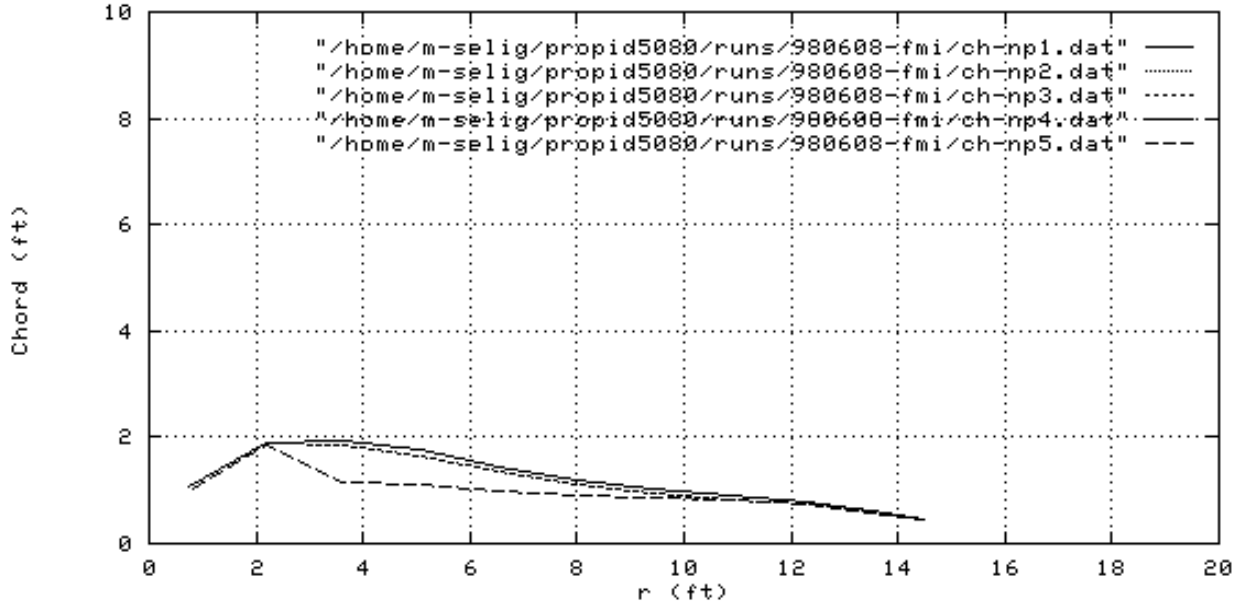


**Fig. 2.8 - Chord distributions for cases NP 1, 2, 3, 4 and 5**

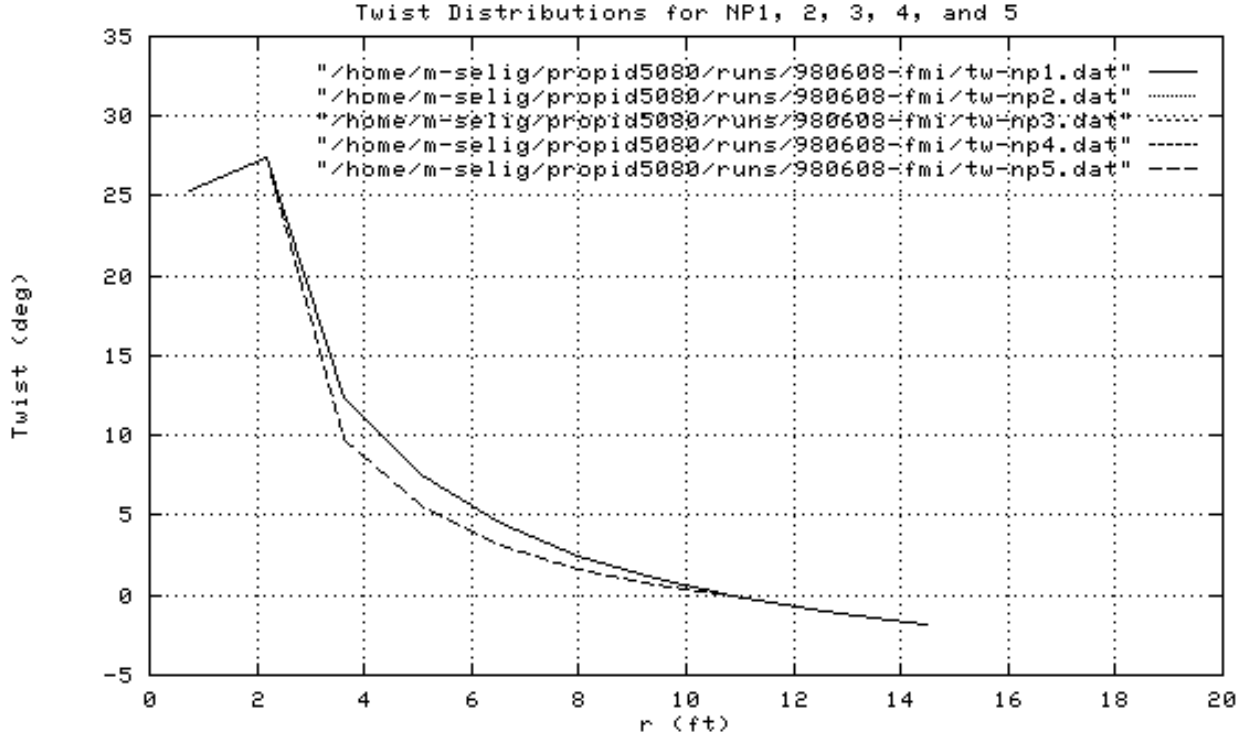


**Fig. 2.9 - Twist distribution for cases NP 1, 2, 3, 4 and 5**

Data plots for NP1, NP2 and NP3 are identical as represented in this graph.

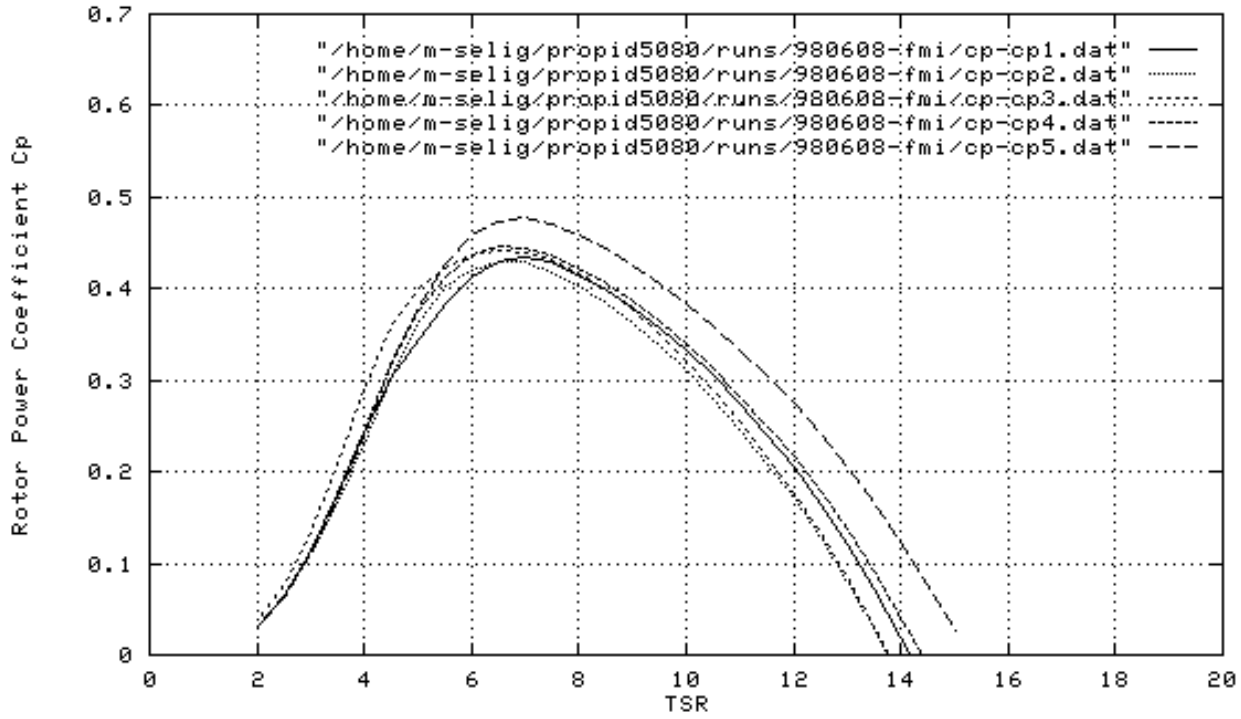


**Fig. 2.10 - Power coefficient curves for cases CP 1, 2, 3, 4 and 5**

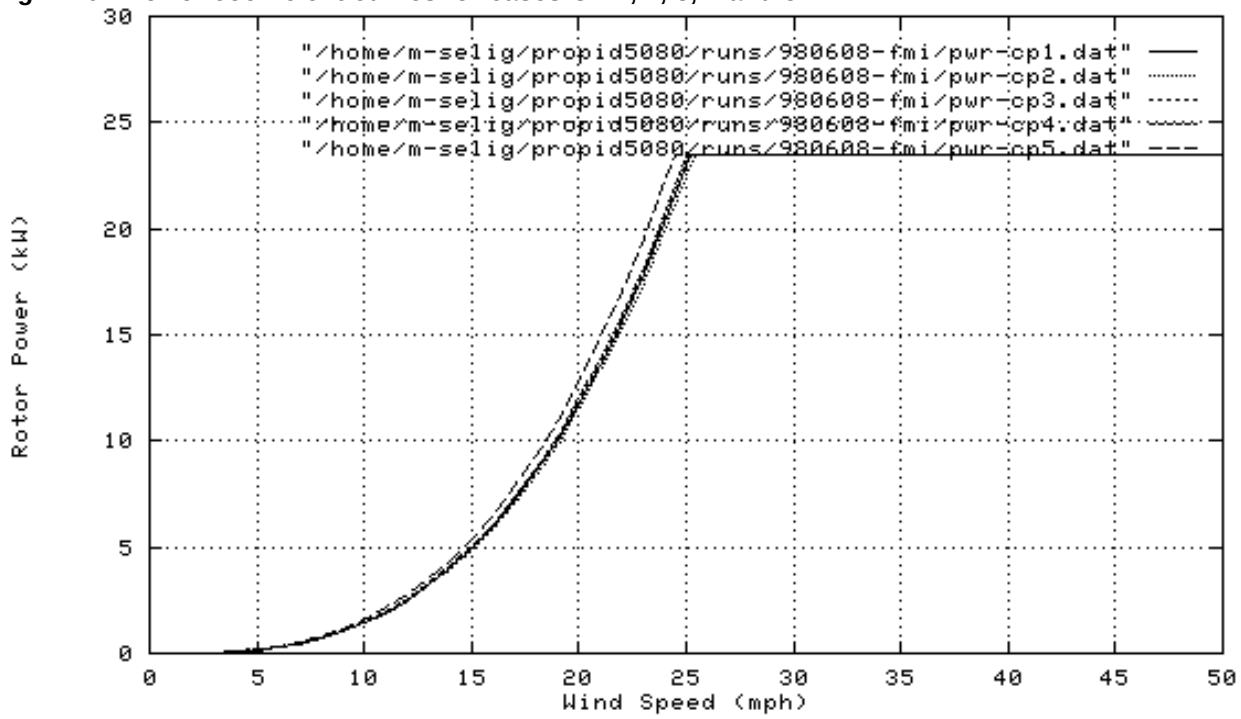


**Fig. 2.11 - Power curves for cases CP 1, 2, 3, 4 and 5 with a TSR of 7**

Data plots for CP1, 2, 3 and 4 are nearly identical as illustrated on this graph.

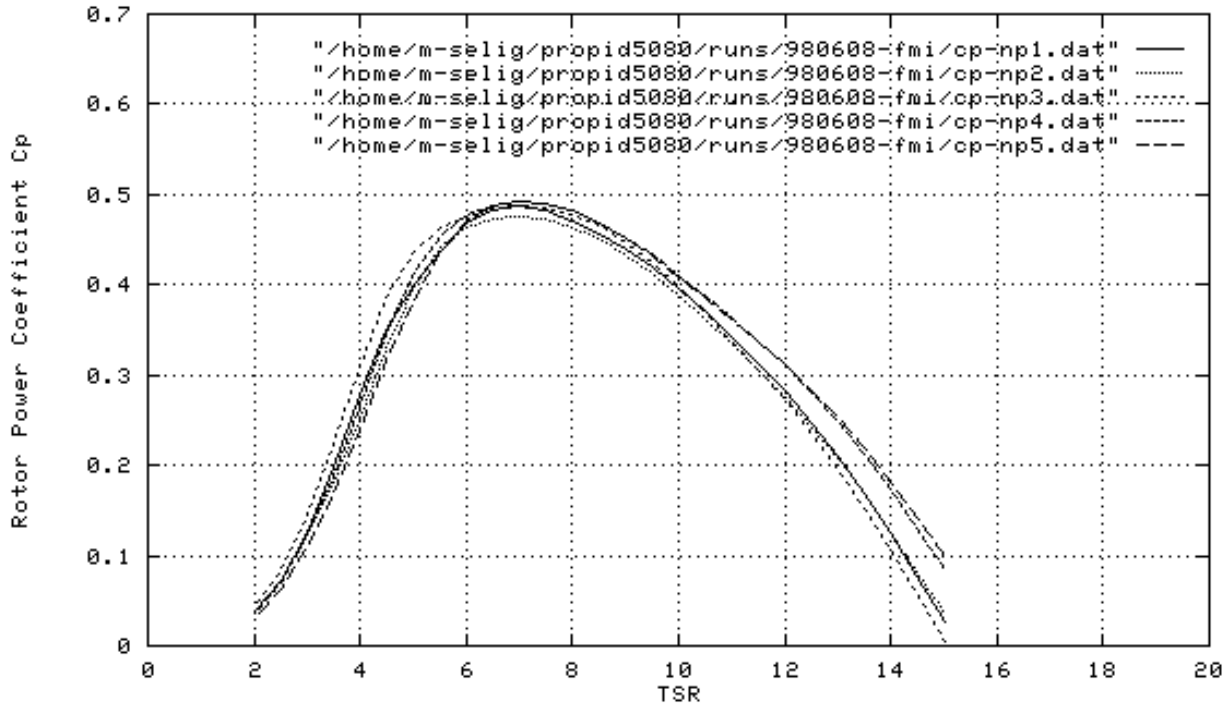


**Fig. 2.12 - Power coefficient curves for cases NP1, 2, 3, 4, and 5**

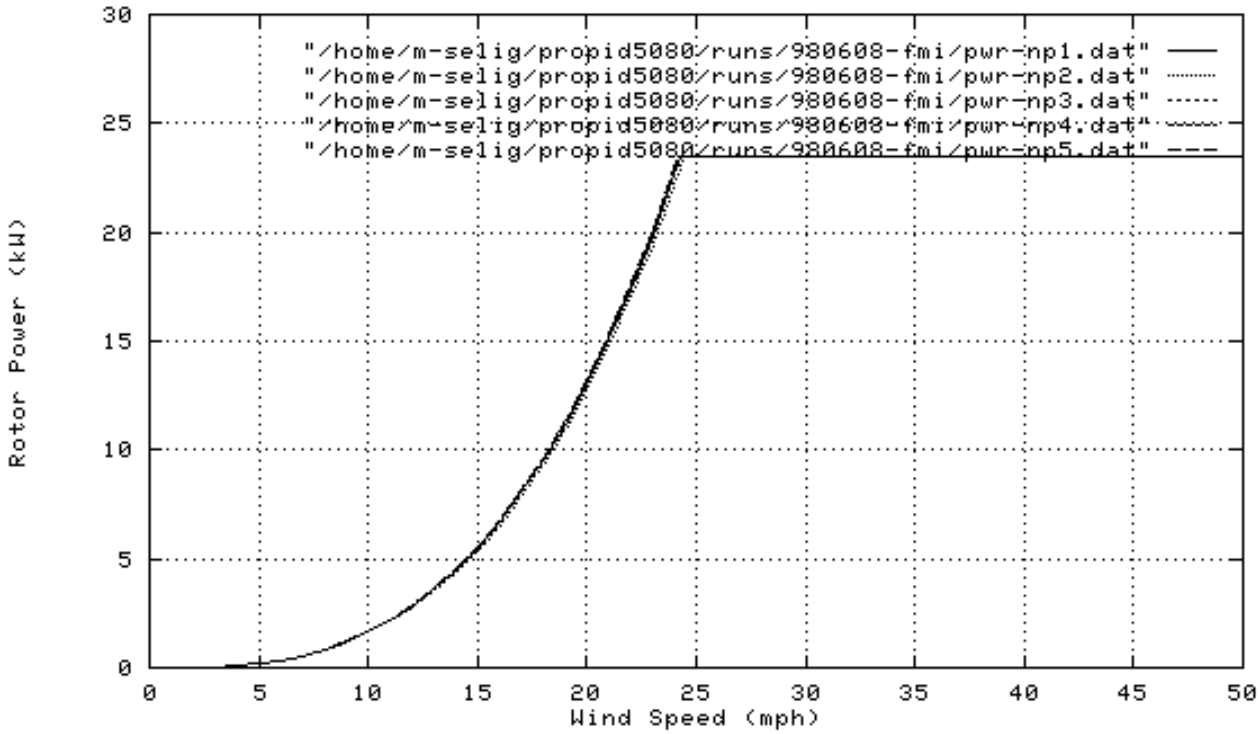


**Fig. 2.13 - Power curves for cases NP1, 2, 3, 4, and 5 for a TSR of 7**
Data plots for NP1, 2, 3, 4 and 5 are nearly identical as illustrated on this graph.

## 2.2.6 Planform Trade Study and Final Design Selection

### 2.2.6.1 Parameter Selection

The selection of the airfoil for the final trade study proceeded as depicted in Fig. 2.14. First, we eliminated the S822 planform from consideration by comparison with the others. Other airfoils produced a larger gain in annual energy and those other airfoils were freely available in the public domain. The SG6050 performance exceeded the performance of the S8036 and the flat bottom of the SG6050 offered some manufacturing advantages, which eliminated the S8036. Next, we eliminated he FX 63-137/SG6051 combination because the gain in annual energy did not outweigh the disadvantages of the FX 63-137 airfoil shape having high camber, much aft loading, and a thin aft section. The SG6050, being thicker than the SG6051, offered structural advantages over the SG6050/SG6051 combination. Finally, given the budgetary constraints, time constraints, risks and the anticipated small advantages to be had from a custom airfoil, the SG6050/SG6051 option was ruled out. Thus, the SG6050 airfoil was selected as the best choice for use in the final trade study and final blade design.

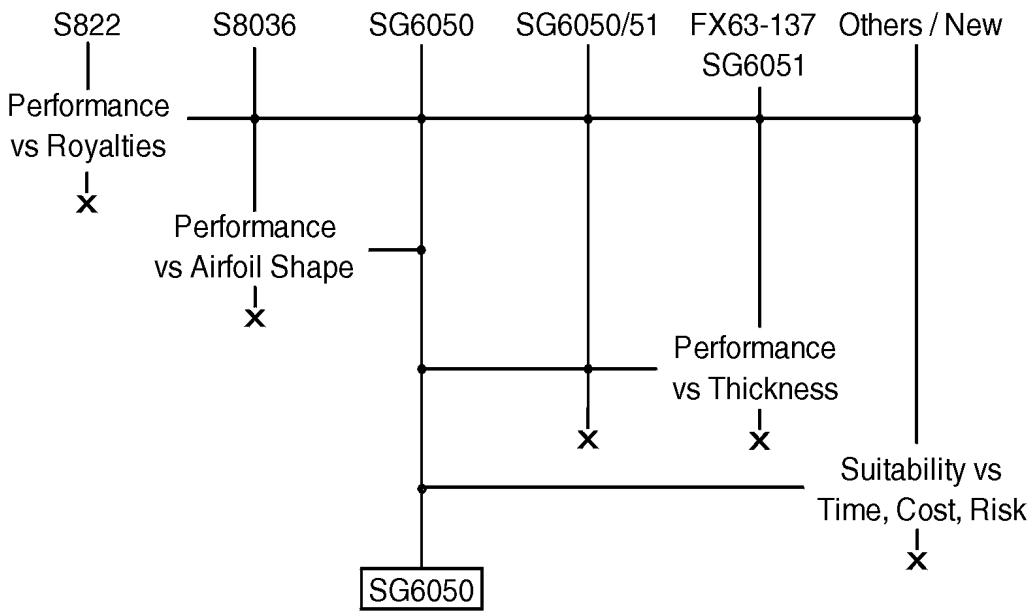


**Fig. 2.14 - Airfoil Selection Decision Tree**

#### 2.2.6.2 Approach

In this final trade study, a linear taper was compared with the fully twisted/tapered blade presented in the last section. The ease of manufacture and greater economic use of materials made the linear taper attractive so long as there were no significant losses in performance.

As in the previous trade study, the rotor speed was fixed at a tip speed ratio of 7 and the rotor power was limited to 23.53 kW, which yielded an output power of 20 kW assuming an 85% constant drive train efficiency. The blade chord was constrained to have a linear taper with the chord at the 75% station unchanged from that of case NP3 (SG6050). In the aerodynamic design process, we prescribed the lift coefficient distribution and PROPID automatically adjusted the twist to achieve the prescribed lift coefficient. The prescribed lift coefficient distribution was the same as that used in the previous trade study.

#### 2.2.6.3 Discussion

Figures 2.15 - 2.20 show the resulting blade geometries and performance predictions of the new blades, and Table 2.3 includes summary data, including the annual energy production values. The important observations include:

- Using a linear taper did not handicap the performance significantly. Over the range of linear tapers considered, the loss was limited to less than 2% (leaving out case LTP5).
- The blade LTP3 had the smallest loss (0.67%) in performance and was compared in Fig. 2.19 with the fully twisted/tapered blade NP3. The largest difference in the shapes was inboard where

the blade LTP3 was narrower than NP3. This result gave some indication of the effect of removing blade chord (material) from the inboard region of the blade. Removing an additional amount of inboard blade chord from case LTP3 (an amount equal to the difference between LTP3 and NP3) would likely yield a similar loss (0.67%). This underscored the diminishing importance of the blade chord over the inboard region.

- To reduce blade costs, it might have been desirable to go with a more narrow blade chord than NP3. The resulting loss in performance was slight, yet still there was a considerable advantage over the baseline Jacobs blade.
- Blade weight was another consideration. The FMI method produced lighter structures than the baseline wood blades. It might have been desirable to have the resulting blade be as heavy as the baseline blades. In this case, the final blade chord distribution would have been broader than the baseline Jacobs, which was the case for LTP3 [Fig. 2.20].

**Table 2.3 - Rotor Configurations for Baseline CP3, NP3 and LTP Planforms With Resulting Performance Gains**

| Case | Airfoil (root/primary/tip) | | AEP (kW hr/yr) | | |
|---|---|---|---|---|---|
| Baseline Jacobs | | | 47949 | | |
| Case | Airfoil (root/primary/tip) | Pitch (deg) | AEP (kW hr/yr) | Diff in AEP vs baseline | |
| Current planform (from previous | | | | | |
| CP3 | SG6050 (16%) | 2.51 | 49666 | 3.58% | |
| Case | Airfoil (root/primary/tip) | Pitch (deg) | AEP (kW hr/yr) | Diff in AEP vs baseline | Diff in AEP vs case CP |
| New planform (from previous section) | | | | | |
| NP3 | SG6050 (16%) | 2.34 | 53461 | 11.50% | 7.64% |
| Case | Airfoil (root/primary/tip) | Pitch (deg) | AEP (kW hr/yr) | Diff in AEP vs baseline | Diff in AEP vs case CP |
| Tapered planforms | | | | | |
| LPT1 | SG650 (16%) | 2.34 | 52503 | 9.50% | -2.00% |
| LPT2 | SG650 (16%) | 2.34 | 53054 | 10.65% | -0.85% |
| LPT3 | SG650 (16%) | 2.34 | 53142 | 10.83% | -0.67% |
| LPT4 | SG650 (16%) | 2.34 | 52595 | 9.69% | -1.81% |
| LPT5 | SG650 (16%) | 2.34 | 51201 | 6.78% | 4.71% |

Airfoils families (root/primary/tip)[5],[6],[7]
Note: Number in parentheses is airfoil thickness.

[5] Annual Energy Production (AEP), see Appendix A.
[6] Airfoil thickness percentage is the maximum thickness ratio over the entire length of the blade.
[7] Pitch in degrees as measured at the 75% spanwise location.

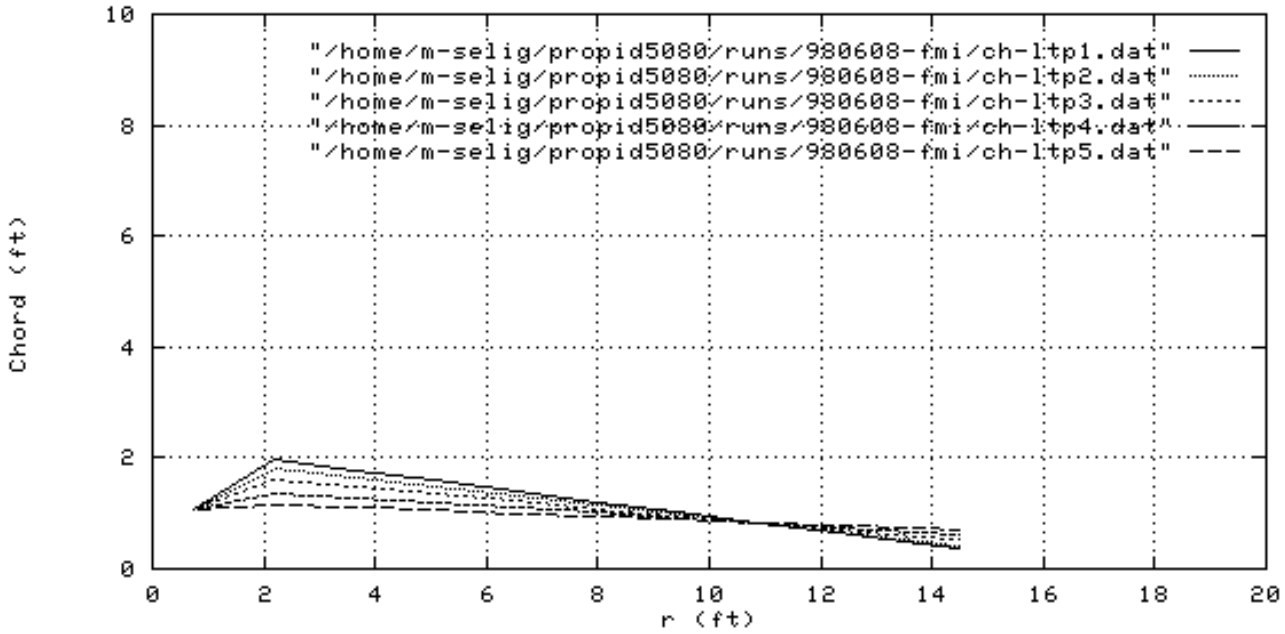


**Fig. 2.15 - Chord distributions for cases LTP1, 2, 3, 4, and 5**

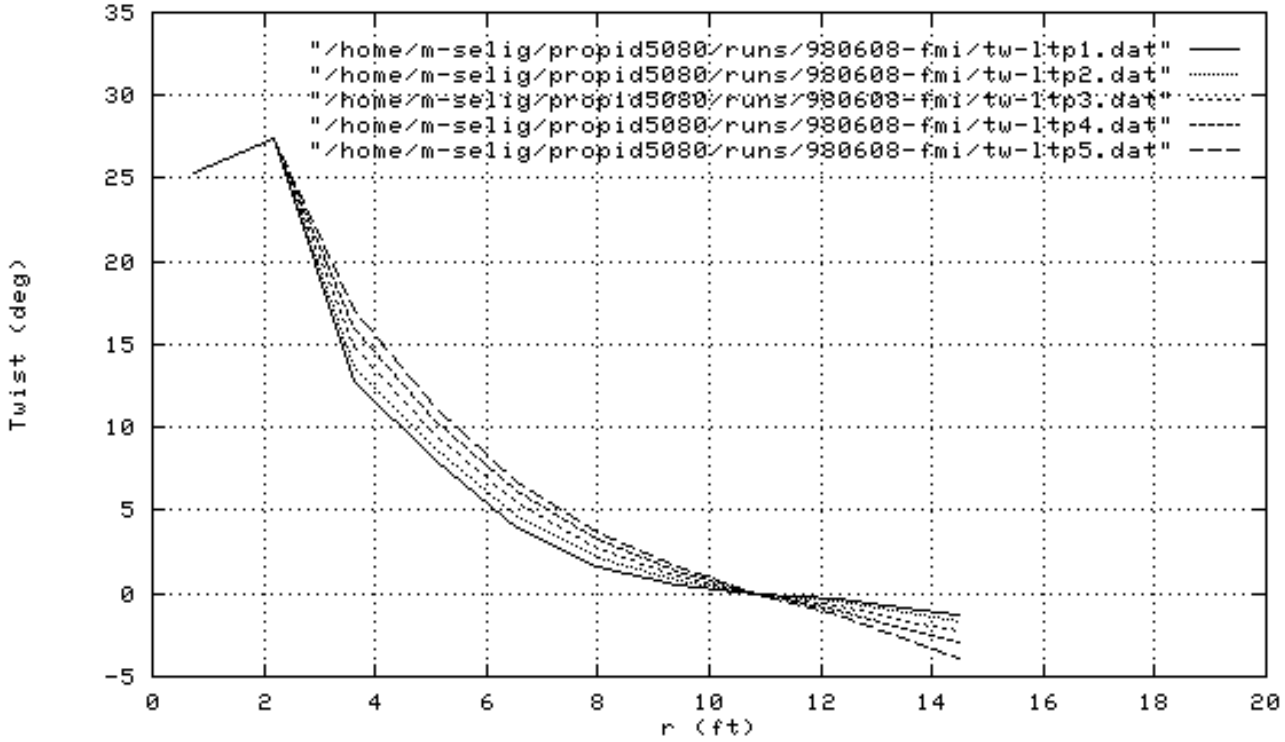


**Fig. 2.16 - Twist Distribution for cases LPT 1, 2, 3, 4 and 5**

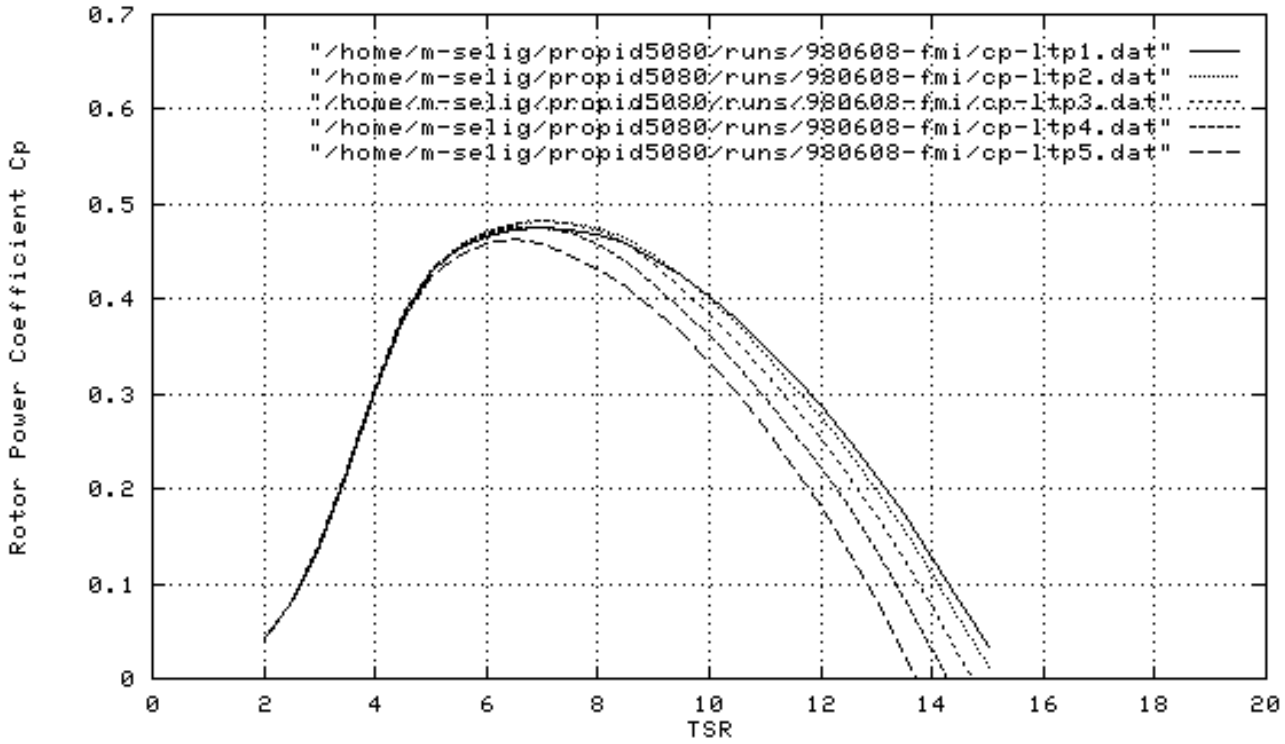


**Fig. 2.17 - Power coefficient curves for cases LTP1, 2, 3, 4, and 5**

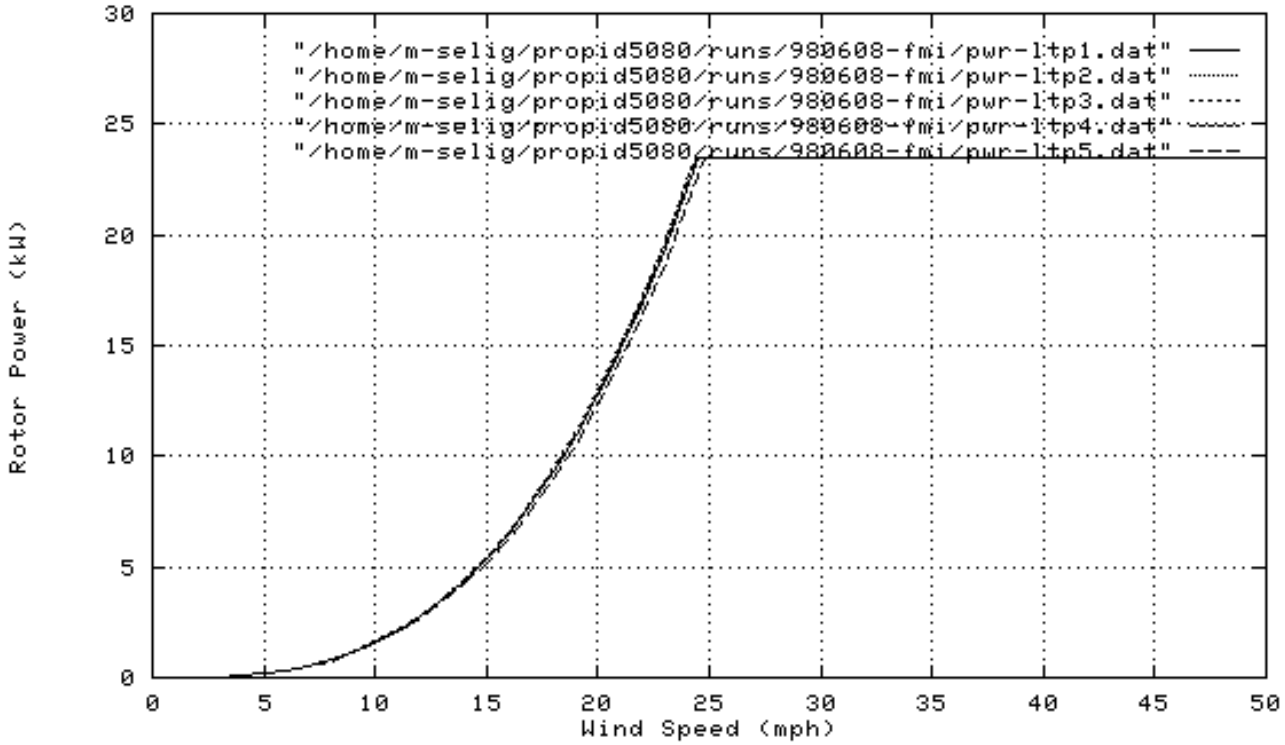


**Fig. 2.18 - Power curves for cases LTP1, 2, 3, 4, and 5**
Some data plots are nearly identical as illustrated by this graph.

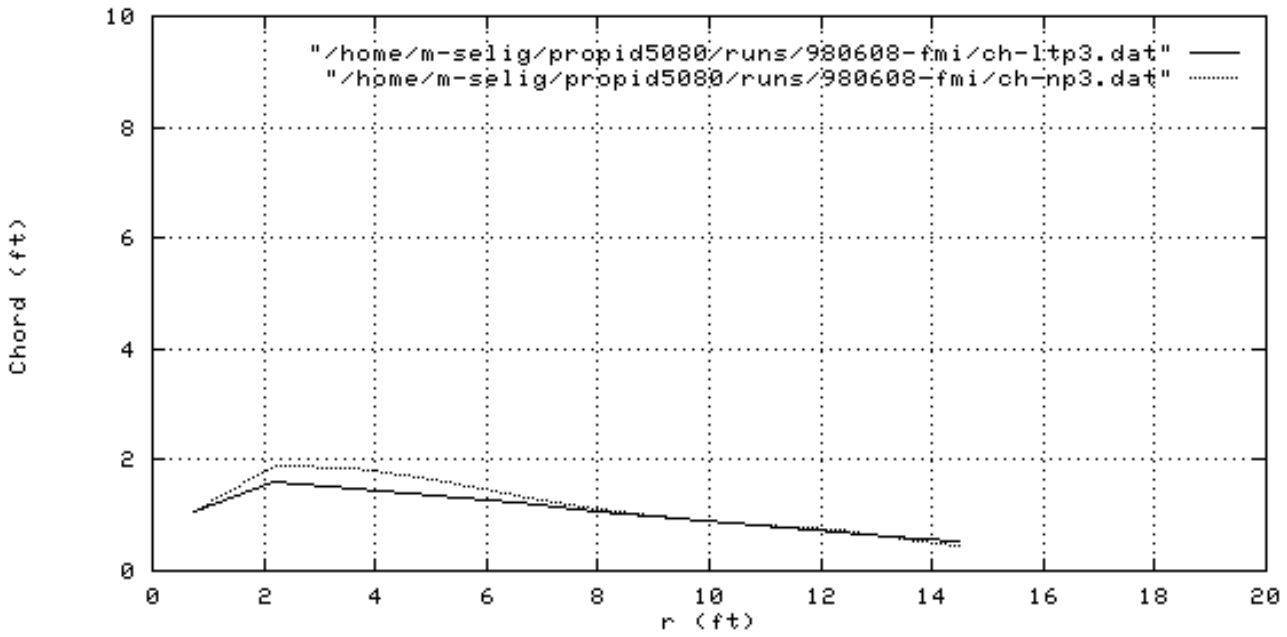


**Fig. 2.19 - Chord distributions for cases LTP3 and NP3**

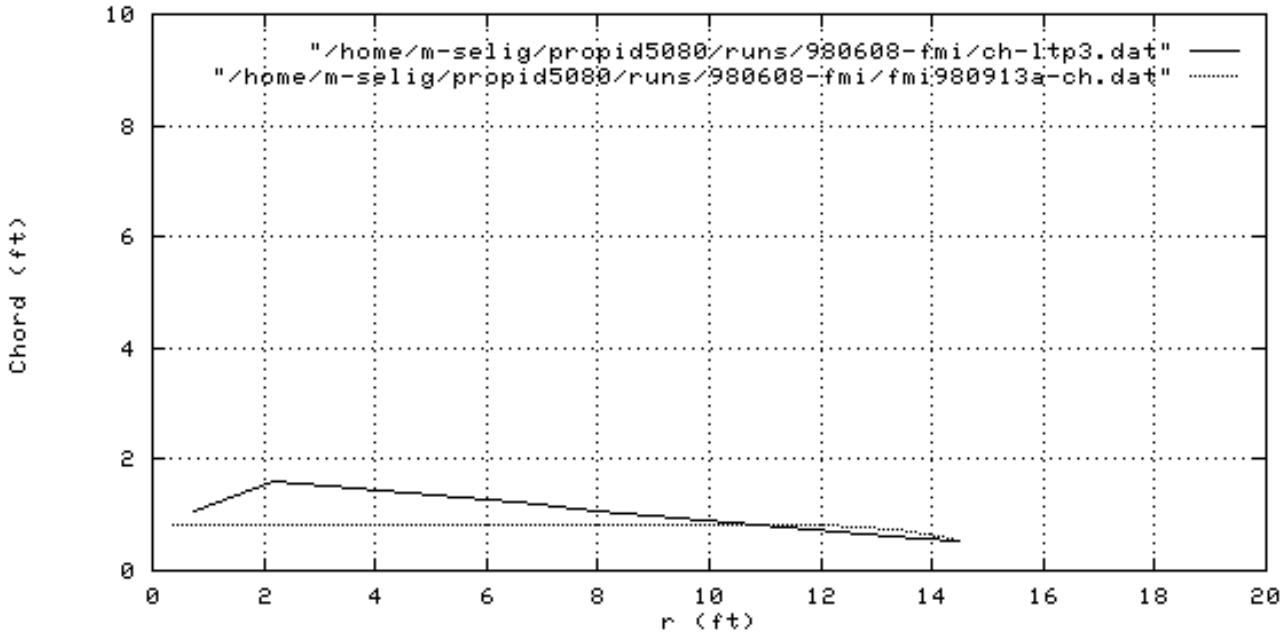


**Fig. 2.20 - Chord distributions for cases LTP3 and Jacobs 29-20**

Figure 2.21 shows the decision tree that led to the final blade selection. First, all of the blades have similar performance, except for case LTP5 that had the lowest performance gain over the Jacobs blade. This eliminated LTP5 from consideration. A large blade chord required more materials and hence cost eliminated LTP1. Between LTP2, LTP3, and LTP4, the best was LTP3 in terms of annual energy production. Moreover, LTP3 has a conventional looking configuration. Again, the linear taper had its advantages with respect to the simplicity of the design, ease of manufacture and economic use of materials. Many blades from LM Glasfiber A/S (headquartered in Lunderskov, Denmark) are of this type. National Renewable Energy Laboratories (NREL) took a similar approach in the design of the new CER blade [Ref. 12] and WindLite in the design of their new 8-kW turbine [Ref. 13]. Thus, our final selection was the blade LTP3 with a 10.83% performance gain over the baseline blade.

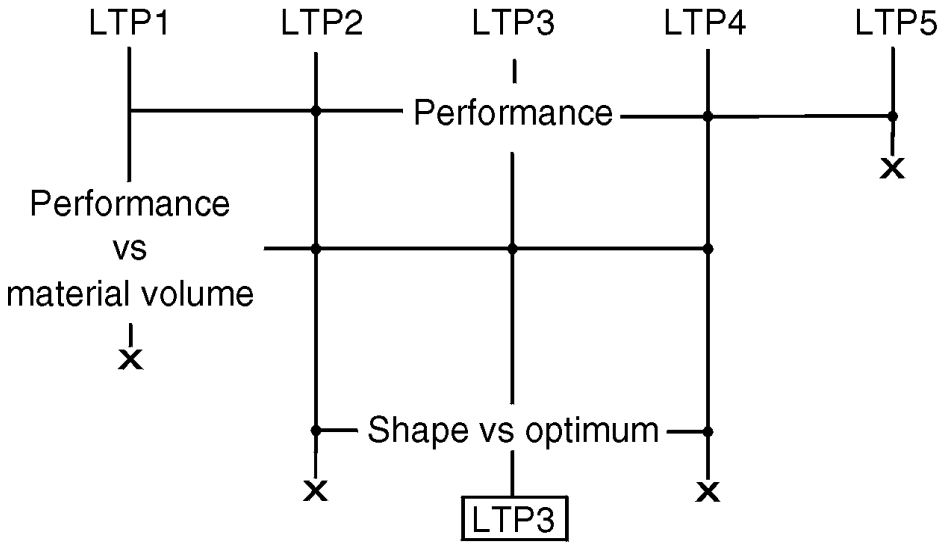


**Fig. 2.21 - Blade Planform Selection Decision Tree**

# 3.0 BMI Prototype Blade Design, Structure and Lamination

## 3.1 Study Goals

### 3.1.1 Study Staging

This was a two-stage study. Both design stages incorporated advanced 3D CAD (Vellum[8], SOLIDWorks[9] and AutoCAD[10]) and Finite Element Modeling (COSMOS/M)[11].

**Preliminary Design (PDR) Blade Design/Trade-Off Study -** This effort researched different aerodynamic parameters, airfoil/planform configurations and the resulting structural configurations to determine optimization parameters for a final blade design.

**Detailed Design Study (DDR) -** This effort developed a final design for fabrication and testing. This effort utilized the findings of the initial trade study to develop an optimized blade.

### 3.1.2 Study Efforts

The task consisted of three interdependent efforts:

**Blade Design/Airfoil Trade-Off Study -** This study followed after a refined aerodynamic definition for a specific blade design. The study was performed by Michael Selig.

**Structural Design/Trade-Off Study** - This study followed after a final blade design. Primary structural design and Finite Element Modeling (FEM) were performed by Chuck Richey

**Design for Manufacturing** - Kent Sherwood and Mike Kramer at FMI were the parties primarily responsible for this study.

## 3.2 Methodology & Modeling

### 3.2.1 Aerodynamic

The study investigated the aerodynamic performance (see Section 2) of derived airfoils and planforms with appropriate twist distributions. Two families of planforms were investigated during the preliminary design period:

1. The “new” NP1–NP5 series - These utilized tapered chords. These were the most efficient, both aerodynamically and structurally.

---

[8] Vellum Drafting Software [Ref. 30]
[9] SOLIDWorks Drawing Software [Ref. 31]
[10] AutoCAD Drafting Software [Ref. 32]
[11] COSMOS/M, a comprehensive analytic modeling software package [Ref. 33]

2. The “current” CP1 and CP5 series - These were essentially constant chord and similar to the original baseline blade airfoil design.

The preliminary design study provided direct input during the detailed design phase of the final blade. The result utilized a modified form of the NP1 planform with a SG6050 airfoil.

### 3.2.2 Structural

The study used Finite Element Modeling (FEM) to perform the analysis. This technique essentially utilized “mathematical bricks” to model structures. The precision varies with the model:

**General Analysis Modeling** - We chose COSMOS/M software for the FEM modeling.

**Geometry Generation** - For this effort, we developed computer tools to generate model properties in order to configure models with consistent geometries and to speed up the analysis process. These tools consisted of Excel spreadsheets to rotate and scale the airfoils and to generate various files required by COSMOS/M to build the FEM models.

**Surface Structure -** We used SHELL4L composite shell elements to model the blade surface structure.

**Core Structure -** We used solid 8-node isotropic elements (SOLID) to model the blade foam core.

**Loads -** Loads were provided for two scenarios:

- ✓ **Maximum Power** was modeled with individual forces on nodes (FND) simulating wind thrust (Y-axis) and torque (in plane toward the leading edge) dependent upon Michael Selig’s analyses.
- ✓ **Hurricane Class II** loads models were determined from Germanischer Lloyd certification specifications. This corresponded to a wind of 59.5 ms or 133.1 mph. The equivalent pressure of 0.157 psi was applied to ***both*** airfoil sides (it would be 0.315 psi if applied to only one side) through the pressure element load (PEL).

**Rotational Forces -** Rotational forces were modeled by applying rotational velocity in radians per second using the “C” (centrifugal) option. Maximum loads correspond to 175 rpm or 18.326 radians per second – negative in the model convention.

**Units -** Modeling was in the English/American pound/inch system.

### 3.2.3 Design for Manufacturing

- ✓ Blade root must fit the Jacobs 29-20 hub.
- ✓ Shape must be simple and have ruled (straight) edges for aerodynamic portions of the blade outboard of the hub area.
- ✓ Laminates must not be complex and must lend themselves to production techniques.

## 3.3 Basic Blade Geometry and Fabrication Details

### 3.3.1 Prototype Blade Dimensions

By combining results of the Blade Design/Airfoil Trade-Off Study with the design requirements of the baseline turbine, a physical blade dimension plan evolved. Once the dimensions of the blade were resolved, tip design and root structure were determined. Fig. 3.1 describes the overall prototype blade planform geometry. Figs. 3.2 and 3.3 define the tip and Figs. 3.4 and 3.5, the root structure.

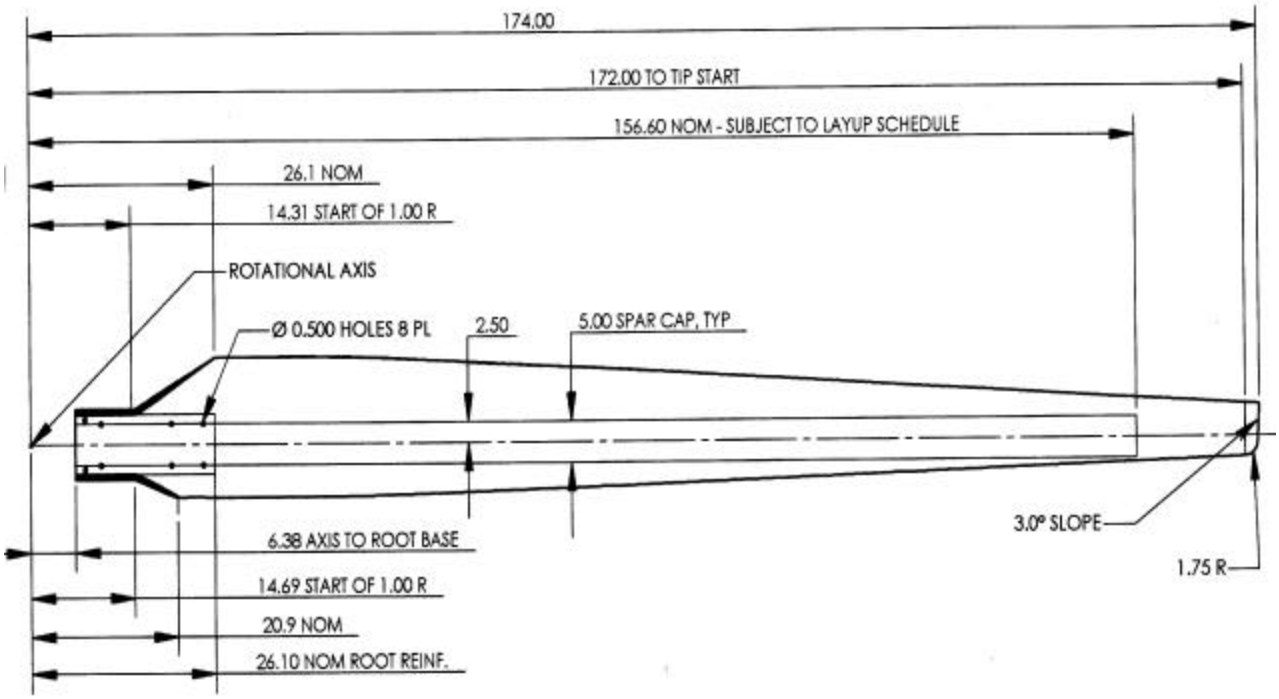


**Fig. 3.1 - LTP3 Blade, Top View Detail of Planform Geometry**

### 3.3.2 Tip Shape

A good tip shape is one that has a sharp outboard edge. To achieve a low noise profile, the design should have the lowest amount of separated flow around the tip and from the trailing edge, including the outer edge of the blade. These edges on the blade should be sharp. The trailing edge should be as sharp as is physically possible; this might mean having a trailing edge as thin as 1/16 in.

The sharp edge along the outer wing edge begins where noted in Figure 3.2, and this edge line follows the camber line of the airfoil. From the last true airfoil station (noted), the upper and lower surfaces of the

blade smoothly taper down to the sharp trailing edge. In this case, the flow cannot wrap quickly around to the top low-pressure surface. Instead, it flows smoothly off the wing tip; thus, the flow does not separate and add to noise. In addition, the now further displaced tip vortex effectively increases the blade span by a small amount. In turn, this results in lower induced drag (more efficient). (See Figures 3.3, 3.6 and Table 3.1.)

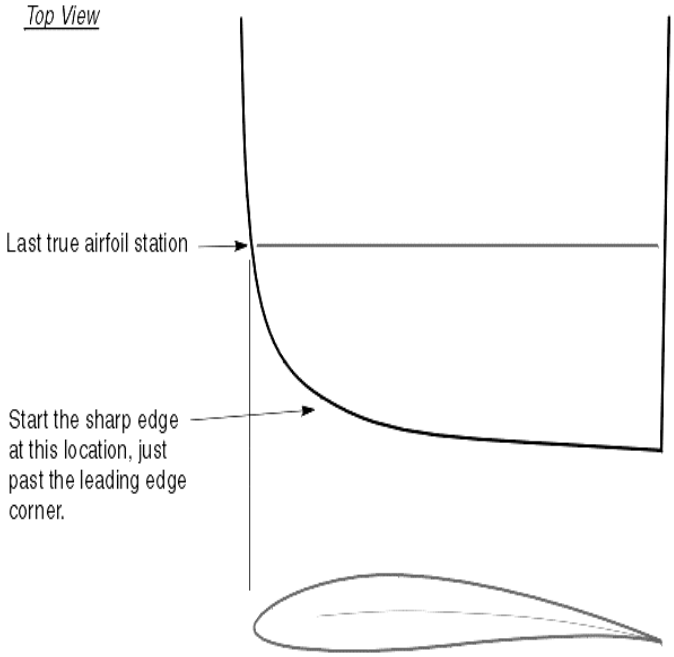


**Fig. 3.2 - Tip Detail**

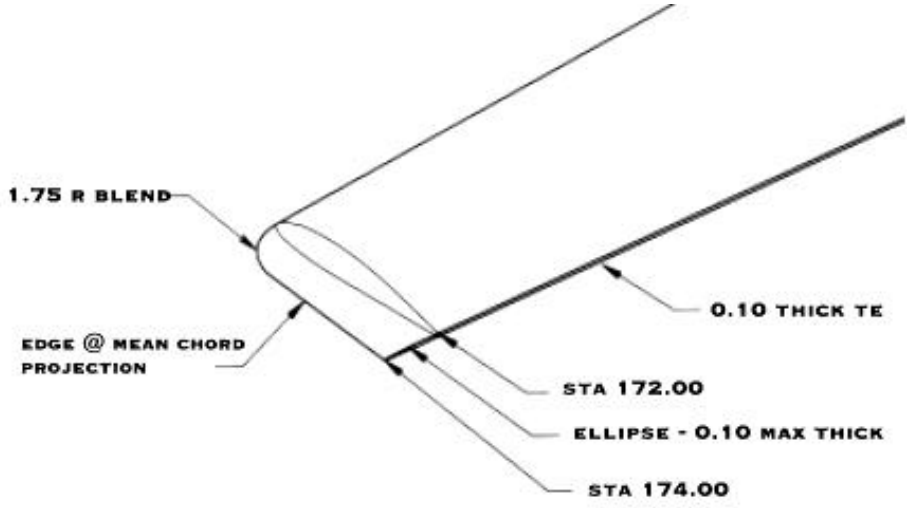


**Fig. 3.3 - Tip shape geometry**

### 3.3.3 Root Connection

In the root area, wood and cast urethane served as a high-density core and provided additional bolt bearing beyond the local heavy glass laminate overwrap. All bolt holes are 0.500" in diameter. The four upper holes and the large 2.75" diameter, central hole were specific to the Jacobs hub configuration. The Ø 2.75" hole was lined with a 0.125" thick aluminum tube for blade retention and as a rotation axis for the over speed system. The two plywood inserts will react to the loads from the tube (bending and in-plane) into the cap structure, with the local fasteners eliminating peel (See Figs 3.4 & 3.5).

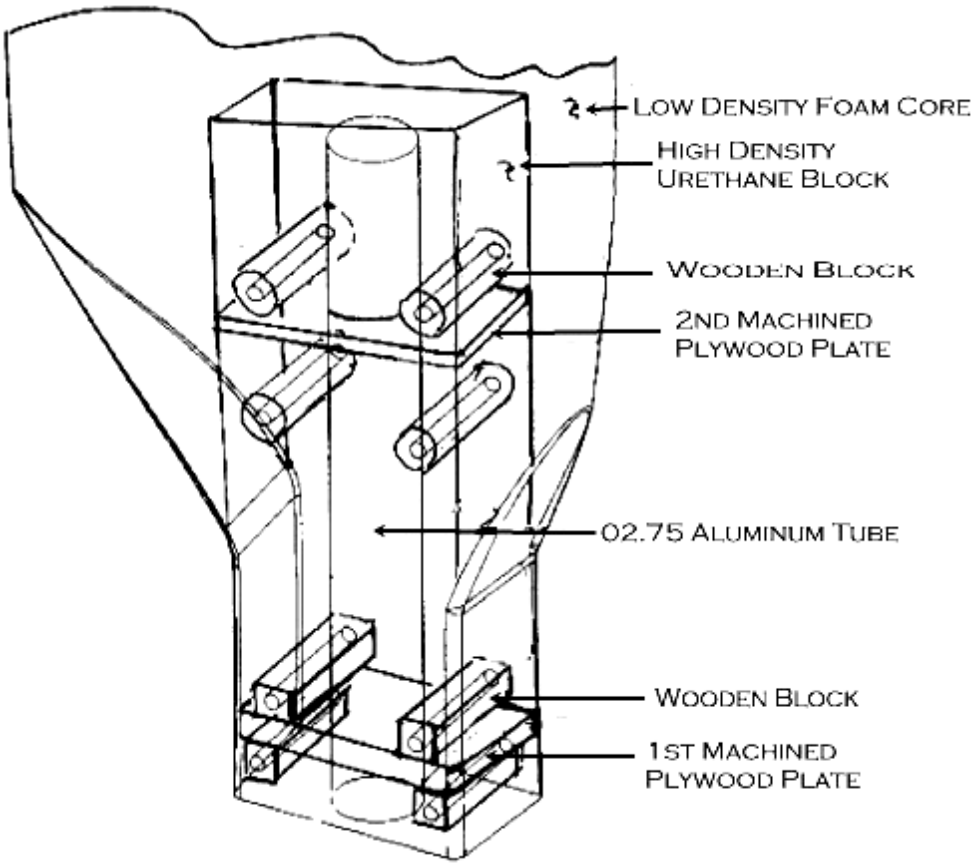


**Fig. 3.4 - Wood and Cast Urethane Root Block**

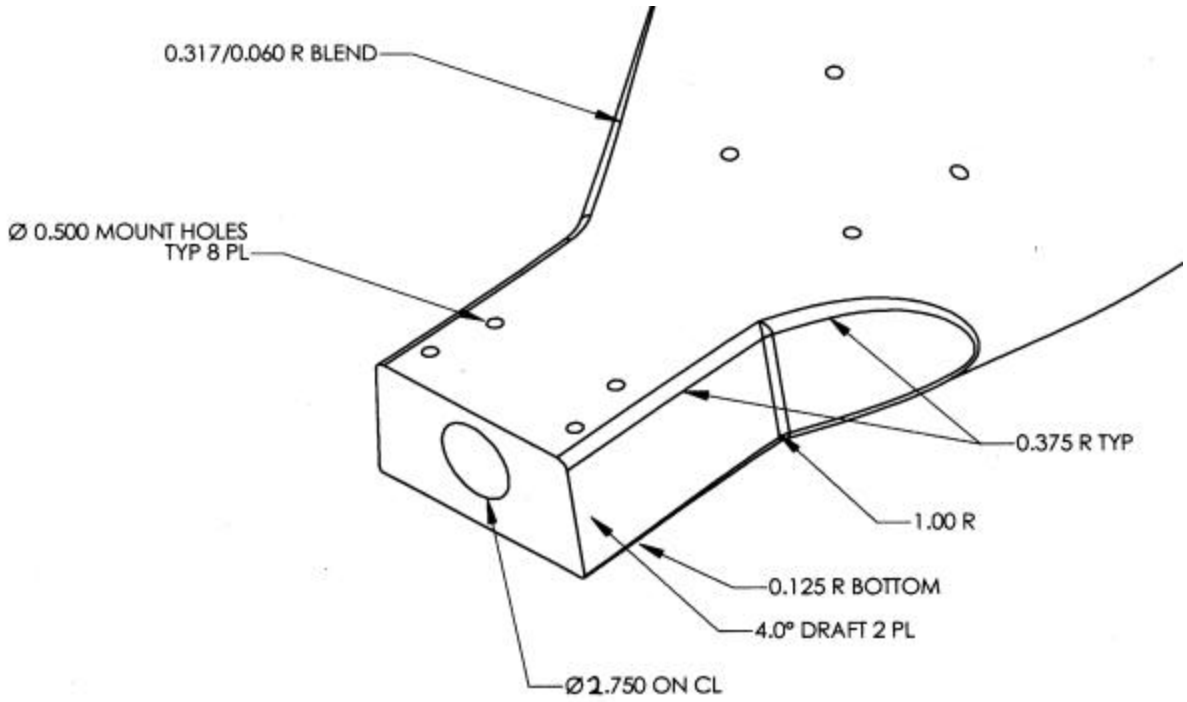


**Fig. 3.5 - Root Detail**

## 3.4 Loft (Shape) Generation

**Table 3.1 - LTP3 Loft (Shape) Generations**

| LPT3 Chord R, fraction | Radius In. | Chord In. | Pitch, Net |
|---|---|---|---|
| 0.15 | 26.1 | 18.113 | -21.711 |
| 0.20 | 34.8 | 18.296 | -22.908 |
| 0.25 | 43.5 | 17.617 | -17.234 |
| 0.35 | 60.9 | 16.097 | -11.994 |
| 0.45 | 78.3 | 14.574 | -7.824 |
| 0.55 | 95.7 | 13.052 | -5.126 |
| 0.55 | 95.7 | 13.052 | -5.126 |
| 0.65 | 113.1 | 11.531 | -3.405 |
| 0.85 | 147.9 | 8.486 | -1.606 |
| 0.95 | 165.3 | 6.965 | -0.557 |
| 1.00 | 174.0 | 6.205 | -0.033 |

Blade generated by airfoil sections. Special sections generated for the hub area.

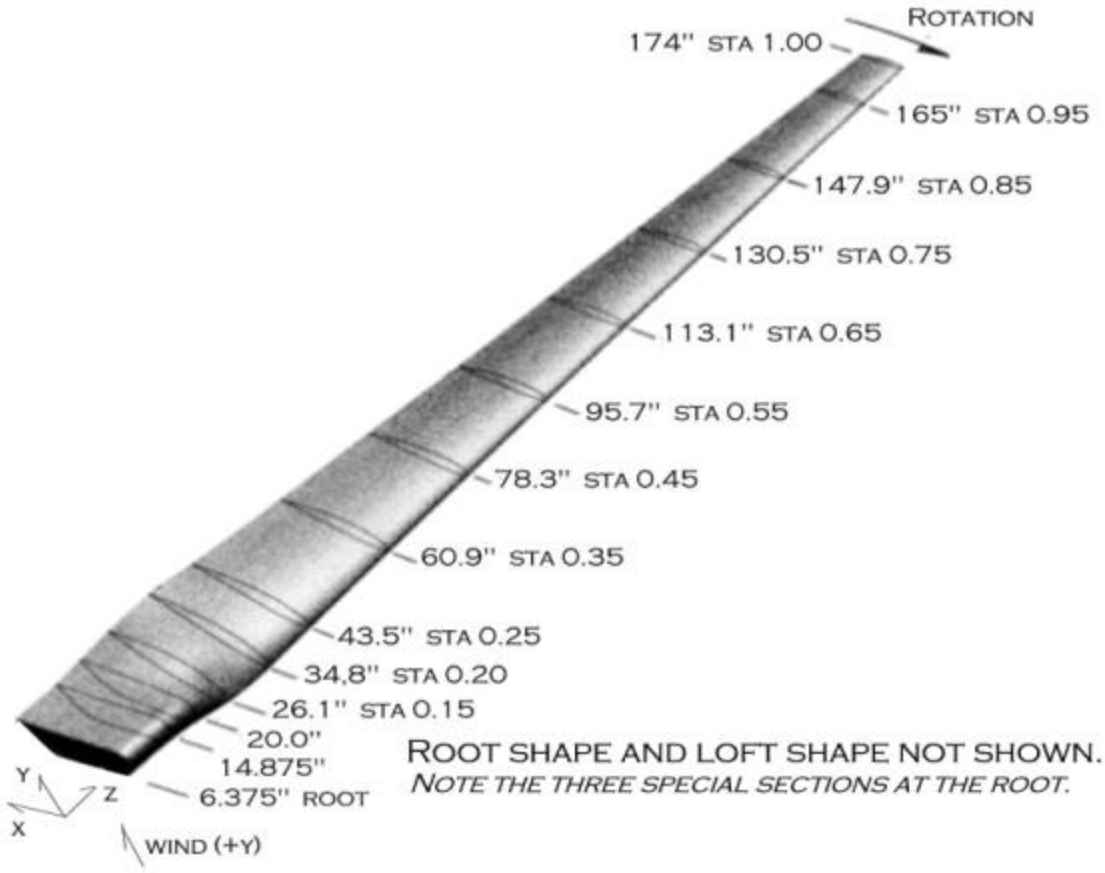


**Fig. 3.6 - LTP3 loft plot**

## 3.5 Material – Preliminary Design/Trade-Off Studies

### 3.5.1 General

The FEM models used materials that are both generic (typical) and specific fabrics from a given manufacture:

- BID = Generic Bi-directional E-glass fabric 10 mils thick. Same as Hexcel Style 7725.
- A130 stitched E-glass fabric. This is a 0° (unidirectional or "UNI") 21 mils thick made by Hexcel.
- DB120 stitched E-glass fabric. This is a ±45° 2-layer fabric 21 mils thick made by Hexcel.
- DB120 –split and stacked into UNI. This is DB120 where the two layers have been cut apart and formed into a single 2-layer UNI. This material was used for laminate data testing for laminate engineering.
- Skin Stack BID(1)/A130(1)/DB120(1). The (N) means "N" layers and the "/" separates layers. Thus, this stack is equivalent to one BID + one A130 + one DB120, where all their reference axes are aligned along the long direction – the BID is 0°/90°, the A130 is 0°, and the DB120 is ±45° with the "0°" orientation along the length of the blade. If not noted, the orientation is inferred as

"0°". A more specific call out is: (0°)$A130_1$/(0°)$DB120_1$/(0°)$A130_1$; where the (XX°) is the alignment in degrees; and, the subscript is the number of layers.

- Cap Stack BID(1)/A130(3). This can be more rigorously written as (0°)$BID_1$/(0°)$A130_3$, where one BID at 0° is followed by three A130 at 0°.

Material properties defined:

- Vf – fiber volume fraction = fiber volume/total volume. This quantity is unitless.
- Ex – Young's Modulus in "x" direction = Stress in x-direction/Strain in x-direction. Units are msi, or millions of pounds per square inch.
- Ey – Young's Modulus in "y" direction = Stress in y-direction/Strain in y-direction. Units are msi, or millions of pounds per square inch.
- Nuxy – Poisson ratio = change in x/change in y for a force in the x-direction. This quantity is unitless.
- Gxy – Shear Modulus in the x-y plane. Units are in msi, or millions of pounds per square inch.
- Fxtu – Ultimate tensile stress in the x-direction. Units are in ksi, or thousands of pounds per square inch.
- Fxcu – Ultimate compressive stress in the x-direction. Units are in ksi, or thousands of pounds per square inch.
- Fytu – Ultimate tensile stress in the y-direction. Units are in ksi, or thousands of pounds per square inch.
- Fycu – Ultimate compressive stress in the y-direction. Units are in ksi, or thousands of pounds per square inch.
- S – Shear stress in the x-y plane of the fabric. Units are in ksi, or thousands of pounds per square inch.
- H0 – Thickness in mils
-

In the FEM models, composite layers were made from epoxy glass laminate. The skins consisted of stacks of *BID(1)/A130(1)/DB120(1)* (52 mils thick); while the cap stack was three layers of the *BID(1)/A130(3)* (73 mils thick each). In the areas of the caps, the skin overlaid the cap structure for a total thickness of 271 mils. The caps were formed four elements wide starting at the fifth element from the trailing edge, traveling in a chordwise direction toward the leading edge (see Table 3.2 and Figs 3.21 - 3.22).

**Table 3.2 - Preliminary FEM Design**

| | Vf | Ex msi | Ey msi | Nuxy | Gxy ms | Fxtu ksi | Fxcu ksi | Fytu ksi | Fycu ksi | S ksi | H0 mils |
|---|---|---|---|---|---|---|---|---|---|---|---|
| **Generic BID/BID (Hexcel 7725)** | 0.44 | 2.83 | 2.83 | 0.140 | 0.90 | 46.30 | -43.60 | 46.30 | -43.60 | 9.70 | 10.0 |
| **DB120 - split & stacked into UNI** | 0.44 | 3.84 | 1.09 | 0.390 | 0.60 | 88.47 | -79.92 | 3.61 | -13.17 | 12.31 | 10.5 |
| **A130 Stitched Fabric - 0°** | 0.45 | 5.26 | 1.27 | 0.320 | 0.50 | 125.89 | -48.44 | 4.90 | -13.53 | 12.63 | 21.0 |
| **DB120 Stitched Fabric - ±45°** | 0.44 | 2.50 | 2.50 | 0.173 | 0.60 | 45.56 | -32.70 | 45.56 | -32.70 | 13.84 | 21.0 |
| **Skin Stack BID(1)/A130(1)/DB120(1)** | 0.44 | 3.76 | 2.04 | 0.360 | 0.87 | 51.28 | -35.51 | 24.50 | -19.88 | 9.78 | 52.0 |
| **Cap Stack BID(1)/A130(3)** | 0.44 | 5.00 | 1.57 | 0.318 | 0.60 | 117.13 | -46.82 | 10.33 | -15.93 | 13.12 | 73.0 |

## 3.6 Design Load Modeling

### 3.6.1 Maximum Power

Maximum power (Fig 3.7) was modeled by individual forces on nodes (FND) simulating wind thrust (Y-axis) and torque (in plane toward the leading edge). These calculations were provided from M. Selig's analysis.

### 3.6.2 Hurricane Class II Loads by the Germanischer Lloyd Certification

Hurricane Class II loads (Fig 3.8) corresponds to a wind of 59.5 m/s or 133.1 mph. The equivalent pressure is 0.157 psi when applied to *both* airfoil sides *or* 0.315 psi if applied to only one side. This is a pressure element load (PEL) in the FEM model.

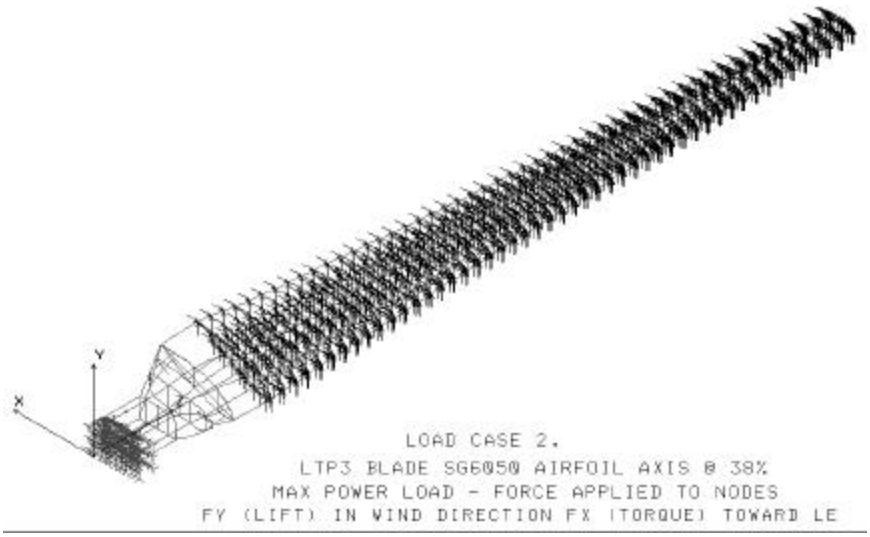


**Fig. 3.7 - Max Power Load FEM Modeling – Final Design**

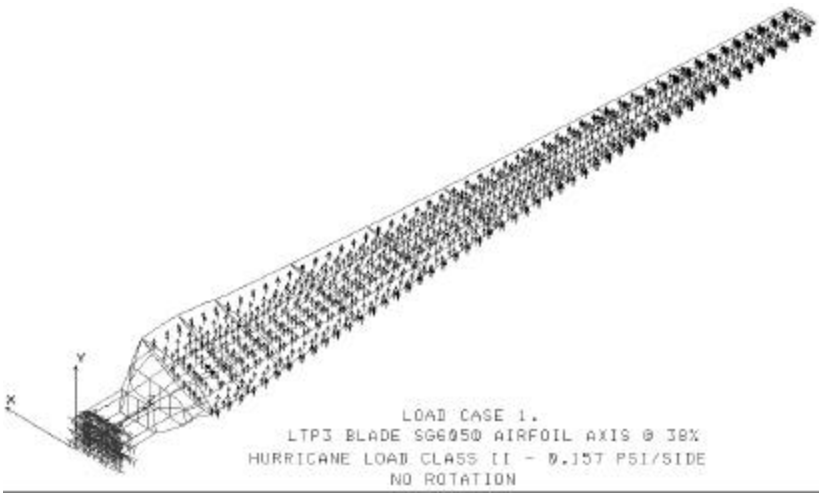


**Fig. 3.8 - Hurricane Load FEM Modeling – Final Design**

## 3.7 Trade-Off Studies

### 3.7.1 Planform Study

**The planform study determined the best way to position the blade axis on the chord. FMI chose three configurations for modeling (see Figs 3.9-3.11).**

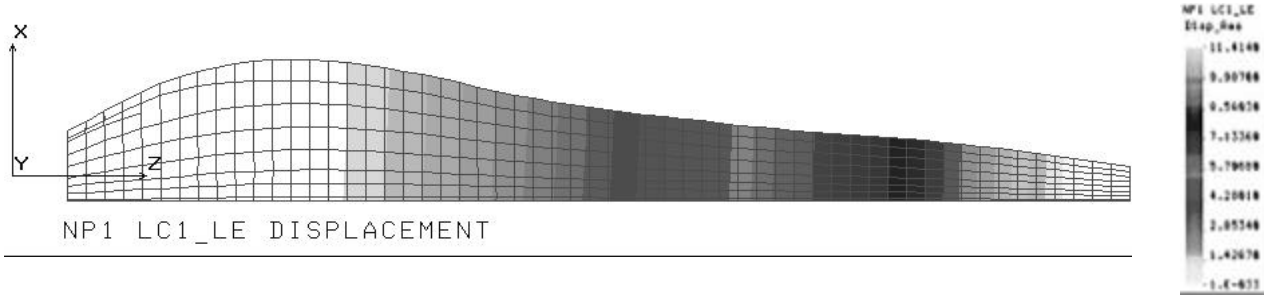


**Fig. 3.9 - Straight L.E., Axis 4.25" AFT – 11.4" Tip Displacement @ Max Power**

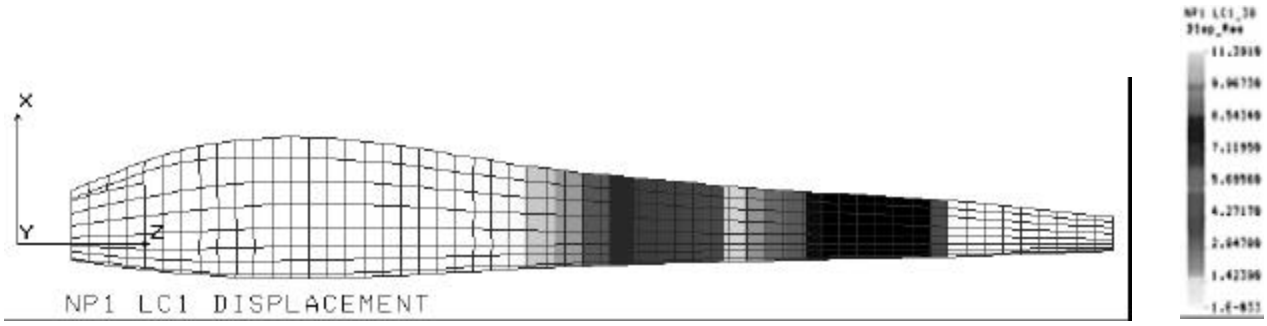


**Fig. 3.10 - Axis @ 25 % CHORD – 11.3" Tip Displacement @ Max Power**

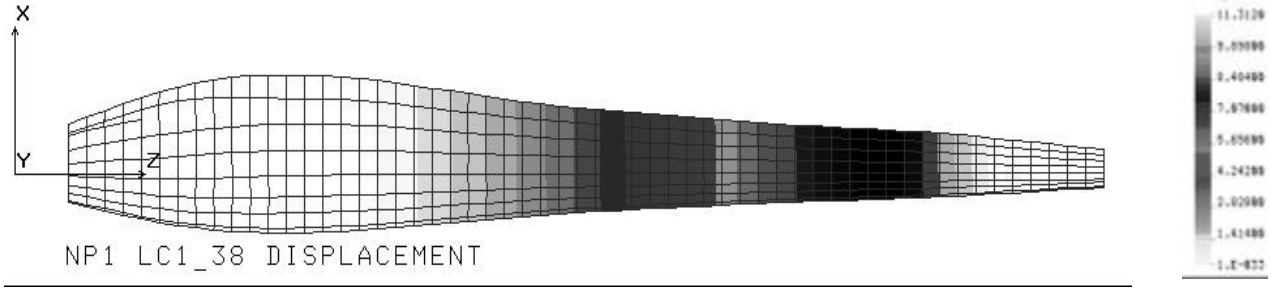


**Fig. 3.11 - Axis @38% CHORD – 11.4" Tip Displacement @ Max Power**

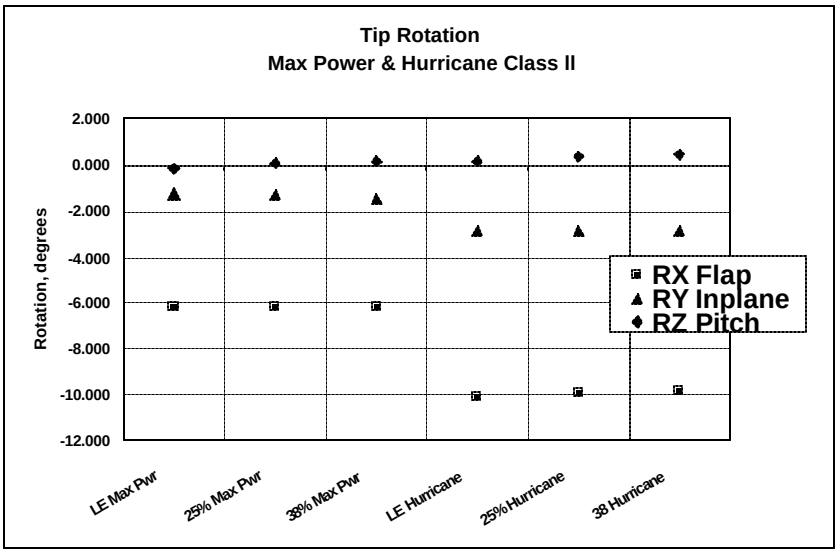


**Fig. 3.12 - Tip Rotation as a Function of Pitch Axis Location**

The baseline constant LE suffered more tip pitch change than would be expected from the tip center of pressure offset, while the remaining is comparable (Fig 3.12).

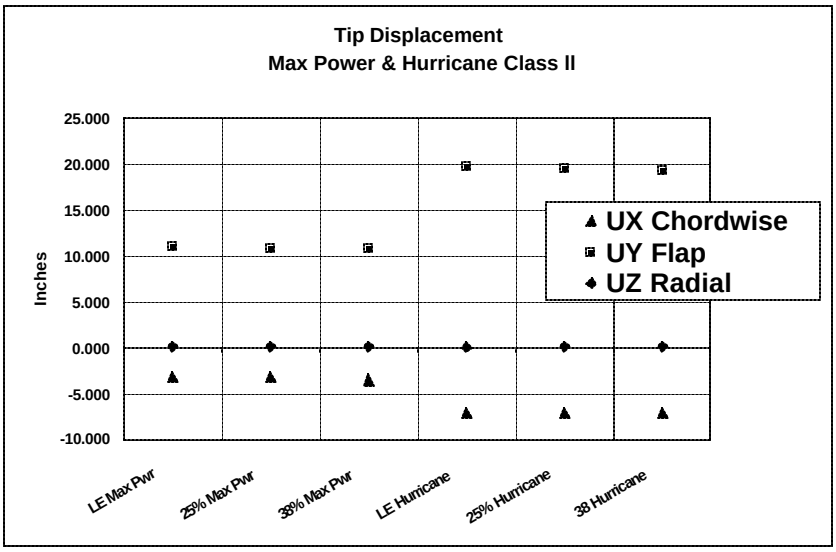


**Fig. 3.13 – Tip Displacement as a Function of Pitch Axis location**

Pitch axis location has little effect on tip displacement (see Fig 3.13).

## 3.7.2 Summary

The pitch axis at 38% chord was the best overall compromise as the spar structure was blended into the hub in a manner that provides efficient fabrication and structure. The 25% and 38% blade curves were very close in performance. The straight LE blade had some tip twist due to the offset of center of

pressure at the tip and suffered slight degradation in buckling.

## 3.8 Comparison of Maximum Displacement

**Von Mises Stress & Tsai-Wu Failure Index.**

### 3.8.1 Comparative Study

This study compared the extremes of section properties with tapered and semi-constant width planforms. We compared New Planform tapered (high performance) and Current Planform with semi-constant width configuration modeled after the Jacobs blade. The comparative study used the 25% axis position on all blades for pitch axis location (see Figs 3.14-3.17). Significant structural reinforcement was required in the root areas of all configurations.

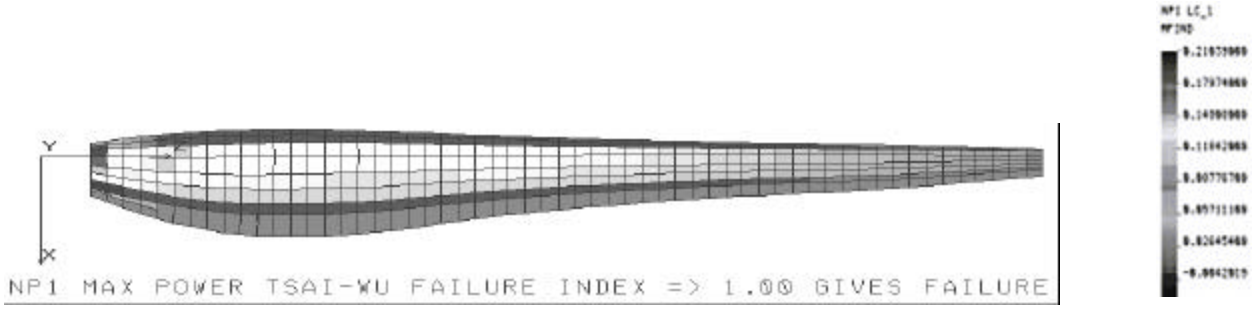


**Fig. 3.14 - NP1 – Smooth structure, with good structural and fabrication characteristics.**

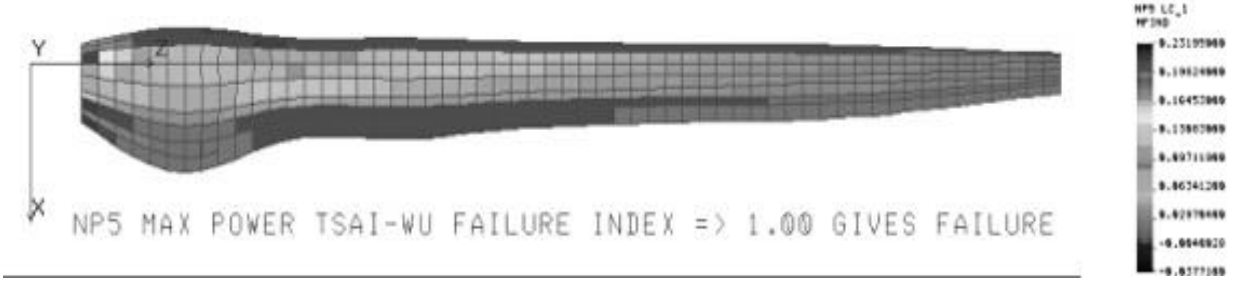


**Fig. 3.15 - NP5 – Exotic loft impractical, but other characteristics are good.**

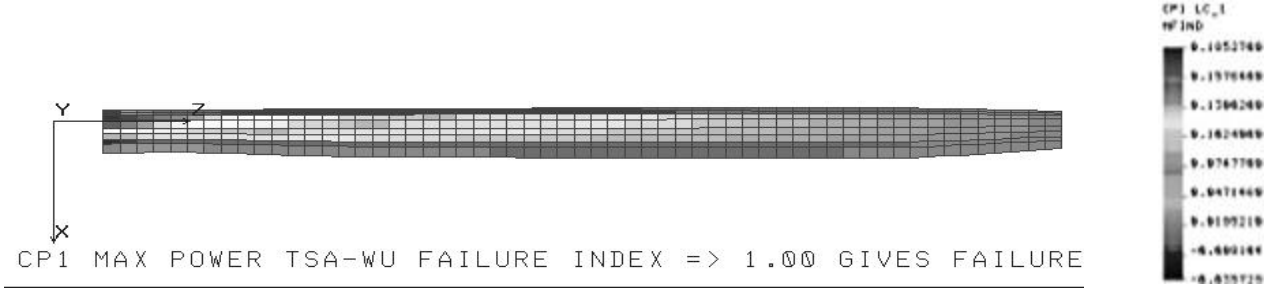


**Fig. 3.16 - CP1 – Easy to build, but efficiency and structural characteristics are poor.**

The thin root section leads to high deflection/stresses and low modal frequencies (Fig. 3.16)

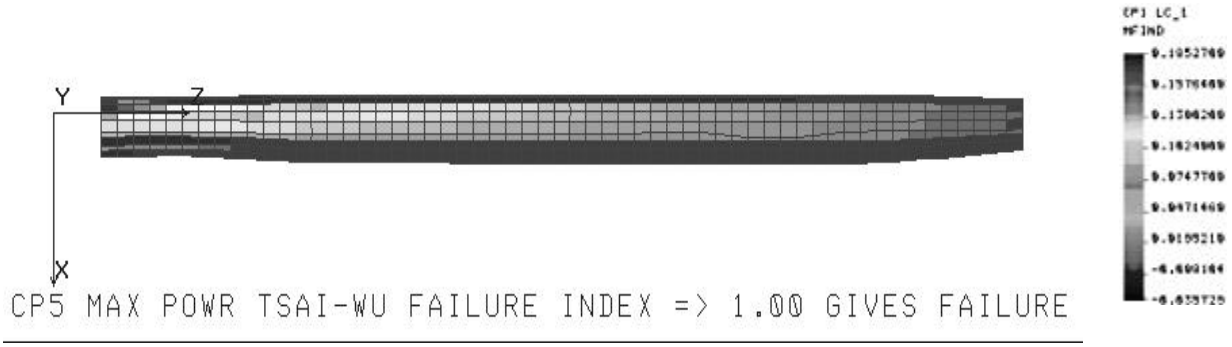


**Fig. 3.17 - CP5 – Easy to build, but efficiency and structural characteristics are poor.**
The thin root section leads to high deflection/stresses and low modal frequencies (Fig. 3.17)

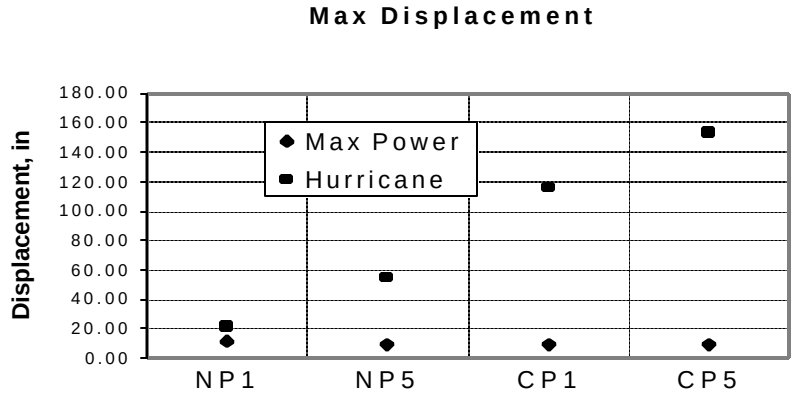


**Fig. 3.18 - Max Displacement**
The displacement increases as the airfoil planform evolves toward constant chord and a thinner root. (See Fig. 3.18.)

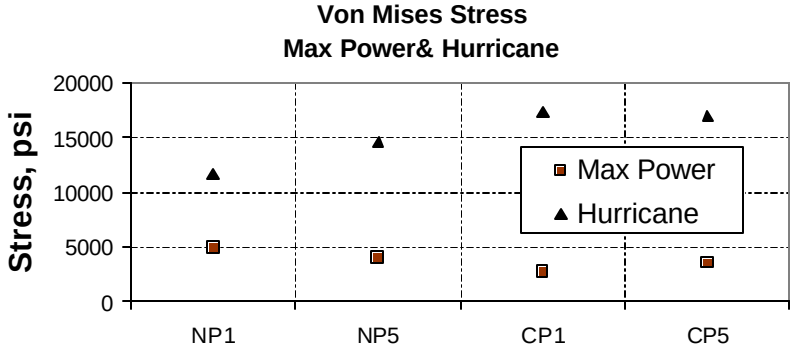


**Fig. 3.19 - Von Mises Stress, Max Power & Hurricane**
As the airfoil planform evolves toward constant chord and a thinner root, the stress, in general, increases. (See Fig 3.19.)

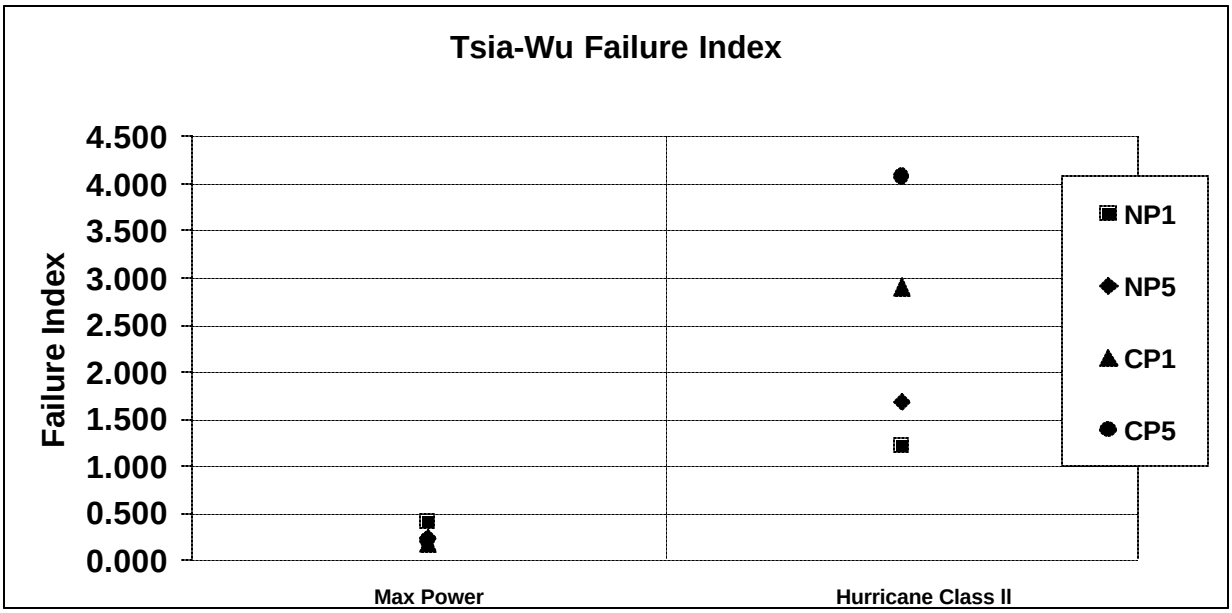


**Fig. 3.20 – Tsia-Wu Failure Index**

As the airfoil planform evolved toward constant chord and a thinner root, the structural margins decreased – additional root reinforcement was required to avert failure in the Hurricane II case (see Fig 3.20).

### 3.8.2 Comparative Study Summary

The major gains in efficiency were realized with the NP configurations and a minimal gain was realized with the CP series. Thus, it was desirable to take the best NP configuration that works structurally.

### 3.8.3 Structure Summary – NP Planform vs. CP Planform

In general, the tapered NP (New Planform) series was the best compromise for both max power and hurricane cases. The CP (Current Planform) stresses were acceptable even in the max power case, as CP thinness limited bending stresses and the blades equalized out-of-plane bending by centrifugal (CF) forces. However, our studies confirmed that CP structures when compared to NP structures, dangerously overstressed under Hurricane II loading and therefore depend upon mechanical feathering.

## 3.9 Final Design

- The Final Design placed the pitch axis at 38% chord.
- FMI chose the SG6050 Selig airfoil. SG6050 has a relatively thick section on either side of the pitch axis.
- This configuration provided an efficient root structure for the spar.
- FMI modified the selected NP1 planform for ruled (straight) loft shape where possible to aid in manufacturing efficiency and to simplify tooling.
- Figs 3.21 and 3.22 illustrate the final design layup definition.

### 3.9.1 Material – Final Design

The skins consist of the Skin Stack of *(0°)A130$_1$/(0°)DB120$_1$/(0°)A130$_1$* (63 mils thick) and the caps consisted of one to six layers of the Cap Stack *(0°)A130$_3$/(0°)BID$_1$* (73 mils thick each). In the areas of the caps, the skin overlaid the cap structure for a total thickness ranging from 478 mils at the root (with additional ±45° BID) to 62 mils in the tip area (see Table 3.3).

**Table 3.3 - Final FEM Design**

| | Vf | Ex msi | Ey msi | Nuxy | Gxy msi | Fxtu ksi | Fxcu ksi | Fytu ksi | Fycu ksi | S ksi | H0 Mils |
|---|---|---|---|---|---|---|---|---|---|---|---|
| **BID (Hexcel 7725)** | 0.44 | 2.83 | 2.83 | 0.140 | 0.90 | 46.30 | -43.60 | 46.30 | -43.60 | 9.70 | 10.0 |
| **Skin Stack A130(1)/DB120(1)/A130(1)** | 0.44 | 4.35 | 1.53 | 0.448 | 0.82 | 96.48 | -40.60 | 18.33 | -15.66 | 8.88 | 63.0 |
| **Cap Stack BID(1)/A130(3)** | 0.44 | 5.00 | 1.57 | 0.318 | 0.60 | 117.13 | -46.82 | 10.33 | -15.93 | 13.12 | 73.0 |

### 3.9.2 Termination of Cap Stacks

The cap stacks were stitched together on a roll and cut to length upon insertion in the tool. The overall cap stack was too thick to terminate all in one step; that would produce an excessive joggle and greatly reduce fatigue life. The solution was to trim the outer most ends in a one ply per inch taper.

### 3.9.3 BID Overlay of Cap Step-Downs

One layer of ±45° BID covered the inside surface of the Cap Stack (Table 3.4) to bleed off stress at the termination and to prevent peel. The detail layup at the root end of the blade required some modification during tooling manufacture. A FEM check confirmed the result.

**Table 3.4 - Lay up Schedule**

| Location | Station/Area/Schedule (Subtract 6.375" to get distance from Blade base) | Schedule |
|---|---|---|
| **Root/Cap** | 6.38 to 21.60 | 5C+5B+1S |
| **Cap - 5.0" Wide** | 21.6 to 46.56 | 5C+1S |
| **Cap - 5.0" Wide** | 46.56 to 63.95 | 4C+1S |
| **Cap - 5.0" Wide** | 63.95 to 84.35 | 3C+1S |
| **Cap - 5.0" Wide** | 84.35 to 124.94 | 2C+1S |
| **Cap - 5.0" Wide** | 124.94 to 136.55 | 1C+1S |
| **Cap/Skin** | 136.55 to 174.00 (tip) | 1S |
| **TE/Kink Reinforcement** | 26.1 Nom | 1S+2B |
| **Base Fore/Aft Inplane Reinforcement.** | 6.38 to 20.0 Nom | 1C+1S |
| **"C" Schedule Cap Stack** | (0°)A130$_3$/(0°)BID$_1$ | 1 Stack 0.073" Thick |
| **"S" Schedule Skin Stack** | (0°)A130$_1$/(0°)DB120$_1$/(0°)A130$_1$ | 1 Stack 0.063" Thick |
| **"B" Schedule ±45° BID** | ±45°BID Hexcel 7725 | 1 Ply 0.010" Thick |

**Table 3.5 - Physical Blade Design Statistics**

| | Max Power 175 rpm | Hurricane Class II | Max Stress/Strain Approx. Dist. from Root in Inches |
|---|---|---|---|
| **Displacement - in** | **6.81** | **9.17** | |
| **Von Mises Stress - psi** | **2679** | **3237** | **Root Edges & 34"** |
| **Txy Shear Stress - psi** | **536/-764** | **693/-549** | **20-32" LE & TE Kink** |
| **Sy Spanwise Stress - psi** | **2622/-2079** | **3041/3170** | **Root Edges & 24-67"** |
| **Sx chordwise stress - psi** | **769/-808** | **963/-1188** | **17"** |
| **Tsai-Wu Failure Index MFIND Failure => 1.00** | **0.06793 Safety Factor = 14.7** | **0.1026 Safety Factor = 9.75** | **34"** |
| **Spanwise Strain EPSY** | **0.001158/-0.000967** | **0.001843/-0.001436** | **34"** |
| **Chordwise Strain EPSX** | **0.000618/-0.000753** | **0.000944/-0.000899** | **NA** |
| **Fatigue Safety Factor Estimate (Tension/Compression)** | **1.57/7.90** | **8.67/13.06** | |

## 3.10 Final Design Summary

### 3.10.1 General Remarks

FMI engineered the detailed design to optimize the blade planform for the Jacobs 29-20 wind turbine. Fabrication methods pioneered by FMI provided improvements in manufacturing and structural performance. FMI also intended for the design to provide a foundation for follow-on applications for other new wind turbines in the 20 kW power category.

- All values in Table 3.5 provide numbers that are consistent with a long-life trouble free blade.
- All displacements and stresses are low. Individual stresses such as shear, tensile, compression, cannot be evaluated separately for safety factors, as the combined stress must be analyzed – in this report, this was provided by the Tsai-Wu Failure Index, which is very low, (see Table 3.5).
- The weight moment that determines the centrifugal load for overspeed agrees within 1.4% of the baseline blade.
- Hurricane Class II conditions produce longitudinal static strains of less than 0.00184 (absolute).
- Bolt-bearing stresses provide safety factors (over 2% yield) of 7.67 (baseline) and 15.34 for a future four-bolt mount blade. The 2% yield criteria means that the stress corresponding to a hole elongation (over yield) is found when the hole has elongated 2% of its original diameter.
- The Tsai-Wu failure index has safety factors of 14.72 (Max Power) and 9.75 (Hurricane Class II).
- Campbell plots show very good frequency isolation for all frequencies.
- Hurricane Class II buckling margins are extremely high – positive (normal) wind direction is 16.56 and 15.28 for negative wind direction. The blade would suffer structural failure well before buckling.
- The structure is very conservative as it consists of a smooth external shell without multiple "hard" interfaces that cause local stress risers.

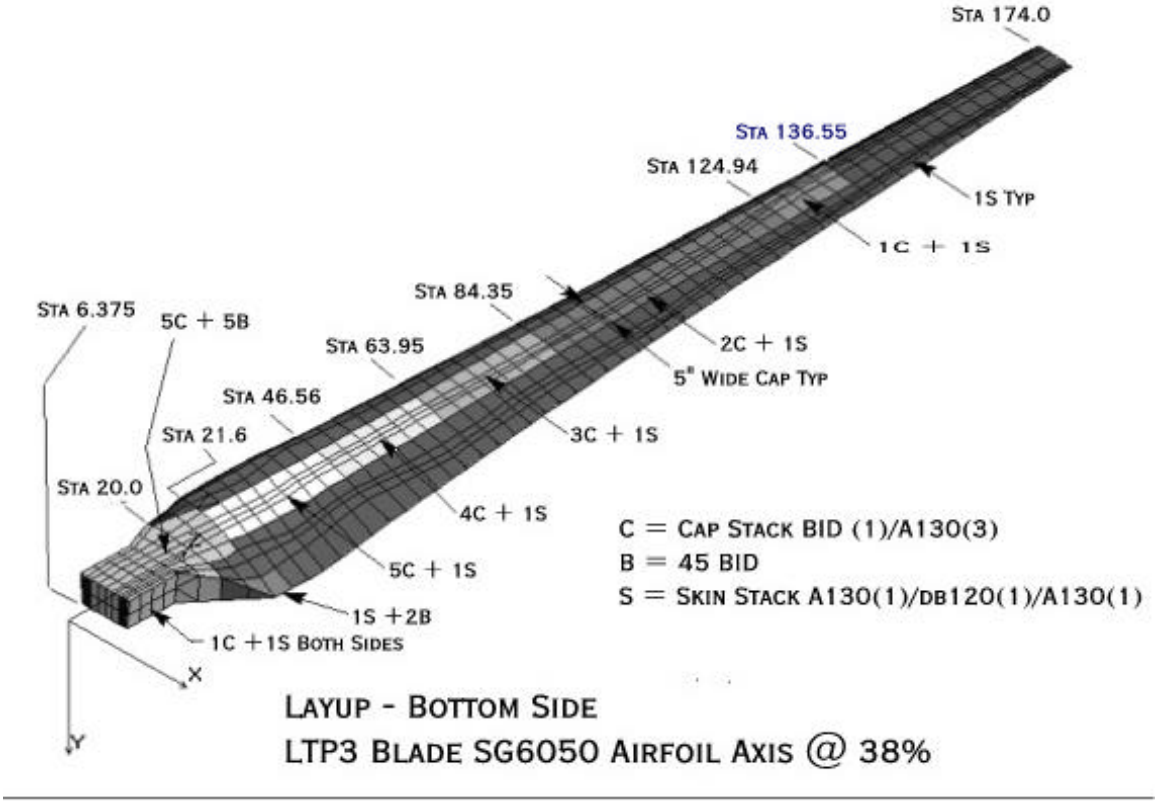


**Fig. 3.21 - Final Design Lay up – ISO Bottom View**

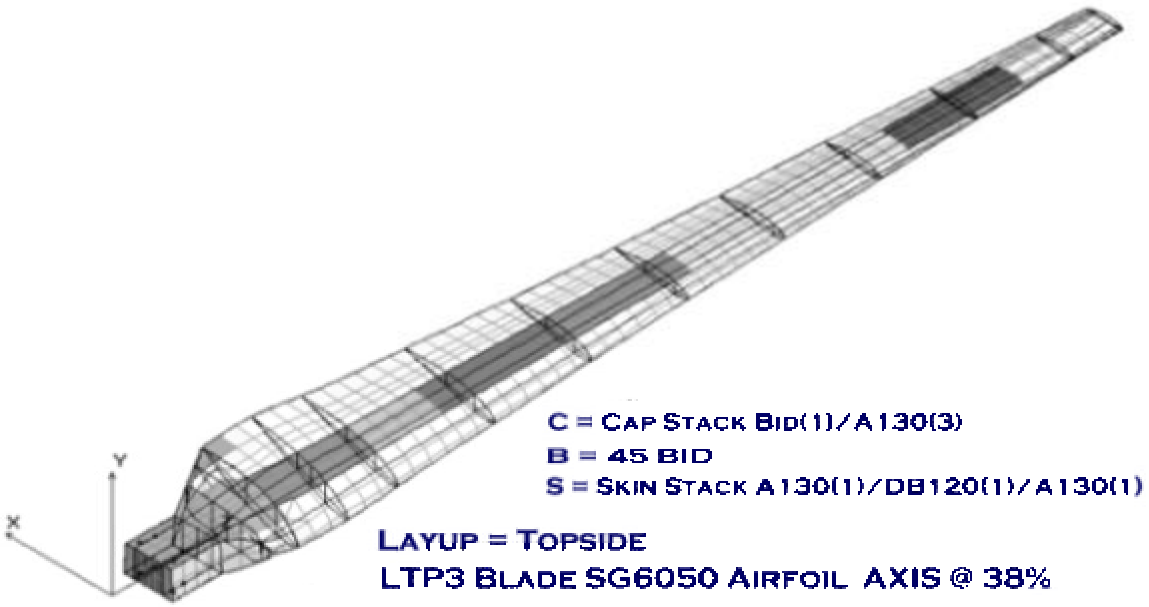


**Fig. 3.22 - Final Design Lay up – ISO Top View**

# 4.0 Foam Matrix Manufacturing

## 4.1 The FMI Solution

The complete FMI wind turbine blade was fabricated in a single tool in two steps: 1) create a molded polyurethane foam core, 2) complete a resin transfer molding (RTM) step.

The core molding fabrication used a patented foam molding process to add strength and reinforcement to the core while simultaneously molding into the core all hard structures such as the root block and attachment points. This procedure provided a means for every surface and aspect of the core to undergo several non-invasive inspections to insure pre-determined conformity before applying laminates.

Pre-cut and stitched dry materials were attached to the core for the spar caps and the skins to complete preparation for the RTM process. The RTM step bonded the laminates to the core and replicated the outer mold line (OML) of the blade design.

Preparation for the RTM process called for removing the reusable skin offset from the tool and then placing the wrapped core into the mold. Within the closed and clamped tool, the vacuum assisted RTM process wetted the entire surface of the core with a precise amount of formulated resin. Heat applied to the tool supplemented the curing process.

After a cooling period, the completed wind turbine blade was removed from the tool for inspection, painting and eventual shipment.

Figure 4.1 shows a typical FMI wind turbine blade cross-section similar to the blade described within this report.

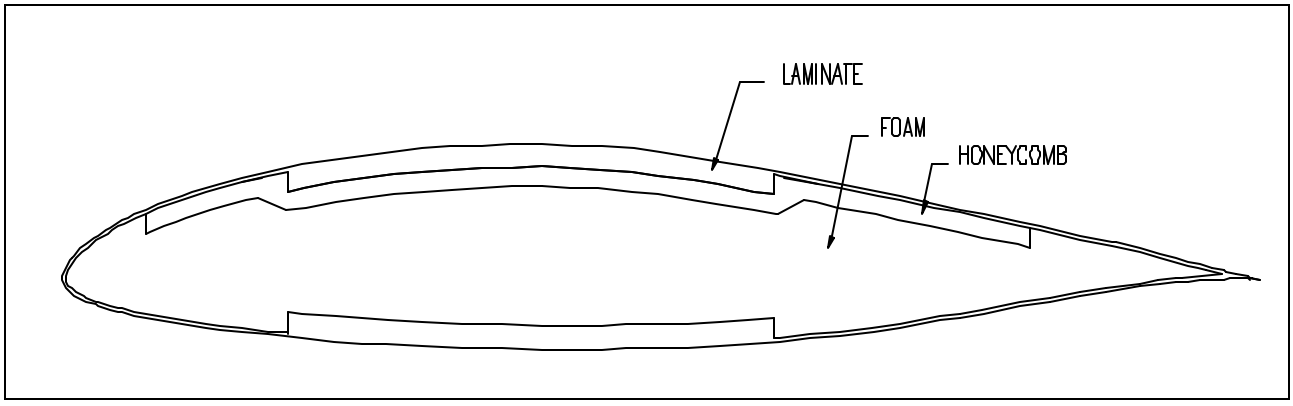


**Fig. 4.1 - Cross Section Typical FMI Wind Turbine Blade**

## 4.2 Tool Design

FMI's tool design plan chose to use numeric control (NC) machining to convert the electronically defined outer mold line (OML) of the engineered prototype blade drawing to a hard form. This process can create either a male plug from which the OML is cast as a "proof of design" tool or as a female OML machined into a steel tool for volume production. FMI chose to create an both an engineered high-density foam male plug and a cradle for that plug. This procedure promoted a close tolerance between the two sides of the closed and clamped tool. As a result, not only did the molded article more exactly replicate the design but it also more precisely shaped the trailing edge and the tip.

During tool fabrication, we planned for injection and vent ports in the tool to facilitate the resin transfer molding (RTM) process. Additional vacuum assisted vent ports were to be located in areas of the tool where resin may not easily flow such as the around the blade tip or along the trailing edge.

The molded foam core/resin transfer molding (MFC/RTM) tool design called for imbedded copper tubing placed between the cavity surface and the outer tool wall in both halves of the tool. The ability to control tool temperature served two purposes. Heated water circulated through the tool during the production cycle maintained a precise temperature for predetermined period to facilitate a $T_g$ temperature[12] and then cold water circulated through the tool reduced time between production cycles.

In a production mode, the opportunity to quickly cycle the tool contributes to both a labor savings and an increased number of cycles over a given length of time.

## 4.3 Tool Construction

Because of cost restraints and the fact that the BMI project required only a limited quantity of blades, FMI constructed an epoxy/fiberglass dual-purpose MFC/RTM tool. Projected service life of this tool was approximately one hundred blades. For a longer production run, FMI would construct metal tools that are capable of producing significantly more parts.

FMI employed NC-machined techniques to fabricate a high-density foam plug using the finalized design coordinates from the computer model replicating the OML of the wind turbine blade. We also fabricated a

---

[12] Composite articles can distort, become more brittle, or otherwise change characteristics when subjected to temperatures beyond the glass transition temperature ($T_g$). The result of this physical reaction to heat can result in a shortened blade fatigue life or even eventual distortion of the airfoil itself. $T_g$ represents a cure temperature that yields a stable article. $T_g$ can be as low as the ambient temperature or as high as several hundred degrees. It is reasonable to expect a turbine blade sited in a desert location to reach an internal temperature of 71°C (160°F). It is difficult to ascertain the degree of damage to the rotor but it is certain damage has occurred and that it has an accumulative effect over time. However, by curing the blade in the fabrication process to a $T_g$ temperature of 80°C (176°F), FMI has negated much of the temperature damage to the article. $T_g$ treatment is a required and common practice for composite articles installed in all military and commercial aircraft, aerospace vehicles and many defense applications [Ref. 34].

cradle from the same high-density foam to accept the low-pressure side of the blade and achieve four-inch flanges at the exact center of the leading and trailing edges. The reverse side of the cradle was machined square. FMI used a rigid flat steel table with a Blanchard ground steel top (the hard back) to support the blade cradle in preparation for the fabrication of the high-pressure side of the tool.

Once the hard back was completed, FMI placed injection ports, vent ports and a male seal strip around the parameter of the plug on the four-inch cradle flange. The high-pressure surface of the blade and flanges were then polished and mold released in preparation for the epoxy/fiberglass shell layup.

The high pressure side of the tool construction included an epoxy/fiberglass shell, a steel supporting structure, copper tubing designed to supply even heat to the tool surfaces using either hot water or hot oil and three inches of supporting/insulating back fill. After completion of these tasks, the tool was turned over, prepared and laminated to form the low pressure half of the tool

After the installation of a clamping system and hinges, FMI opened the tool. Both exposed mold surfaces needed some detailed preparation for the construction of the skin offsets.

Reusable skin offsets reduced the dimension of the foam core by the net thickness of the lamination composite material applied during the RTM process step. The offsets defined cap spar buildups on both the high and low-pressure sides of the blade as well. FMI used prepreg fiberglass material to construct these reusable skin offsets for both surfaces of the tool.

The completed skin offsets represented the last step of the OML tool fabrication.

## 4.4 Root Block

### 4.4.1 Procedure

Because of the large twist in the blade from the root to 26.1” toward the tip, FMI designed a molded root block, fitted precisely into the root cavity of the tool, to accommodate hub loads and secure the blade to the root [Fig. 4.2].

With the skin offsets positioned inside the tool, a splash, extending 26.1” towards the tip of the root area of the tool provided the OML dimensions for a root block plug. This plug was the model for an epoxy/glass tool constructed to mold the root block. See Fig. 3.4 and Fig. 3.5 for design details.

The butt end of the root block tool was flanged to allow for the clamping of an aluminum end plate to the tool. Eight 1½ ” x 1 ½ ” wood blocks were cut to length and keyed into the mold to take the compression loads that were exerted by the mounting bolts. We machined two marine grade plywood pieces to fit inside the mold. Precisely placed, these two plywood pieces matched the sides, top and bottom of the tool. These two plywood pieces also aligned and held the internal 2.75” OD 2024 T3 aluminum sleeve. After securing the end plate to the tool, we poured 12 pound per cubic foot foam into the tool and

clamped the top section to the bottom section of the tool with 0.5” bolts. The end plate had an expanding plug that matched the inside dimension of the aluminum sleeve that prevented foam from filling the tube.

After cure and a small amount of de-flashing and abrading of all surfaces, the completed root block auto-fitted into the blade tool. Since the root block was inside the OML tool as we poured the core, expanding foam encapsulated the root block and made the root structure an integral part of the molded foam core.

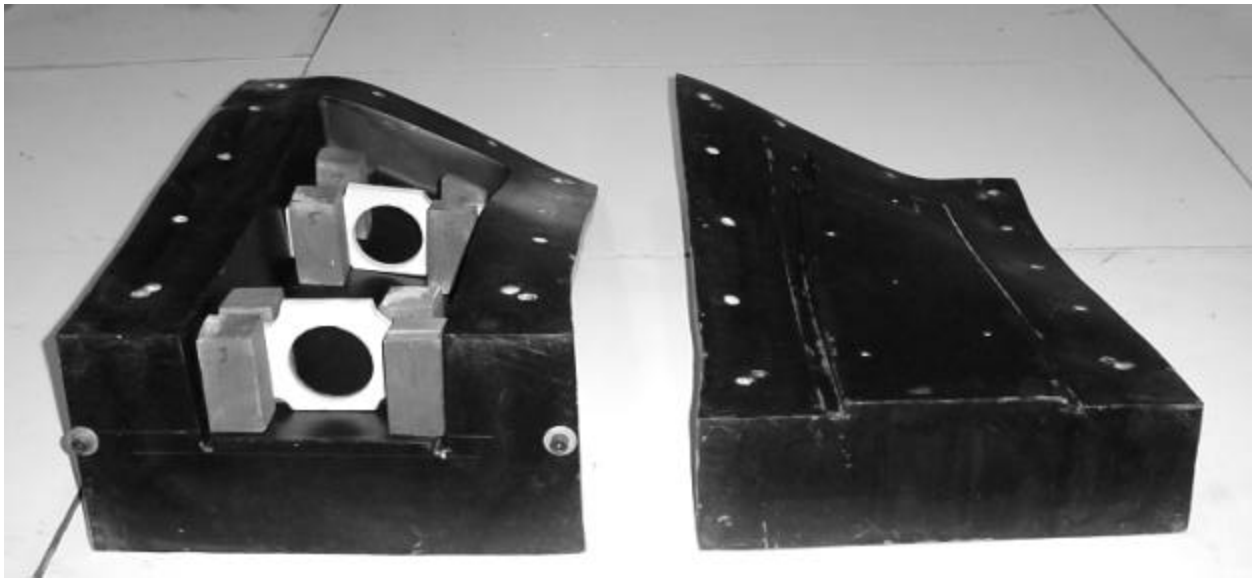

**Fig. 4.2 - Root Block casting tool with wood blocks and plywood mounting tube jigs.**

**Fig. 4.3 - Open tool with engineered plug**

The plug defines all surfaces of the molding tool shell. This view (Fig.4.3) shows the open tool with the engineered plug used as a dimensional reference to verify OML location. This view also shows some of the molding tool details such as the manual latches and the lock pins. The light colored line near the perimeter of the shell defines the location of the rubber O-ring sealing gasket.

Figures 4.4 – 4.7 show additional views of the tool and some of the fabrication steps.

**Fig. 4.4 - Open tool surface conditioning**
A FMI technician checks for surface blemishes. Note hinge detail and latches on the backside of the tool. Copper pipes on either side of the hinge are liquid inlet and outlet ports to heat or cool the tool during process or curing cycles.

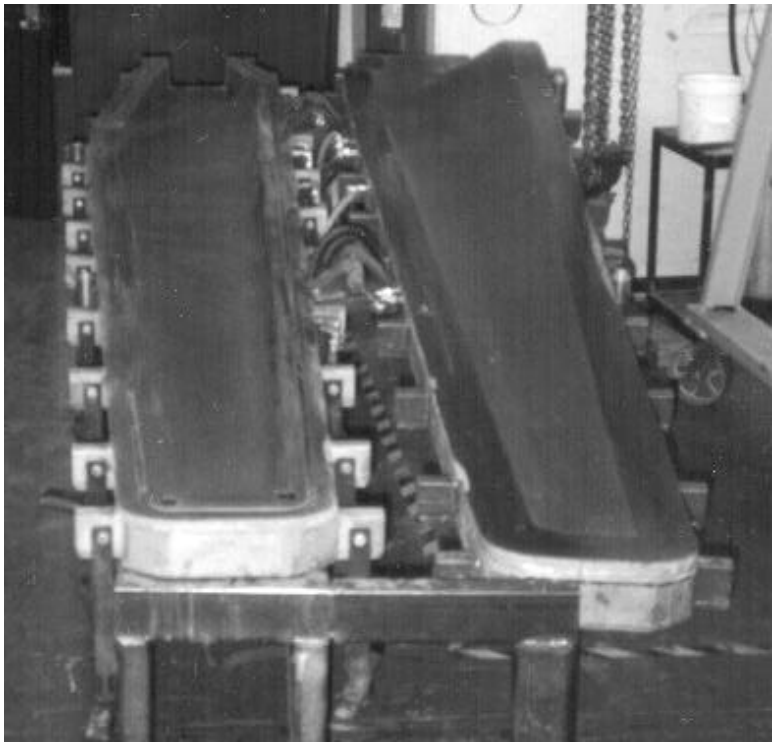

**Fig. 4.5 - Open production Tool**

Fig. 4.5 shows the open tool positioned for cleaning or maintenance.

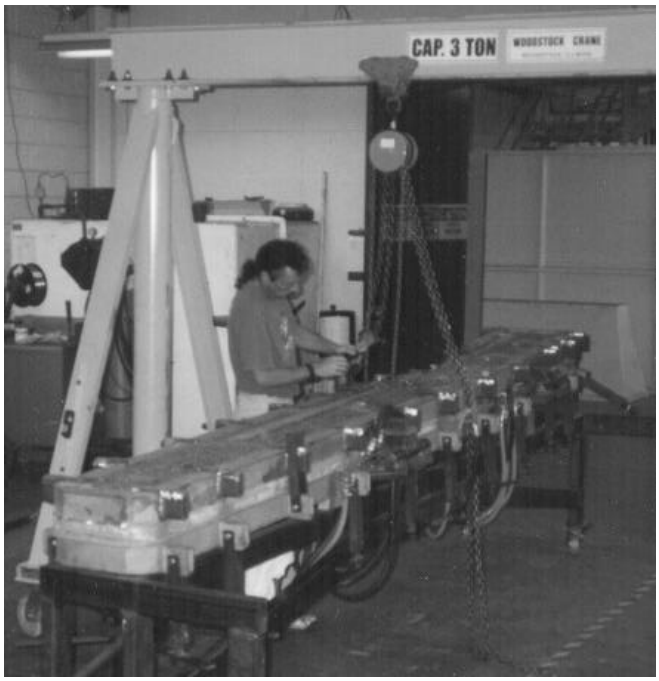


**Fig. 4.6 - Closed tool from rear**
This view affords a better look at the placement of the heating and cooling ports.

The overhead crane opens and closes the tool in both production and cleaning cycles. In actual production, FMI uses a smaller and more ergonomic hydraulic life positioned behind and over the lifting eye.

A volume production tool uses automated hydraulics that not only open or close the tool, but also secure and release the tool latches.
.

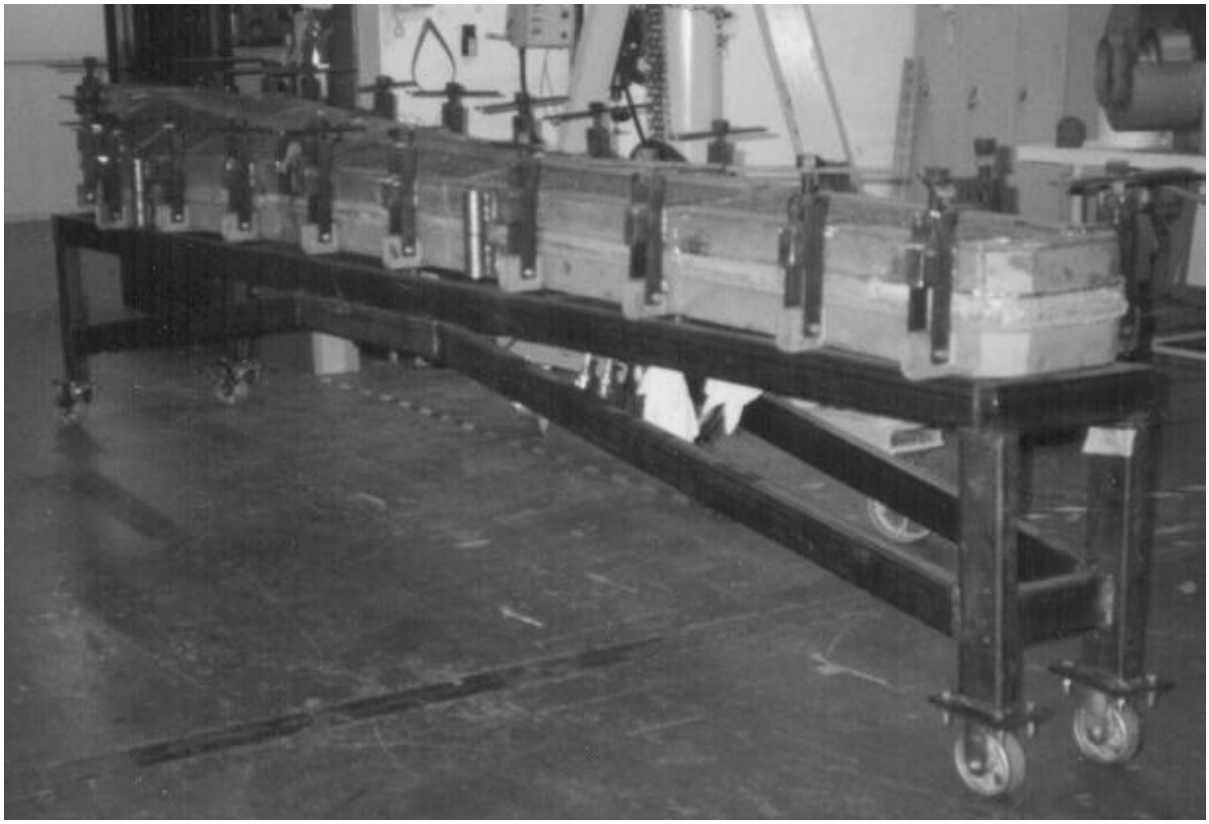

**Fig. 4.7 - Closed and latched tool**

Fig. 4.7 shows the closed tool as it would appear during a production cycle with closed and secured latches. The 4,500-pound structure rests upon a welded beam bridge to provide a solid and secure platform for the tool. Wheels allow the tool to move as required.

## 4.5 Blade Fabrication

### 4.5.1 Fabrication Steps

These consecutive fabrication steps produced finished blades.

- Mold the structural root block with all hard points and interior mounting hard points.
- Place the molded root block into the blade tool cavity with the skin offsets in place and mold the foam core.
- Detail the completed core and dry wrap glass fabric, according to the lamination schedule, around the foam core.
- Remove the reusable skin offsets from the MFC/RTM tool and place the glass wrapped core back into the MFC/RTM tool.
- Clamp the MFC/RTM tool and attach all vents and injection tubes.
- RTM the blade.
- Raise and hold tool temperature to achieve cure.
- Cool tool to ambient temperature and release the latches.
- Remove the blade. Detail where necessary. Paint where necessary.

### 4.5.2 Fabrication Detail

The first step was to craft a foam core in the MFC/RTM tool with the skin offsets in place. The tool held the pre-cast root structure in place during the foaming process creating a single integrated composite structure. Internal tool heat accelerated foam cure and achieved $T_g$.

Curing racks served as temporary storage for completed core and a means to extend the cure for several days. They also provided a platform for a close visual inspection before proceeding to the next step.

Meanwhile, uniform lengths of dry cap stack material and dry skin stack material were prepared according to the lamination schedule. Then we laid the cap stack material into the molded spar cavities of the core and stapled or tacked them in place. We wrapped the skin stack of woven and double bias glass completely around the leading and trailing edge to meet at the spar cap. We then carefully placed the wrapped core inside the MFC/RTM tool, closed it and clamped the latches. With the vent/vacuum and inlet tubes attached, resin began flowing into the tool under vacuum and pressure. Hot water, flowing through the tool, elevated the internal temperature to a pre-determined point. A constant temperature, held for a pre-determined time, assisted the cure and $T_g$ compliance.

The RTM process thoroughly wetted out the material, bonding the skin and core into a monolithic unit.

The result of the RTM process was a very smooth surface ready for primer and paint. An additional improvement would be to gel coat the tool surfaces to save the primer and painting steps. This would reduce touch labor and paint cost. We chose not to gel coat the test blades, as it was more advantageous that we were able to visually check the quality of the laminate.

## 4.6 FMI Fabrication Attributes

There are four main attributes associated with polyurethane foam molding/RTM structures in the wind turbine blade application.

- The density of cured polyurethane foam increases when it expands into confined areas of a sealed mold. For example; with a finished core, foam density will increase as measured from the center of the core to the surface. The result is that the skin surface has higher compression strength than it would if the foam maintained a uniform density throughout the part. One of Mr. Sherwood's patents covers a procedure using various materials to reinforce the core surface creating a foam/matrix skin[13].
- Aerodynamic loads are carried by the skin surface while the underlying core provides structural and adhesive support. When the lamination schedule calls for span support beyond the compression loading limits of the skin, two unidirectional multi-ply glass cap spars, one on either side of the core, are laminated onto the foam core during the RTM phase of the process.
- In some cases, aerodynamic loads require an increase in load bearing strength on the low-pressure side of the blade to resist compression failure in that direction. Rather than suffering the weight and expense penalty of enlarging the low-pressure side spar cap, the FMI solution can incorporate another of Mr. Sherwood's patents described as a procedure for placing honeycomb in the exact location requiring additional strength. The result is that the foam packs the honeycomb cells causing measurably higher density foam in the cells during the molding process. The diffusion of foam throughout the honeycomb matrix produces exceptionally high compression load bearing strength with a very small weight penalty[14].
- Manufacturing benefits include: reduced fabrication time when compared to hand layup, VARTM[15] or other methods that require the top and bottom sides having to be bonded in a second step, lower part count, reduced per unit labor costs, lower weight, elimination of voids and cavities, no edge joined seams, no water absorption, and minimal field preparation prior to blade mounting.

### 4.6.1 The Tool

- Only one set of tooling is required for moderate production rates
- Ovens not required.
- A closed mold procedure significantly reduces the amount of volatiles entering the atmosphere.

---

[13] U.S. Patent # 4,664,974 Kent Sherwood, May 12, 1987
[14] U.S. Patent # 4,797,312 Kent Sherwood, Jan. 10, 1989 and U.S. Patent # 4,857,830 Kent Sherwood, Aug.15, 1989
[15] Vacuum Assisted Resin Transfer Molding usually described as vacuum bagging to a single engineered surface.

- Fast part production.
- Close dimensional tolerances.
- Foam and resin metering results in weight consistency and a predictable CG from blade to blade.
- No seam fabrication
- No tolerance stack up

### 4.6.2 Materials

- Inexpensive materials
- Lamination schedules can change without modifying aerodynamic characteristics.
- The molded foam core encapsulates all internal parts such as root structure.

### 4.6.3 Labor and Cost Containment

- Low labor cost per unit.
- Low part count results in large savings in inventory and greater quality control.

## 4.7 FMI Final Fabrication Product

FMI fabricated seven prototype blades for static, fatigue and field-testing. FMI modified three painted blades for field-testing on a Jacobs 29-20 turbine. The NWTC facility used another three unpainted blades for the static and fatigue testing. The last blade served as a “proof of concept” display. FMI also fabricated a production quality test specimen to afford visual inspection points of internal blade construction as part of quality control procedures.

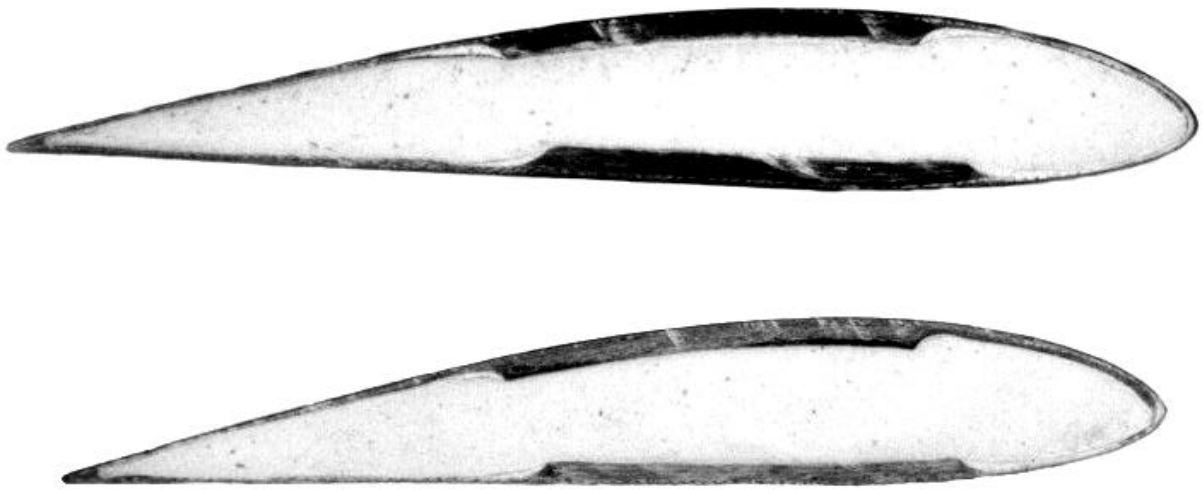

**Fig. 4.8 - FMI Prototype blade cross-sections**

Top cross-section in Fig. 4.8 was cut from a pre-production test blade at Station 61” and the lower cross-section cut from the same test blade at Station 75”.

The cross-sections in Fig. 4.8 illustrate both blade taper and internal construction architecture. This view shows the foam core tightly bonded with the glass fiber and the several laminate plies in the spar caps. Comparing the two sections provides a visual illustration of the spar cap step-down that occurred at station 63.95” as described in Table 3.4. These specimens also show a sharply formed and well-supported trailing edge.

Figs. 4.9, 4.10, 4.11, 4.12 show the transition between the flat root of the blade and the airfoil. Fig. 4.2, the root block-casting tool, shows the contour of the root block from station 0 extending to station 26.1 (see Fig 3.1). The airfoil transition begins at station 6.38 and is fully evolved by station 26.1. Incorporating the root block into the foam core as intrinsic to the blade structure contributes added strength at the root without interfering with the airfoil design.

Fig. 4.10 illustrates the advantage of a seamless structure. As discussed in Paragraph 3.7, lowered amounts of separated flow are anticipated to yield a lower noise profile. Separated flow around the tip can come from the trailing edge and/or the outer edge of the blade. Both of these edges should be as sharp as physically possible; this might mean having a trailing edge as thin as 1/16 in. Fig. 3.2 and 3.3 show design details that call out a 0.10 thick trailing edge. Figures 4.11 and 4.12 show root details.

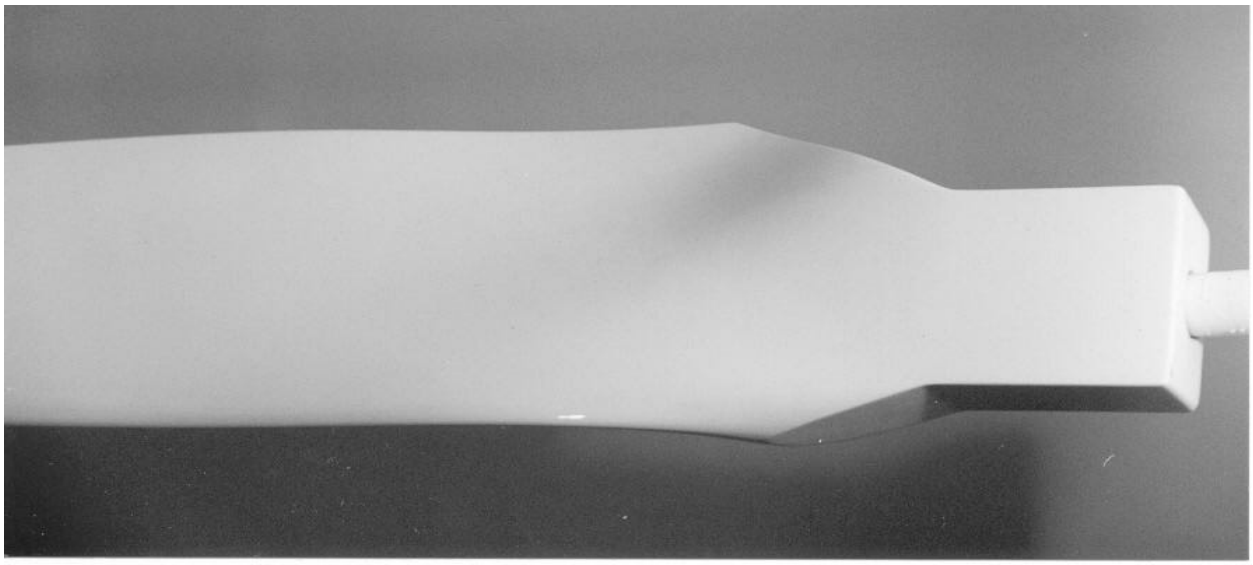

**Fig. 4.9 - Finished and painted prototype blade, upwind side**
(To about station 43” of 174”.)

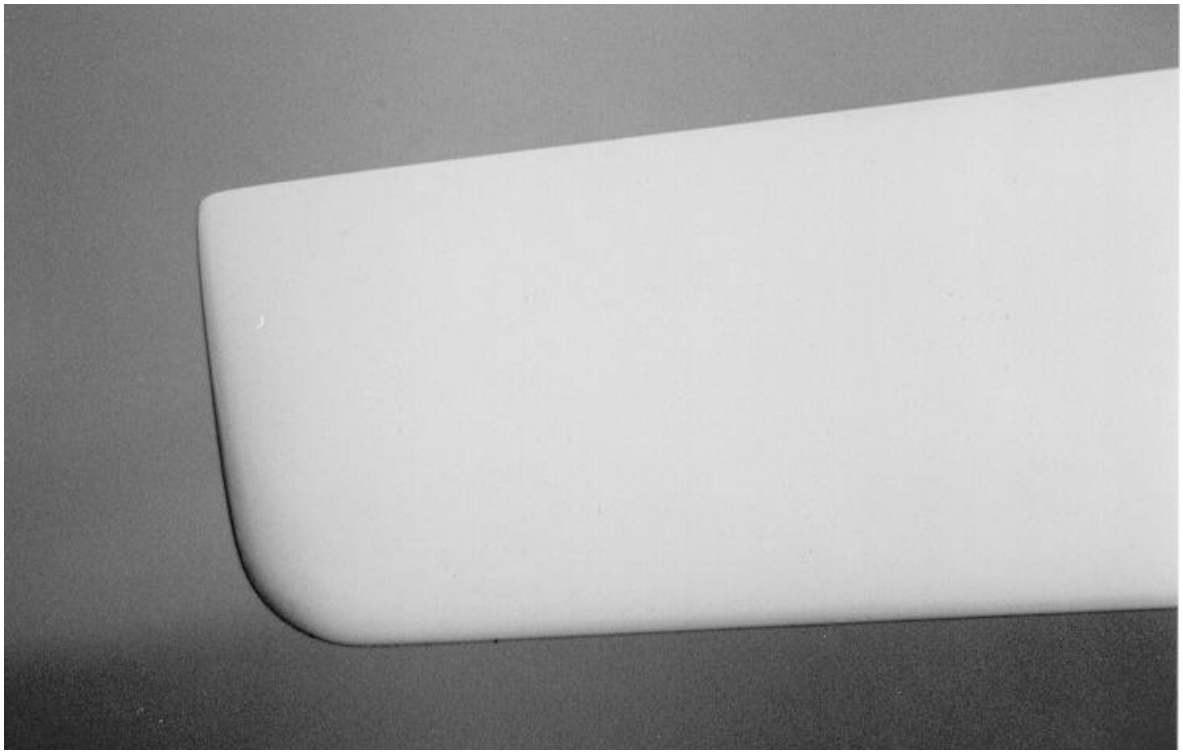

**Fig. 4.10 - Tip Detail: Prototype blade tip, upwind side, after painting**

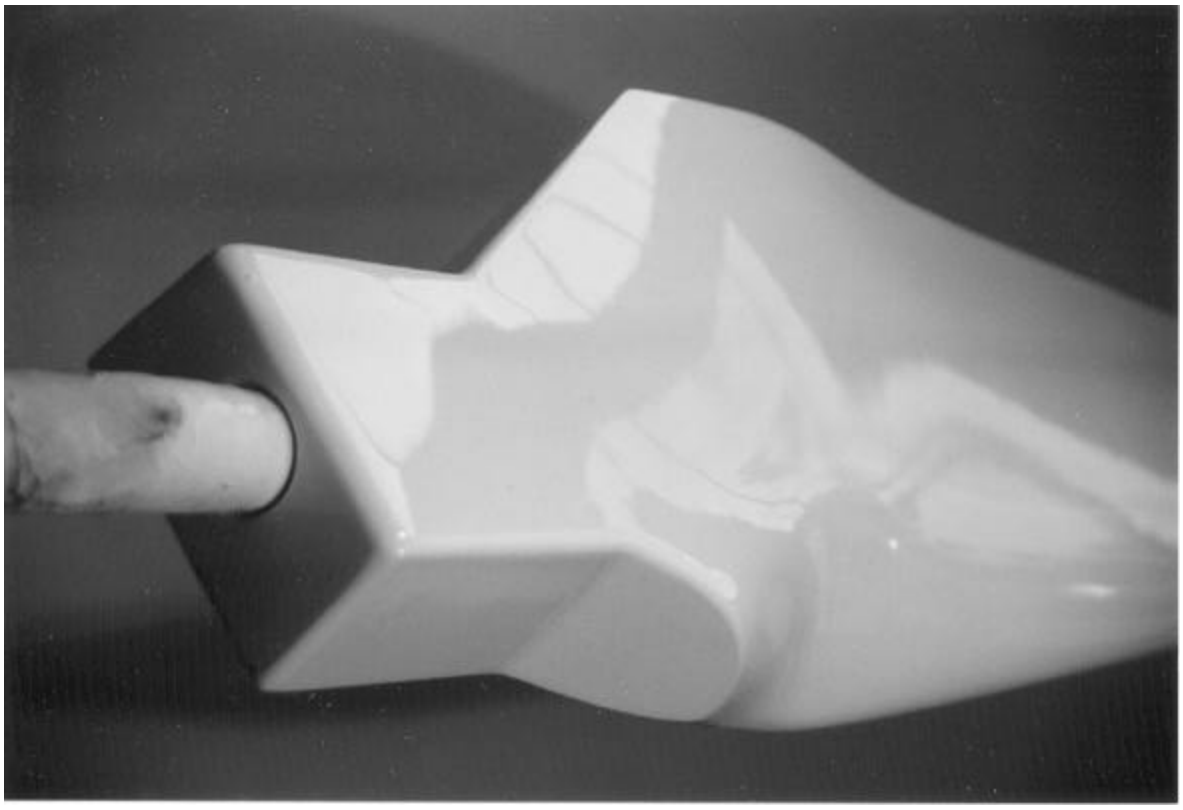

**Fig. 4.11 - Root Detail, downwind side**

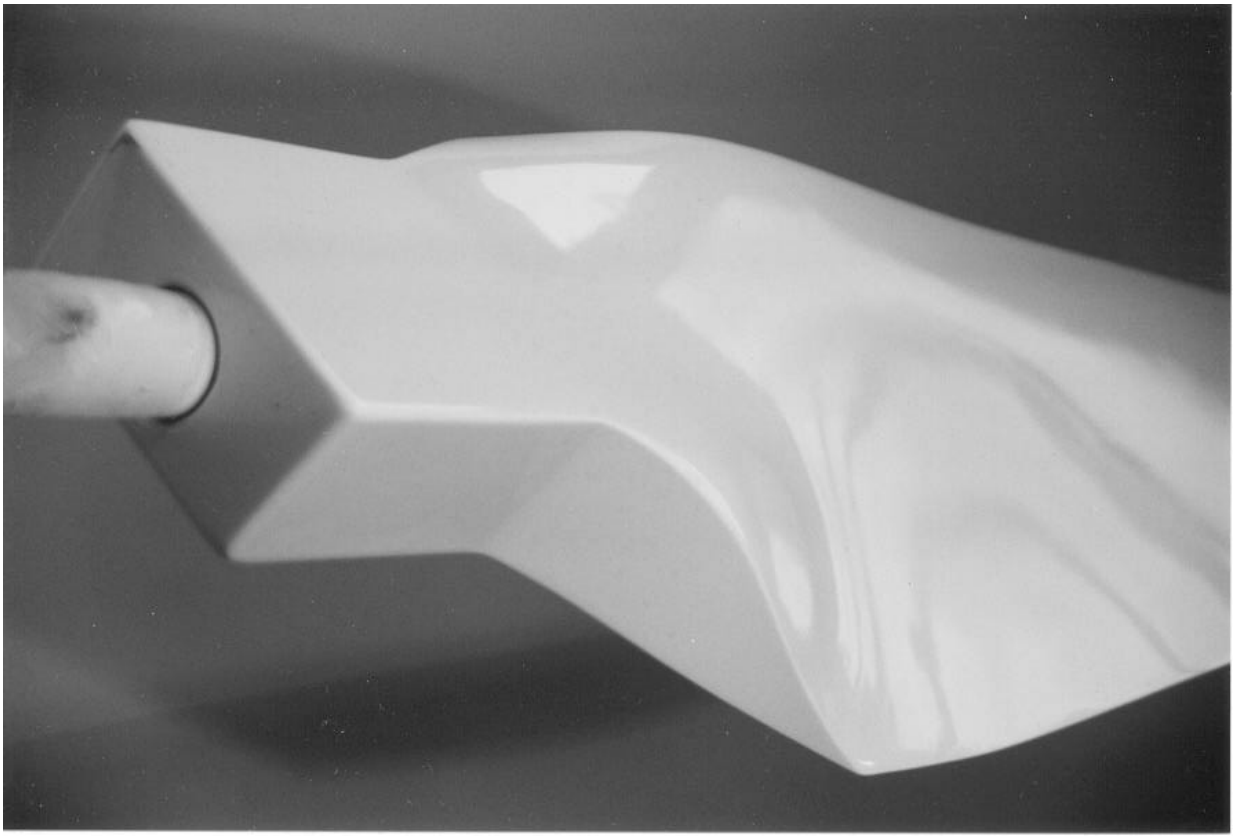

**Fig. 4.12 - Root Detail, upwind side**

### 4.7.1 Jacobs 29-20 Attachment Plate Modification

In order to mount the prototype blade on the Jacobs 29-20 turbine hub, FMI molded and bonded attachment plate pads to the unpainted blade.[16] These attachment plate pads, located on either side of the blade, are contoured to the blade shape assuring a tight bond between the blade surface and each attachment plate pad. Each pad presents a flat face on the same plane as the root surface to accommodate the Jacobs mounting hardware. Fig. 4.13 shows both sides of the blade, including the root modification and drilled mounting bolt holes. See Figures 3.4 and 3.5 for root design detail for the Jacobs attachment hardware.

An appendix photo (Fig. A.1) of the Jacobs 29-20 turbine with baseline rotor shows how the blade, attachment plate and blade springs are mounted.

[16] The possibility that the BMI Prototype Blade may be deployed on turbines other than the Jacobs 29-20 was always a design consideration. The prototype blade root structure design accommodates either the Jacobs hub or a hub of a more conventional design. Because attachment plates are unique to the Jacobs hub, FMI determined that dealing with them as a modification best resolves the hub issue of a universal blade.

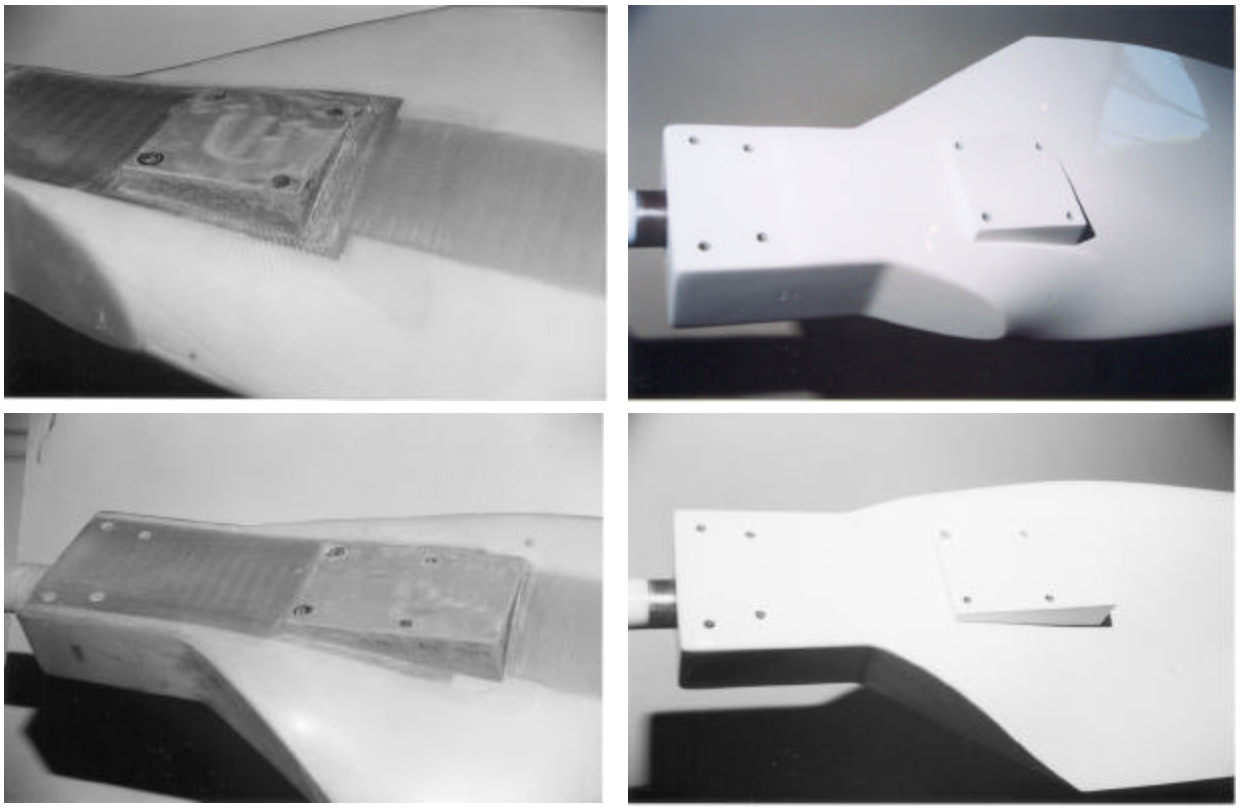

**Fig. 4.13 - Prototype Blade with Jacobs 29-20 Attachment Plate Modifications**

## 4.8 Conclusion

The BMI project has allowed FMI to investigate new methods of achieving high capability rate production using a minimum of tooling. The tool constructed with integrated heating and cooling played an especially important part of this project as rapid cycle times could be achieved. The fact that the molded blades can be cured in the tool eliminates the need for large curing ovens. This not only speeds up the cycle time but also greatly reduces cost and required floor space.

For production rates of 150 blades per year, a more costly steel tool would be required. FMI is convinced that because of single tool production, the overall tooling cost is actually less expensive than the multiple tools required for most other composite construction. Higher production rates would require additional tools.

# 5.0 Qualification Testing

## 5.1 Introduction

The AX-2111 Statement of Work (SOW) required that FMI conduct a series of tests in accordance with the Production, Assembly and Qualification Test Plan. These tests determined levels of quality and reliability and verified that the prototype blades met all pre-determined quality acceptance criteria.

Qualification tests included:

- Measurements of the surface contours and surface finish to verify pre-determined specifications.
- Coupon tests.
- Fatigue tests of blades and joints.
- Non-destructive testing to determine quality of manufactured blades.
- Static tests.
- Modal testing – full or partial blade.

The NREL National Wind Technology Center (NWTC) [17] [18] in Golden, CO conducted a test series, including a full blade modal test and static tests, under the direction of Walt D. Musial, NREL Certification Test Manager, and Scott Hughes, NREL Certification Test engineer, with technical assistance from Chuck Richey, FMI structural consultant. FMI provided the NWTC with three production quality prototype blades for test purposes. NWTC defined the test criteria and designed the test planforms. This section reports the results of their work.

## 5.2 Computer Simulations, Certification and Testing

- **Max Power Loads & Fatigue**. The actual maximum power loads were derived aerodynamically. A Rayleigh wind distribution as defined by Germanischer Lloyd was calculated and applied to obtain a spectrum of loads vs. cycles. This computation was further adjusted using a Cumulative Damage calculation to provide a constant test load for a chosen number of cycles. The relationship between stress and number of cycles is $S/S_o = 1 - b \cdot LOG(N)$; where, b = 0.10 for fiberglass, S= failure Stress at N cycles, and $S_o$ = maximum static stress.

---

[17] NWTC-ST-FMI-STA-01-1000-FR "Static Testing of the Foam Matrix BMI Blade", July 9, 2001, All work performed under the DOE/NREL Wind Program subtask WER00 2420 in support of Sandia National Laboratories Blade Manufacturing Improvement Project AX-2111; National Renewable Energy Laboratory, National Wind Technology Center, Golden, CO.

[18] NWTC-ST-FMI-FAT-02-0201-FR "Fatigue Testing of the Foam Matrix BMI Blade" , August 20, 2001, All work performed under the DOE/NREL Wind Program subtask WER1 2455 in support of Sandia National Laboratories Blade Manufacturing Improvement Project AX-2111; National Renewable Energy Laboratory, National Wind Technology Center, Golden, CO.

- **Hurricane Class II Loads** according to the Germanischer Lloyd certification specifications correspond to a wind of 59.5 m/s or 133.1 mph. The equivalent pressure is 0.157 psi applied to ***both*** airfoil sides – it would be 0.315 psi if applied to only one side. The turbine must survive this load test with an appropriate safety factor.
- **Modal Frequencies**. Campbell frequency plots were derived and verified by testing to assure that there are no mode interactions, a possibility that may cause loads resulting in turbine damage or life reduction.
- **Tower Strike**. Analytical and/or experimental data must show that tower strikes will not occur under normal operating conditions.

## 5.3 Computed Final Design Results with Analysis

### 5.3.1 Frequency Modes

Modes 1, 3,4 and 5 are flapping modes. Mode 2 is in-plane and Mode 6 is the first torsion mode. Modes 1, 2, and 6 are illustrated in Fig. 5.1, 5.2 and 5.3.

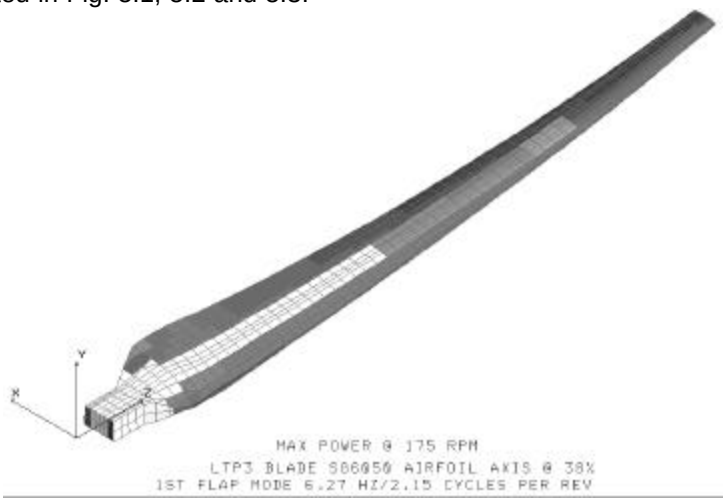


**Fig. 5.1 - 1st Flap Mode (Mode 1)**

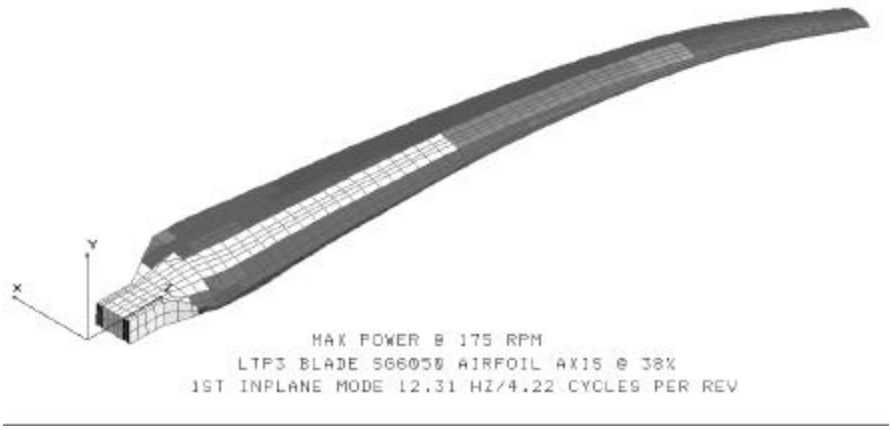

**Fig. 5.2 - 2nd First in Plane Mode (Mode 2)**

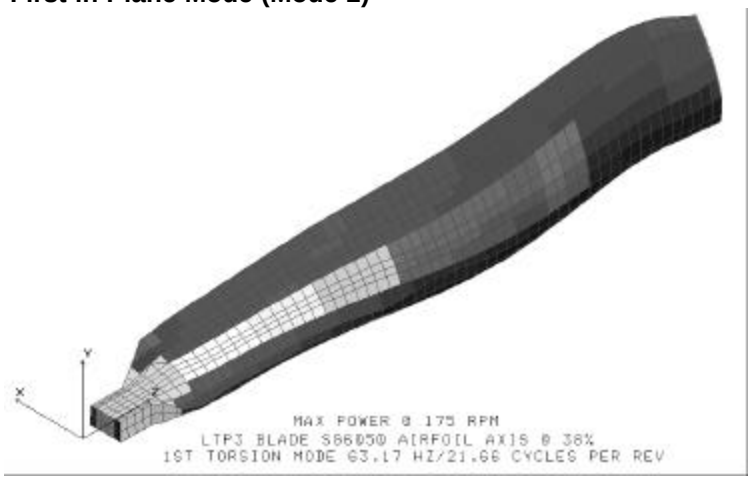


**Fig. 5.3 - First Torsion Mode (Mode 6)**

## 5.4 Campbell Frequency Diagrams

Figures 5.4 – 5.7 show Campbell diagrams in two flap modes and a first in-plane edge mode. All test measurements are for "0" RPM – the remaining test curve is extrapolated.

Modes 1, 3,4 and 5 are flapping modes, while mode 2 is an in-plane mode and mode 6 is the first torsion mode.

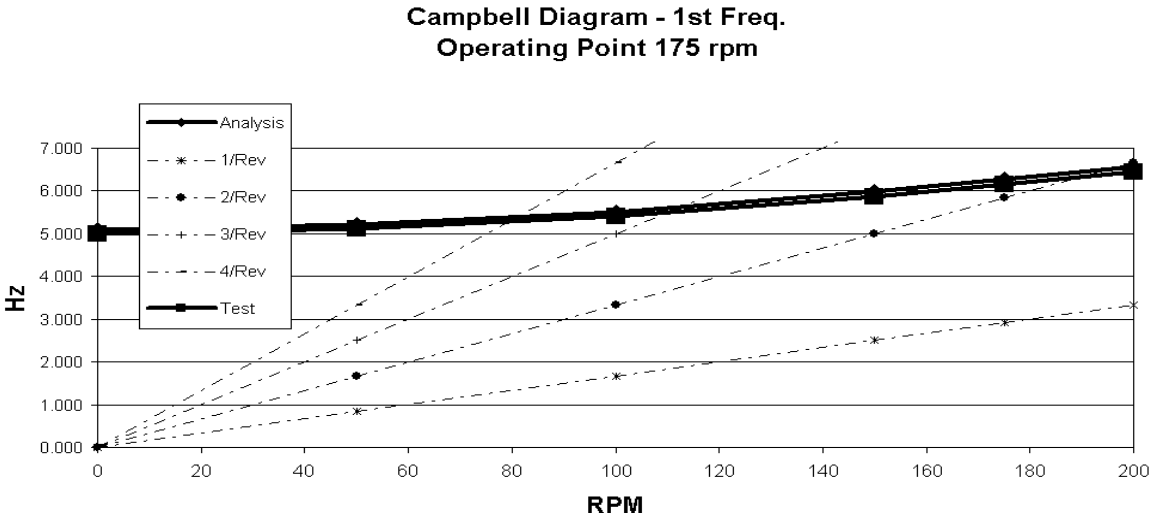


**Fig. 5.4 - First Flap Mode – 5.01 Hz by analysis, 5.0 Hz by NREL Test**

Data plots of analysis and test are nearly identical as illustrated by Fig. 5.4.. The first flap mode is supercritical – the first intersection is 2/Rev at about 190 RPM – 15 RPM above operating RPM.

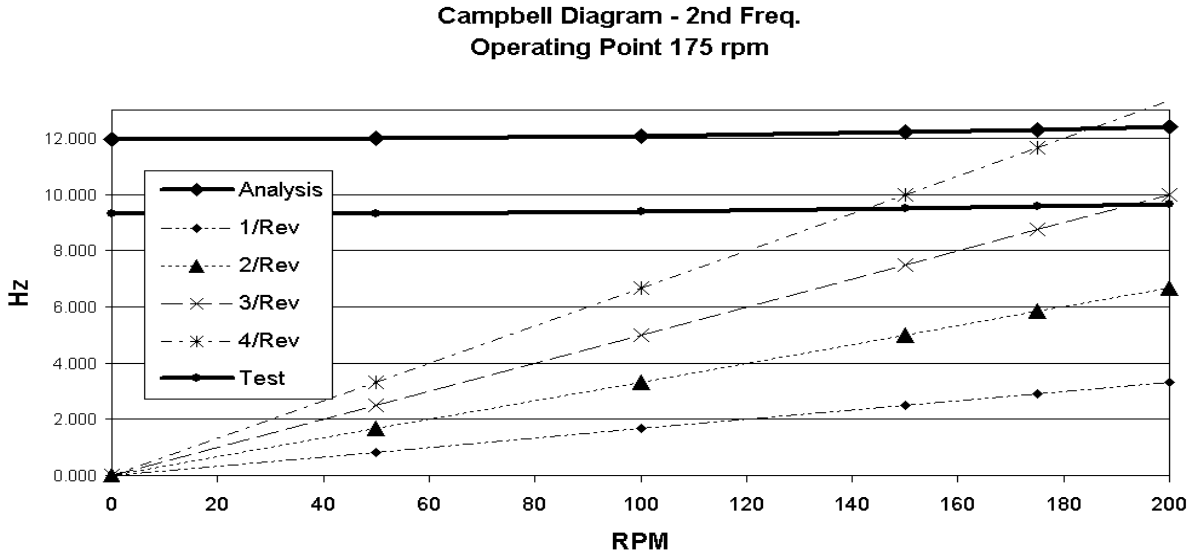


**Fig. 5.5 - First In-Plane (Edge) Mode – 11.95 Hz by analysis, 9.3 Hz by NREL Test**

As illustrated in Figure 5.5, the first in plane mode intersects 4/Rev *below* the target operating speed. The second intersection is 3/Rev at about 195 RPM – well above the 175-RPM operating speed. This mode shows the largest difference between analysis and test results – indicating that actual blade in-plane stiffness is lower than that modeled.

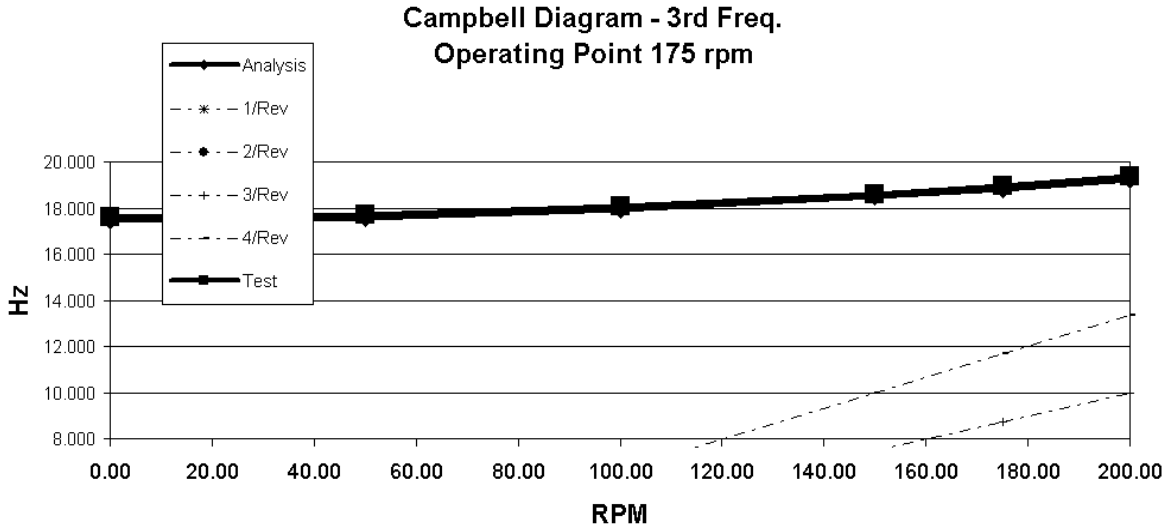


**Fig. 5.6 - Second Flap Mode – 17.47 Hz by analysis & 17.6 by NREL Test**

Data plots of analysis and test for the 2nd flap mode are nearly identical, as illustrated by Figure 5.6. The second flap mode is well above the first four per rev modes.

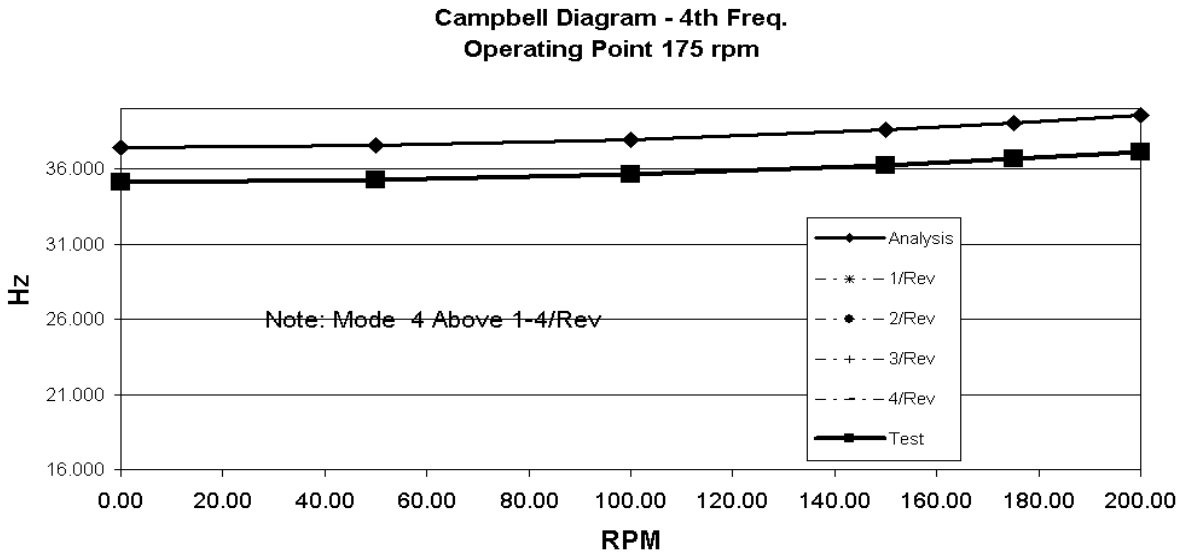


**Fig. 5.7 - Third Flap Mode – 37.4 Hz by analysis & 35.1 by NREL Test**

Figure 5.7 shows that the third flap mode is supercritical and is well above per revs through 4/Rev. The slight difference between analysis and test is probably due to a small in-plane coupling for this mode, although it is primarily a flap mode.

## 5.5 Hurricane Loads

### 5.5.1 Hurricane Loads – Buckling Analysis

Analysis reveals that the first buckling mode will occur at loads nearly an order of magnitude above hurricane Class II loads, so a non-linear analysis is not required. Figures 5.8 – 5.10 show the first three buckling mode shapes.


**Fig. 5.8 - Hurricane Loads Buckling Shape – 1st Negative Mode**


**Fig. 5.9 - Hurricane Loads Buckling Shape – 1st Positive Mode**


**Fig. 5.10 - Hurricane Loads Buckling Shape – 2nd Positive Mode**

**Table 5.1 - Design and Test Load Data**

| FEM BL Blade Station (inches) | Class II Hurricane Shear Loading (Lbs) | Class II Design Moments (in-lbs) | Test Moment 2 Point Load (in-lbs) | Test Moment Shear (lb) |
|---|---|---|---|---|
| 0.0 | 604.00 | 45438 | 45438 | 548.8 |
| 11.0 | 604.00 | 38782 | 39391 | 548.8 |
| 28.4 | 555.21 | 29121 | 29842 | 548.8 |
| 45.8 | 460.25 | 21113 | 20294 | 548.8 |
| 50.0 | 438.00 | 19300 | 18000 | 548.8 |
| 50.0 | 438.00 | 19300 | 18000 | 257.1 |
| 63.2 | 371.99 | 14640 | 14601 | 257.1 |
| 80.6 | 292.11 | 9558 | 10126 | 257.1 |
| 98.0 | 220.73 | 5717 | 5652 | 257.1 |
| 115.4 | 157.67 | 2973 | 1178 | 257.1 |
| 120.0 | 140.00 | 2450 | 0 | 257.1 |
| 120.0 | 140.00 | 2450 | 0 | 0 |
| 132.8 | 102.72 | 1186 | 0 | 0 |
| 150.2 | 55.72 | 217 | 0 | 0 |
| 163.3 | 16.60 | 0 | 0 | 0 |

Table 5.1 reports baseline design and test load values as computed by Chuck Richey.

## 5.6 Validation Testing

### 5.6.1 Test Background

FMI provided three prototype blades identified as numbers AT 10688, AT 10689 and BT 10742 to NWTC to complete the qualification testing requirements of the BMI project. The test blades, without drilled mounting holes necessary for attachment to the hub or modifications necessary to attach the pitch springs, were otherwise exact production replicates of the field test qualified blades. Unpainted blades facilitated visual inspections during the testing process.

NWTC used the small blade test stand located in Building 254 (IUF) at NREL's National Wind Technology Center (NWTC) north of Golden, CO for this test series.

## 5.7 Static Testing

### 5.7.1 Summary

NWTC conducted a static test on a project blade on October 5, 2000. At the completion of testing, the blade had not failed. The maximum root bending moment reached 94,872 in-lb before testing was concluded due to a root fixture failure. The failed root fixture was not a standard part of the test blade or of a representative Jacobs turbine hub. Instead, it was manufactured for this test to approximate the stiffness of the Jacobs turbine's hub connection. This maximum bending moment was 209% of the IEC Class II Hurricane load (with no test factors applied) [Ref 35,36]. With IEC 61400-23 test load factors applied, the blade was tested to 173% of the IEC Class II Hurricane load.

### 5.7.2 Scope

This section covers static testing of the FMI blade developed under Sandia National Laboratories BMI solicitation. Included in the static-testing portion were blade mass and center of gravity measurements, a blade modal survey, and the structural static test.

### 5.7.3 Objectives

The objectives of the FMI static blade tests were to:

- Determine the static strength of the blade under IEC 61400-01Class II extreme wind loading conditions.
- Determine the eigenfrequencies of the blade.
- Determine the weights and center of gravity of the blades sent to NREL.
- Provide strain versus load data for FEM validation.

### 5.7.4 Blade Identification

FMI inscribed this test blade with the identifying mark BT10742. NREL marked this blade for tracking

purposes as Blade #1. The distance from the center of rotation to the blade root is 6.38-in.

### 5.7.5 Blade Weight and Center of Gravity

FMI reported the prototype blade weight at 57.80 lbf. The target weight for the BMI blade was 57.52 lbf according to FMI design documents. The target static root moment was 3725 in-lbf.

A Pelouze platform scale, checked with calibration weights ensuring the measurement was within ± 0.5-lbf, confirmed blade #1 weight to be 57.2-lbf before drilling the root attachment holes.

The center of gravity (CG) was determined by balancing the blade on the corner of an inverted length of angle iron. A tape measure, with a measurement uncertainty of ±1/8-in, indicated the length of the blade as 167.375-in measured along the low-pressure surface of the blade

### 5.7.6 Eigenfrequencies

A brief modal survey of blade identified as AT10689 was conducted prior to the static test. Note that this was not the blade statically tested. The blade was cantilevered horizontally from NREL's small blade test stand, positioned with the tip chord perpendicular to the laboratory floor, trailing edge up, and having the pitch axis parallel to the floor. Mounting to the test stand provided greater stiffness inboard of the root plane, as compared to the in-field installation of the blade.

NREL staff placed two uni-axial accelerometers on the blade at the tip chord, with one located near the trailing edge and the other next to the leading edge. The accelerometers were affixed to the blade using petro-wax. Depending on the measurement, the accelerometers were aligned with an inclinometer to coincide with either the flap or lead-lag orientation. Accelerometer cable was taped to the blade for strain relief.

Blade frequencies were determined from the frequency response functions (FRF) generated by the dynamic signal analyzer (DSA). A Force/Exponential window was used for all measurements. The dynamic signal analyzer was set at 400 lines of resolution, with a valid frequency bandwidth of 0-50 Hz. Each orientation (flap or lead-lag) was tested in independent runs. Five hammer excitations / accelerometer responses were recorded and averaged for each run.

For flapwise tests the blade was excited by driving (impacting) the hammer against the high-pressure side of the blade, directly opposite the leading or trailing edge accelerometer. Using either the leading or trailing edge accelerometer resulted in the same eigenfrequencies. Lead-lag tests had the hammer driving the trailing edge (parallel to the tip chord), and using the response of an accelerometer mounted parallel to the tip chord at the leading edge.

Figure 5.11 shows the FRFs for both flapwise and lead-lag tests. Resulting eigenfrequencies are noted on the figure.

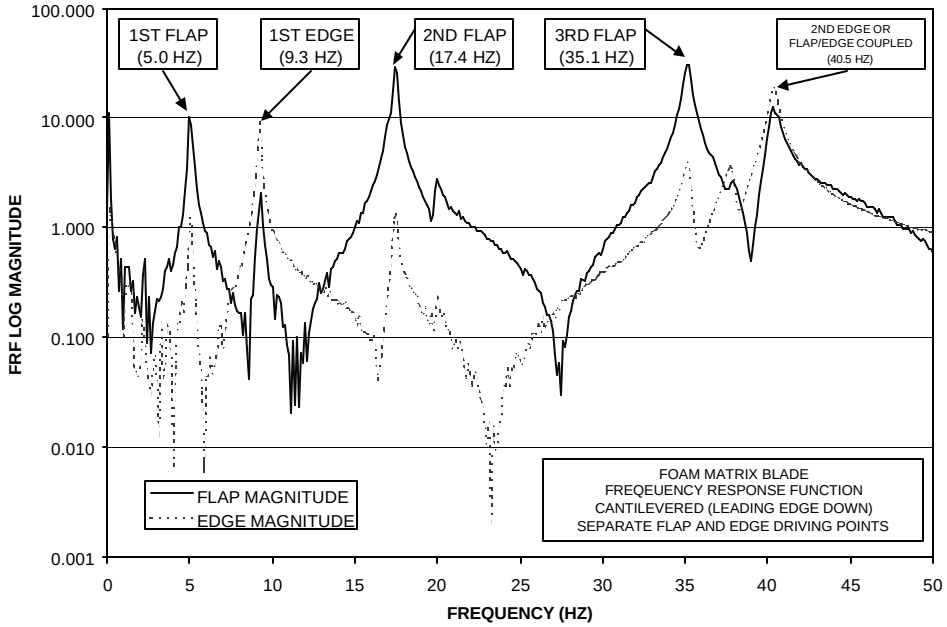


**Fig. 5.11 - Modal survey results**

An attempt at determining the 1st torsional eigenfrequency of the blade did not produce a definitive value. We observed very weak resonant peak at 25-Hz when the leading and trailing edge accelerometers were out of phase, but the magnitude was not large enough to verify it. A more extensive modal survey, with a greater number or driving points would be necessary to determine the 1st torsion eigenfrequency.

## 5.8 Test Setup

### 5.8.1 Testing Apparatus

All test apparatus had at least a factor of safety of 3.0, based on the extreme hurricane loading. The exception to this was the original Jacobs hub adapter, which had an unknown design and history. Test hardware design was such that in the event of a hub adapter failure, catastrophic damage would not occur. The test setup oriented the root of the blade (chordwise) perpendicular to the lab floor in order to apply the flapwise loading. The measured inclination of the root was to be 0.0 +/- 0.1 deg, in both the spanwise and flapwise directions prior to testing.

### 5.8.2 Root Fixture

The blade was attached to the test stand using a NREL built test fixture based on an original Jacobs' pitch shaft that inserts into the 21-inch deep, 2.5-inch diameter radial sleeve in the blade root along the pitch axis. A 2-in steel rod inserted to the full sleeve depth replicated the Jacobs' pitch shaft. A length of structural tubing (4"OD, 2.5"ID) was welded on to the fixture. This structural tubing was then clamped to

the test stand. Figure 5.12 shows a sketch of the root fixture.

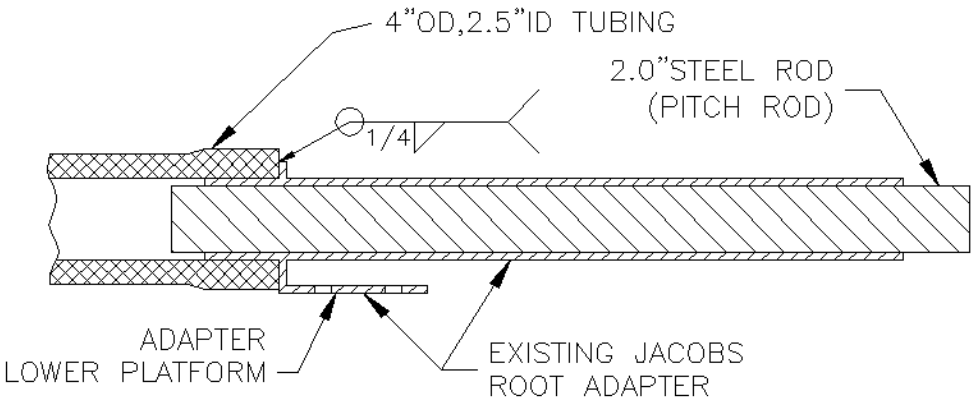


**Fig. 5.12 - Test root fixture section view**

An original Jacobs hub shaft adapter was taken from an actual Jacobs hub and modified to fit the blade. The gap between the lower platform and the hub shaft collar of the Jacobs root adapter was 0.76-in. The corresponding dimension of the blade was 0.9-in. Due to this, staff cut, relocated and then welded the lower platform in order for the blade to fit.

NREL staff drilled four blade-mounting holes. These holes were drilled (parallel to the mainshaft) in the out-of-plane direction through the thickness of the blade to match the root fixture bolt pattern. Drill hole diameter was 0.5010 to 0.5020. The blade was mounted by fitting it onto the shaft of the root fixture and installing the bolts perpendicular to the shaft. A ¼ -plate was fabricated to serve as the upper platform for the root attachment fasteners, opposite the lower platform. Four 1/2-in, Grade 8 bolts clamped the blade to the root fixture through the upper and lower platforms. Staff torqued these fasteners to 12 ft-lb as specified by FMI. This torque number was recommended for use with the original Jacobs wood blades. The function of these 1/2-in bolts was to transmit only the radial loads, as moments are reacted through the pitch shaft. These torque values were less critical than for primary root attachment fasteners in similar wind blade designs, where this situation has resulted in long-term ovaling of the through holes, and caused blade root failure. A lightly torqued fastener here, however, will allow all the radial (centrifugal) loads to be carried by these fasteners and the blade bearing material in shear.

The 4-in OD structural tubing was clamped to a fixture of the test stand using six 1-8 Grade 8 cap screws. Staff torqued these cap screws to 200 ft-lb. The test stand had a fatigue rated maximum overturning moment capacity of 100,000 ft-lbs.

### 5.8.3 Loading Apparatus

The diagram shown in Figure 5.13 indicates how loads were applied using a two-point whiffle tree

arrangement. The whiffle tree was composed of the load saddles, spreader bar, and attaching hardware. Staff constructed two load saddles, one 50-inches (inboard saddle) from the root and one 120-inches (outboard saddle) from the root. The single point pull location was located 82.8-in from the blade root. 36-in length wire rope connected the spreader bar to the load saddles. The load saddles consisted of 2-in thick laminated plywood with airfoil sections cut out for each load introduction station (50 and 120-in from the root). A 1/2-in thick urethane layer molded between the wood and the airfoil better distributed the load to reduce stress concentrations. Aluminum channel served as the load carrying structure around the plywood. A ballast weight was placed on the spreader bar in order to statically balance the whiffle tree.

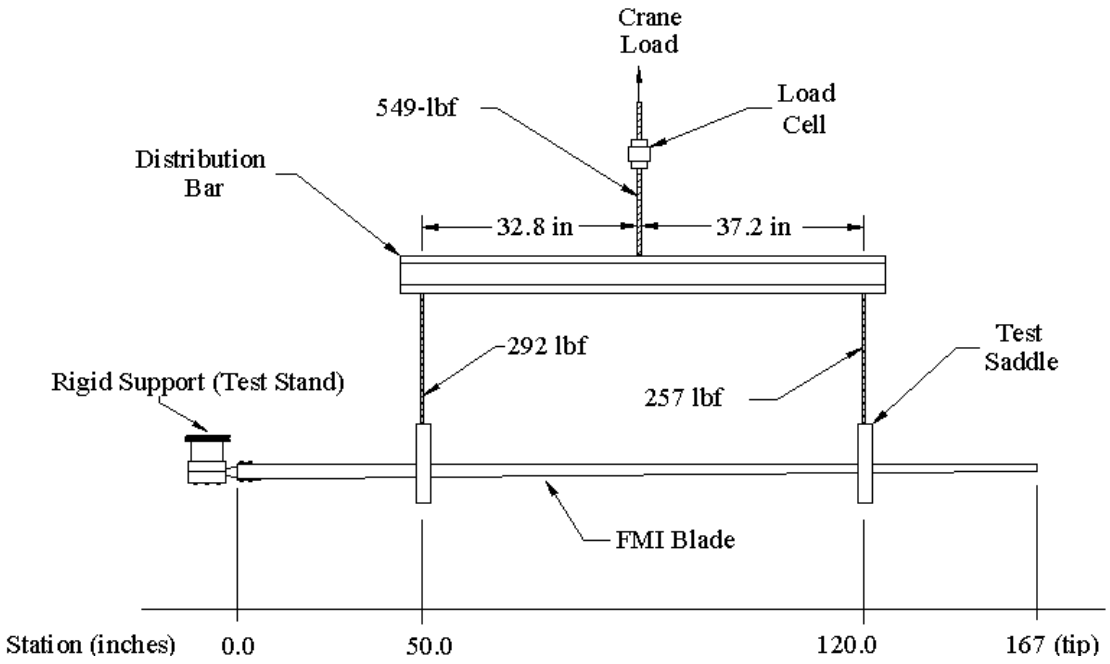


**Fig. 5.13 - Whiffle Tree Geometry (loads for extreme hurricane load)**

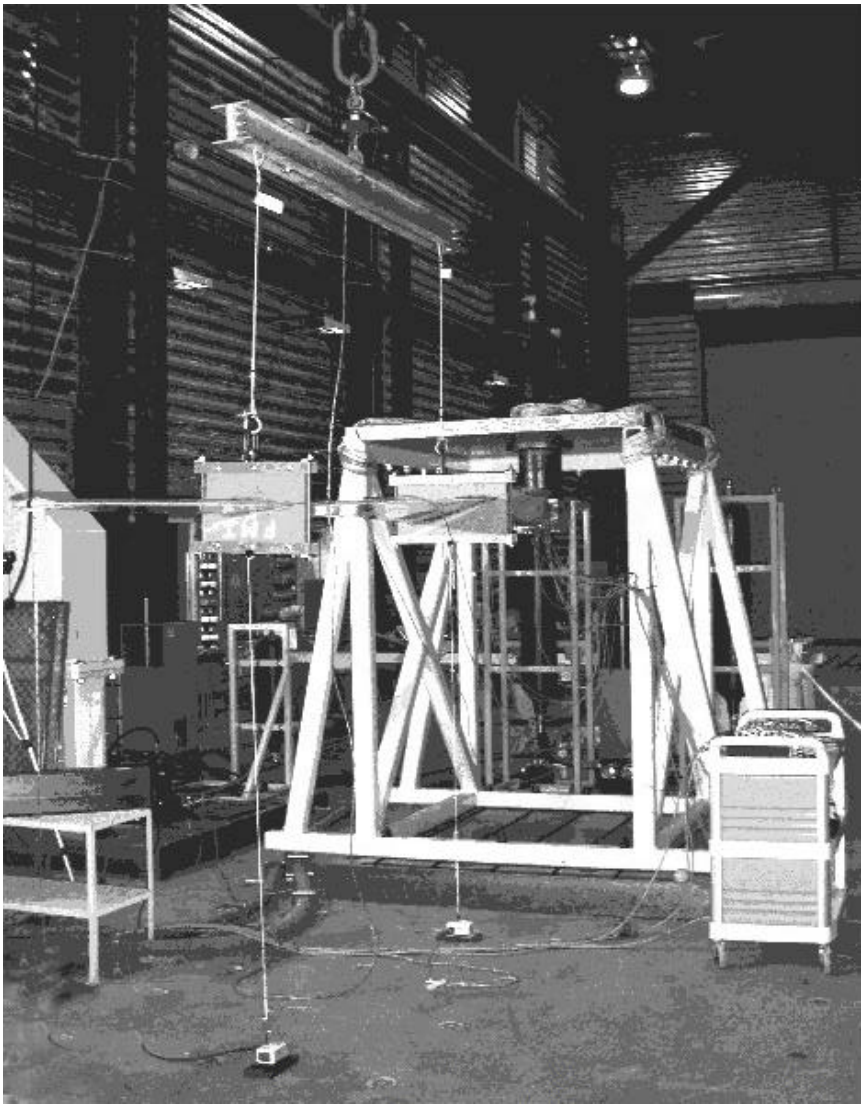

**Fig. 5.14 - Static test stand setup with blade and test saddles**

### 5.8.4 Test Loads

The static load test was performed on the blade specimen using the IEC Class II hurricane design loads as a basis. FMI consultant, Chuck Richey, of Mechanical and Composite Engineering (MCE) provided extreme design loads. NREL staff did not verify these loads to assure compliance with the IEC design criteria. Figure 5.15 shows the Design IEC Hurricane loading with the design test load (at a test load of 549-lb) created by the loading setup in Figure 5.13. The recommended test load factors in IEC 61400-23 blade testing guideline [Ref 35,36] are not incorporated in the data in Figure 5.15. The test loading shown in Figure 5.15approximates the design bending moment from the root to around the 100-in station. Table 5.1 shows numerical values for the flapwise design loads. Figure 5.14 shows the test stand, the prototype blade and the whiffle tree.

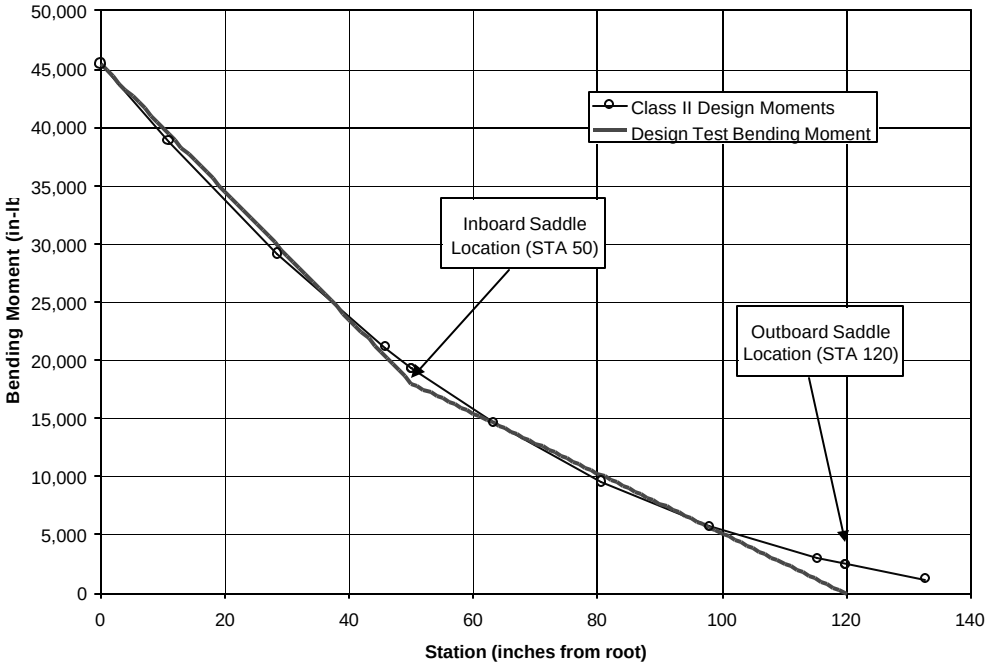


**Fig. 5.15 - Bending Moment Distribution**

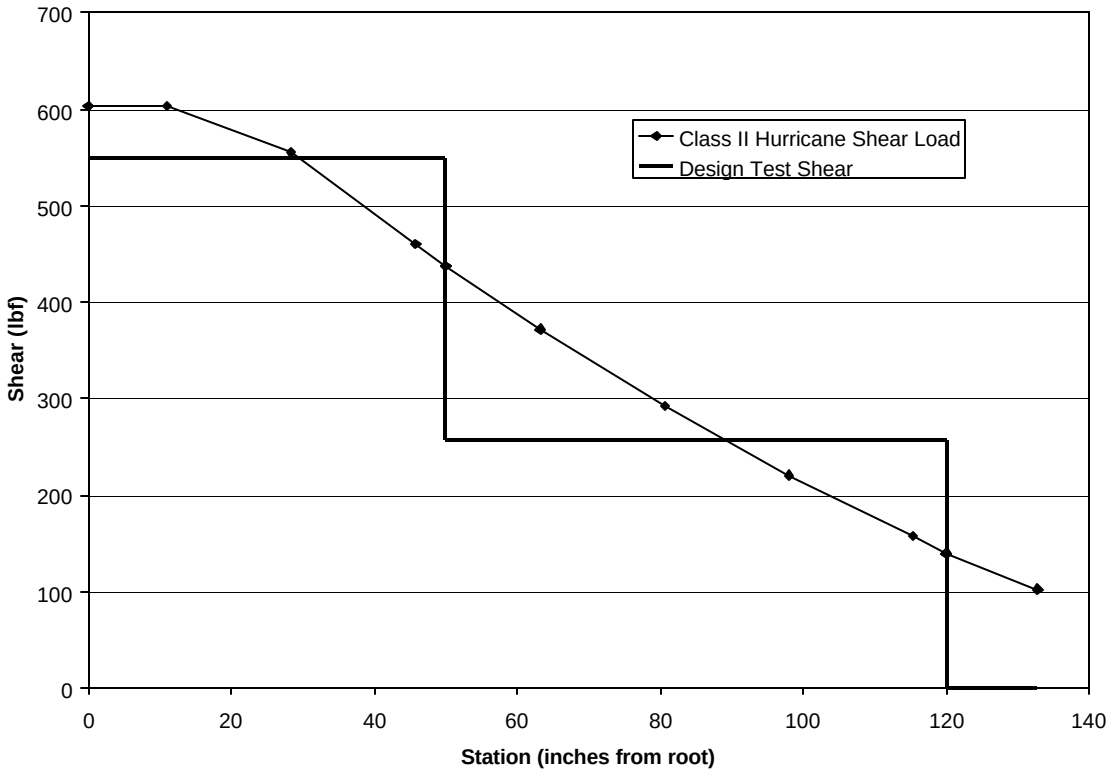


**Fig. 5.16 - Shear Loading**

Figure 5.16 compares the design Class II Hurricane shear load (no IEC test factors) with the test shear loading applied during the test(at the design test load of 549-lbf).

NREL staff used two factors to scale the design loads to IEC 61400-23 equivalent test loads. In a hot-wet environment, the blade materials lose strength and stiffness. Since the test lab is a more benign environment and the blade is stronger than under its design condition, a test load factor of 1.1 was used to scale the blade design loads for environmental conditions. An additional factor of 1.1 accounts for the uncertainty in testing one blade from a population of various strengths, accounting for the possibility that the tested blade may be from the stronger side of the manufactured population. These combined factors result in a test load factor of 1.21.

### 5.8.5 Tare Weight

Tare weight is the gravity-induced load due to the test apparatus and blade weight that the load cell measures. Tare weight is subtracted from the recorded load cell reading to obtain the true test load. The following equation gives the test load as a function of the load cell reading and associated tare weights:

*Test Load = Load Cell Reading – (Blade Tare + Apparatus Tare)*

Blade tare weight was determined by calculating the load required (at the load cell spanwise station) to zero the bending moment at the root of the blade. For the measured weight of 57.2-lbf and a CG 52.0-in from root, the calculated blade tare load was determined to be 36-lbf.

The apparatus tare weight includes the weight of all loading equipment between the load cell and the blade, including the spreader bar and load saddles. The 120-in station load saddle was modified (described later) between the 175% and 200% loadings. Due to this modification, two apparatus tare loads were used; initially 80-lbf, and after the modification, 67-lbf.

Combining the blade tare with the apparatus tare, the total tare load was 116-lbf initially, and 103-lbf after modifying the outboard saddle.

### 5.8.6 Instrumentation

All load sensors and instrumentation were calibrated in accordance with NREL's A2LA accredited blade testing procedures. For specific information on hardware see Appendix B, Sheet B.1.

#### 5.8.6.1 Data Acquisition System

NREL staff used their Blade Structural Testing Real-Time Acquisition Interface Network (BSTRAIN) for acquiring test data. BSTRAIN is described in [Ref 37,38]. Appendix B Sheet B.2 shows a schematic of the BSTRAIN system.

The data acquisition system (DAQ) hardware was composed of the following main components; National

Instruments (NI) SCXI-1321 terminal blocks, SCXI-1121 filter/amplifiers, SCXI-1001 chassis, and an AT-MIO-16XE A/D board. The SCXI-1321 terminal blocks served as wire-termination hard points, with four channels per block. The SCXI-1121 modules were configured with a low-pass frequency of 4-Hz, with gains and excitation voltages that were instrument dependent as described below. The A/D board had16-bits of resolution and a maximum sampling rate of 100 kS/s. Data sample rate was 5 Hz.

#### 5.8.6.2 Load Cell

Staff used a LeBow 5,000-lbf-load cell to record loads. The load cell was located between the whiffle tree and the loading crane. The load cell measurement included both the test load and tare load (see section 5.8.5). Prior to testing the load cell was checked using calibrated 1,000-lbf and 2000-lbf dead weights. The result of this check showed the load cell to be reading within .01% of the dead-weight values. The nameplate accuracy (including hysteresis and non-linearity) was 0.05% of full scale.

#### 5.8.6.3 Strain Gages

Strain gages placed at critical sections on the blade surface verified FEM strain and monitored peak strain values at various loads. Strain was measured at 19 separate gage locations.

Table 5.2 defines strain gage placement. (The key below the table describes the gage nomenclature.) Note that the first four channels (0 through 3) were reserved for the load cell and displacement measurements.

**Table 5.2 - Strain Gage Placement Data**

| Channel | Name | % Span | Span Station (in) | % Chord | Curvelinear Distance to Trailing edge | Distance to blade root (in) | Orientation | Gage Type | Blade Side HP/LP |
|---|---|---|---|---|---|---|---|---|---|
| 4 | 06S11LA | 6.8 | 11.13 | 50.0 | n/a | 5.5 | 0° | Single | LP |
| 5 | 14S34HA | 14.4 | 24.23 | 34.6 | n/a | 18.6 | 0° | Single | HP |
| 6 | 14S43LA | 14.4 | 24.23 | 43.9 | n/a | 18.6 | 0° | Single | LP |
| 7 | 16S34HA | 16.7 | 28.23 | 34.7 | 12.03 | 22.6 | 0° | Single | HP |
| 8 | 16S42LA | 16.7 | 28.23 | 42.2 | 10.81 | 22.6 | 0° | Single | LP |
| 9 | 16R14LA | 16.7 | 28.23 | 14.3 | 16.00 | 22.6 | 0° | Rosette | LP |
| 10 | 16R14LB | 16.7 | 28.23 | 14.3 | 16.00 | 22.6 | 45° | Rosette | LP |
| 11 | 16R14LC | 16.7 | 28.23 | 14.3 | 16.00 | 22.6 | 90° | Rosette | LP |
| 12 | 16S72LA | 16.7 | 28.23 | 72.5 | 5.00 | 22.6 | 0° | Single | LP |
| 13 | 21S34HA | 21.7 | 37.03 | 34.9 | 11.81 | 31.4 | 0° | Single | HP |
| 14 | 21S37LA | 21.7 | 37.03 | 37.2 | 10.69 | 31.4 | 0° | Single | LP |
| 15 | 21R72LA | 21.7 | 37.03 | 72.6 | 5.00 | 31.4 | 0° | Rosette | LP |
| 16 | 21R72LB | 21.7 | 37.03 | 72.6 | 5.00 | 31.4 | 45° | Rosette | LP |
| 17 | 21R72LC | 21.7 | 37.03 | 72.6 | 5.00 | 31.4 | 90° | Rosette | LP |
| 18 | 21S13LA | 21.7 | 37.03 | 13.7 | 15.81 | 31.4 | 0° | Single | LP |
| 19 | 27S35HA | 27.6 | 47.23 | 35.6 | 11.13 | 41.6 | 0° | Single | HP |
| 20 | 27S40LA | 27.6 | 47.23 | 40.3 | 10.44 | 41.6 | 0° | Single | LP |
| 21 | 52S37HA | 52.5 | 90.63 | 37.6 | 8.44 | 85.0 | 0° | Single | HP |
| 22 | 52S39LA | 52.5 | 90.63 | 39.5 | 8.38 | 85.0 | 0° | Single | LP |

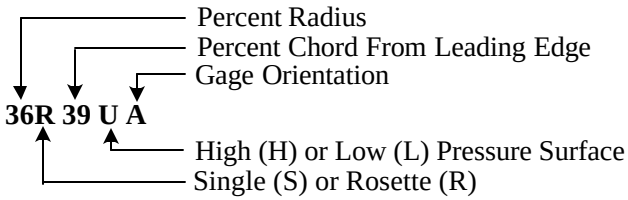


**Symbols for Gage Orientation:**

A - 0 Degrees From Spanwise Direction
B - 45 Degrees From Spanwise Direction
C - 90 Degrees From Spanwise Direction

FMI consultant Chuck Richey requested the gages be located at 22.6-inches, 31.4-inches, and 41.6-inches (inches from the blade root) for FEM validation. These gages were placed along the blade axis at the center of the spar cap on the upper and lower surfaces. In addition, NREL added gages at 85-inches on both surfaces to get a measurement between the saddles. They also added a single gage at 5.5 inches on the compression surface corresponding to the termination of the root flange bracket. A gage was added on the upper and lower surfaces at 18.6 inches to get a measurement on top of the pitch shaft cavity. Finally, a series of single gages and rosettes were added at the 22.6 and 31.4 stations to measure skin strains on the compressive surface in the area where critical buckling was most likely to occur.

Rosette strain gages were Measurements Group model WK-09-250RD-10C gages, and single element

gages were Measurements Group model CEA-13-250UW-10C gages. Both of these gages are 1000-Ohm, with a 09 STC (self-temperature compensation), and an active gage length of 0.25-in. All gages were wired as quarter-bridges, with a three lead-wire configuration. Strain gage signals had a gain of 200, and an excitation voltage of 3.333 V. With these settings, the smallest differential strain measurable was 0.5 microstrain. Including factors such as misalignment, bridge non-linearity, and thermal effects, the uncertainty of the strain gage signals is given as ±5% of the indicated value (not full-scale). Figure 5.17 shows strain gages positioned on the low-pressure surface of the blade.

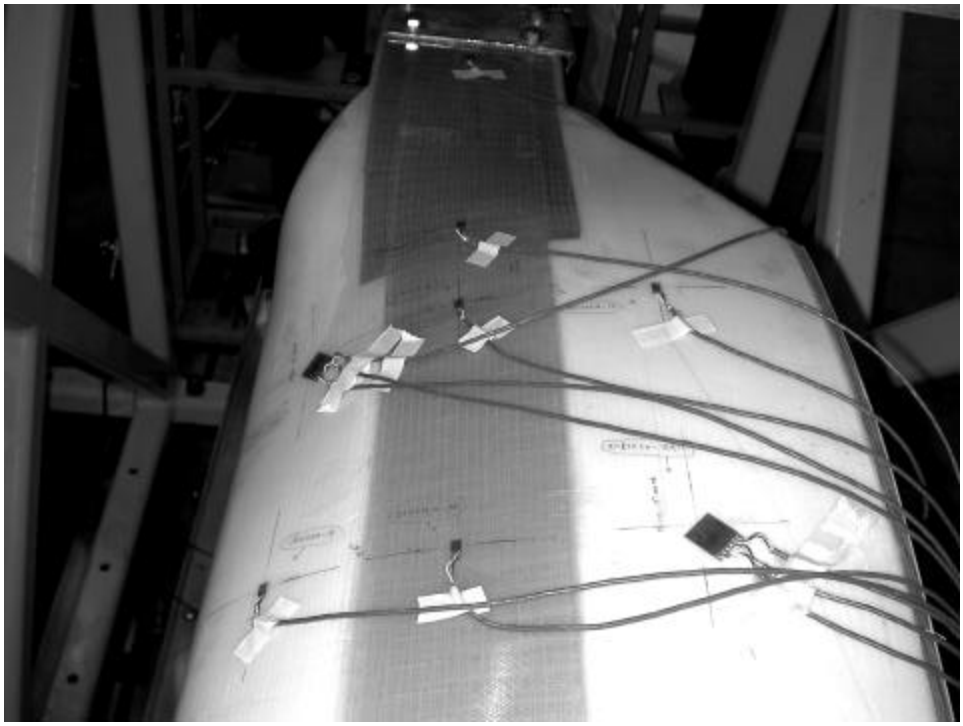

**Fig. 5.17 - Low-pressure surface gages**

Staff performed several checks prior to testing to ensure accurate readings. They made gage resistance measurements where the strain gage wires connect to the BIB (Blade Interface Box) modules. Simulating a gage signal using a decade resistor performed a second check. The decade resistor, inserted into the signal path at the BIB module, changed the resistance and the recorded signal for the corresponding strain measurement. Results of both of these checks indicated the strain gage channels were functioning within specification.

Staff used three 8-channel BIB modules for the test. These modules provided bridge completion and streamlined wiring between the data acquisition system and the strain gages.

#### 5.8.6.4 Deflection Measurements

Instruments recorded deflection measurements at the load saddle stations and at the blade tip (167-in station). String potentiometers measured deflections at the load saddles. The uncertainty of the string

pot measurements is ± 0.05-in. Staff manually recorded tip deflections by reading a retractable tape measure attached to the tip. The uncertainty of the tip deflection measurement is ±. 0.1-in.

### 5.8.7 Film and Video

Staff took still photographs of the test during and after the test. Video cameras recorded the test from three angles; overhead from tip to root, leading edge from tip to root, and a close-up of the leading edge focusing on blade station near the root.

## 5.9 Static Test Execution

Testing was conducted under NREL's A2LA accredited test procedures for static blade testing. Testing followed the test plan [Ref 39], with the following exceptions: staff conducted testing in Building 254 instead of Building 251, they used a LeBow 5-Kip load cell and the blade tare load was calculated to zero the root moment instead of the total blade weight. Figure 5.18 shows a photograph of the test. Not visible is the whiffle tree, which is located above the photograph frame.

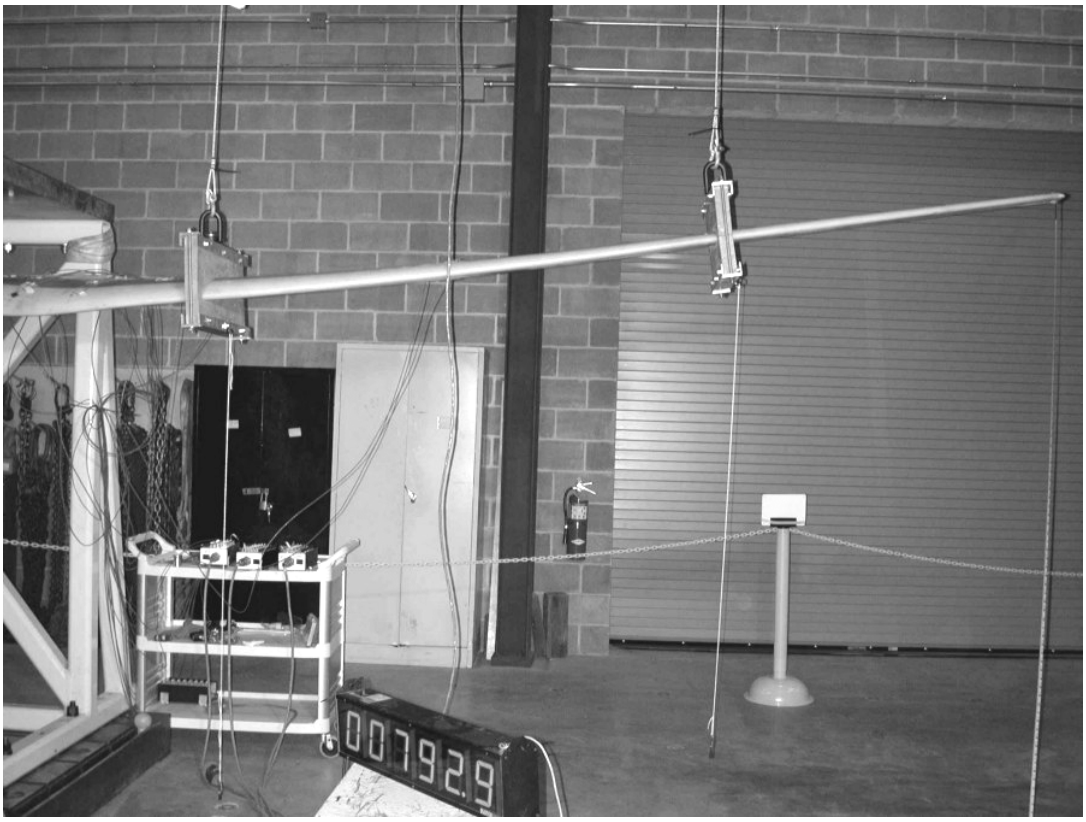


**Fig. 5.18 - Leading edge view of test**

A manually controlled overhead bridge crane applied the loads. The slowest crane speed provided a loading rate of approximately 10 lbf/sec. With the crane load applying the tare load of 116-lbf, all strain

gages and string pots were zeroed. Staff conducted the static test in a series of load steps. These load steps started at the tare load, then ramped to a target load level, held the load level a length of time (load plateau), then ramped down to the tare load. The test plan called for load steps (based on the design test load of 549-lbf) of 50%, 75%, and 100%, then increasing in steps of 25% until failure occurred. Figure 5.19 shows crane load versus time from test data and Table 5.3 provides load step plateau statistics. Some of the data collected at the tare load were removed from the graph to allow tighter display of the data on the x-axis (time). Staff held load step plateaus for a minimum of 10-seconds with a maximum length determined by the time the test operator needed to record the tip deflection.

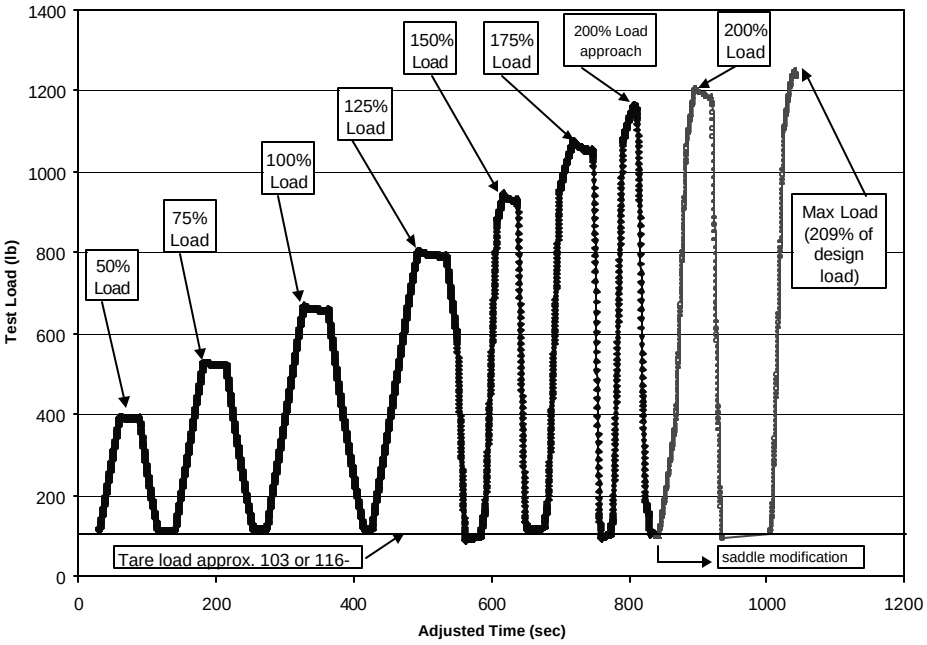


**Fig. 5.19 - Crane load versus time**

**Table 5.3 - Load Step Plateau Statistics**

| | Target Values | | | Empirical Test Data (crane load) | | | |
|---|---|---|---|---|---|---|---|
| Plateau (% of Design Load) | Target Test Load | Tare Load | Target Crane Load | Plateau average | Plateau Maximum | Plateau Minimum | Plateau Time |
| | lb | lb | lb | lb | lb | lb | sec |
| 50 | 274 | 116 | 390 | 391 | 395 | 389 | 27.4 |
| 75 | 412 | 116 | 528 | 524 | 530 | 521 | 31.6 |
| 100 | 549 | 116 | 665 | 660 | 668 | 657 | 34.0 |
| 125 | 686 | 116 | 802 | 795 | 807 | 791 | 39.6 |
| 150 | 823 | 116 | 939 | 932 | 945 | 927 | 18.6 |
| 175 | 961 | 116 | 1077 | 1059 | 1078 | 1051 | 26.4 |
| 200 | 1098 | 103 | 1201 | 1192 | 1207 | 1183 | 23.4 |

It was noted with the test approaching the 200% load step that the outboard saddle (120-in station) was rotating about the chordwise axis and applying an unintended moment to the blade due to large blade deflections. To alleviate the rotation, the test was briefly stopped in order to modify the saddle. Material was removed from the saddle in order to place the wire rope / saddle attachment point closer to the blade, thereby reducing the moment arm causing the saddle to rotate. After the modification was performed the whiffle tree was balanced and weighed using a Transducer Techniques 2-Kip load cell. The tare load with the modified saddle was 103-lbf (including blade tare). After the modification, the displacement potentiometers were re-zeroed (these provide relative displacement measurements). The 200% load step and failure loading were performed after the saddle modification.

During the 225% (failure) loading, the root fixture failed at a crane load of 1248.8-lbf. Figure 5.20 shows the test bending moment applied to the blade at the time that the root fixture failed along with the IEC Class II hurricane load.

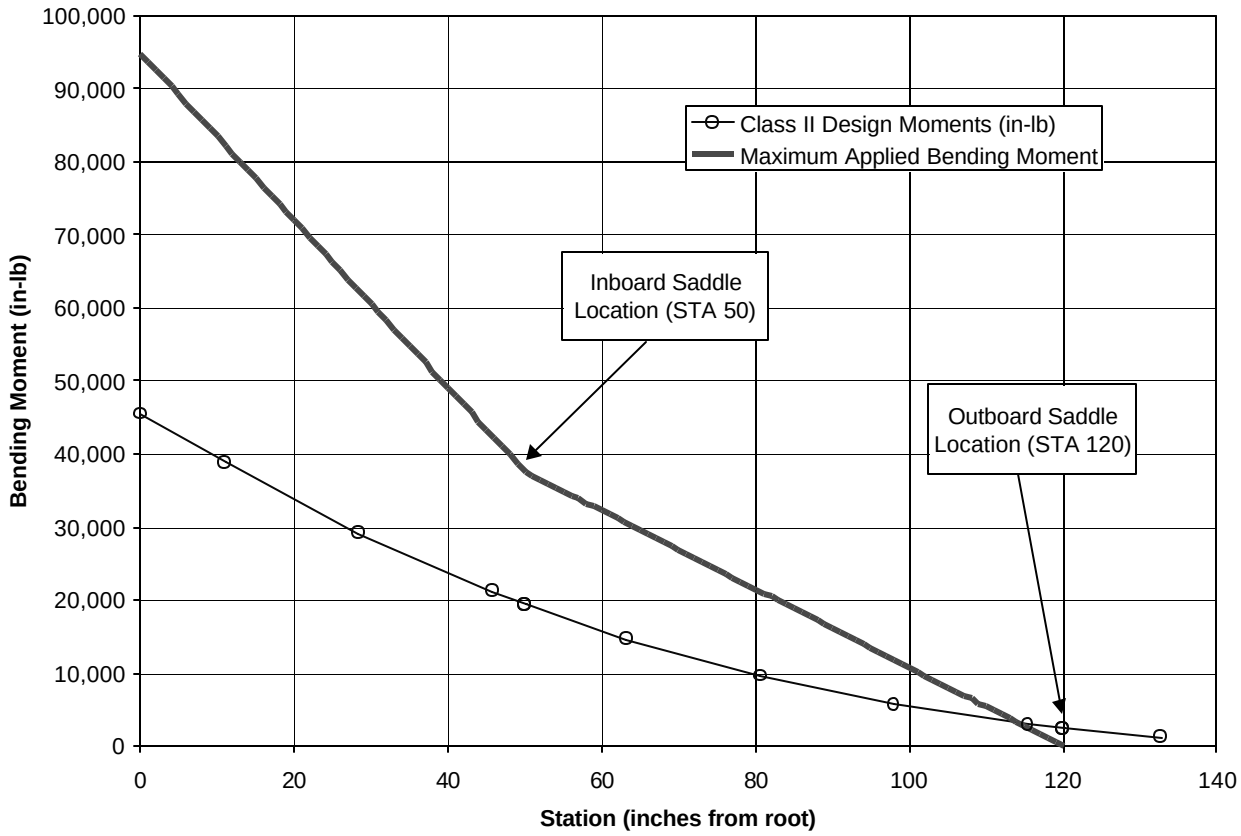


**Fig. 5.20 - Test bending moment at point of failure**

## 5.10 Results

The root fixture failed at a maximum crane load of 1248.8-lb. This crane load was equivalent to a test load of 1145.8-lb, or a root bending moment of 94,872 in-lb, which indicated 209% of the unfactored Class II hurricane load root bending moment. The root fixture failed when the hollow shaft inserted into the sleeve pulled away from the main structure of the fixture due to a weld failure on the original Jacobs fixture. Figure 5.21 shows a photo of the root attachment after failure.

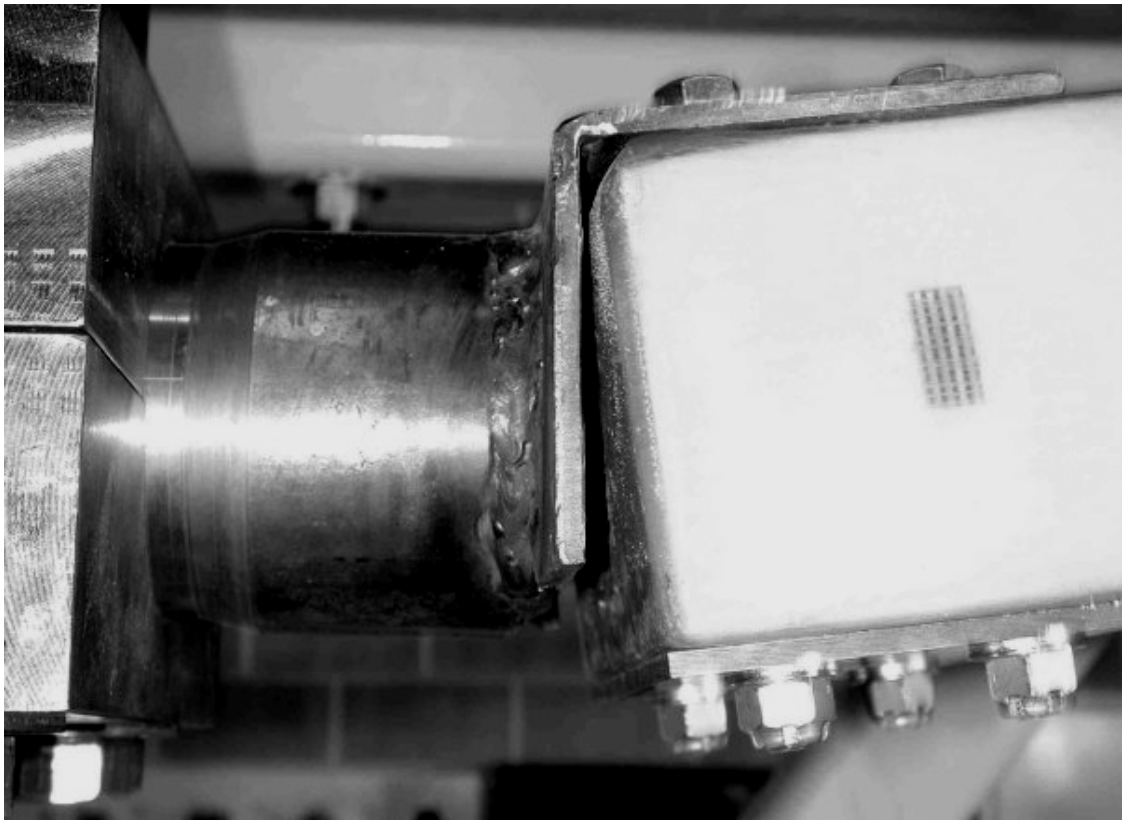

**Fig. 5.21 - Root attachment after failure**

During the load plateaus, the load was observed to relieve slightly. This relaxation was most likely due to the yielding of the root fixture. The load relaxation during the load plateaus was more evident at higher loads.

The majority of strain signals were linear-elastic, but several gages exhibited plastic behavior due to yielding of the test fixture. Staff observed some non-linear behavior from gages near the root and gages on the low-pressure (compression) surface.

Only minor audible acoustic emissions were detected at higher loads. There was no obvious blade damage at the conclusion of testing.

### 5.10.1 Deflections

Figure 5.22 shows deflection data taken at the load saddles. Deflections reported here are probably smaller than the in-field deflections, as the test root fixture is believed to be stiffer than the actual in-field root attachment. Data presented were for positive loading (load ramping up) for each of the loadings. The offset in displacement around the tare load was due to the yielding of the root adapter fixture. The yielding of the root fixture was evident as a “knee” in the displacement-load curves.

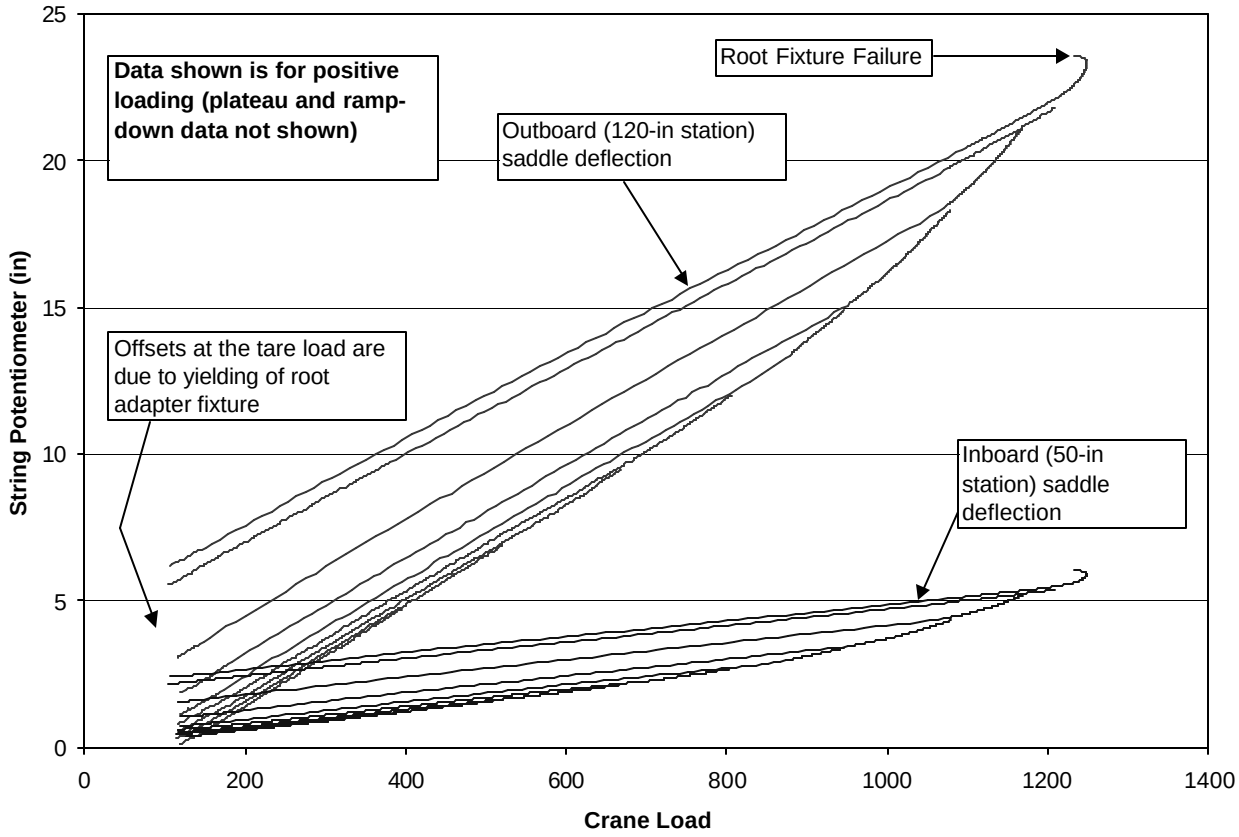


**Fig. 5.22 - Deflections at saddle locations**

Taking the linear portion of the final loading, the deflections at the saddles can be characterized by the following relations, based on the applied root moment:

For the inboard saddle: $d_{inboard} = 3.38 \cdot 10^{-5} \cdot M_{root}$

For the outboard saddle: $d_{outboard} = 17.27 \cdot 10^{-5} \cdot M_{root}$

Using these relations at the failure moment of 94,872 in-lb, the 50-in station saddle deflection would be 3.2-in, and the 120-in station saddle deflection would be 16.4-in.

Figure 5.23 shows the single-point tip deflection as recorded by a test operator. Note that zero displacement occurs at the tare load. Values were recorded during the load plateaus. Tip deflection data is lower than actual deflections due to the absence of loading between the outer saddle (120-in station) and the tip. The failure loading deflection was not recorded. However, at the 200% load plateau, the tip deflection was recorded as 31.7-in.

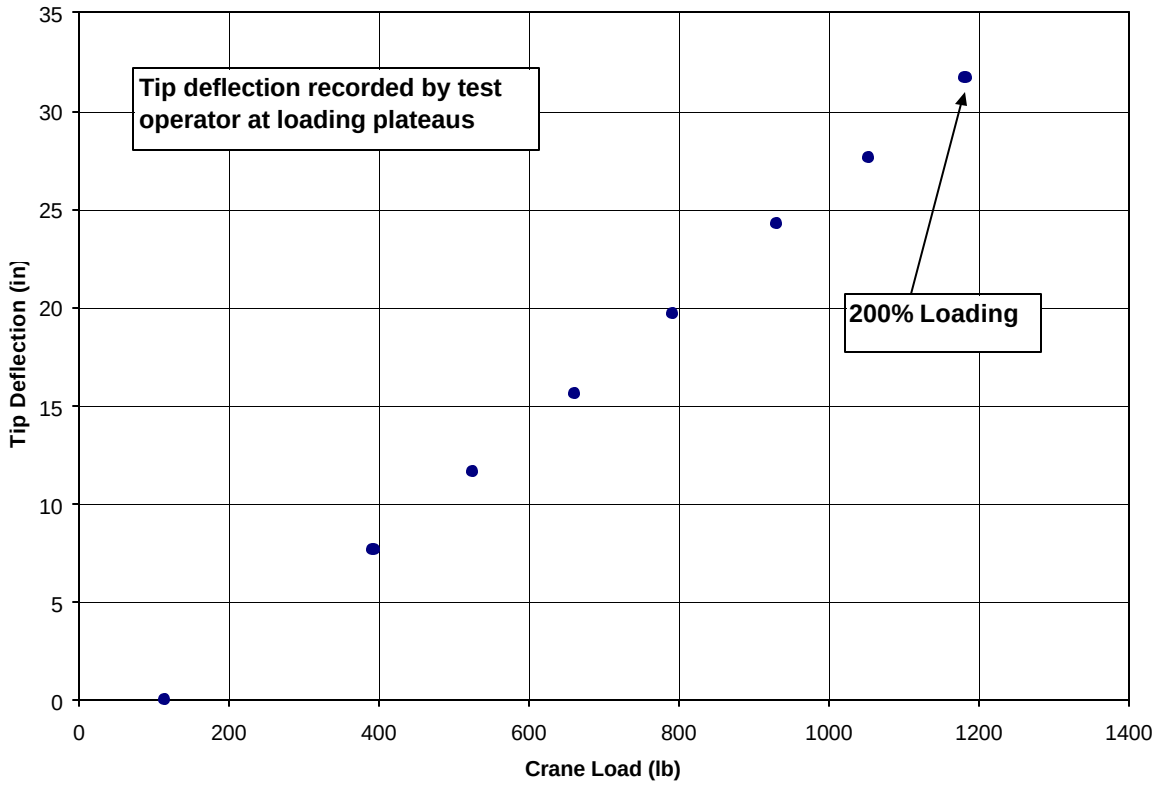


**Fig. 5.23 - Tip deflection**

### 5.10.2 Strain gage data

Strain gage plots of load versus strain for the individual strain gages are shown in Appendix B, Figures B.3 through B.17. These strain charts contain two traces, one before the saddle modification (50% through 175% loadings) and the other trace after the saddle modification (200% and failure loadings). The slight differences between the strains for these traces may be attributed to the saddle modification. Table 5.2 describes the strain gage nomenclature. Strain data is presented as a function of the test load (tare load has been removed).

Gage 06S11LA (Figure B.1) exhibited some hysteresis, some of which can be attributed to the yielding of the root fixture. Strain gages located at 14% to 16% span displayed a discontinuity (increase in strain magnitude on low-pressure side, slight decrease on high-pressure side) around a test load of 1080-lb. The localized discontinuity appeared to be based on strains outboard of this region not showing a similar shift. The shift was more pronounced on the low-pressure surface. Gage 16S42LA shows definite structural non-linear behavior.

Figure 5.24 shows strain gage data versus spanwise station, for gages located on the chordwise-center of the spar caps.

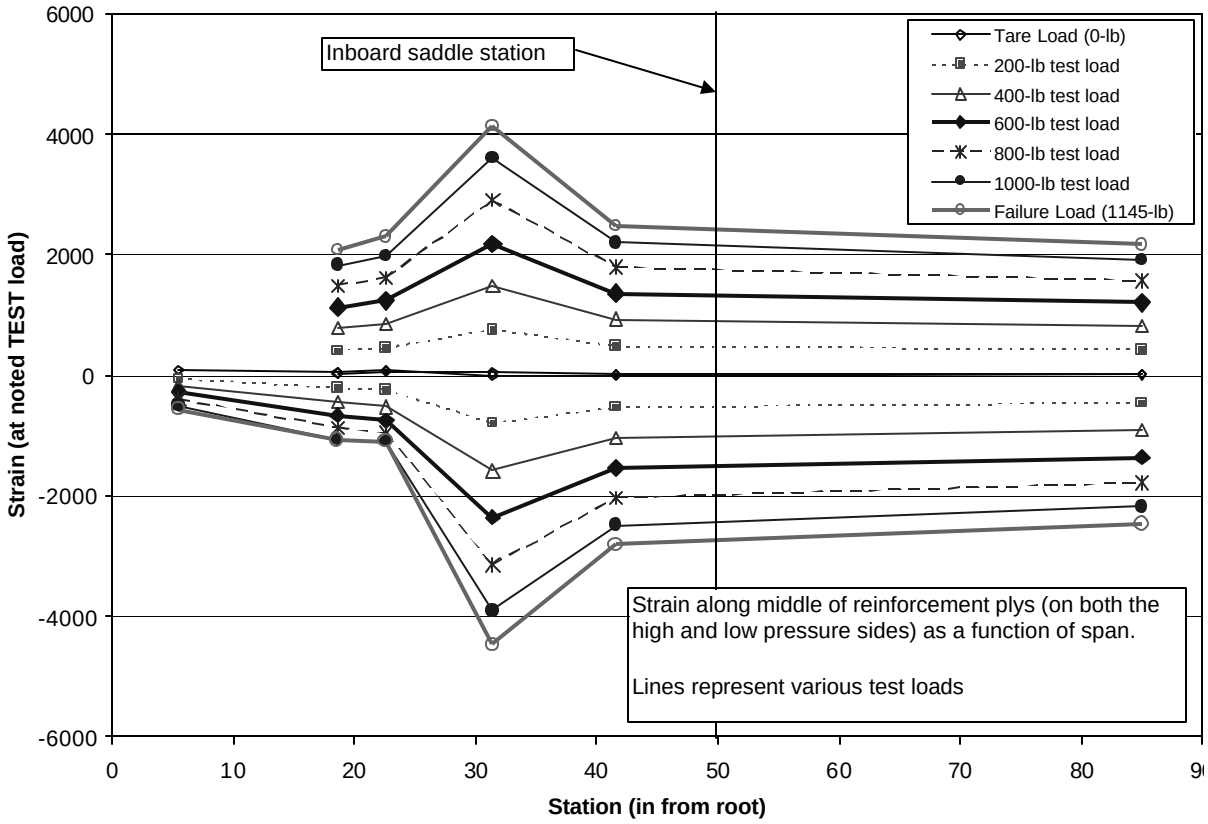


**Fig. 5.24 - Strain versus spanwise station for mid-spar cap strain gages**

# 5.11 Conclusions

## 5.11.1 Summary

A static test was performed on an FMI test blade on October 5, 2000 at the National Wind Technology Center. The root fixture failed at a maximum crane load of 1248.8-lb. This crane load is equivalent to a test load of 1145.8-lb, or a root bending moment of 94,872 in-lb. Based on these numbers, the blade was tested to 173% of the factored IEC 61400-23 test load using the IEC 61400-01 class II design loads (209% of the unfactored IEC 61400-01 design loads). Strain gage results indicate that partial structural damage may have occurred around 160% of the factored design load, based on strain discontinuities on the low-pressure surface around 15% span. No visible damage was evident at the conclusion of testing.

## 5.11.2 Future Work

We suggest that a second FMI blade be subjected to a fatigue test [Ref 40].

## 5.12 Fatigue Tests

### 5.12.1 Fatigue Calculations at Maximum Power Operation

#### 5.12.1.1 Using Longitudinal Strain, EPSY[19]

Material static strain ultimate allowables, see Materials section 3.5, are scaled by 0.352 corresponding to $S/S_0$ for 3,000,000 fatigue test cycles with slope, b = 0.10, where $S/S_0 = 1\text{-}b \cdot LOG\ (N)$ and the LOG is to the base 10. The choice of b=0.100 is predicated upon the following:

- Although the referenced SAND97-0032 document has several materials similar to those used in the subject blade, with differing "b" values, the overall average seems to be near 0.100, a choice consistent with Germanischer Lloyd acceptable values.
- The simplified approach is justified because the material groups used are not specifically tested.
- The calculated margins are high enough that the choice is somewhat academic, as any typical number would result in a decent margin of safety – see Remarks below.

Peak EPSY tensile and compression strains are 0.00116 (tension) and –0.00097 (compression) as the reference strain values for the calculated Max Power $\varepsilon/\varepsilon_0$ values. (See Figures 5.25 and 5.26.) The strain margins of safety become[20]:

- **Cap Tensile Strain Margin of Safety: = 0.00845/. 00116 = 7.30 (Limiting Value)**
- **Skin Tensile Strain Margin of Safety: = 0.00867/. 00116 = 7.49**
- **Cap Compression Strain Margin of Safety: = -0.00338/-0.00097 = 3.50 (Limiting Value)**
- **Skin Compression Strain Margin of Safety: = -0.00365/-0.00097 = 3.77**

---

[19] COSMOS/M label used for strain in the y-axis (the longitudinal direction in this model).

[20] The numerators are the max strain for the each case: cap tensile, cap compression, skin tensile, and skin compression. The minimum of all of these is cap compression @ 3.50. The overall minimum is 3.50 for cap compression - this is the overall limit (weakest link) for the blade. We choose a very conservative Safety factor of 2.0 over this that requires a MS of 3.50/2 = 1.75. This choice yields the 97,034,557 cycles calculation, which is 32 times the required lifetime.

**Remarks**

These margins essentially give infinite life. If we use a safety factor of 2.00, then the minimum margin required is = 3.50/2 = 1.75. To reduce this to a margin of safety of "0" (zero), the corresponding cycles would be 97,034,557 cycles, or 32 times the required lifetime; that is:

**1.75 = (1-0.100·LOG(3,000,000))/ (1-0.100·LOG(97,034,557)).**

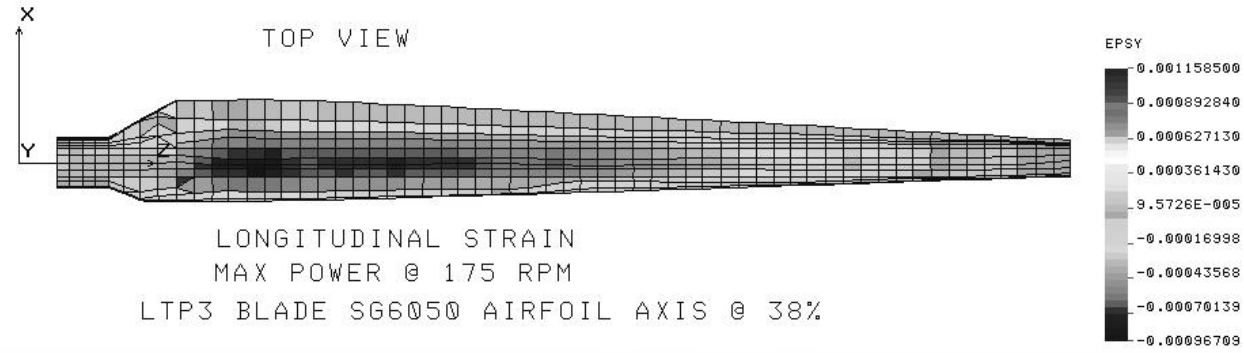


**Fig. 5.25 - Strain on blade top surface**
(See Reference 22)

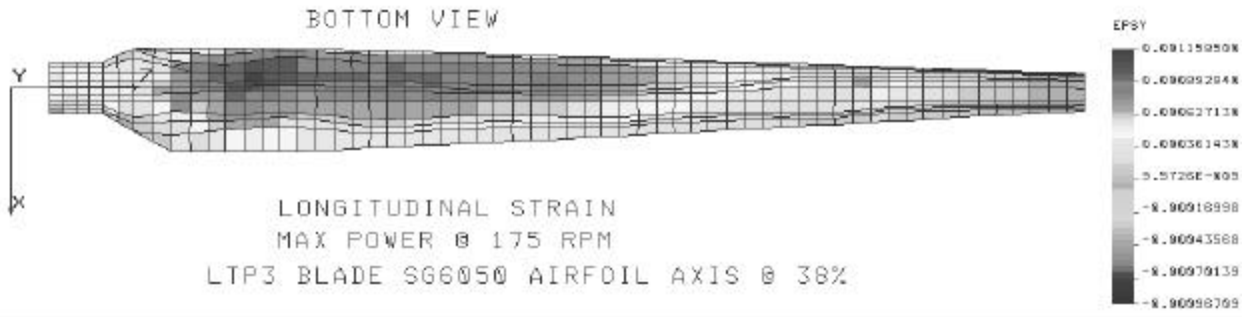


**Fig. 5.26 - Strain on blade bottom surface**
(See Reference 22)

# 5.13 Fatigue Test Introduction

## 5.13.1 Background

A separate prototype blade was static tested prior to this fatigue test [Ref 42]. The static test did not result in a failure of the blade, but did result in a failure of the Jacobs OEM root attachment fixture. The failure occurred at 173% of the IEC 61400-01 Class II extreme wind loading using IEC 61400-23 blade testing criteria.

The National Wind Technology Center (NWTC) also conducted a fatigue test of an FMI (Foam Matrix Inc.) prototype blade between January 31 and February 17, 2001. The test program used a hydraulic actuator to apply a constant amplitude cyclic flap-wise load to the blade at a single spanwise location to represent

equivalent damage for a FMI-derived fatigue load spectrum. The test was conducted in progressively more damaging load blocks of 1,000,000 cycles each and was concluded when failure occurred during the third block at 2,739,100 cycles. The failure was a compressive skin failure due to a ply drop 93.25-in from the root.

### 5.13.2 Scope

This section documents the fatigue testing of the prototype blade developed under the Sandia National Laboratories BMI solicitation.

### 5.13.3 Objective

The objective of this test was to determine the fatigue life of critical structural features of a prototype blade in terms of the FMI flap-wise load spectrum. The area of primary concern was skin-to-foam core adhesion over the entire blade. The Foam Matrix MFC/RTM process eliminates the shear web that exists in most conventional designs.

### 5.13.4 Blade Weight and Center of Gravity

The fatigue test article was one of three blades shipped to NREL. FMI inscribed this test blade with the identifying mark 'AT 10688'. The weight of the specimen was 55.8-lbf. This weight was for the as-received blade with no holes drilled for root attachment. A Pelouze platform scale, checked with calibration weights, ensured the measurement was within ± 0.2-lbf before drilling the root attachment.

The center of gravity (CG) was determined by balancing the blade on the corner of an inverted length of angle iron. The CG was determined to be 51.5-in from the root, as measured along the low-pressure surface of the blade. A tape measure, with a measurement uncertainty of ±1/8-in, indicated the length of the blade as 167.375-in, measured along the low-pressure surface of the blade.

## 5.14 Test Setup

### 5.14.1 Test Location

NREL used the small-blade test stand located in Building 251 at NREL's National Wind Technology Center (NWTC) north of Golden, CO for fatigue testing.

### 5.14.2 Test approach

The test used a hydraulic actuator to apply a single-point constant amplitude fatigue load, located 129.63 inches from the root of the blade in the flap direction only. Other load components such as edge and radial forces are important but were not available to use in the test. Figure 5.27 shows a schematic of the test layout.

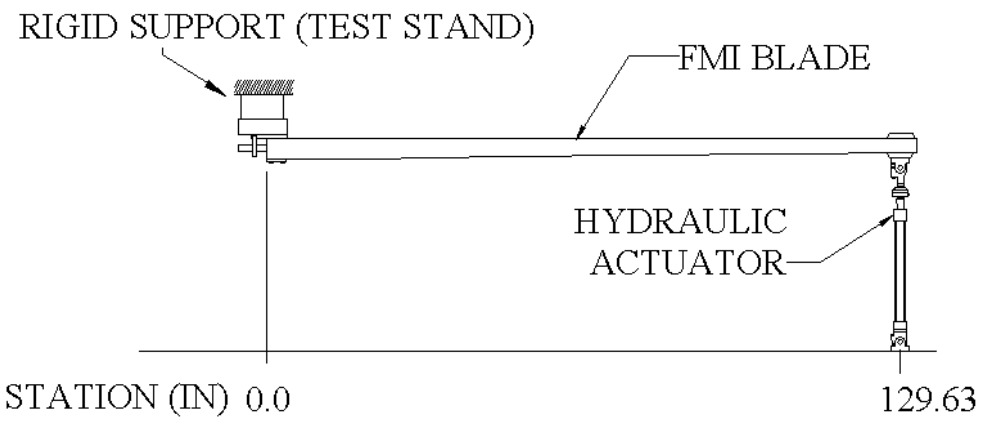


**Fig. 5.27 - Test layout schematic**

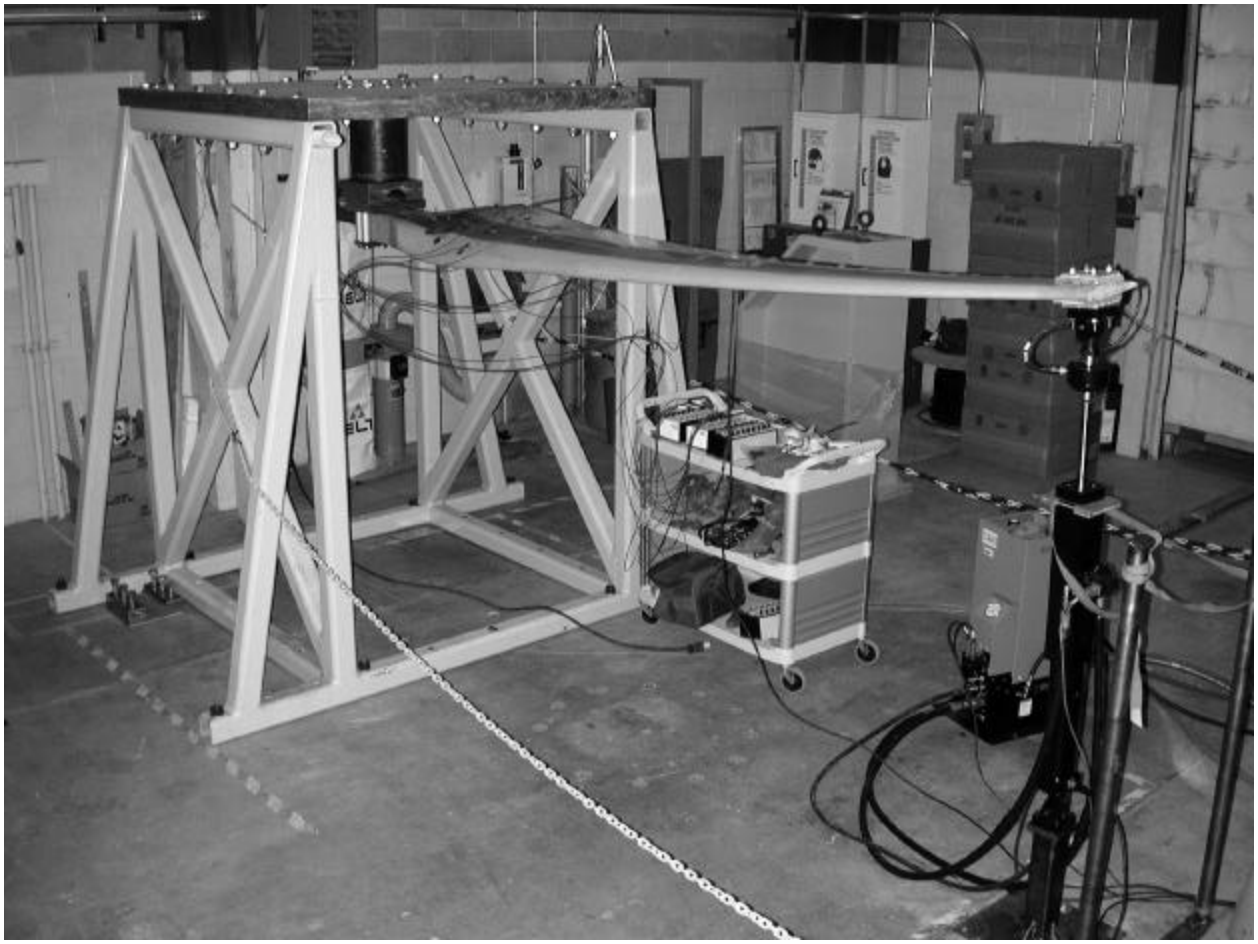

**Fig. 5.28 - Photograph of test in progress**

Figure 5.28 shows the test setup. Note that the test was running during this photo. Visible in the photograph are the small-blade test stand, test article, and the hydraulic actuator.

## 5.15 Test Hardware

### 5.15.1 Load Introduction Hardware

A servo-hydraulic actuator applied the loads. The actuator used for testing had a load capacity of 1-kip (1,000-lbf) in both tension and compression. The actuator had a 12-in stroke A 90-gpm (at 3000-psi) hydraulic power supply pumped hydraulic oil to the actuator. A hydraulic service manifold controlled oil flow to the actuator and provided accumulation capacity.

NREL staff constructed a 14-in tall pedestal base to locate the actuator above the laboratory floor at the proper test height.

Table 5.4 itemizes the hydraulic equipment used for testing.

**Table 5.4 - Hydraulic-loading hardware**

| Item | Model | Manufactu | Serial Number | Note |
|---|---|---|---|---|
| Hydraulic Controller | FlexTest IIm | MTS Inc. | System 838.69 | |
| Hydraulic Power Supply | 506.62A | MTS Inc. | 0147886 | 75-GPM |
| Hydraulic Service Manifold | 293.11 | MTS Inc. | 1008854 | 50-GPM |
| Actuator | 242.01 | MTS Inc. | 1009808 | 12-in stroke, 1-kip load |
| Servo-valve | 252.25 C-01 | MTS Inc. | B348225-01 | 25-GPM |
| Load Cell | 661.19 E-01 | MTS Inc. | 103281 | 1.1-kip |

### 5.15.2 Load Application Fixture

The blade was cut 131.75 in from the root of the blade to facilitate the installation of the load application fixture. Figure 5.29 shows the load application fixture. In an effort to re-enforce the blade for the load application fixture, staff removed a quantity of the foam core and filled the resulting cavity with epoxy. They installed aluminum plates on both sides of the blade to react the actuator load. Next, they poured epoxy leveling pads between the blade skins and the aluminum plates to align the aluminum plates parallel to the flats of the blade root. Four 3/8-24-all thread studs extended through the blade and the plates to fasten the blade to the swivel-head of the actuator. The 3/8-24 stud nuts were torqued to 30 ft-lbf.

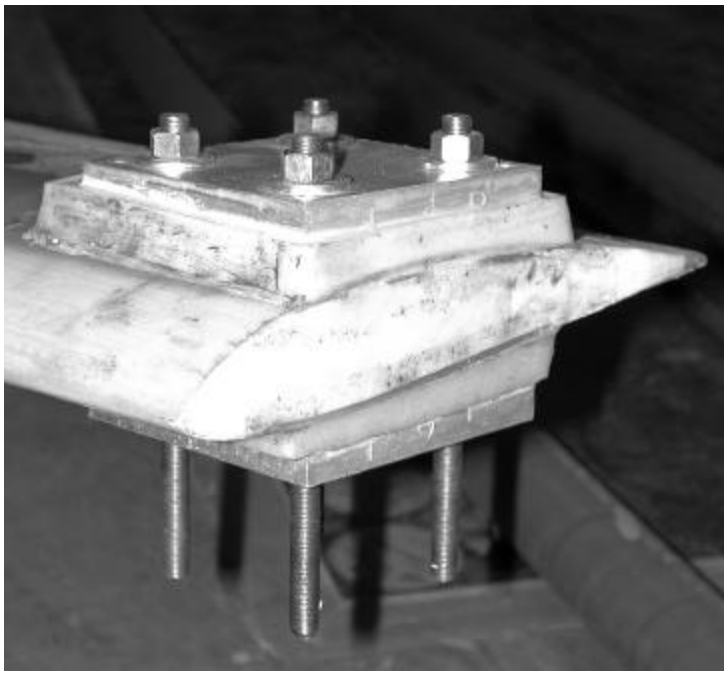

**Fig. 5.29 - Load application fixture**

### 5.15.3 Root Fixture

Staff connected the blade to the test stand through an adapter fixture. The adapter fixture was designed to have a compliance similar to the Jacobs root attachment fixture, but with an increased strength. They bolted the root to the stand with four ½ -in bolts using the same bolt pattern as the Jacobs OEM fixture. This arrangement held the low-pressure surface rigidly to the test stand. Additionally, two bolts on each side of the root clamped the blade root to the test stand. These bolts clamped through aluminum cylinders (spacers), which added strength to the fixture design. Staff torqued all of the root clamp bolts to 35 ft-lb in order to avoid crushing the 1.75-in square plywood dowels inside the blade root. A solid steel rod placed into the blade sleeve simulated the pitch rod of the hub. The rod had a machined step in order to insert to the full depth of the pitch rod hole of the blade. This solid rod extended 5 inches inboard of the blade root where it was rigidly attached to the test stand. Figure 5.30 shows the root attachment fixture.

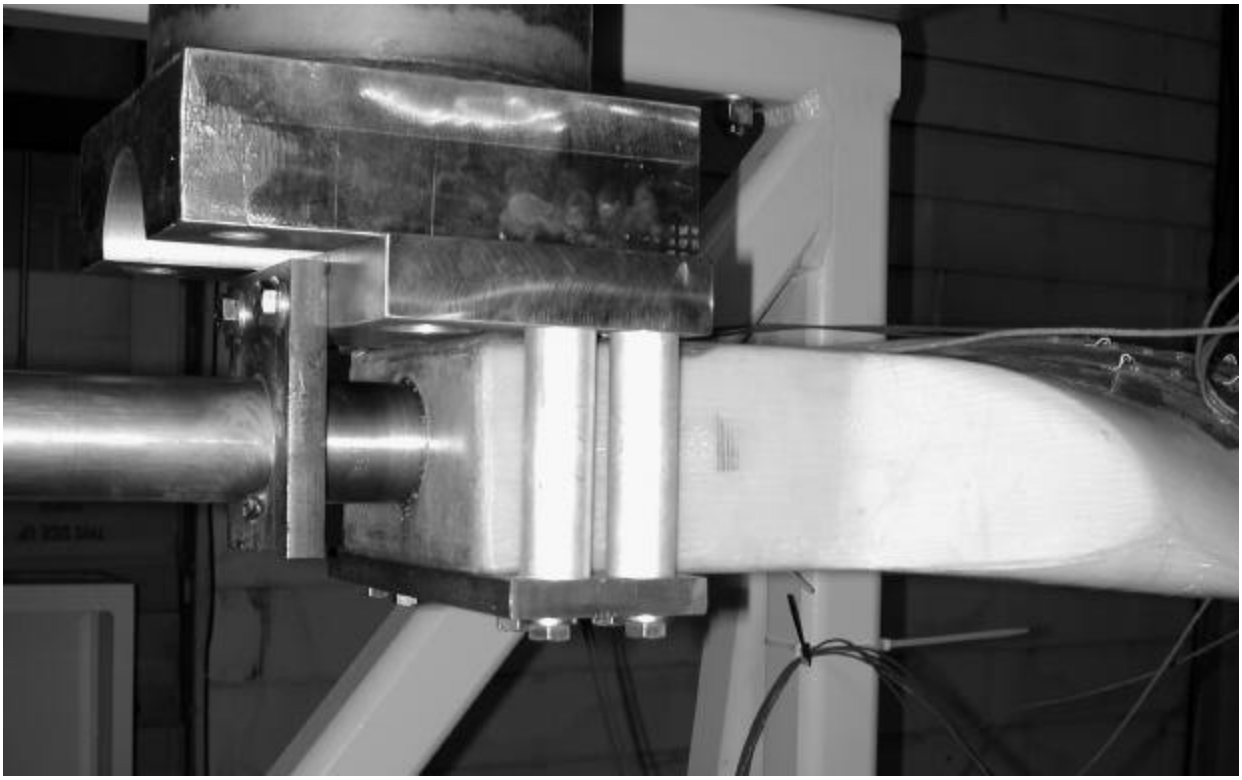

**Fig. 5.30 - Fatigue test root fixture**

## 5.16 Fatigue Loading

### 5.16.1 Fatigue Design Loads

FMI consultant Chuck Richey of Mechanical & Composites Engineering (MCE) provided the baseline fatigue loads. These fatigue loads used a non-conservative cutout wind speed base of 11 m/s and steady

wind loading, and did not include turbulent winds or extreme load cases. Due to the lack of available data from the Jacobs 29-20 turbine operation, NREL used Richey's loads as a baseline fatigue load. However, these loads are probably lower than the actual fatigue loads. Tables C.1 and C.2 of Appendix C show the design fatigue loads document.

### 5.16.2 Tare Weight Corrections

Staff considered tare weight prior to testing. The tare weight includes all testing hardware and blade weight that reacted to the load introduction station. The testing hardware includes the swivel-head and attaching fasteners. Staff calculated the blade tare weight required to null the blade-weight induced bending moment at the root of the blade. Prior to mounting the blade, and after the load application apparatus had been installed on the blade, staff determined the weight and center of gravity of the cut section. The modified blade, including the load application station materials, had a weight of 57.4 lbf, with a center of gravity 51.5 in from the root of the blade, producing a static tare moment of 2,956 in-lbf. In order to nullify this root bending moment, a load of 23 lbf was necessary at the load introduction station. The weight of the test apparatus between the load cell and blade (swivel head and fasteners) was 5 lbf. Therefore, the total tare weight was 5 lbf + 23 lbf = 28 lbf. This tare load was added to both the maximum and minimum fatigue design fatigue loads to obtain the fatigue test loads.

### 5.16.3 Test Loading

NREL staff applied the test loading using constant-amplitude block loading. They applied fatigue loads using an R-ratio of 0.1 (R-ratio = minimum load / maximum load). They applied an initial load of 247 lbf / 24.7 lbf for 1 million cycles. Subsequently, they applied additional load blocks for 1 million cycles, raising the maximum load 20% (relative to the initial maximum load) for each block while maintaining the R-ratio of 0.1, until a failure occurred.

Table 5.5 gives the design and test loads used for this test.

**Table 5.5 - Test load matrix**

| | Load Block | | | | | |
|---|---|---|---|---|---|---|
| | 1 | | 2 | | 3 | |
| | Maximum Load (lb) | Minimum Load (lb) | Maximum Load (lb) | Minimum Load (lb) | Maximum Load (lb) | Minimum Load (lb) |
| Design Load | 247.0 | 24.7 | 296.4 | 29.6 | 346.0 | 34.6 |
| Tare Load | 28 | 28 | 28 | 28 | 28 | 28 |
| **Test Load** | **275.0** | **52.7** | **324.4** | **57.6** | **374.0** | **62.6** |

Test Load = Design Load + Tare Load

The hydraulic actuator applied test loads at a frequency of 3 Hz. The first flap natural frequency of the modified blade, with the load attachment fixture installed, measured 5.6 Hz.

The actuator controller used displacement control for dynamic stability [Ref 43]. The test operator determined quasi-statically displacement parameters that related to the test loads.

Stiffness checks were performed every 30 minutes (5,400 cycles). During stiffness checks, the blade was cycled at a reduced frequency of 0.1 Hz (quasi-static) to minimize dynamic effects. Stiffness checks were done to record the blade stiffness (load range / displacement range) and to zero the strain gages, nullifying thermal effects.

Underpeak fault detection was set up for the load cell channel. If the load did not reach a specified level for the programmed displacement, which could indicate a possible specimen failure, the hydraulic controller shut off the oil supply to the actuator, stopping the test.

## 5.17 Test Instrumentation

### 5.17.1 Load Cell

A load cell mounted between the blade and the actuator piston measured loads. The load cell had a calibrated full-scale range of 1,000 lbf. The nameplate accuracy of the load cell is 0.08% FS (full scale), which results in a load uncertainty of ±0.8 lbf. MTS personnel calibrated the load cell on site prior to testing. The MTS controller sent high-level analog signals (± 5V) to the DAQ (data acquisition system) for load data collection.

### 5.17.2 Displacement

An LVDT (Linear-Variable Differential Transformer) recorded the displacement of the actuator piston. The LVDT was factory installed inside of the actuator piston. MTS personnel calibrated the LVDT prior to testing. The LVDT accurately tested in the range of ±0.08 in. The MTS controller sent high-level analog signals (±5V) to the DAQ for LVDT data collection.

### 5.17.3 Strain Gages

Measurements Group manufactured the model WK-09-250RD-10C three-element rectangular rosette strain gages and model WK-09-250BF-10C single element gages used in this test. All gages had a 0.25-in active grid length and a nominal resistance of 1000 Ohm. All gages used a three-wire, quarter-bridge configuration connection. Gage Self-Temperature-Compensation (STC)[21] was matched to the FRP of the

[21] STC is the Self-Temperature-Compensation number. Its units are in ppm/deg F, (for the gages used, 9e-6 in/in/deg F). Essentially if the STC number of the gage is not matched to the coefficient of thermal expansion, the gage will produce an output due to the thermal expansion of the material to which it is bonded (gage would expand at a different rate than the base material). Typical 0-degree fiberglass laminates have a coefficient of thermal expansion (CTE) close to 9e-6 (in the transverse direction the CTE is typically larger). Since the strain gages were autozeroed, the STC is not as critical compared with no-autozeroing.

blade laminate (STC=09). All bridges used a 3.333-V excitation voltage with a gain of 200. With these settings, the smallest differential strain measurable was 0.5 microstrain (effectively a 16-bit A/D board).

Bridge completion used BIB (Blade Interface Box) units mounted near the blade. These units provided (8) strain gage channels of bridge completion, had selectable settings for 1000-Ohm or 350-Ohm quarter bridges and for half- or full-bridges for any gage resistance. BIB units used Measurement Group MR1-10C-129 Bridge completion modules. Excitation voltages and signal outputs from the BIB units were connected to the data acquisition hardware through a 40-wire, 24-gauge shielded cable.

Several checks were made prior to testing to ensure accurate readings. Staff measured gage resistance where the strain gage wires connect to the BIB modules. A second check simulated a gage signal using a decade resistor. A decade resistor, inserted into the signal path at the BIB module, changed resistance to two different levels and the corresponding strain measurement was recorded in the data acquisition system. Results of both of these checks indicated the strain gage signals readings were within 2 percent of the actual strain. In general, considering systematic errors (gage misalignment, bridge non-linearity, thermal effects, and electrical noise), the accuracy of strain gage signals reported is estimated as within ±4 percent of the indicated value.

Strain gages were autozeroed during the stiffness checks, as described above in Section 5.16.3. The autozero algorithm zeroed the strain signals at the test tare load, which compensates for the thermal output of the strain gages. Staff used the same strain gage layout as with the static test, recording nineteen strain gage signals. Table 5.6 shows the strain gage layout used for the test.

**Table 5.6 - Strain gage placement**

| Channel | Name | % Span | Span Station (in) | % Chord | Curvelinear Distance to Trailing | Distance to blade root (in) | Orientation | Gage Type | Blade Side HP/LP |
|---|---|---|---|---|---|---|---|---|---|
| 4 | 06S11LA | 6.8 | 11.13 | 50.0 | n/a | 5.5 | 0° | Single | LP |
| 5 | 14S34HA | 14.4 | 24.23 | 34.6 | n/a | 18.6 | 0° | Single | HP |
| 6 | 14S43LA | 14.4 | 24.23 | 43.9 | n/a | 18.6 | 0° | Single | LP |
| 7 | 16S34HA | 16.7 | 28.23 | 34.7 | 12.03 | 22.6 | 0° | Single | HP |
| 8 | 16S42LA | 16.7 | 28.23 | 42.2 | 10.81 | 22.6 | 0° | Single | LP |
| 9 | 16R14LA | 16.7 | 28.23 | 14.3 | 16.00 | 22.6 | 0° | Rosette | LP |
| 10 | 16R14LB | 16.7 | 28.23 | 14.3 | 16.00 | 22.6 | 45° | Rosette | LP |
| 11 | 16R14LC | 16.7 | 28.23 | 14.3 | 16.00 | 22.6 | 90° | Rosette | LP |
| 12 | 16S72LA | 16.7 | 28.23 | 72.5 | 5.00 | 22.6 | 0° | Single | LP |
| 13 | 21S34HA | 21.7 | 37.03 | 34.9 | 11.81 | 31.4 | 0° | Single | HP |
| 14 | 21S37LA | 21.7 | 37.03 | 37.2 | 10.69 | 31.4 | 0° | Single | LP |
| 15 | 21R72LA | 21.7 | 37.03 | 72.6 | 5.00 | 31.4 | 0° | Rosette | LP |
| 16 | 21R72LB | 21.7 | 37.03 | 72.6 | 5.00 | 31.4 | 45° | Rosette | LP |
| 17 | 21R72LC | 21.7 | 37.03 | 72.6 | 5.00 | 31.4 | 90° | Rosette | LP |
| 18 | 21S13LA | 21.7 | 37.03 | 13.7 | 15.81 | 31.4 | 0° | Single | LP |
| 19 | 27S35HA | 27.6 | 47.23 | 35.6 | 11.13 | 41.6 | 0° | Single | HP |
| 20 | 27S40LA | 27.6 | 47.23 | 40.3 | 10.44 | 41.6 | 0° | Single | LP |
| 21 | 52S37HA | 52.5 | 90.63 | 37.6 | 8.44 | 85.0 | 0° | Single | HP |
| 22 | 52S39LA | 52.5 | 90.63 | 39.5 | 8.38 | 85.0 | 0° | Single | LP |

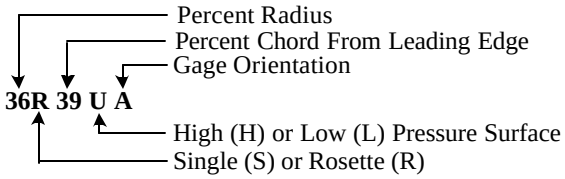


**Symbols for Gage Orientation:**

A - 0 Degrees From Spanwise Direction
B - 45 Degrees From Spanwise Direction
C - 90 Degrees From Spanwise Direction

## 5.17.4 Data Acquisition System

Staff used a custom NREL program, BSTRAIN as the front-end for data acquisition. National Instruments manufactured the 16-bit data acquisition hardware consisting of SCXI-1321 terminal blocks, SCXI-1121 isolation amplifiers, a SCXI-1001 12-slot chassis, and a PCI-MIO-16XE A/D board. All data channels used10-kHz low-pass anti-aliasing filters. Sampling occurred on each data channel at 120 samples per second. Data were recorded as Peak / Valley pairs for each cycle. Appendix C, Sheet C.3 gives the data acquisition schematic for this test.

## 5.17.5 Video

A video camera recorded the test. The permanently mounted camera is located on the high bay wall. The camera provided an overhead view of the blade's leading edge.

## 5.18 Test Execution

NREL staff ran several cycles in order to determine the maximum stable test frequency of 3 Hz. They used this frequency for the duration of the test.

The testing started on February 2, 2001, using the baseline test loads of 275 / 52.7 lbf (which include tare). Testing continued with this loading until the load block finished at 1,014,632 cycles. Staff observed no unusual blade behavior during this first load block. The displacement analog output from the hydraulic controller was not functioning properly during the first load block. This did not affect the test itself but the data acquisition system did not record any displacement data. Staff rectified this problem at cycle number 1,028,500.

On February 9 and starting at cycle 1,014,632, staff increased the loads by 20% for the second load block. This load block continued until the total test cycle count reached 2,000,000 cycles. Around cycle 1,800,000, a region at 16% span developed some apparent de-bonding of the skin from the foam core evidenced by an increase in observed out-of-plane panel movement. This de-bonding region was on the high-pressure side, towards the trailing edge at the chordwise end of the uni-directional laminate plank. Staff continually monitored this region during the test but it exhibited only significant panel deflections, never surface cracks.

NREL started the third and final load block on February 13. They increased the maximum load by 20% of the original maximum load to 346-lb (374-lb including tare). They installed a 1-in thick spacer underneath the actuator to allow for the test displacements of this load block. At cycle 2,382,000, several other regions around 16% span developed apparent de-bonding of the laminate from the foam core. These widespread de-bonded areas could be located by both visual inspection (visible out of plane deflection) and by noting the sound produced by tapping a coin on the laminate. De-bonded areas exhibit a hollow, or lower frequency sound, compared with intact laminates. Regions on both the high-pressure and low-pressure surfaces at 16% span exhibited signs of de-bonding.

Around cycle number 2,686,000, a new damage region appeared 93 inches from the root. This damage exhibited a light color compared with the surrounding laminate. The damage appeared to be a spanwise abnormality with a length of about 1.5-in and was located on the compression side on the uni-directional laminates. Tap tests indicated that the area had a subsurface delamination. In addition, the temperature measurements of this region were about 5 degrees F warmer than the surrounding laminates. Figure 5.31 shows this region at around cycle 2,686,000.

Catastrophically blade failure occurred 739,100 cycles into the third load block at cycle 2,739,100. The test shut down three cycles later from a load underpeak. The blade failed 93.25 inches from the blade root. The failure was a compressive-surface buckling of the entire chord.

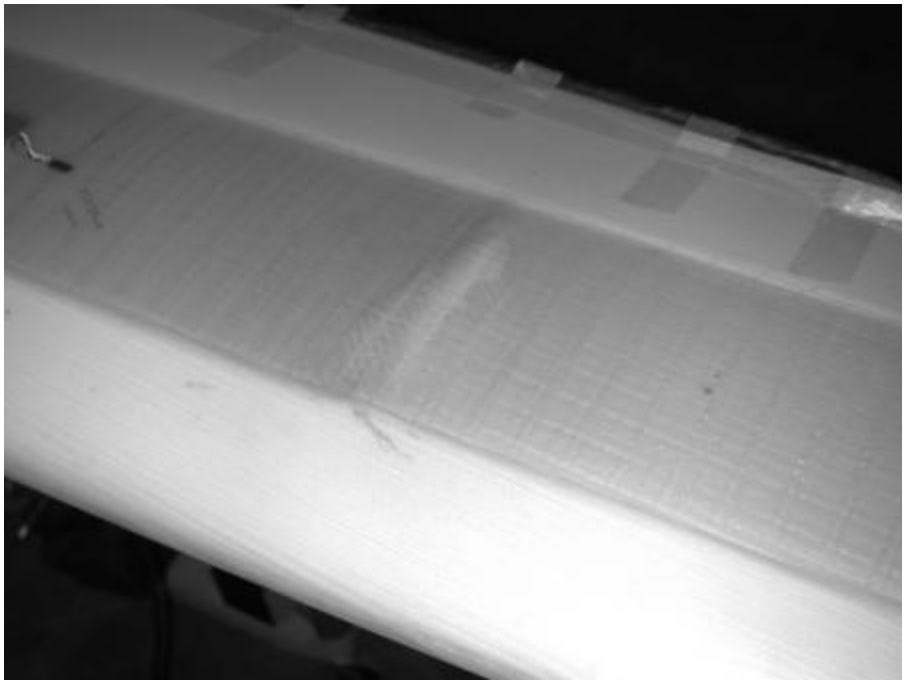

**Fig. 5.31 - De-bonding region 93-in from root around cycle 2,686,000**

Table 5.7 gives the history of the test loading. Loads given in Table 5.7 are the design loads, which do not include tare. To obtain the test loads, add 28-lb to the loads listed in Table 5.7

**Table 5.7 - Design load test history**

| Load Block | Maximum Load (lb) | Minimum Load (lb) | Number of Cycles |
|---|---|---|---|
| **1** | 247 | 24.7 | 1,014,632 |
| **2** | 296.4 | 29.6 | 985,368 |
| **3** | 346 | 34.6 | 739,100 |
| | | **Total cycles** | **2,739,100** |

Table 5.8 gives the displacement control parameters used for the test. Changes in the control parameters at cycles 0, 1,014,632, and 2,000,000 represent new load blocks. Changes in the control parameters at cycles 580,000, 1,813,823, and 2,686,300 compensated for the softening of the blade.

**Table 5.8 - Test displacement control parameters**

| | | Cycle | | | | | |
|---|---|---|---|---|---|---|---|
| | | 0 | 580,000 | 1,014,632 | 1,813,823 | 2,000,000 | 2,686,300 |
| Load Block 1 | LVDT @ 28-lb | -5.4 | -4.8 | | | | |
| | LVDT @ 53-lb | -4.8 | -4.0 | | | | |
| | LVDT @ 275-lb | 2.4 | 3.0 | | | | |
| | | | | | | | |
| Load Block 2 | LVDT @ 28-lb | | | -4.8 | -4.6 | | |
| | LVDT @ 58-lb | | | -3.9 | -3.6 | | |
| | LVDT @ 324-lb | | | 4.6 | 4.9 | | |
| | | | | | | | |
| Load Block 3 | LVDT @ 28-lb | | | | | n/a | -5.6 |
| | LVDT @ 62.6-lb | | | | | -4.8 | -4.4 |
| | LVDT @ 374-lb | | | | | 5.4 | 5.8 |

## 5.19 Test Results

### 5.19.1 Result Summary

The blade failed at cycle 2,739,100 during the third load block as listed in Table 5.8. Failure was due to a compressive-side skin failure at 93.25 inches from the root. A ply drop, where the unidirectional layers transition from four to three layers, appears to be the primarily cause of the failure. The failure region was immediately outboard of this ply-drop. The failure area was a crease, initiated at the center of the unidirectional plank, that ran across the entire chord. Figures 5.32, 5.33 and 5.34 show the failure region.

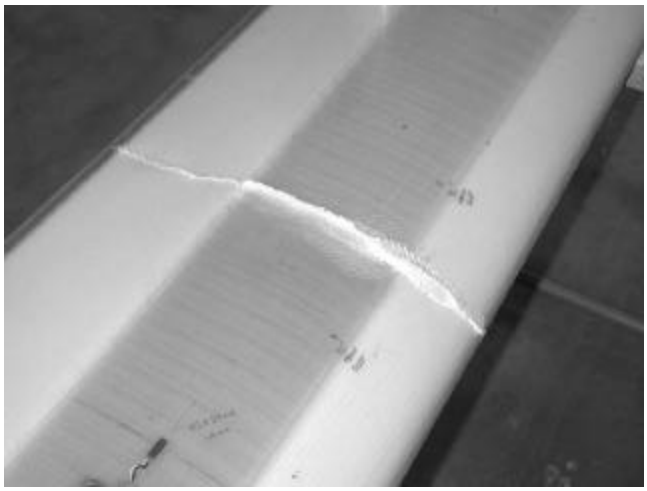

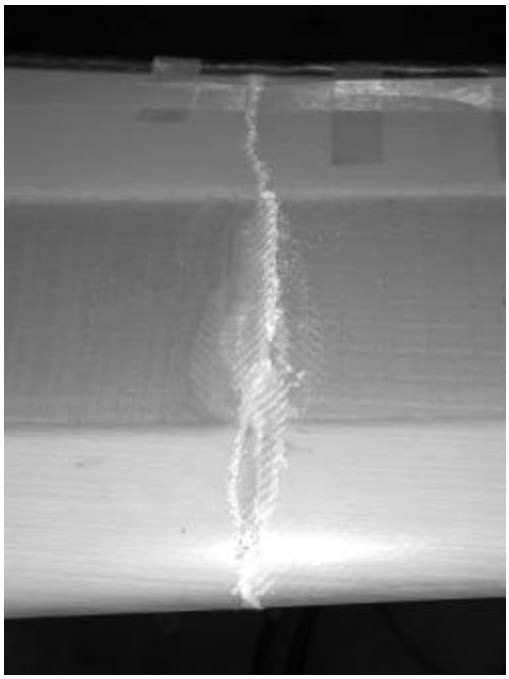

**Fig. 5.32 - Longer view of blade fracture**

**Fig. 5.33 - Close-up of blade fracture**

**Fig. 5.34 - Blade fracture showing load application fixture and test stand**

## 5.19.2 Load and Displacement

Figure 5.35 displays measured loads collected during the stiffness checks at a reduced frequency of 0.1 Hz. Note that during the stiffness check cycles[22], the minimum load was around zero while the maximum load increased with each load block. The stiffness checks were performed to allow autozeroing of the strain gages and to allow the load to pass through the tare load of 28 lb. The discontinuities in maximum load along each of the three load blocks were due to actuator displacement adjustments that accounted for softening of the blade.

[22] The stiffness of the blade is a global stiffness, load range divided by actuator displacement range. This includes all softening along the span of the blade. Something such as a root stiffness would need to be inferred from strain gage data, which is a local property (not a sectional value). To obtain a root stiffness, the test specimen would need to be outfitted with a displacement transducer at the station of interest (attach a string potentiometer or something of that nature).

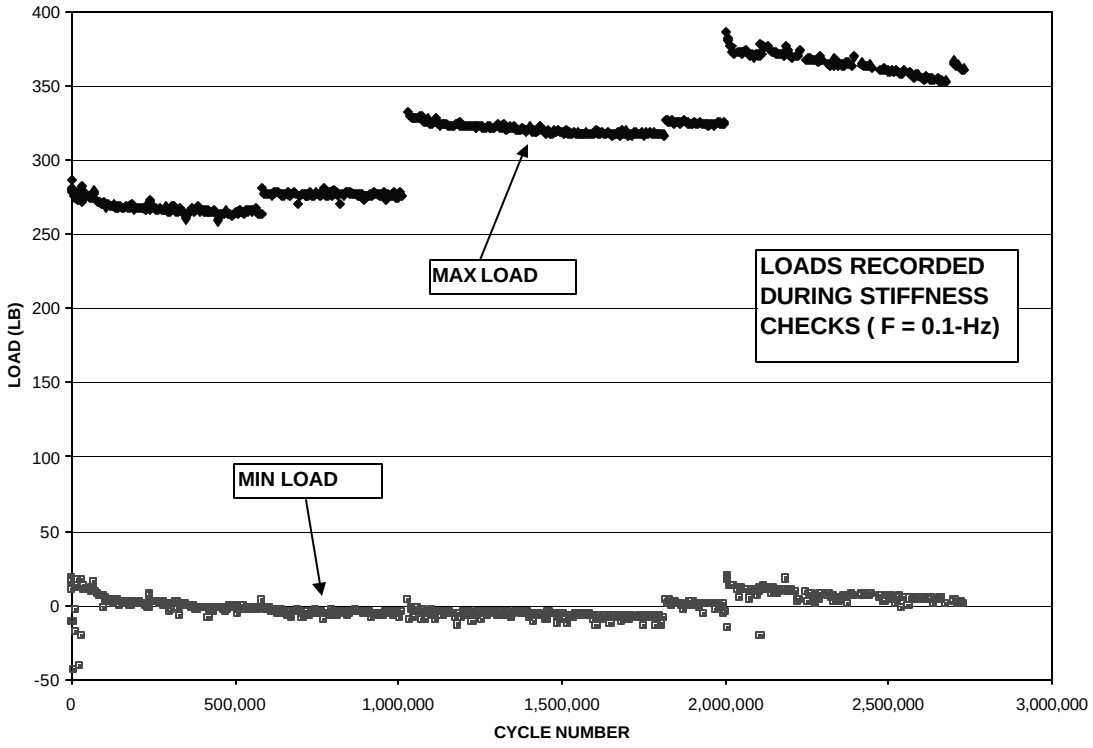


**Fig. 5.35 - Stiffness check-cycle load history**

Figure 5.36 shows the stiffness history of the test. Stiffness is defined as the load range divided by the displacement range. BSTRAIN computed stiffness data using load and displacement data collected during quasi-static stiffness checks. Note how the rate of stiffness degradation started to increase beginning around 2,000,000 cycles. Stiffness data was not available for the first million cycles due to anon-functional LVDT analog output described in Section 5.20.

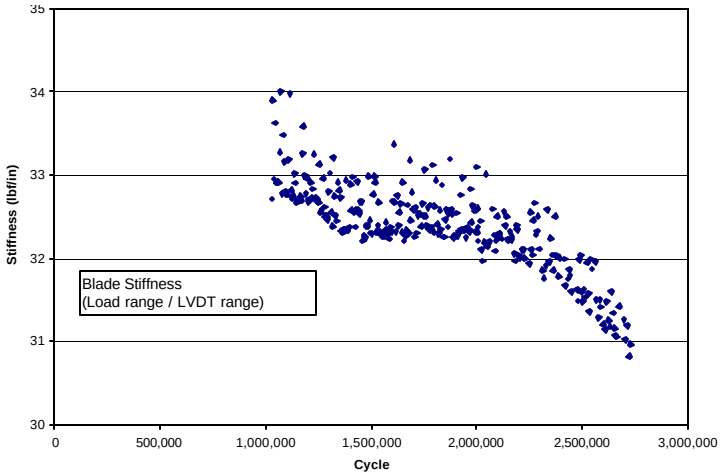

**Fig. 5.36 - Measured blade stiffness record**

Figure 5.37 presents the load history for the test. These collected data were the peaks and valleys during the 3-Hz cycle frequency. The load varied slightly due to drift in the LVDT because of changes in the temperature of the hydraulic oil bath. Note the loss of load during the final load block.

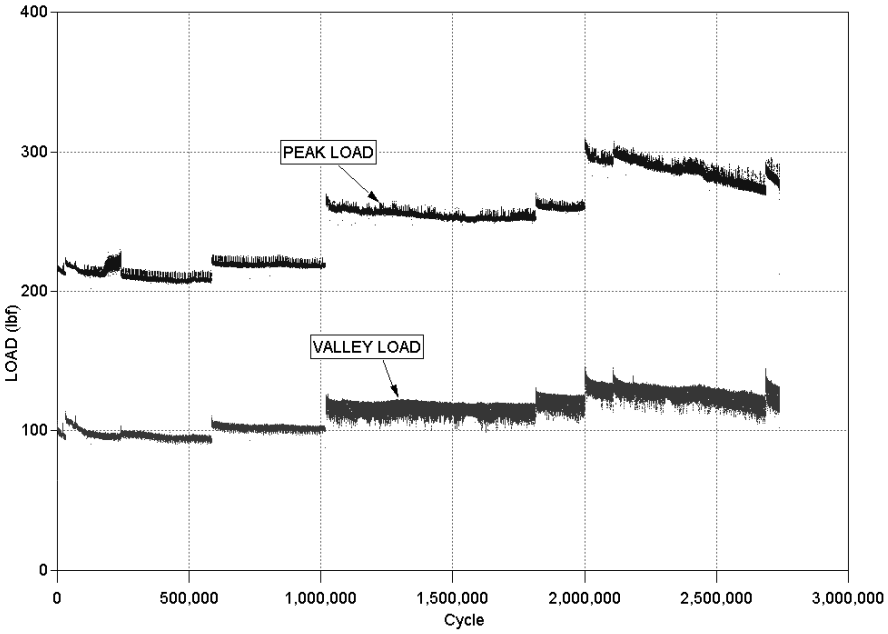


**Fig. 5.37 - Dynamic load history**

Figure 5.38 shows the range and mean displacement (LVDT) data for the test. Again, displacement data are not available for the first 1,000,000 cycles

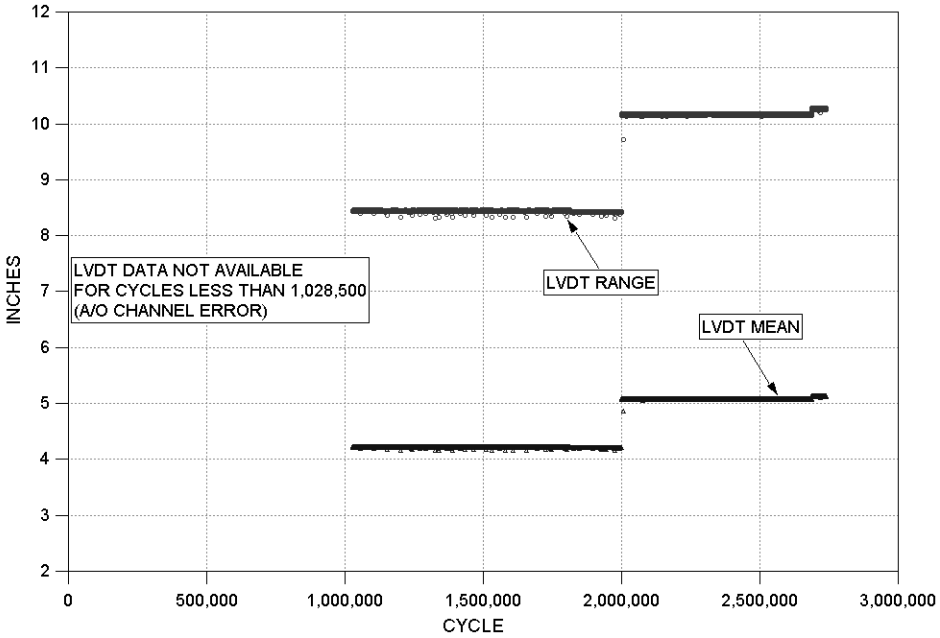


**Fig. 5.38 - LVDT range and mean data**

### 5.19.3 Strain Data

Appendix C, Figures C.1 through C.19 plot strain versus cycle data for each strain gage signal. These data had been block-averaged at 20 data points per block. Approximately 136,000 points represent each curve.

Note that the Y-axis (microstrains) had a different scaling for each graph. Strain data were labeled as "peak" or "valley" on each graph, with "peak" values corresponding to the absolute value of the peak actuator load.

While conducting the test, NREL staff anticipated a possible failure in the region between the end of the pitch shaft tube and 21% span. Visual observations of panel de-bonding and the trends of the strain gage signaled an anominally in this region.

The gage located on the middle of the uni-directional plank (16S42LA) tended to shed strain throughout the test, while the gages toward the leading and trailing edges (16R14Lx and 16S72LA, respectively) tended to exhibit a strain increase throughout the test. Prior to the failure (which occurred outboard of this region), the gage located towards the trailing edge (16S72LA) measured an event where the strain was decreasing, then suddenly increased. We don't know if this event would have progressed to a failure at this location.

Observation also indicated softening inboard of the tube-end at gages 14S34HA and 14S43LA. During the final load block, both of these gages exhibited local softening, with the magnitude greater on the low-pressure side.

Each gage of the rosette strain gage at 21% span (21R72Lx) was in compression for the entire test. This is typically indicative of non-linear panel deformation (blister). During the post-mortem inspection, the skin was intact to the foam core. During the third load block the axial strain at this location was seen to decrease, while the chordwise strain increased in magnitude.

The strain decreases observed for gages in the outboard regions of the blade (27S35HA, 27S40LA, 52S37HA, and 52S39LA) may be in part attributed to softening of the blade in the failure region.

Several of the gages exhibited strain reversal (zero crossing). Typically, strain reversal would not be expected for a tension-tension test. When a strain reversal is observed, plastic deformation has occurred on the test article, usually during the initial cycle of the block. Since the strain reversal was not seen in every strain gage, it is most likely that the test article yielded locally.

Some of the graphs exhibit spikes in the data that were artifacts resulting from cycles before and after the stiffness check transition. As the actuator slows from a 3-Hz to a 0.1-Hz frequency, a ¾ amplitude cycle was executed to smooth the load transition. These ¾ amplitude cycles, which appeared as spikes in the

data, were counted as cycles (about 500 for the entire test).

Strain data variation (scatter) can generally be attributed to slight variations in load due to dynamic effects. The data scatter seen in Figures C.9 and C.12 was likely due to poor strain gage solder connections.

## 5.20 Post Mortem Inspection

NREL staff preformed a post-mortem inspection of the test article on May 9, 2001. They sectioned the blade in the failure region 93 in from the root. Chordwise section cuts at 22.6 in (16% span), 31.4 in (21% span), and 41.6 in (27% span) from the root of the blade exposed the blade for inspection.

Figure 5.39 shows a cross-section of a spanwise cut through the failure region. The tip of the blade is to the left and the top surface is the compression-side failure region. The spanwise cut, shown in this figure, is 5.5-in from the leading edge. Buckling failure caused the void in the foam near the compression skin, whereas the void near the tension skin was there before failure. Note that the failure region was immediately outboard of a laminate ply-drop.

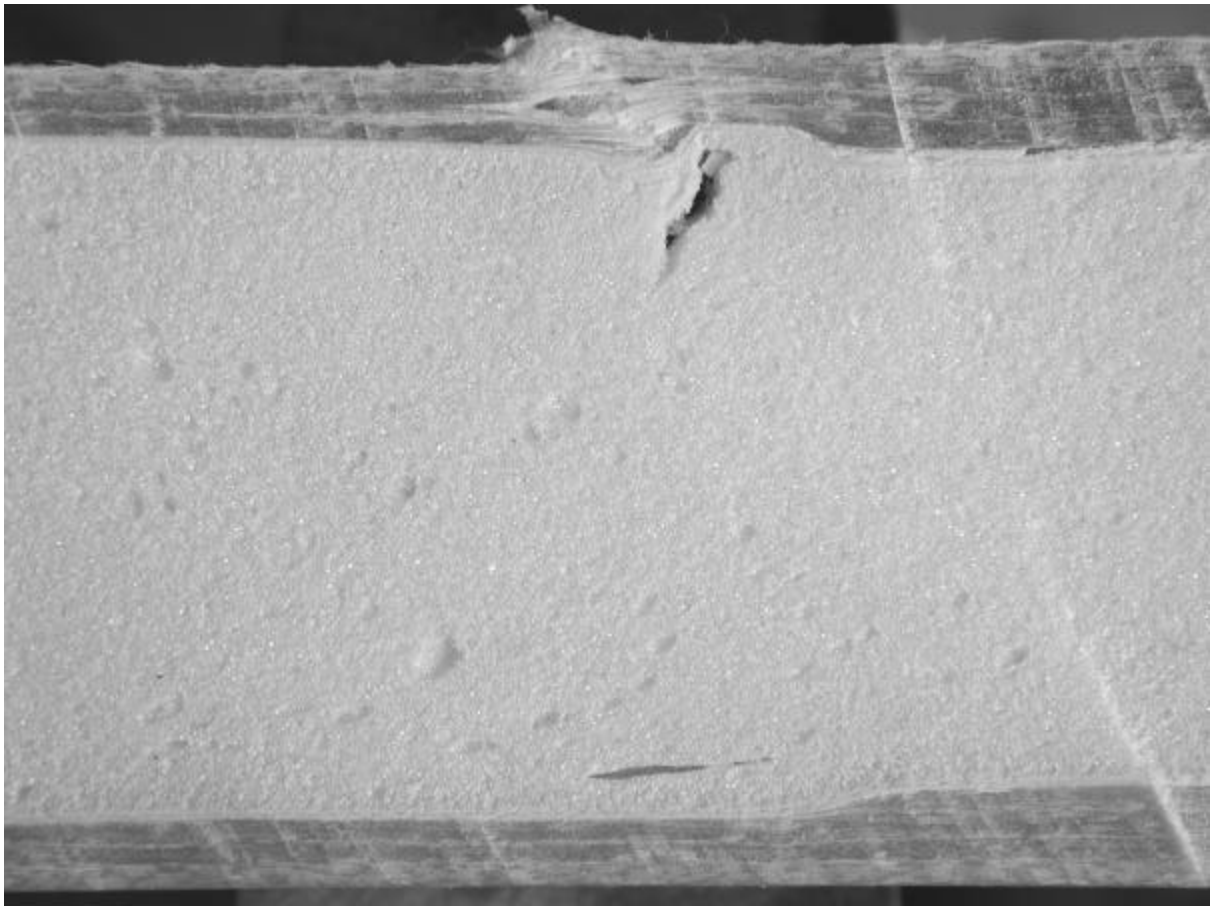

**Fig. 5.39 - Spanwise section photograph of failure region**

Figure 5.40 shows a cut airfoil section 22.6-in from the root of the blade (16% span). The high-pressure side is on the bottom of the photograph. The figure shows the cracks where the foam/skin separation occurred on both the high and low-pressure surfaces. The cracks were enhanced with a permanent marker to make the cracks more visible. The arrows indicate the start and end of the cracks. The crack on the high-pressure skin is about 7-in long and the crack on the low-pressure side is about 4-in long.

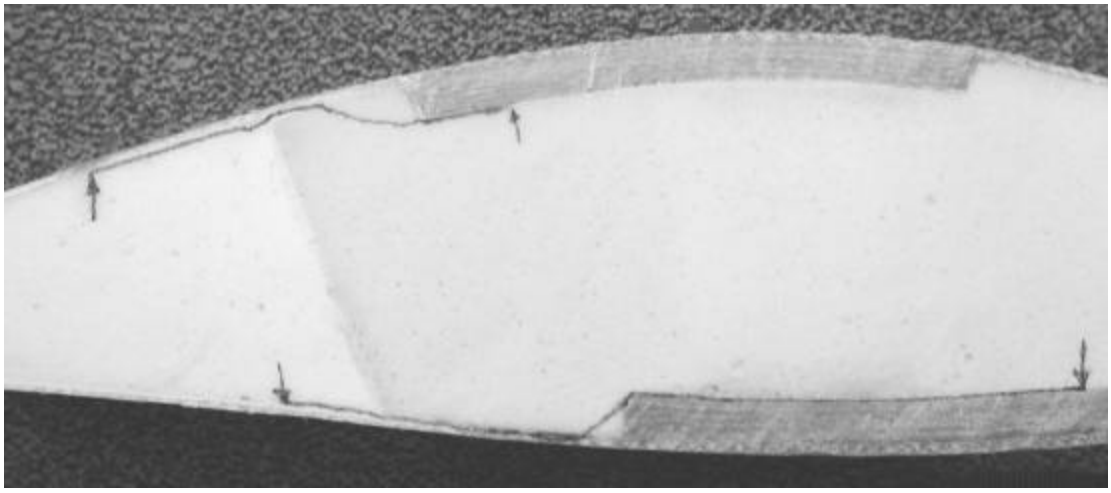

**Fig. 5.40 - Cut airfoil section at 16% span**

Figure 5.41 shows the cut airfoil section 31.4-in from the root of the blade (21% span). This crack runs through the foam in the leading edge section, but does not reach either the high-pressure or the low-pressure skins. The crack has been enhanced with a permanent marker. The damaged strain gage visible on the top skin in the Figure 5.41 is gage 21S13LA.

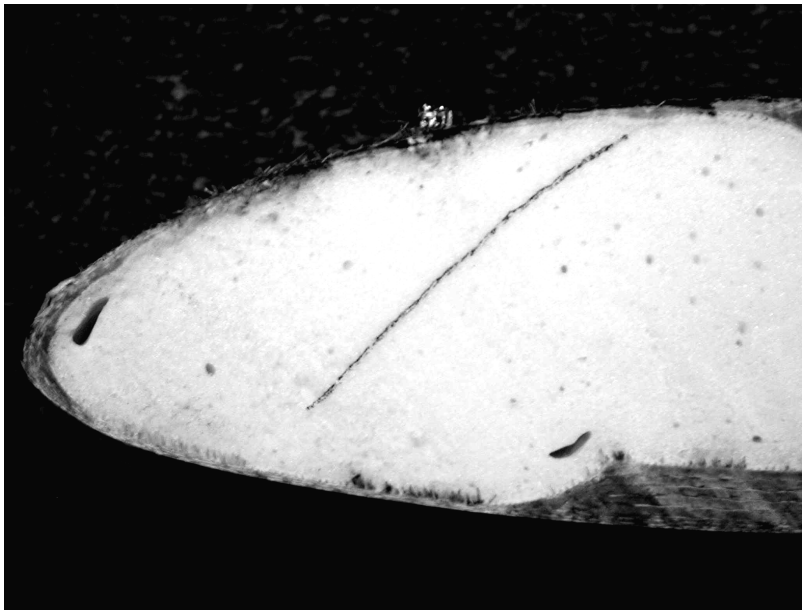

**Fig. 5.41 - Cut airfoil section at 21% span.**

Results from the post mortem indicated there were regions where the laminates had de-bonded from the foam core (or experienced foam failure near the skin/foam interface), notably at 16% span. Coin tap tests and visual observations of non-linear panel movements revealed de-bonding in this region during the test,

## 5.21 Conclusions

Due to the blade failure, the fatigue test concluded at cycle 2,739,100. The blade failure was a compression fatigue failure of the spar cap at a ply-drop located 93.25 in from the blade root. The failure occurred 739,100 cycles into the third load block of 346 lbf / 34.6 lbf. This failure region began delaminating several thousand cycles before the final failure, starting in the spar cap region.

Large regions of the blade root exhibited separation of the foam core from the skin during the course of the test, but were still able to carry the test loads at the time of failure. Damage in these regions was propagating during the test and could have progressed to a less benign state.

The fatigue load spectrum used for this test used non-conservative assumptions about the turbine cutout wind speed and turbulence environment. Therefore, no conclusions about the suitability of this blade to survive the operating loads on any specific turbine may be drawn.

# 6.0 BMI Field Test

## 6.1 Test Objective

**The purpose of the Field Test was to obtain data to verify blade performance and structural integrity**.

Acting upon the recommendation of WTI, FMI made arrangements with the Pacific Energy Conservation Services of Kamuela, HI[23] for the use of two of their production turbines to test prototype blades on operational turbines. These turbines are located on the Lalamilo Wind Farm in Hawaii County, HI. This is an established field with 60 installed Jacobs 17.5kW and 20kW turbines with 1,087.5kW of production capacity. It was our intention, with assistance of Lalamilo Wind Farm personnel, to install and calibrate instrumentation, operate the turbines and conduct testing as described in the test plan. Unfortunately, FMI was unable to complete the structural integrity test called for in the test plan and due to conditions beyond our control, unable to gather wind data in a timely manner. Combinations of equipment failures and wind conditions delayed and then precluded our ability to measure operational data such as cut-in and furling wind speeds, power data, and other measurable data. This report does not include any data collection event or any such other wind data.

## 6.2 Field Test Plan

FMI submitted the field test plan, [Ref 15, 17, 18, 19, 20] to Sandia for approval as contractually provided for in the BMI Statement of Work. The test plan followed details and tasks outlined in the Mechanical Loads Test Report [Ref 16]. FMI field test engineers made specific modifications to accommodate the mechanical requirements of the Jacobs 29-20 turbine and the geographic layout of the Lalamilo site.

## 6.3 Field Test

In June 2000, FMI shipped three BMI prototype blades and support test equipment to Hawaii for subsequent attachment to the project test turbine.

Per the test plan, FMI technicians bonded load sensors and quarter-bridge strain gauges to one blade. Then they attached instruments to gather blade performance data such as blade bending. A radio telemetry system transferred data from the rotating hub to a transducer placed in the turbine controller to monitor power output. Hub position and rotor speed sensors attached to the main shaft gearbox also collected and transmitted additional data.

[23]The Lalamilo Wind Farm is owned by Pacific Energy Conservation Services, P.O. Box 2195 - Puako Mauka, Kamuela, HI 96743. The field contact is Willard B. Dill, Supervisor, Lalamilo Wind Farm, 808-882-7315

Technicians also instrumented a second and identical turbine equipped with a baseline rotor baseline rotor to measure wind and energy performance and to provide comparative wind data and power generation data.

As prescribed in the test plan, technicians erected several meteorological sensors. These included a calibrated cup-style anemometer to measure wind speed, a wind vane sensor to report wind direction, an absolute pressure transducer to gather air pressure data and an ambient 3-wire resistive temperature device to provide air temperature.

Instrumentation acquired and recorded raw data from data acquisition modules, stored it as an ASCII record, then read and processed it using CRUNCH-GPP[24], Version 6 software. These files are records of analog voltages, digital and pulse channels in ASCII format. During processing, these files generated a series of graphs showing the response of the turbine to a variety of winds and operating conditions. Air density and low speed shaft speed provided additional data values.

From the collected data, FMI expected to produce a series of data reports, among them were; Azimuth Averaging Results, Power Spectral Density Results including Blade Flap and Blade Edge Bending and Cycle Counting Results. In addition we expected to obtain Type A and Type B uncertainty analysis results.

Table 6.1 details the instrumentation of the Jacobs 29-20 turbines, and information specific to the Jacobs 29-20 Turbine is given in Table 6.2.

**Table 6.1 - Test Equipment List**

| Parameter | Units | Instrument | Location | Range +/- V | Excit. V | Freq. Hz | Mfgr. | Model No. |
|---|---|---|---|---|---|---|---|---|
| Blade Flapwise Bending | Strain | ¼ bridge straingage | Blade | 1 - 5 | 5 | 40 | PR | 2262 |
| Blade Chordwise Bending | Strain | ¼ bridge straingage | Blade | 1 - 5 | 5 | 40 | PR | 2262 |
| Wind Speed | m/s | Anemom. Maximum | Turbine Tower | 1 - 5 | | 40 | PR | 2212 |
| Wind Direction | Deg. | VWindvane Maximum | Turbine Tower | 1 - 5 | | 40 | PR | 2202 |
| Air Pressure | kPa | Pressure Sensor | Turbine Tower | 1 - 5 | | 40 | | 700-1200 |
| Air Temperature | $^0$C | PT 100 | Turbine Tower | 1 - 5 | | 40 | PR | 2203 |
| Power Output | kW | Watt Transduc. | Controller | 1 - 5 | | 40 | | |
| Hub Position | Deg. | 1000 puls. Inductive | Mainsh/belt | 1 - 5 | | 40 | PR | 2214 |
| Rotor Speed | rpm | 1000 puls. Inductive | Mainsh/belt | 1 - 5 | | 40 | PR | 2212 |

[24] CRUNCH-GPP Software, NWTC, LF24 991229 Test Plan Template, R.Santos , Harold Link.

**Table 6.2 - Test Turbine Configuration and Operational Data, [Ref 14]**

| **General Configuration:** | |
|---|---|
| Make, Model, Serial Number | Jacobs 20-29 kW |
| Rotation Axis (H / V) | Horizontal |
| Orientation (upwind / downwind) | Upwind |
| Number of Blades | 3 Blade |
| Rotor Hub Type | |
| Rotor Diameter (m) | 8.84 m |
| Hub Height (m) | 36.6 m |
| **Performance:** | |
| Rated Electrical Power (kW) | 20kW |
| Rated Wind Speed (m/s) | |
| Cut-in Wind Speed (m/s) | 3.6 m/s |
| Cut-out Wind Speed (m/s) | 12.2 m/s |
| Extreme Wind Speed (m/s) | 34 m/s |
| **Rotor:** | |
| Swept Area ($m^2$) | 61.36m² |
| Minimum On-line Rotational Speed (rpm) | 90 rpm |
| Maximum On-line Rotational Speed (rpm) | 175 rpm |
| Coning Angle (deg) | |
| Tilt Angle (deg) | 12 deg. |
| Blade Pitch Angle (deg) | |
| Direction of Rotation | Counter Clock Wise |
| Power Regulation | |
| Overspeed Control | Blade actuated governor |
| **Drive Train:** | |
| Gearbox Make, Type, Ratio | Off-set hypoid, gear drive 1:6.1 |
| Generator: Make, Type, Speed, Voltage, Frequency | Winco, brushless 3-phase synchronous,1067.5 rpm<br>0-180 volt AC @ 0-45Hz |
| **Braking System:** | |
| Parking / Service Brake: Make, Type, Location | Manually operated disk type |
| Normal Shutdown Brake: Make, Type, Location | |
| Emergency Shutdown Brake: Make, Type, Location | |
| **Yaw System:** | |
| Wind Direction Sensor | None (tail vane) |
| Yaw Control Method | Dual fold tail vane |
| **Tower:** | |
| Type | 3-leg, free standing, galvanized steel |
| Height (m) | |
| **Control / Electrical System:** | |
| Controller: Make, Type | |
| Power Converter: Make, Type | Master mind, energy phase |
| Logic System | |
| Monitoring System | |
| Electrical Output: Voltage, Frequency, Number of Phases | 0-165 VAC, 0-45 Hz, single phase |

## 6.4 Site Map and Description

Lalamilo Wind Farm provided the layout of the Wind Farm location (Fig 6.1).

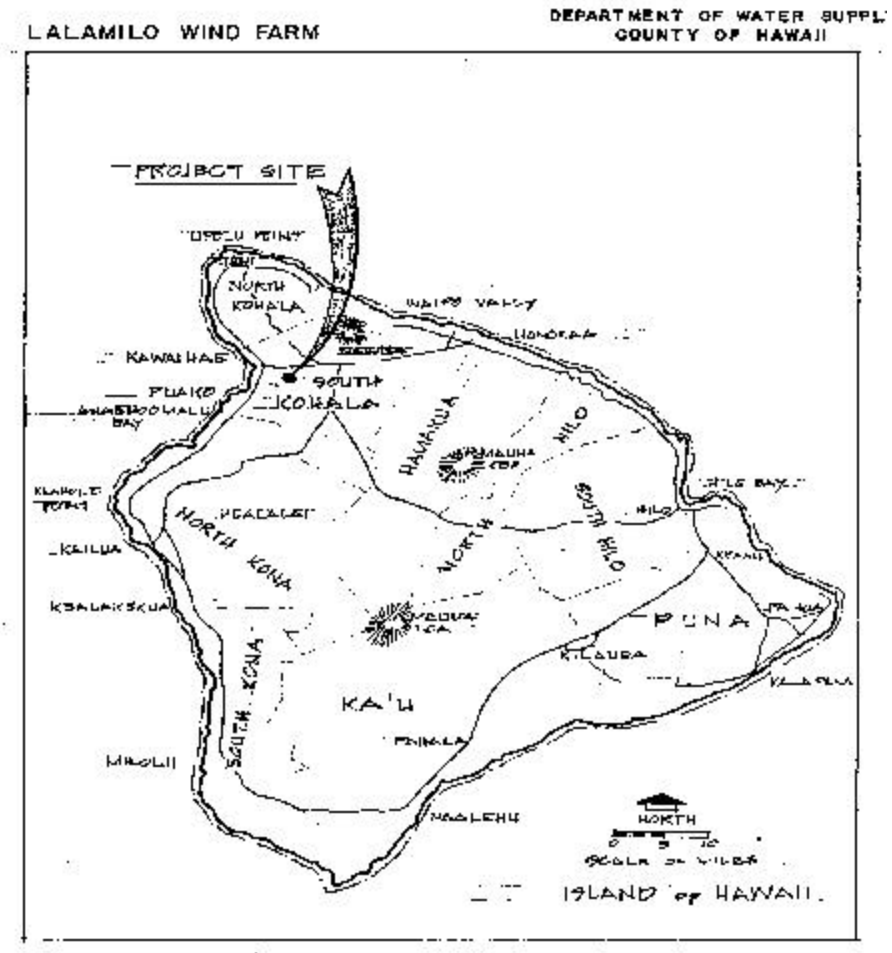


**Fig. 6.1 - General Location Plan**

## 6.5 Field Test Results

*After extensive effort by both FMI contractors and Pacific Energy personnel over nearly 10 months, all efforts to gather any significant data of either test loads or wind energy production were abandoned. This report does not contain, nor can it substantiate, any claims of blade load characteristics gathered under field conditions or any claims of energy production as a result of real world tests.*

It may be instructive to briefly review a variety of the problems FMI field technicians and the Lalamilo field service representatives encountered in their attempt to instrument and measure various data collection segments.

Trade winds at this site seem to vary from nearly nothing during the winter to very strong during the rest of the year, occasionally interrupted by severe storm conditions. There are very few light wind days. Since late spring of 2000, higher- than- predicted winds at the Hawaiian site complicated the installation and testing process. The Jacobs turbines, mounted on 36.6m (122 feet) towers, necessitated the use of a high crane in calm winds to service the equipment. From the very first effort, wind conditions caused delay after delay.

A second problem concerned attaching recording instrumentation to the turbine in a manner that would provide accurate data collection. The configuration of the hub yields very few useful surfaces for instruments and radio transmitters. As a result, the technicians had to improvise. Once strain gages were attached to the test blade, the technicians waited for an opportunity to lift the rotor and waited for calm winds to zero the instrumentation. Fine-tuning and adjustments also awaited favorable conditions.

The Jacobs turbine employs several features to either hold the rotor into the wind or take the rotor out of the wind when indicated. (See Appendix A.) As wind speed increases, a mechanical furling device feathers the rotor and swings the tail vane to position the rotor out of the wind. With the original rotor in place, this process works well. However, as wind approaches cut-out speed, the furling device releases and the turbine increasingly yaws back and forth until either the rotor pitched out of the wind or the wind velocity decreased. Yaw activity is continually episodic on “good wind” days as the rotor nears maximum power output.

One unexpected consequence of the BMI prototype blade design was that this yaw activity started at a much lower wind speed than with the baseline blades. Unfortunately, it also occurred at a less than “best power” rotor rotational speed. We now believe that the new blade put a greater surface area into the wind and that the furling device compensated for the increased torque by working as designed.

Lalamilo personnel used wire cable to tie the tail vane and hold the rotor into the wind. A more satisfactory fix was to increase the tail vane area to overpower the furling device and the yaw event. When lower winds in mid-December allowed turbine maintenance, Lalamilo field technicians fabricated and installed a larger tail vane. We have since learned that changes to the tail vane failed and were, in themselves, insufficient to hold the rotor into the wind. In fact, the tail vane suffered a mechanical failure once it encountered stronger than anticipated winds.

Because the field test represents an important segment of the BMI Statement of Work, we have made continued efforts to collect significant data for this report. These efforts were to no avail. On March 19, 2001, we discontinued any attempt at data collection and shortly thereafter, removed the test equipment from the turbines and from the site.

# 7.0 Project Findings and Conclusions

The scope of this project focused on the concept of advancing the fabrication process of wind turbine blades in ways to lower blade costs and improve their quality and reliability.

## 7.1 Blade Design and Fabrication

FMI determined a set of ideal design parameters based on the early decision to prototype the Jacobs 29-20 turbine and to characterize a rotor for a generic 20kW turbine. The following parameters describe both design limits and the finished product.

- 4.42 meter blade root to tip
- Linear tapered planform
- Soft stall regulated
- Blade weight, 27.2-kilogram approx. (60 pounds)
- Low noise
- Low blade displacement in Hurricane Class II wind
- Specifically designed flat surface root section

We thus can conclude;

- *The FMI manufacturing process replicates the exact blade design. A blade can be fabricated to meet a variety of loading conditions as dictated by turbine or environmental demands and with internal features such as operational tip brakes, imbedded de-icing materials or other fittings as required.*
- *Blades are net molded with a high reproducibility relative to the tool and to the master blade design that described the tool.*
- *The finished product is a monolithic structure with no bonded joints.*
- *Blade replication is nearly identical from one part to the next. Production blades weights should be within 200 grams.*
- *Only a 204 gram weight difference existed between three blades fabricated for field test, (before adding Jacobs attachment plate modifications and paint).*

  Blade # BT10740 27.670 kilograms

  Blade # BT10806 27.535 kilograms

  Blade # BT10805 27.466 kilograms

- *Low touch labor and lean manufacturing techniques are key contributors to both quality control and lower manufacturing overhead.*
- *FMI can substantially decrease tool cycle time and increase productivity by introducing automated controls for materials handling, tool mechanicals and tool temperature controls.*

- *Implanting internal heating and cooling in the molding tool to control cure time and reduce cycle time may increase both the quality of the product and the number of production turns.*
- *The FMI process is environmentally friendly. Minimal quantities of volatile organic compounds (VOC) are released into the atmosphere during the fabrication cycle.*
- *Detail work instructions document each fabrication and inspection step. FMI is ISO 9001 certified which requires the maintenance of detailed documentation of each task on the manufacturing and inspection process.*

## 7.2 Cost Reductions Identified

This project identified several elements of cost reduction attributed to the FMI blade fabrication process.

- *Low touch labor, fast cycle production time, low cost raw materials, good surface finish and the incorporation of lean manufacturing techniques.*
- *Near perfect blade replication from one part to the next reduces on-site installation costs. Production blades will be within a few grams of the same weight and within a few millimeters of balance.*
- *Additional cost reduction contributions are expected as a result of reduced blade maintenance costs and extended blade useful life.*

## 7.3 Marketing

There seems to be little movement among the small turbine manufacturers as it pertains to a universal design of blades and rotors. We could expect substantially reduced rotor costs if a common rotor family capable of powering a number of turbine models were to emerge. This is the basic model as used in large wind where only a few blade manufacturers enjoy market share across a wide spectrum of turbine manufacturers. Moreover, the many small turbine companies who use in-house or captive blade manufacturing facilities make entering into the small wind market difficult.

A rotor sold in sufficient volumes to take advantage of manufacturing efficiencies and positioned to power a number of competing turbines would have compelling marketing appeal. FMI sees an opportunity in that niche. FMI intends to persist in the wind industry so long as the opportunity for small wind appears profitably feasible.

## 7.4 Future Work

Opportunities exist for the manufacture of utility grade turbine blades. Much of FMI's technology has direct application when considering the construction implications of rotors in the greater than 40 meter range. Nothing in this paper specifically addresses scaling up to large blades; however, additional

research and testing may identify FMI technology applications.

We are confident that FMI can significantly contribute talent, energy and expertise to the many projects now underway to further the development of an efficient domestically manufactured utility grade rotor.

## 7.5 Conclusions and Recommendations

- *This iteration of the FMI manufacturing approach appears to deliver a long-lived small wind blade capable of withstanding a Class II hurricane wind event.*
- *The FMI manufacturing strategy replicates the exact blade design. It can be fabricated to meet a variety of loading conditions as dictated by turbine or environmental demands and with internal features such as operational tip brakes, imbedded de-icing materials or other fittings as may be required. It is lightweight and durable.*
- *Within certain limitations, these modifications may also include blade weight and/or blade stiffness.*
- *As a conservative estimate, it seems likely that FMI wind blades using BMI prototype blade manufacturing techniques could be economically scaled from as small as 3 meters to perhaps 12-16 meters in length without manufacturing or weight penalties. Because of the variety of lamination materials available to its designer, the FMI blade is ideally suited for the 10-85kW wind turbine sited in difficult locations. Sites where occasional high winds jeopardize blade durability or sites located in extreme climatic conditions are ideal candidates.*
- *The FMI manufacturing process may have direct application to production of utility grade rotors, rotors in the greater than 80 meter rotor range. Additional research and testing in this arena may mandate eventual application of FMI technology.*
- *The BMI Prototype blade is ready for production. This design, both aerodynamically and structurally, could be of significant value to a turbine manufacturer when matched with a turbine capable of capitalizing on its characteristics. Design collaboration between FMI and an enterprising turbine engineer holds strong promise for an efficient, low cost and durable small wind energy product.*
- ***The BMI Prototype blade cannot be characterized as a replacement blade for the Jacobs 29-20 turbine. The blade could be a key component of a Jacobs 29-20 turbine reconfiguration or upgrade if certain structural and control changes are incorporated to support the increased power produced by the prototype blade. This reconfiguration may, or may not, be economically justified.***

# Appendix A Baseline Blade

## A.1 Jacobs 29-20 Technical Specifications

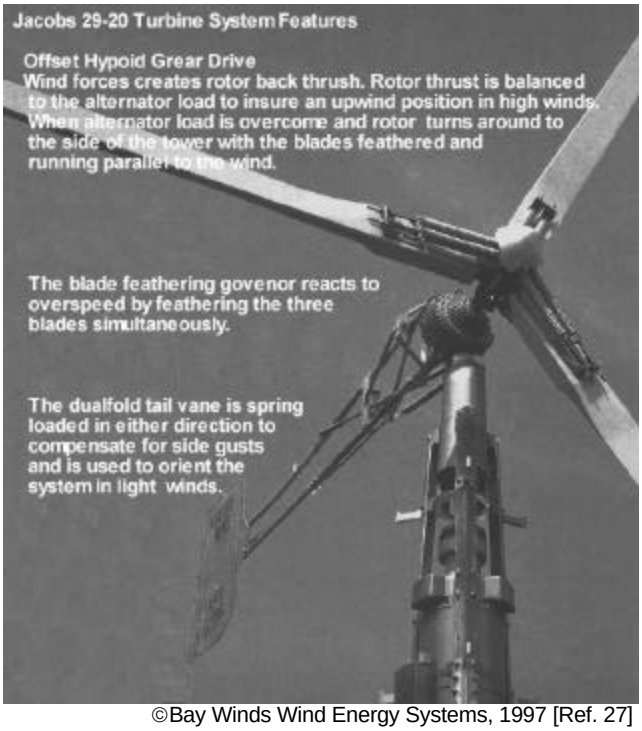




**Fig. A.1 - WTI Jacobs 29-20 Turbine and Rotor**

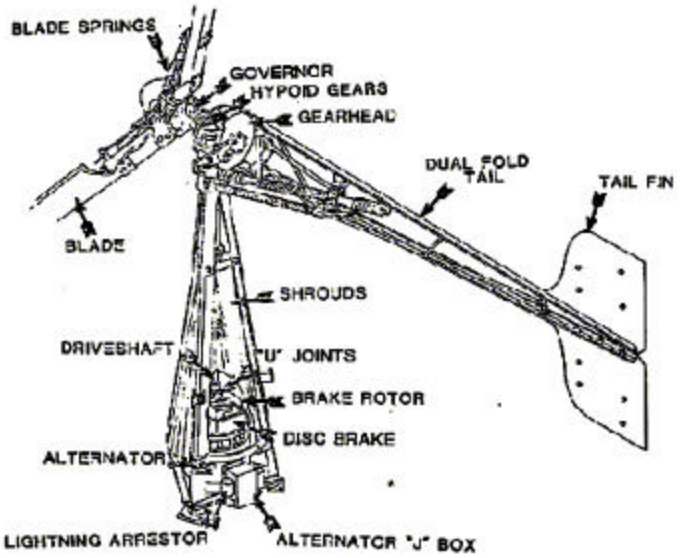


**Fig. A.2 - Jacobsä Power System Cutaway Drawing of Power System Features**
(Reprint © 1981 Jacobs Wind Energy Company, Minneapolis, MN; [Ref. 28].

## A.1.1 WTI Sales Literature

***JACOBS POWER SYSTEM FEATURES:*** *The Jacobs Power System consists of three key elements: an Inclined Hypold Gear Drive, a Powerhead using our Blade Actuated Governor, and an Automatic Storm Protection Control on the Folding Tail vane. By using the Inclined Hypoid design, our Powerhead is close to the tower. This allows the propellers to pass above and behind the tower center. The Powerhead can quickly turn about the tower center as turbulent storm gusts strike. Violent wind direction changes are inherent in storms and the free turning Jacobs'- Wind Energy System has a design based on our 50 years' experience in minimizing storm damage potential to Wind Systems. Power System weight is also a major factor in designing long-lived Wind Systems. Our new Jacobs Wind Energy System has greatly reduced the free turning weight on the lower cap by mounting the heavy alternator down in the tower. The weight of the Power System that Is free to track the wind is under 500 pounds. This is less than that of our older designs, where the generator was mounted above the tower, even though our new systems have over three times greater output capacity.*

***HYPOID GEAR DRIVE SYSTEM****: Cutaway of Gear Case shows the Off-Set Hypold Gear Drive System (patented), which balances gear torque against propeller back thrust pressure to give a steady equalized power delivery to the alternator. Note that the drive pinion is at the top of the gear case, preventing oil drag power losses. The sealed tube below the pinion encases the drive shaft. By eliminating any oil seal at the bottom of the gear case, oil can never leak out of the case and destroy the gears. Designed for long life and trouble free operation, the Inclined Hypoid Gear Drive (patented) has wide spaced propeller hub bearings to withstand storm induced stresses. Short-coupled bearing shafts, common on many interior wind systems can wear allowing the propellers on such systems to spring and flop around after a few years. The Jacobs designed Gear Drive is made to operate year after year with no bearing maintenance.*

***BLADE ACTUATED GOVERNOR:*** *Our newly patented Blade Actuated Governor has a simple, failsafe design that improves on the governor that has already been field proven on Jacobs equipment since the early 1940's. Thousands of our Blade Actuated Governors have powered remote pipeline cathodic protection systems all over the world. Thousands more since 1950 have powered Jacobs Wind Energy Systems for remote farms and ranches worldwide. Note that there are no complicated electric or hydraulic governor systems to fail with Jacobs Energy Systems, as are common on most newly designed Wind Energy Systems. Any Wind System propeller speed control method that does not turn all the propeller blades to regulate the speed cannot withstand high winds or storms without severely stressing the propeller and tower support systems. Jacobs Wind Energy Systems have led the industry in simplicity of design since we started the mass production Industry for consumer sized wind electric plants fifty years ago.*

***AUTOMATIC STORM PROTECTION CONTROL:*** *The Spring Snubber Control on the folding tail vane automatically folds the Powerhead and Gearbox around to the side of the tower in winds over 40 MPH. This simple and automatic folding system requires no electric or other complicated controls that can fall or cause maintenance problems. System output is maintained, even in storms. Properly designed wind systems do not need to "Shutdown" in high winds. Our pipeline wind plant systems in service since the 1930's never had the luxury of human supervision or shutdown controls. Automatic Shutdown controls presume a slowly increasing wind. Storm gusts, however, can occur almost instantaneously, before most manual or automatic controls have time to shutdown a Wind System or crank it out of the wind. These high wind gusts can instantly apply thousands of pounds of pressure that can strain or wreck the plant or the tower. The free turning automatic Jacobs Storm Protection Control, when coupled with our Blade Actuated Governor, prevents wind pressure stress on the Powerhead and tower from exceeding that of a 40± MPH wind. These design and construction features are the result of 50 years of experience in controlling propeller systems In storms. All Jacobs features are covered by current and pending patents.*

*ã1981 Jacobs Wind Energy Systems [Ref. 29]*

**Table A.1 - Jacobs 29-20 Turbine Specifications**

24-37m mast

8.8m rotor diameter

Output @ 10m/s 10.6 kW

Optional tiltable tower

Cut in speed 3.6m/s 8 mph

Survival wind speed 54m/s

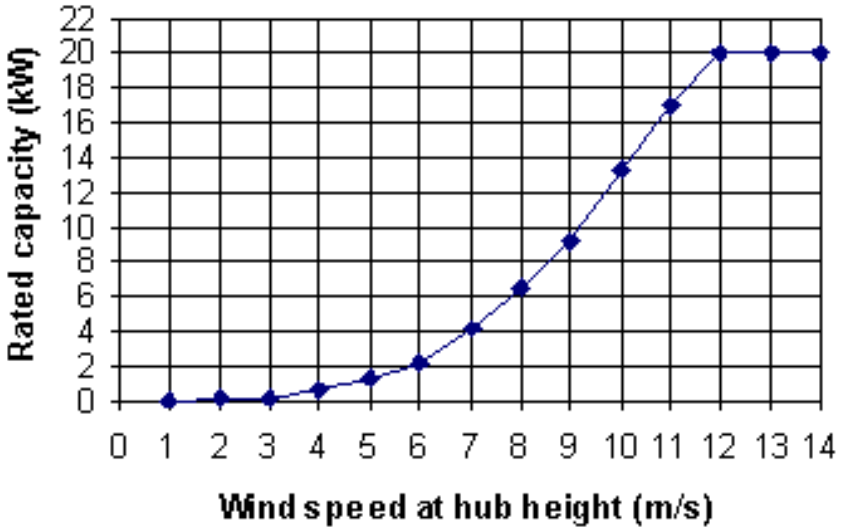


©Galeforce.uk.com, [Ref. 28]

**Table A.2 - Annual Power Output Estimate**

| Wind Speed mph/mps | Estimated Performance Output (kWh/y) |
|---|---|
| 10/4.47 | --19727 |
| 11/4.92 | --25704 |
| 12/5.36 | --32297 |
| 13/5.81 | --39289 |
| 14/6.26 | |

--46468

15/6.7
--53646

16/7.15
--60665

17/7.6
--67398

18/8.05
--73743

All outputs are based on Rayleigh Distribution, outputs will vary based on tower height!

## A.1.2 Baseline Blade Physical Characteristics

From various sources [Refs.1- 4], information on the baseline 20-kW Jacobs 29-20 turbine blade was gathered for the purposes of aerodynamically modeling the rotor. These parameters are listed in Table A.3 below. Many of these values were used as constraints in the design trade studies that are presented in the sections following this section.

**Table A.3 - Various Parameters for the Jacobs 20-kW Turbine**

| | |
|---|---|
| General rotor configuration | Upwind<br>3 blades<br>Passive dual-fold tail vane for yaw control<br>Automatic furling (blade actuated governor)<br>Offset hypold gear drive (1:6.1) |
| Blade diameter | 8.839 m<br>(29 ft) |
| Hub dia (non-aerodynamic region) | 1.77 m<br>(5.81 ft)<br>0.20 R |
| Blade chord and twist | (see figures) |
| Airfoils | Hub: Flat plate<br>50% radius: USNPS6 (19.9% thick)<br>90% radius: USNPS5 (15.9% thick)<br>Tip: USNPS4 (12.0% thick) |
| Airfoil performance data | USNPS4 (tip) from UIUC wind tunnel test data (Ref. 5)<br>Inboard stations synthesized from experimental data on USNPS4 |
| "Rated" rotor speed and wind speed | 175 rpm @ 26 mph |
| Reynolds number | 825,000 (75% station)<br>for a wind speed of 16 mph |
| Blade pitch | 3.53 deg @ 75% station<br>(E.E.S.I. engineering drawing, 1985, Ref. 2) |
| Maximum generator (output) power | 20 kW |
| Maximum rotor power | 23.53 kW<br>(based on known rated power and estimated efficiency) |
| Generator efficiency | 85% (estimate) |
| Cone angle | unknown, 0 deg used |

The wind-regime parameters listed in Table A.4 represent a **standard** reference site used by NREL. The defining parameters lead to an average wind speed of 15.09 mph for the Jacobs turbine on a 100-ft tower. This wind speed will be used for making the annual-energy comparisons to be discussed later.

**Table A.4 - Wind Regimes Considered**

| | |
|---|---|
| **Average wind speed** | **5.4 m/s @ 10 m height (12.08 mph @ 32.81 ft) as per standard reference site used by NREL.** |
| **Wind shear exponent** | **0.2** |
| **Weibull K** | **2** |
| **Average wind speed at hub height** | **6.748 m/s @ 30.48 m (15.09 mph @ 100 ft)** |

Figures A3 – A5 shows the airfoils, chord and twist distributions, respectively, that were used in modeling the Jacobs blade geometry. The "twist" distribution is that taken from the E.E.S.I. engineering drawing [Ref. 2]. This distribution includes the blade pitch. The modern standard convention with wind turbines is that the blade pitch is referenced to the 75% station at which location the blade twist is zero. Based on this convention, the blade pitch is 3.53 deg (the original twist at the 75% station). In the blade design effort, the blade pitch and twist will follow the standard convention of setting the twist to zero at the 75% station.

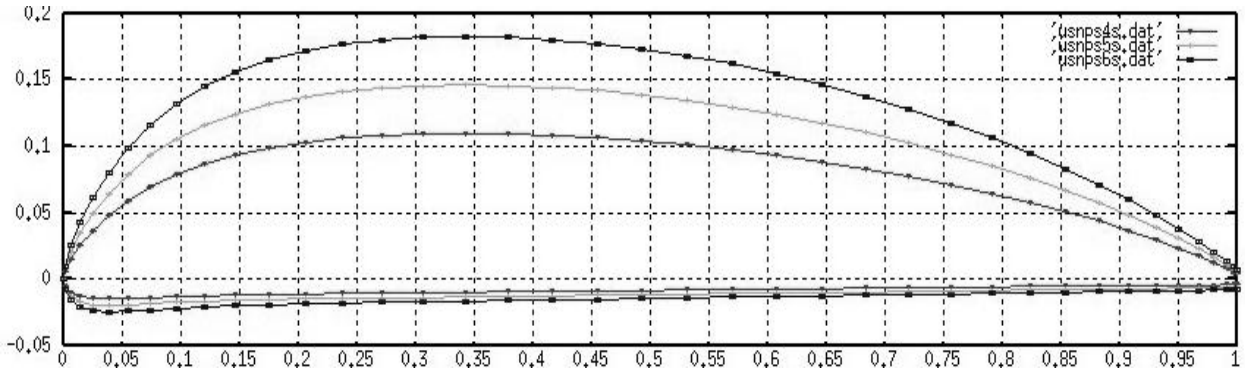


**Fig. A.3 - USNPS airfoils used along the blade span (to scale)**

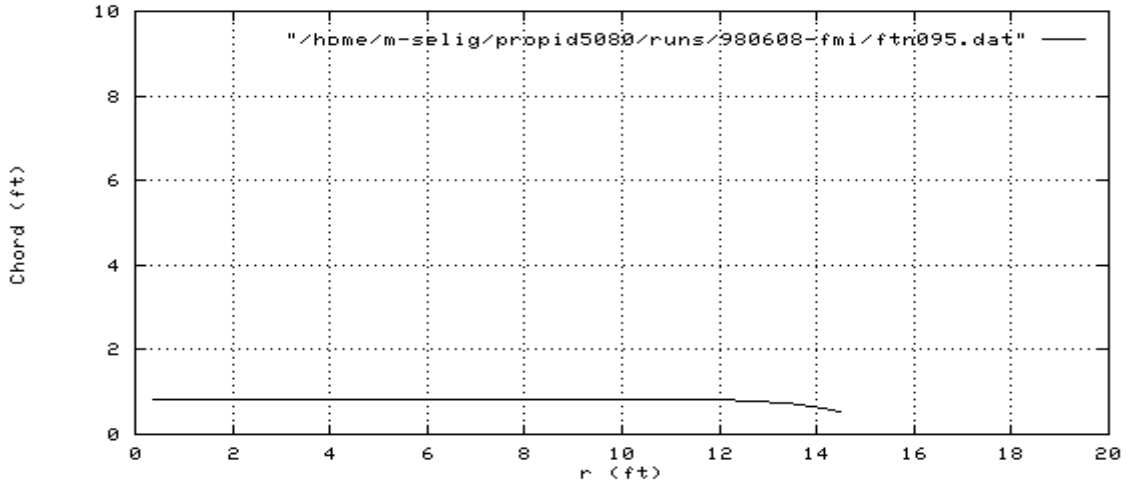


**Fig. A.4 - Jacobs 29-20 chord distribution**

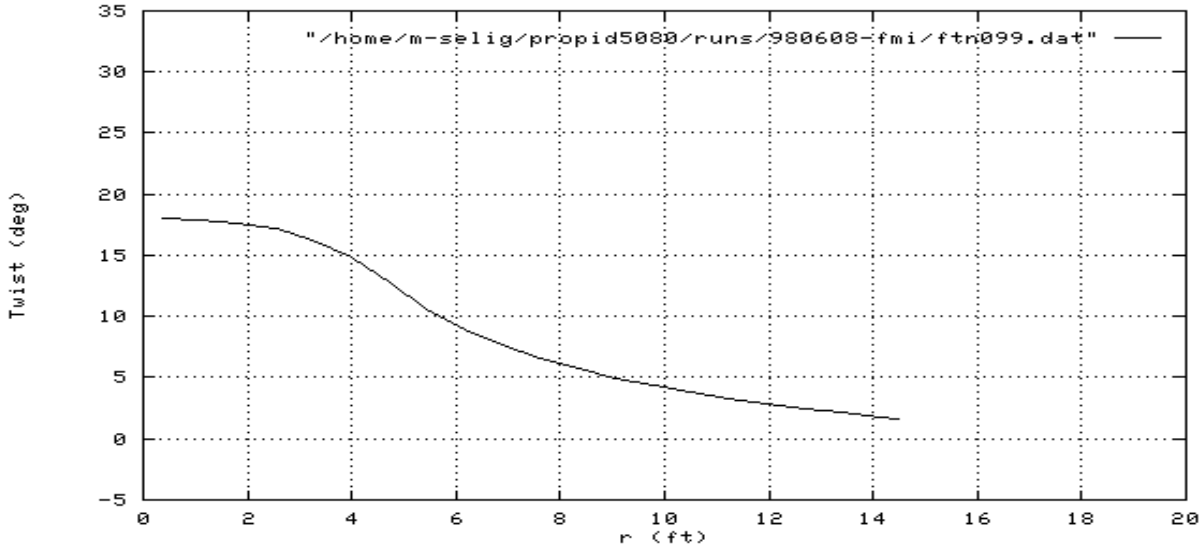


**Fig. A.5 - Jacobs 29-20 twist distribution**

The blade shape design and analysis process was carried out through the use of the PROPID computer program [Ref. 6]. This code includes both inverse design and direct analysis capabilities. The analysis module of the code is based on the PROP program, which is widely used for its accuracy in predicting wind turbine rotor performance. The design capability of the code allows for the prescription of desired aerodynamic characteristics from which the corresponding blade shape is determined.

# Appendix B Static Test[25]

**Table B.1 - Data Acquisition test equipment**

| ITEM | MODEL | SERIAL NUMBER |
|---|---|---|
| COMPUTER | GATEWAY G6-400MHz | 12453836 |
| A/D BOARD | NI PCI-MIO-16XE-10 | 0xA85558 |
| CHASSIS | NI SCXI-1001 12 SLOT | 1977 |
| SLOT #1 SIGNAL CONDITIONING MODULE | NI SCXI-1121 4 CHANNEL | 2312 |
| SLOT #2 SIGNAL CONDITIONING MODULE | NI SCXI-1121 4 CHANNEL | A6A451 |
| SLOT #3 SIGNAL CONDITIONING MODULE | NI SCXI-1121 4 CHANNEL | A6A44E |
| SLOT #4 SIGNAL CONDITIONING MODULE | NI SCXI-1121 4 CHANNEL | A6A44B |
| SLOT #5 SIGNAL CONDITIONING MODULE | NI SCXI-1121 4 CHANNEL | A6A46A |
| SLOT #6 SIGNAL CONDITIONING MODULE | NI SCXI-1121 4 CHANNEL | 2263 |
| SLOT #1 TERMINAL BLOCK | NI SCXI-1321 4 CHANNEL | 1492 |
| SLOT #2 TERMINAL BLOCK | NI SCXI-1321 4 CHANNEL | 1470 |
| SLOT #3 TERMINAL BLOCK | NI SCXI-1321 4 CHANNEL | 1478 |
| SLOT #4 TERMINAL BLOCK | NI SCXI-1321 4 CHANNEL | A6A539 |
| SLOT #5 TERMINAL BLOCK | NI SCXI-1321 4 CHANNEL | A6A53B |
| SLOT #6 TERMINAL BLOCK | NI SCXI-1321 4 CHANNEL | 1466 |
| BLADE INTERFACE BOX #1 | NREL SPECIFIC | 03 |
| BLADE INTERFACE BOX #2 | NREL SPECIFIC | 09 |
| BLADE INTERFACE BOX #3 | NREL SPECIFIC | 06 |
| LOAD CELL | LEBOW 5-KIP MOD. 3187-5K | 2827 |
| OUTBOARD STRING POT | PATRIOT MOD. P-40B(A56) 40" RANGE | 19540 |
| INBOARD STRING POT | UNIMEASURE MOD. PA-30 30" RANGE | 29070305 |
| TIP DEFLECTION LINEAR TAPE MEASURE | NREL SPECIFIC | NREL-9 |
| SINGLE ELEMENT STRAIN GAGES | MICROMEASUREMENTS CEA-13-250UW-10C | LOT R-A55AF11 |
| ROSETTE STRAIN GAGES | MICROMEASUREMENTS WK-09-250RD-10C | LOT DJ-K47FE02 |
| PLATFORM SCALE | PELOUZE MODEL 4010 125-LB CAPACITY | 1136183 |
| LOAD CELL (TARE MEASUREMENT) | TRANSDUCER TECHNIQUES 2-KIP MOD. SWO-2K | 87257 |

| MODAL SURVEY HARDWARE | | |
|---|---|---|
| **ITEM** | **MODEL** | **SERIAL NUMBER** |
| DYNAMIC SIGNAL ANALYZER | HEWLETT-PACKARD | 3431A01613 |
| ACCELEROMETER CHARGE AMPLIFIERS | PCB MOD.480C06 , X10 AMPLIFICATION | 648, 642 |
| FORCE HAMMER CHARGE AMPLIFIER | PCB 482A16, X10 GAIN SETTING | 143 |
| ACCELEROMETERS | PCB 303A, 1.0 V/g | 1176, 1177 |
| FORCE HAMMER | PCB 208A03, 970 mV/g | 1550 |

| STATIC TEST HARDWARE | | |
|---|---|---|
| **ITEM** | **MODEL** | **SERIAL NUMBER** |
| LOAD CELL READOUT | UTICOR TECH MOD. 1406-1 | 10303 |
| TEST STAND | NREL SMALL BLADE TEST STAND | N/A |
| OVERHEAD CRANE | IUF 35-TON OVERHEAD BRIDGE CRANE | N/A |
| INBOARD (50-IN STATION) LOAD SADDLE | NREL SPECIFIC | FMI-01 |
| OUTBOARD (120-IN STATION) LOAD SADDLE | NREL SPECIFIC | FMI-02 |
| INCLINOMETER | LUCAS DP-45 ANGLE STAR | 90190017 |

[25] Appendix B presents selected data from an internal NREL report “NWTC-ST-FMI-STA-01-1000-FR” Ref. 42

**Table B.2 - BSTRAIN Data Acquisition Schematic**

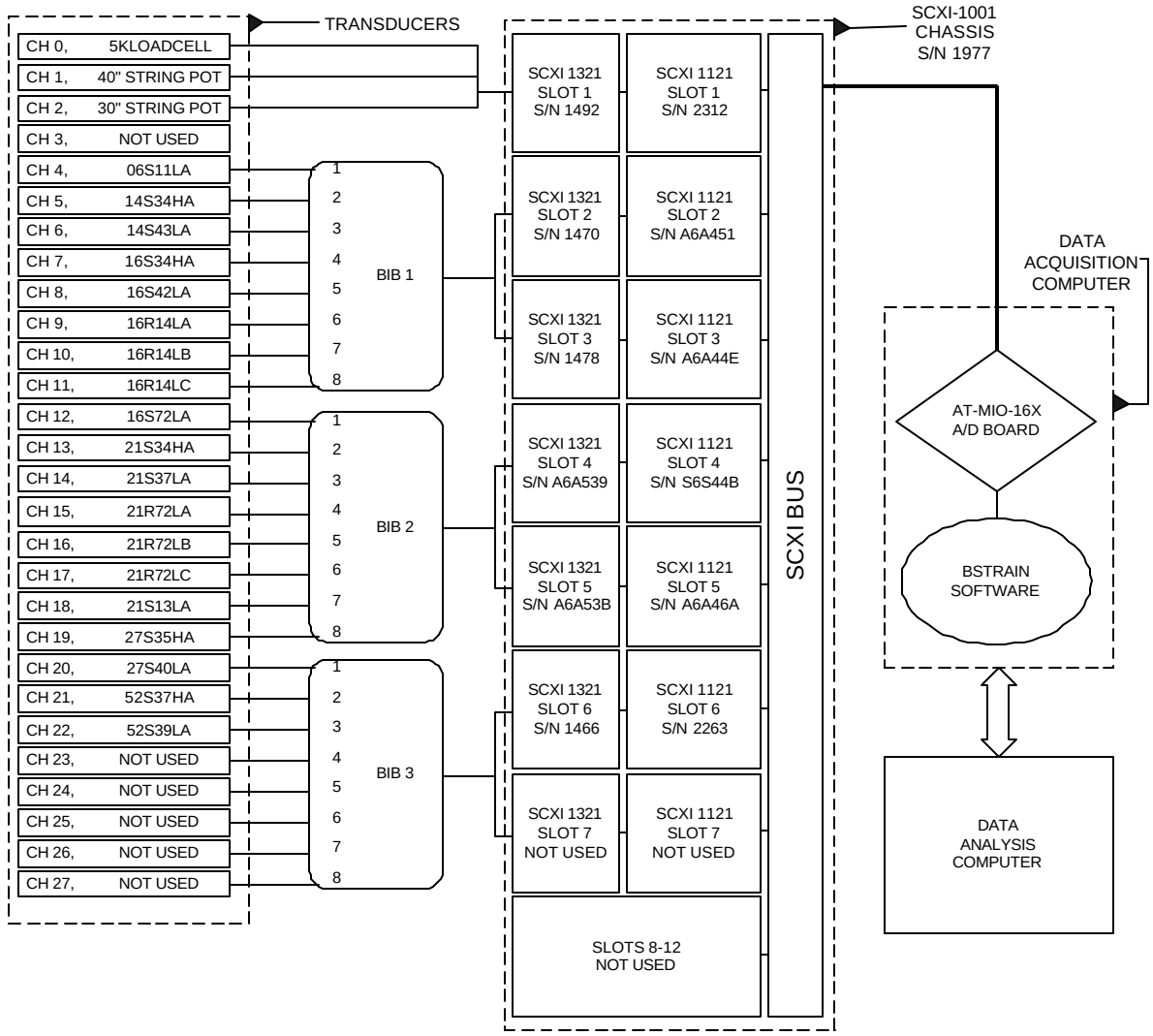

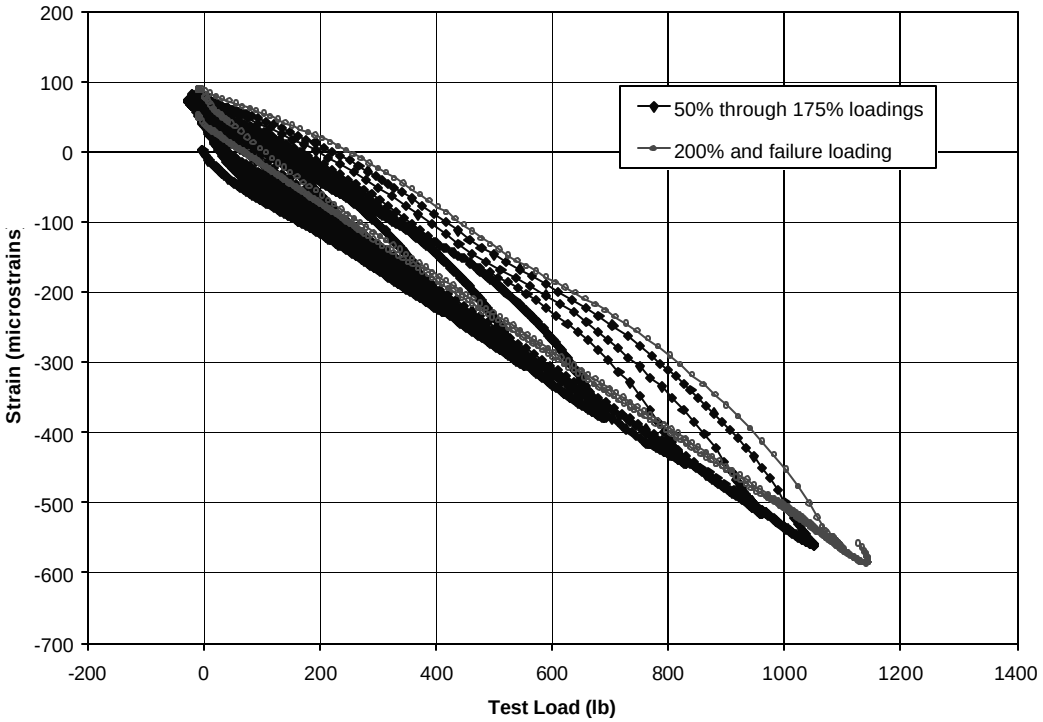


**Fig. B.1 - Gage 06S11LA strain data**

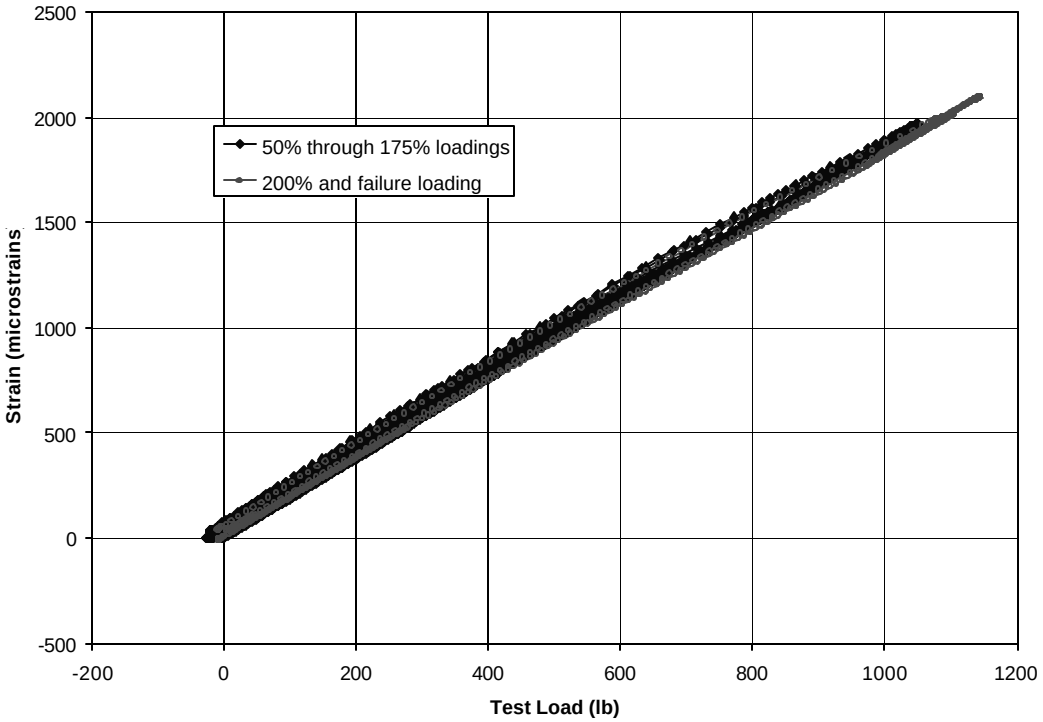


**Fig. B.2 - Gage 14S34HA strain gage**

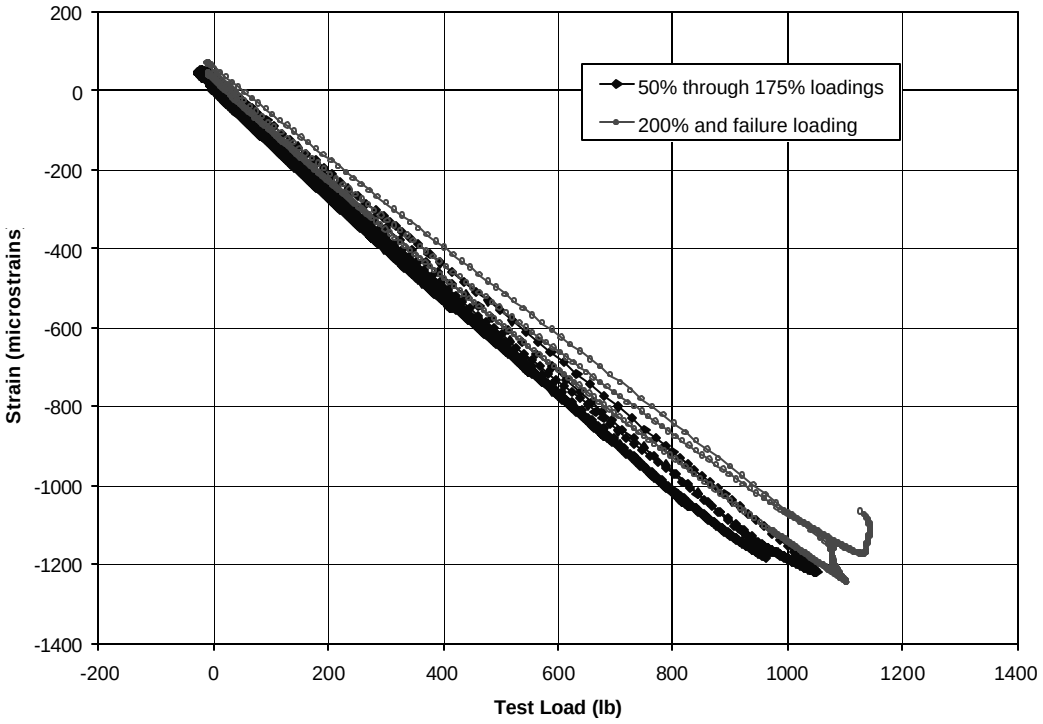


**Fig. B.3 - Gage 14S43LA strain gage**

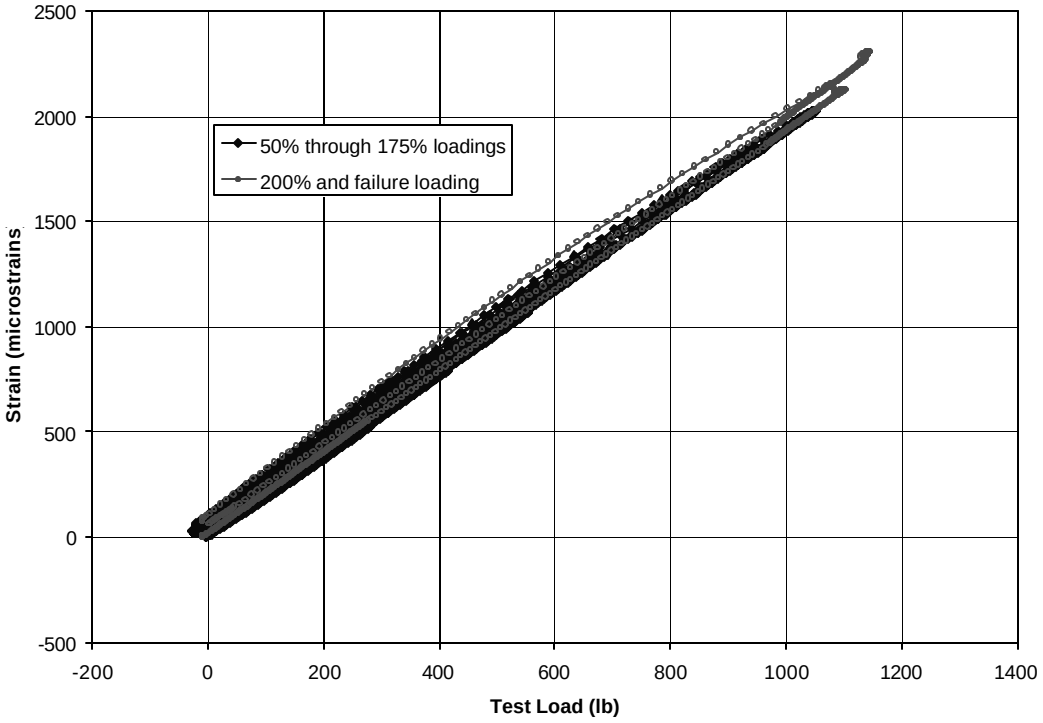

**Fig. B.4 - Gage 16S43HA strain data**

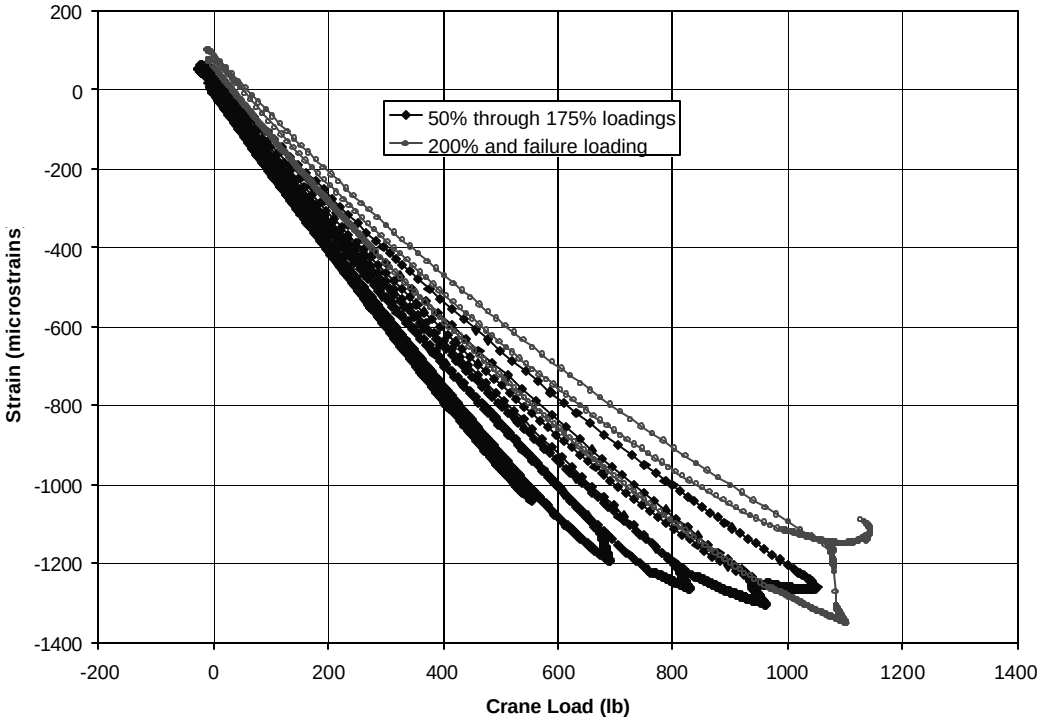


**Fig. B.5 - Gage 16S42LA strain data**

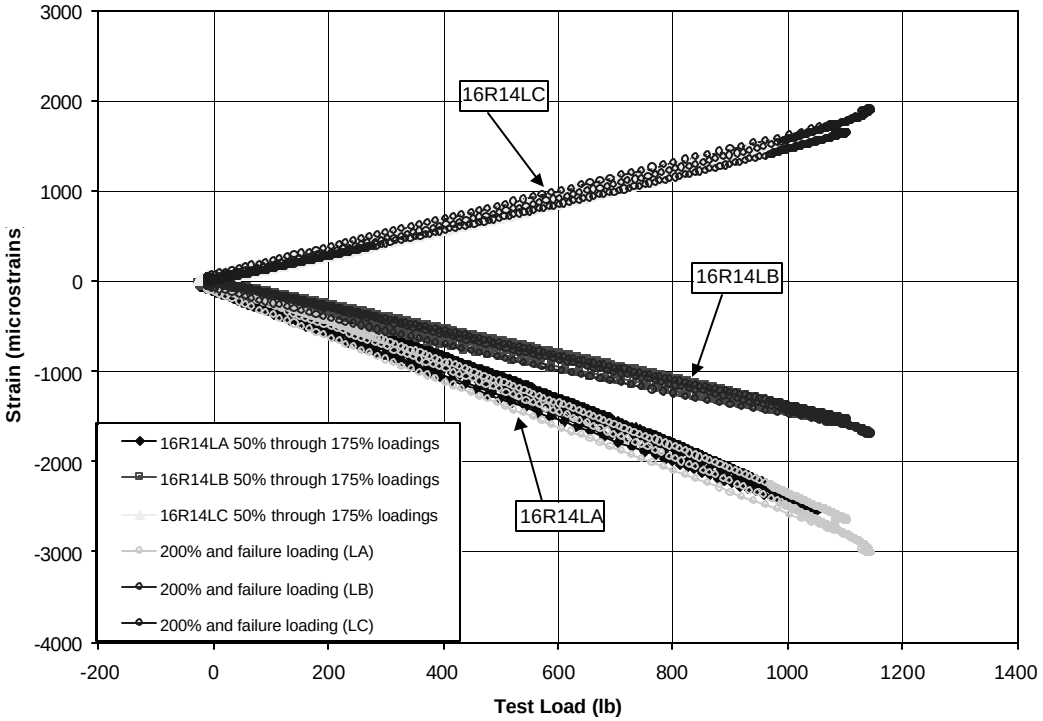


**Fig. B.6 - Rosette gage 16R14L(0,45,90 degree) strains**

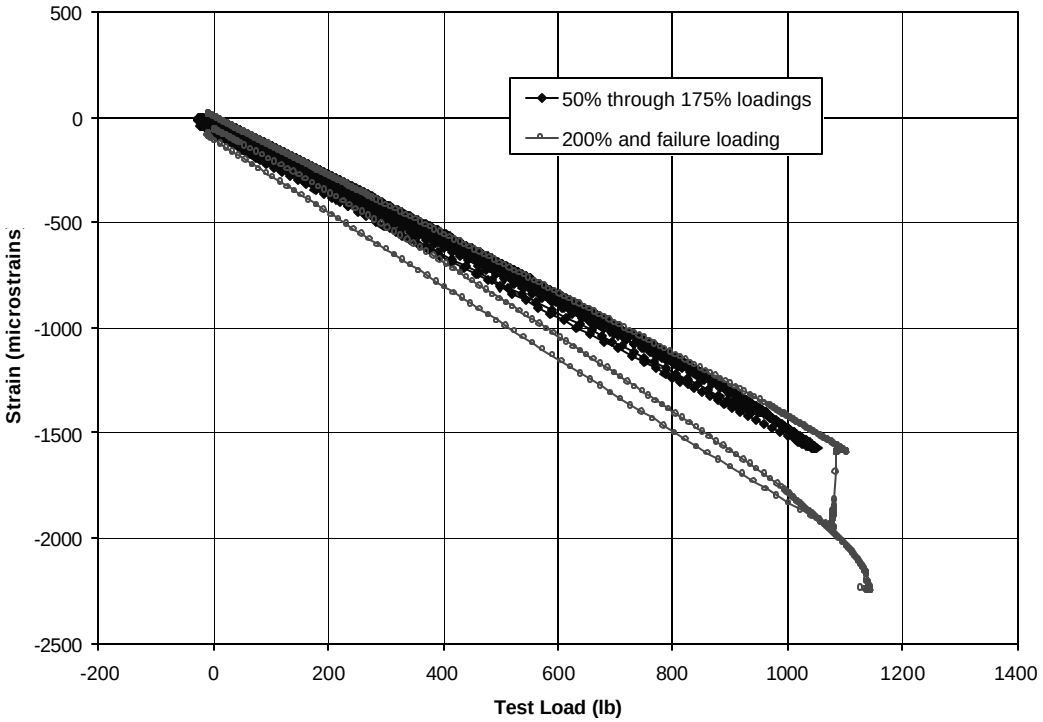


**Fig. B.7 - Gage 16S72LA strains**

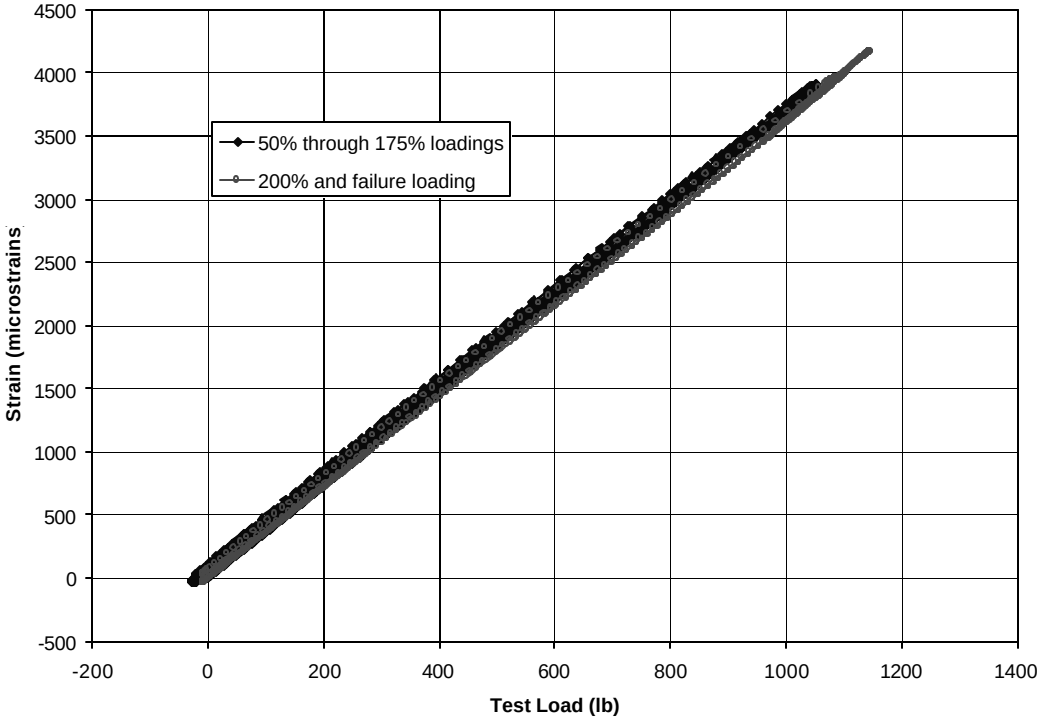


**Fig. B.8 - Gage 21S34HA strains**

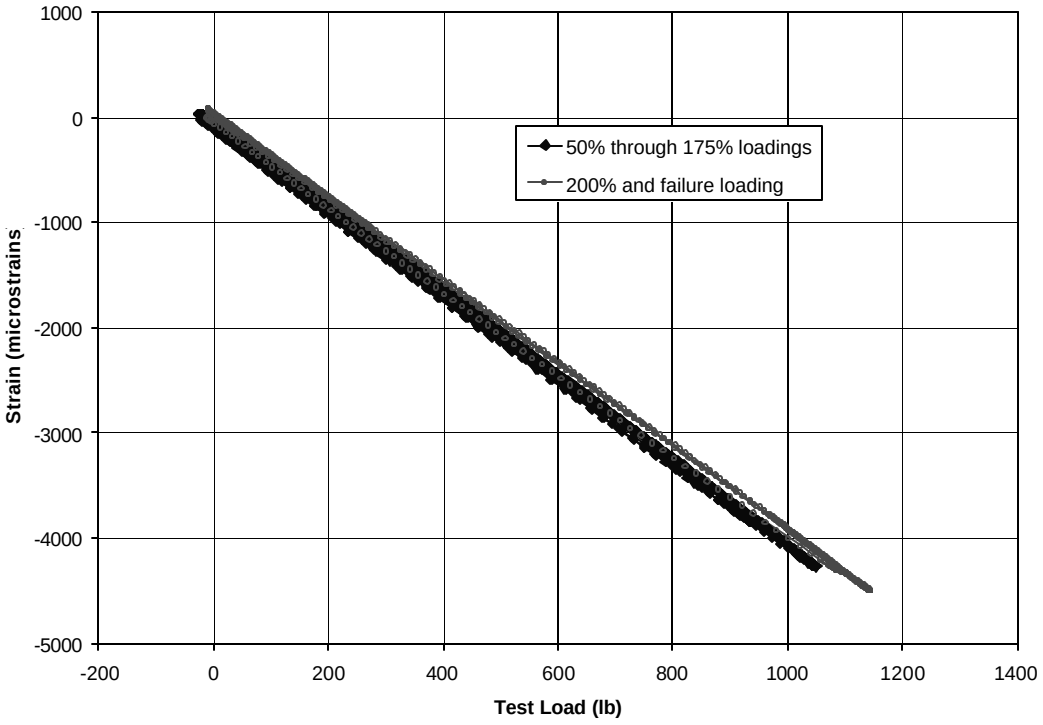


**Fig. B.9 - Gage 21S37LA strains**

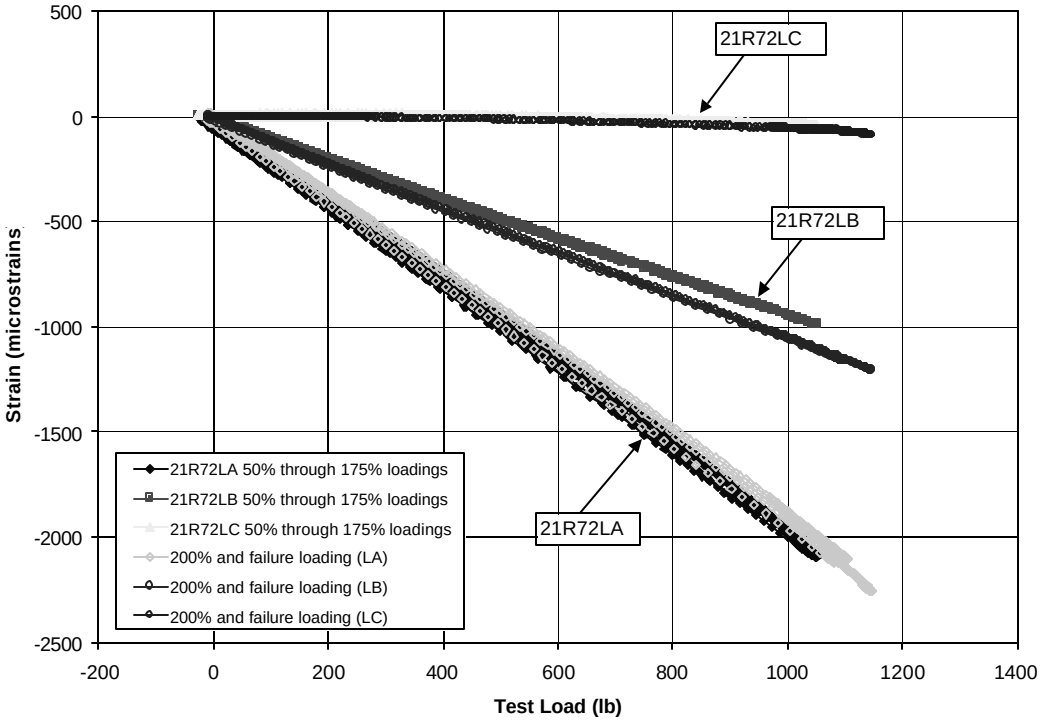


**Fig. B.10 - Rosette gage 21R72L(A, B, C) strains**

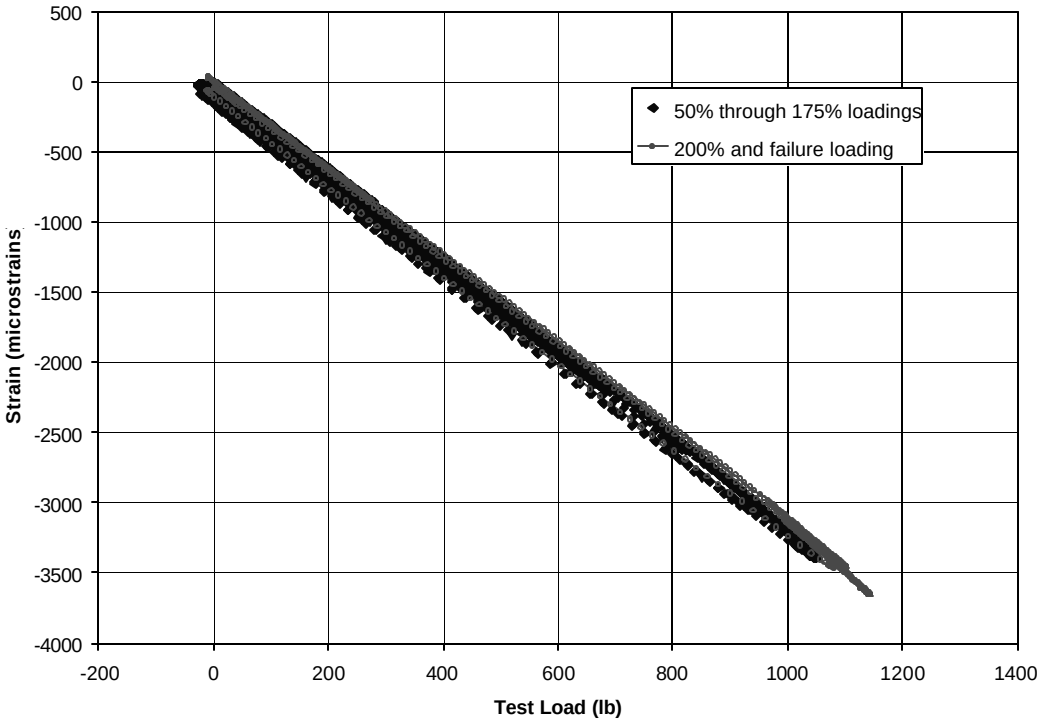


**Fig. B.11 - Gage 21S13LA strains**

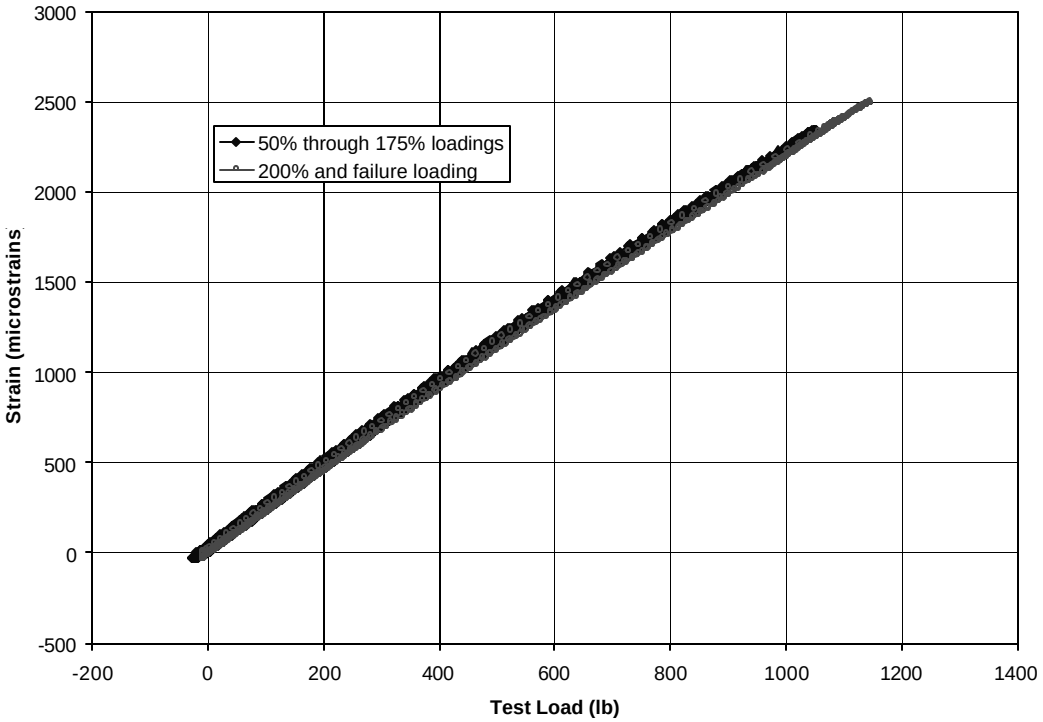


**Fig. B.12 - Gage 27S35HA strains**

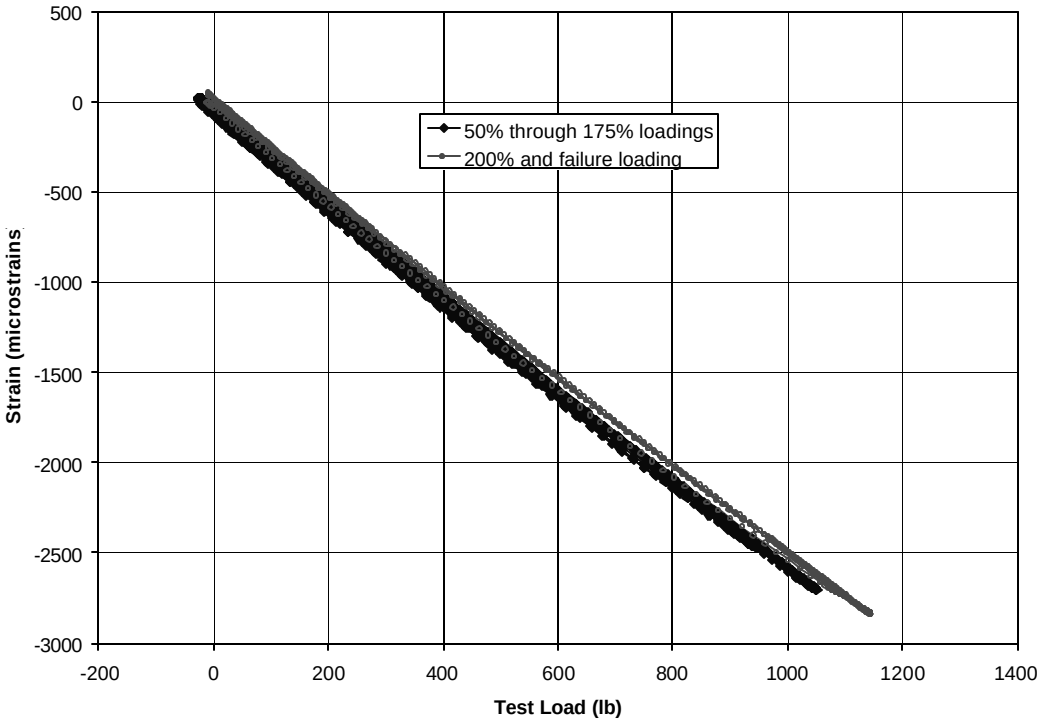


**Fig. B.13 - Gage 27S40LA strains**

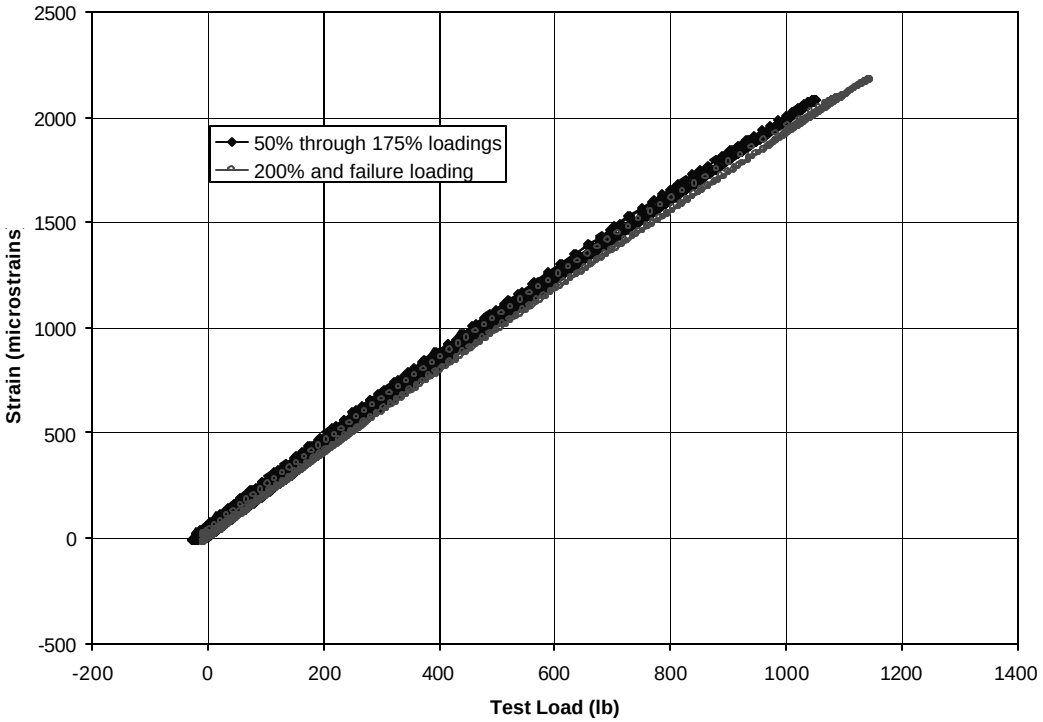


**Fig. B.14 - Gage 52S37HA strains**

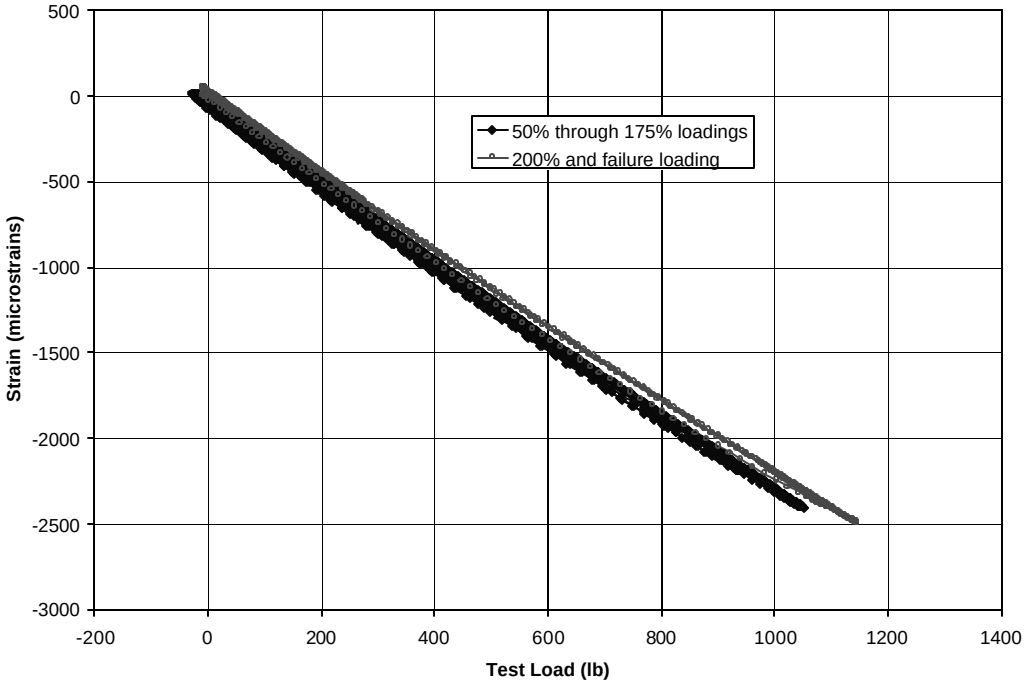


**Fig. B.15 - Gage 52S39LA strains**

# Appendix C Fatigue Test[26]

## Table C.1 - Loads document, page 1

**BMI BLADE - FATIGUE TEST CALCULATIONS**
**REGULAR OPTION - 11.7 to 3.5 M/S (26.2 to 7.8 MPH)**
**5.4 m/s Average Wind Speed**

File: Fatigue Rayleigh Based Rev b=0.0699 12-19-00.xls
Rev: 12/19/00 C. Richey

**IEC Class 2 A**
**Average V** **5.4** m/s
**Cut Off V** **11.7** m/s

S/So Slope Inverse 1/ b 14.3 Input
S/So Slope b 0.0699
Where S/So = 1-b·LOG(N);
And, S2 = S1 + b·LOG(N1/N2)

Blade Actuator Force Constant, Ks = 49.6 lb/in

N = Sum Nnorm/Nsum*HRactive*AVERAGE RPM*Kavail

| | Wind Speed m/s | Normalized Cycles Nnorm | Sum Nnorm | Moment Fraction M/Mmax (V/13.4)^2 | Bin Power Kw 29.14*(V/13.4)^3 | RPM 175*(V/11.7) (1 Cycle/Rev)) | Power* Count Kw*N |
|---|---|---|---|---|---|---|---|
| 1 | 3.5 | 0.0274 | | 0.089 | 0.78 | 52.4 | 0.02134 |
| 2 | 3.7 | 0.0277 | | 0.100 | 0.92 | 55.3 | 0.02557 |
| 3 | 3.9 | 0.0280 | | 0.111 | 1.08 | 58.3 | 0.03022 |
| 4 | 4.1 | 0.0281 | | 0.123 | 1.25 | 61.3 | 0.03528 |
| 5 | 4.3 | 0.0281 | | 0.135 | 1.45 | 64.3 | 0.04070 |
| 6 | 4.5 | 0.0280 | | 0.148 | 1.66 | 67.3 | 0.04646 |
| 7 | 4.7 | 0.0278 | | 0.161 | 1.89 | 70.3 | 0.05251 |
| 8 | 4.9 | 0.0275 | | 0.175 | 2.14 | 73.3 | 0.05880 |
| 9 | 5.1 | 0.0270 | | 0.190 | 2.41 | 76.3 | 0.06526 |
| 10 | 5.3 | 0.0265 | | 0.205 | 2.71 | 79.3 | 0.07184 |
| 11 | 5.5 | 0.0259 | | 0.221 | 3.03 | 82.3 | 0.07847 |
| 12 | 5.7 | 0.0252 | | 0.237 | 3.37 | 85.3 | 0.08508 |
| 13 | 5.9 | 0.0245 | | 0.254 | 3.74 | 88.2 | 0.09159 |
| 14 | 6.1 | 0.0237 | | 0.272 | 4.13 | 91.2 | 0.09795 |
| 15 | 6.3 | 0.0229 | | 0.290 | 4.55 | 94.2 | 0.10407 |
| 16 | 6.5 | 0.0220 | | 0.309 | 5.00 | 97.2 | 0.10990 |
| 17 | 6.7 | 0.0211 | | 0.328 | 5.47 | 100.2 | 0.11538 |
| 18 | 6.9 | 0.0202 | | 0.348 | 5.98 | 103.2 | 0.12044 |
| 19 | 7.1 | 0.0192 | | 0.368 | 6.51 | 106.2 | 0.12503 |
| 20 | 7.3 | 0.0182 | | 0.389 | 7.08 | 109.2 | 0.12911 |
| 21 | 7.5 | 0.0173 | | 0.411 | 7.68 | 112.2 | 0.13264 |
| 22 | 7.7 | 0.0163 | | 0.433 | 8.31 | 115.2 | 0.13558 |
| 23 | 7.9 | 0.0154 | | 0.456 | 8.97 | 118.2 | 0.13793 |
| 24 | 8.1 | 0.0144 | | 0.479 | 9.67 | 121.2 | 0.13966 |
| 25 | 8.3 | 0.0135 | | 0.503 | 10.40 | 124.1 | 0.14076 |
| 26 | 8.5 | 0.0126 | | 0.528 | 11.17 | 127.1 | 0.14124 |
| 27 | 8.7 | 0.0118 | | 0.553 | 11.98 | 130.1 | 0.14110 |
| 28 | 8.9 | 0.0109 | | 0.579 | 12.83 | 133.1 | 0.14037 |
| 29 | 9.1 | 0.0101 | | 0.605 | 13.71 | 136.1 | 0.13906 |
| 30 | 9.3 | 0.0094 | | 0.632 | 14.63 | 139.1 | 0.13720 |
| 31 | 9.5 | 0.0086 | | 0.659 | 15.60 | 142.1 | 0.13483 |
| 32 | 9.7 | 0.0079 | | 0.687 | 16.61 | 145.1 | 0.13198 |
| 33 | 9.9 | 0.0073 | | 0.716 | 17.65 | 148.1 | 0.12869 |
| 34 | 10.1 | 0.0067 | | 0.745 | 18.75 | 151.1 | 0.12502 |
| 35 | 10.3 | 0.0061 | | 0.775 | 19.88 | 154.1 | 0.12099 |
| 36 | 10.5 | 0.0055 | | 0.805 | 21.06 | 157.1 | 0.11667 |
| 37 | 10.7 | 0.0050 | | 0.836 | 22.29 | 160.0 | 0.11210 |
| 38 | 10.9 | 0.0046 | | 0.868 | 23.56 | 163.0 | 0.10733 |
| 39 | 11.1 | 0.0041 | | 0.900 | 24.88 | 166.0 | 0.10240 |
| 40 | 11.3 | 0.0037 | | 0.933 | 26.25 | 169.0 | 0.09737 |
| 41 | 11.5 | 0.0033 | | 0.966 | 27.67 | 172.0 | 0.09226 |
| 42 | 11.7 | 0.0030 | | 1.000 | 29.14 | 175.0 | 0.08713 |
| | 11.9 | | | | | | |

BIN 4
M= 0.1509*Mmax
Sum Nnorm = .3021
TOTAL
N = 4.33E+06

4.33E+06 = N = Cycles
0.1509 = Avg(M/Mmax)
0.3021 =Sum Nnorm

BIN 3
M = 0.3519*Mmax
Sum Nnorm = .2604
TOTAL
N = 5.72E+6

5.72E+06 = N = Cycles
0.3519 = Mavg
0.2604 =Sum Nnorm

BIN 2
M = 0.6634*Mmax
Sum Nnorm = .11156
TOTAL
N = 3.50E+6

3.50E+06 = N = Cycles
0.6634 = Mavg
0.1156 =Sum Nnorm

BIN 1
M= 0.9334*Mmax
Sum N norm= .0187
TOTAL
N = 6.73E+5

6.73E+05 = N = Cycles
0.9334 = Mavg
0.0187 =Sum Nnorm **4.24731**

**Sum** **0.697** = Nsum (See Top)

[26] Appendix C presents selected data from an internal NREL report "NWTC-ST-FMI-FAT-02-0201-FR" Ref. 40

## Table C.1 - continued – Loads document, page 2

### BMI BLADE - FATIGUE TEST CALCULATIONS
**REGULAR OPTION - 11.7 to 3.5 M/S (26.2 to 7.8 MPH)**
**5.4 m/s Average Wind Speed**

| | |
|---|---|
| **0.697** | Nsum WIND TURBINE ACTIVE FRACTION - BINS 1-4 SUM |
| **0.373** | WIND TURBINE INACTIVE FRACTION - OUTSIDE of BINS 1-4 |
| **0.900** | Kavail ASSUMED AVAILABILITY (ON LINE) FRACTION |
| **0.627** | WTactive WIND TURBINE ACTIVE FRACTION = 0.697*0.900 => TOTAL ACTIVE FRACTION |
| **1.422E+07** | Nactive = No. ACTIVE CYCLES for 30 YEARS @ 175 to 52.4 RPM |
| **1.648E+05** | HRactive ACTIVE HOURS +0.627*365*24*30 |
| **129.63** | BL inches @ BLADE END |
| **34748** | Mmax in-lb BASELINE MOMENT @ MAX POWER 11.7 m/s and 175 rpm |
| **268.06** | BASELILNE SHEAR lb @ BL 129.63 @ MAX POWER |

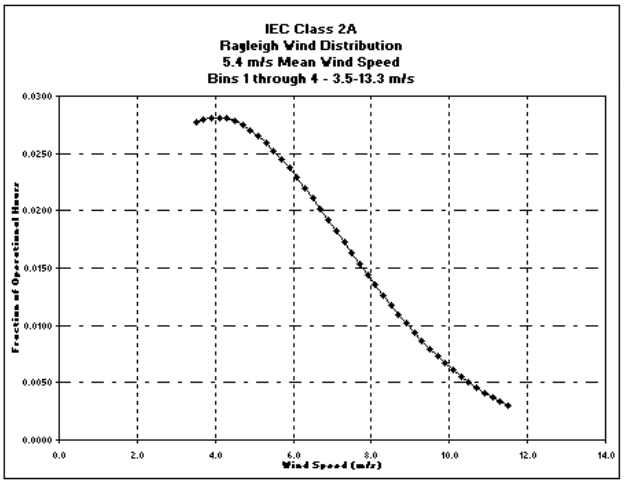


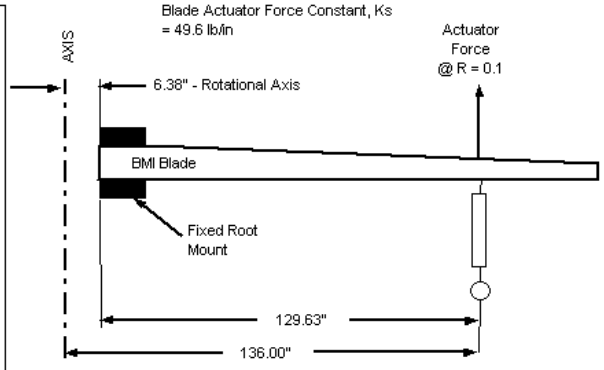


### BMI BLADE - FATIGUE TEST CALCULATIONS
**REGULAR OPTION - 11.7 to 3.5 M/S (26.2 to 7.8 MPH)**
**5.4 m/s Average Wind Speed**

| | |
|---|---|
| **700,096 KWH** | **30 YR Output** |
| **64 KWH** | **Average Output Per Day** |

**CUMULATIVE DAMAGE - BASELINE**

**BASELINE 2.11+E9 CYCLES - 4 LOADS**

Nfact0 **1.000E+00** **(Scales N)**

| | N Cycles | M/Mmax | Max Moment in-lb | Max Force lb |
|---|---|---|---|---|
| **BIN 1** | 672,933 | 0.9334 | 3.243E+04 | 250 |
| **BIN 2** | 3,497,061 | 0.6634 | 2.305E+04 | 178 |
| **BIN 3** | 5,721,816 | 0.3519 | 1.223E+04 | 94 |
| **BIN 4** | 4,328,956 | 0.1509 | 5.242E+03 | 40 |

**N Total:** 14,220,766

**CUMULATIVE DAMAGE - 3,000,000 CYCLES**

**TEST @ 3.00+E6 CYCLES - 4 LOADS**

b = 0.0699

Nfact1 **2.110E-01** **(Scales N)**

| | N Cycles | M/Mmax | Max Moment in-lb | Max Force lb |
|---|---|---|---|---|
| **BIN 1** | 141,961 | 0.9806 | 3.407E+04 | 263 |
| **BIN 2** | 737,737 | 0.7106 | 2.469E+04 | 190 |
| **BIN 3** | 1,207,069 | 0.3991 | 1.387E+04 | 107 |
| **BIN 4** | 913,233 | 0.1981 | 6.884E+03 | 53 |

**N Total:** 3,000,000

**CUMULATIVE DAMAGE - 1,000,000 CYCLES**

**TEST @ 1.00+E6 CYCLES - 4 LOADS**

b = 0.0699

Nfact2 **7.032E-02** **(Scales N)**

| | N Cycles | M/Mmax | Max Moment in-lb | Max Force lb |
|---|---|---|---|---|
| **BIN 1** | 47,320 | 1.0140 | 3.523E+04 | 272 |
| **BIN 2** | 245,912 | 0.7440 | 2.585E+04 | 199 |
| **BIN 3** | 402,356 | 0.4325 | 1.503E+04 | 116 |
| **BIN 4** | 304,411 | 0.2315 | 8.043E+03 | 62 |

**N Total:** 1,000,000

**KEY:**

**Bin 1 => 11.7 to 10.9 m/s**
**Bin 2 => 10.9 to 8.3 m/s**
**Bin 3 => 18.3 to 5.7 m/s**
**Bin 4 => 5.7 to 3.5 m/s**

| | |
|---|---|
| **700,096 KWH** | **30 YR Output** |
| **64 KWH** | **Average Output Per Day** |

**TEST @ 3.00+E6 CYCLES - 1 LOAD**

b = 0.0699

| | N Cycles | M/Mmax | Max Moment in-lb | Max Force lb |
|---|---|---|---|---|
| **BIN 1** | 2,997,844 | 0.8880 | 3.086E+04 | 238 |
| **BIN 2** | 2,156 | 0.8879 | 3.085E+04 | 238 |
| **BIN 3** | 0 | 0.8879 | 3.085E+04 | 238 |
| **BIN 4** | 0 | 0.8879 | 3.085E+04 | 238 |

**N Total:** 3,000,000

**TEST @ 1.00+E6 CYCLES - 1 LOAD**

b = 0.0699

| | N Cycles | M/Mmax | Max Moment in-lb | Max Force lb |
|---|---|---|---|---|
| **BIN 1** | 999,286 | 0.9214 | 3.202E+04 | 247 |
| **BIN 2** | 714 | 0.9214 | 3.202E+04 | 247 |
| **BIN 3** | 0 | 0.9214 | 3.202E+04 | 247 |
| **BIN 4** | 0 | 0.9214 | 3.202E+04 | 247 |

**N Total:** 1,000,000

**Table C.2 - Data acquisition system wiring diagram**

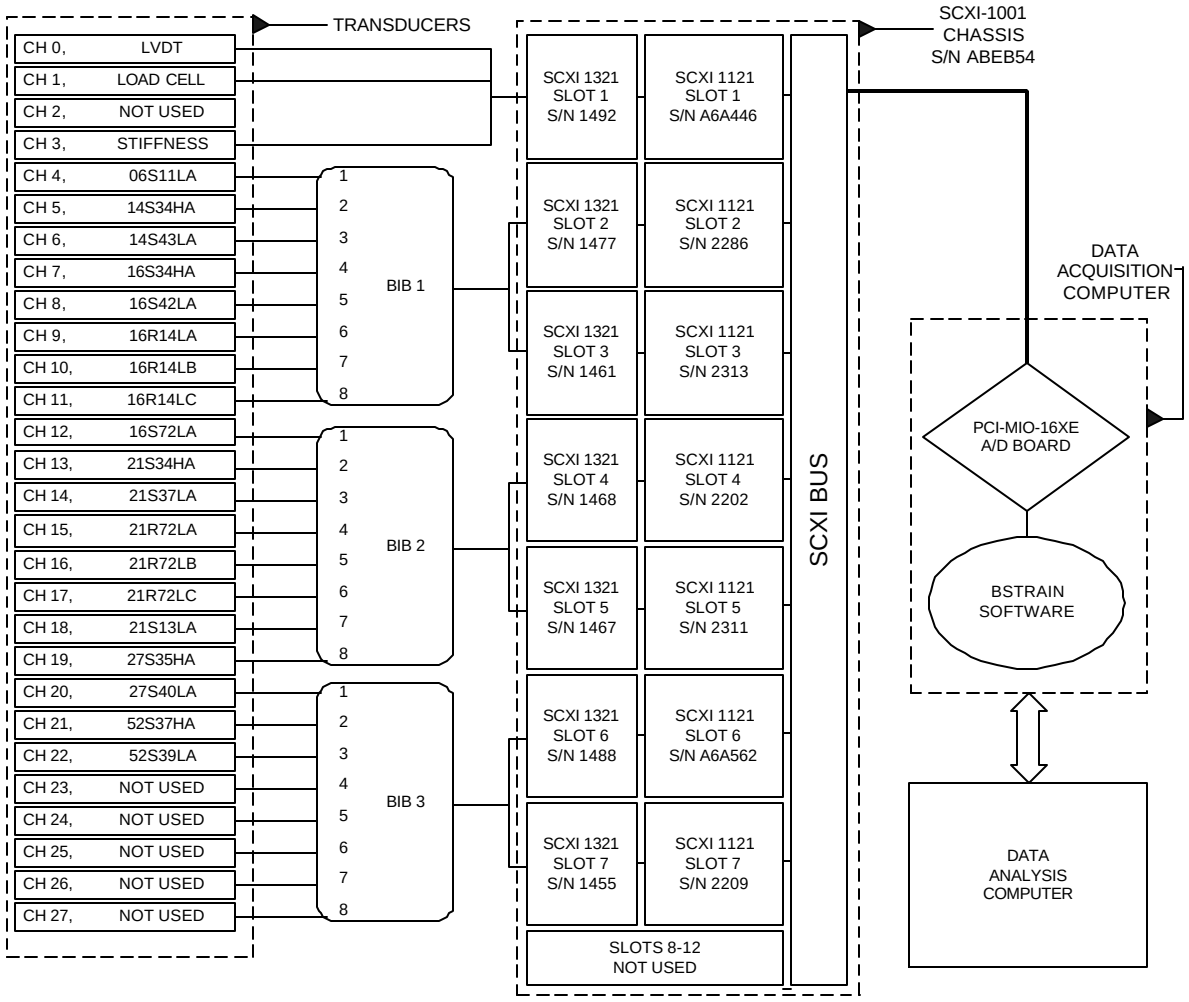

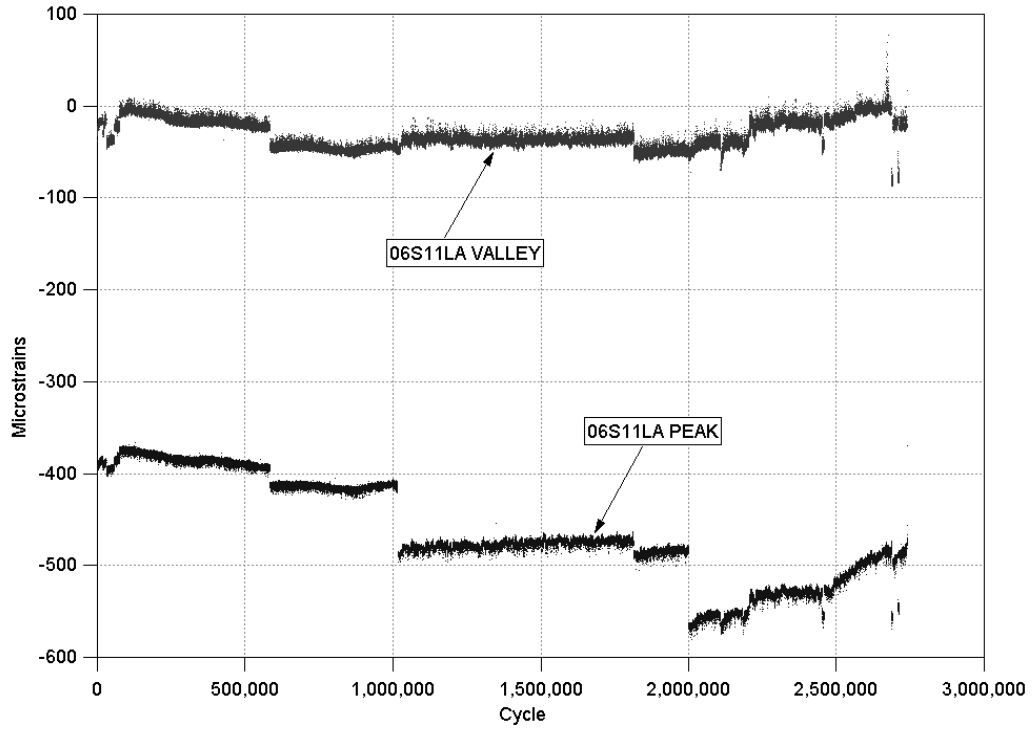


**Fig. C.1 - Gage 06S11LA peak/valley strain data**

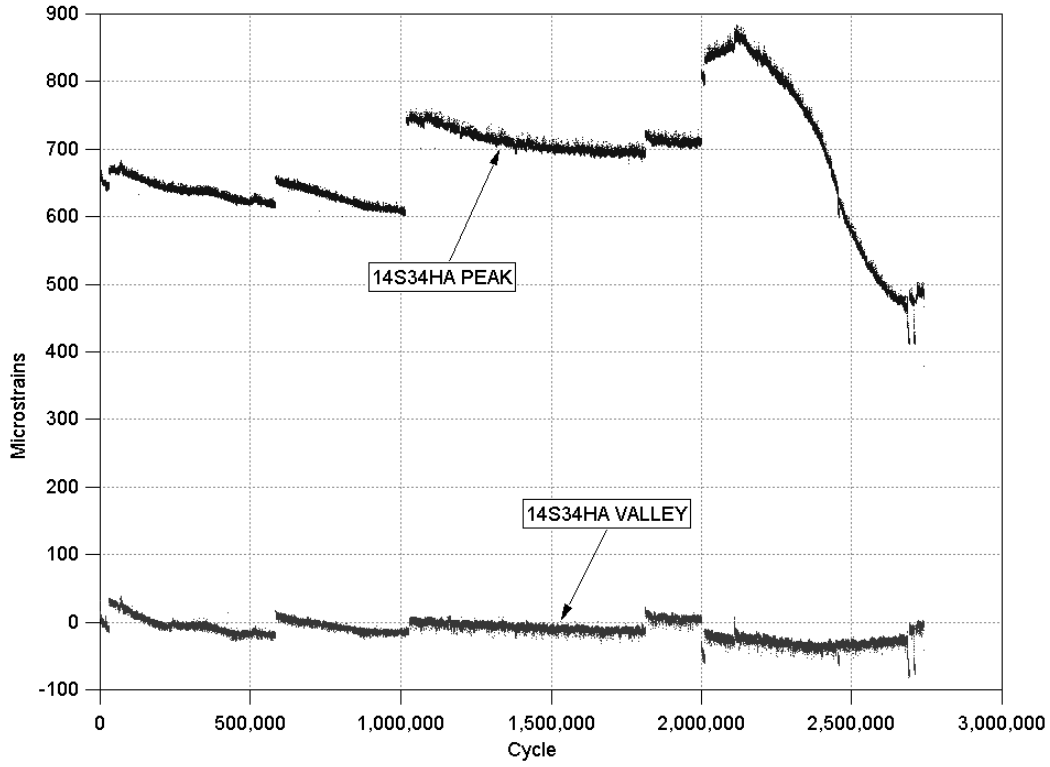


**Fig. C.2 - Gage 14S34HA peak/valley strain data**

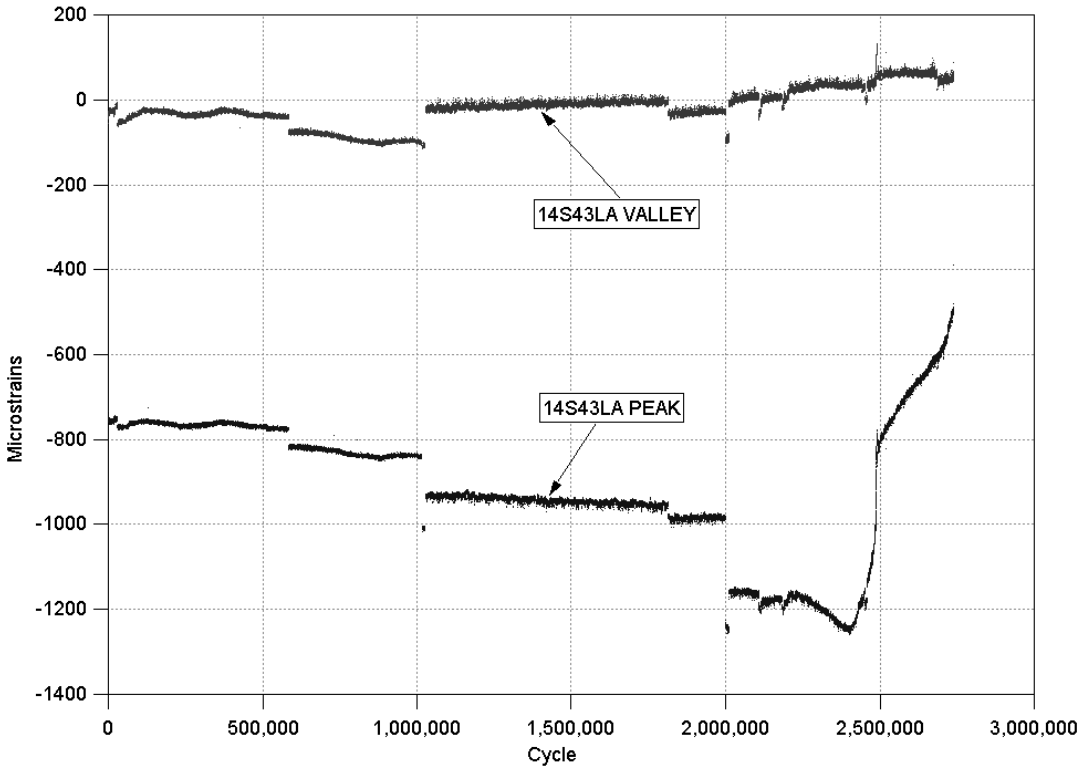


**Fig. C.3 - Gage 14S43LA peak/valley strain data**

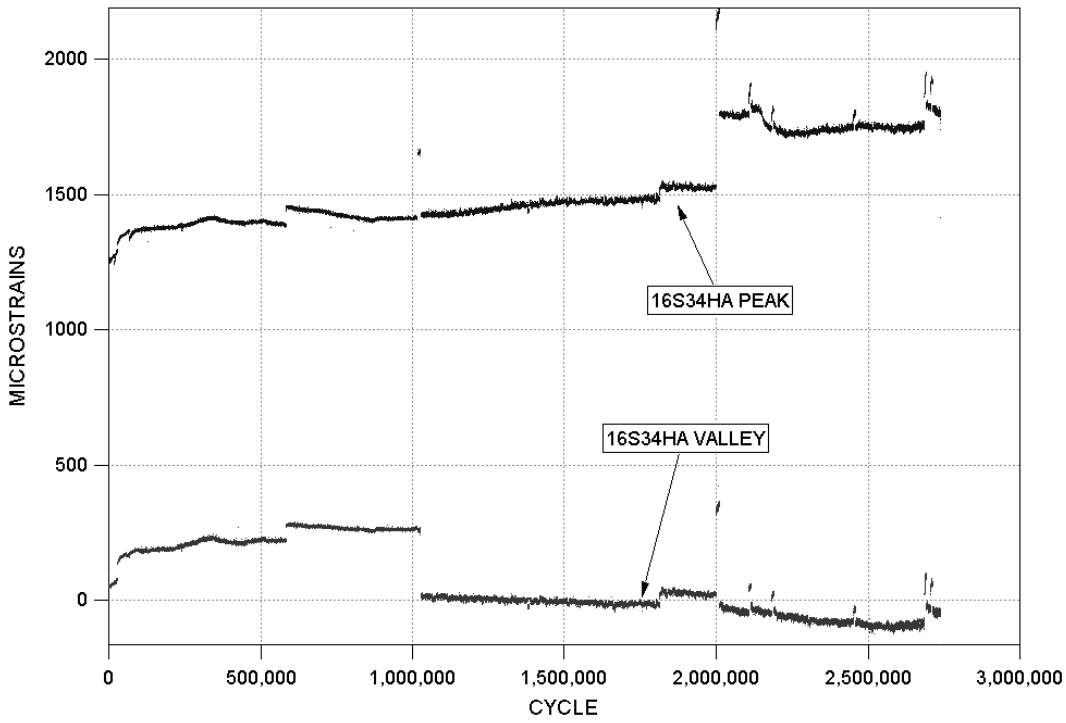

**Fig. C.4 - Gage 16S34HA peak/valley strain data**

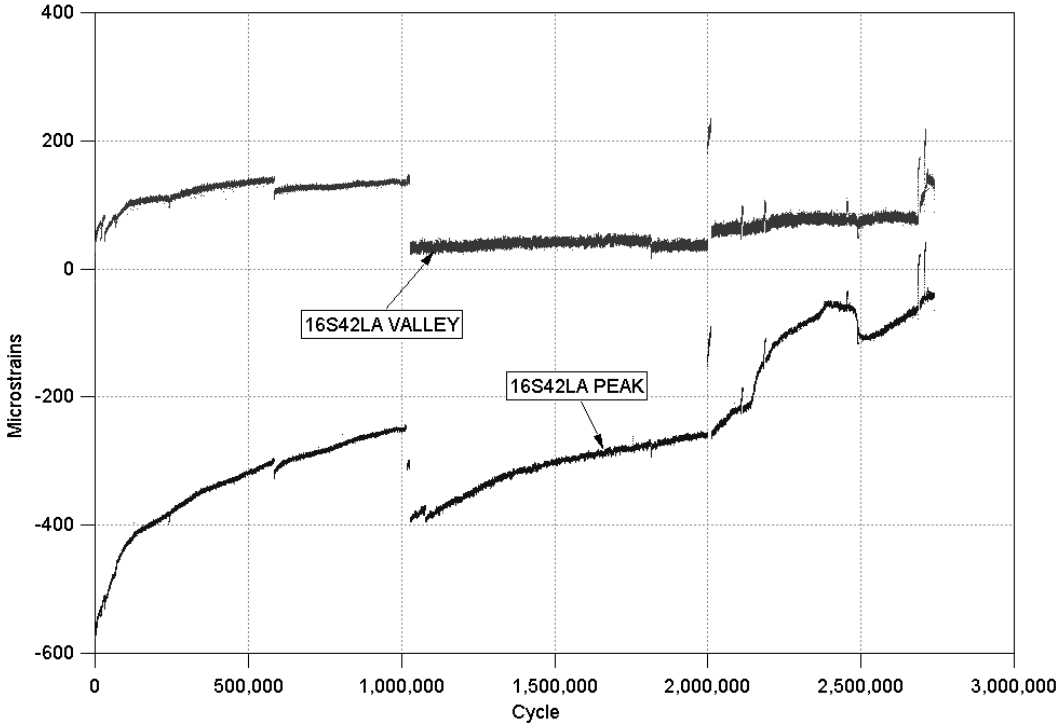


**Fig. C.5 - Gage 16S42LA peak/valley strain data**

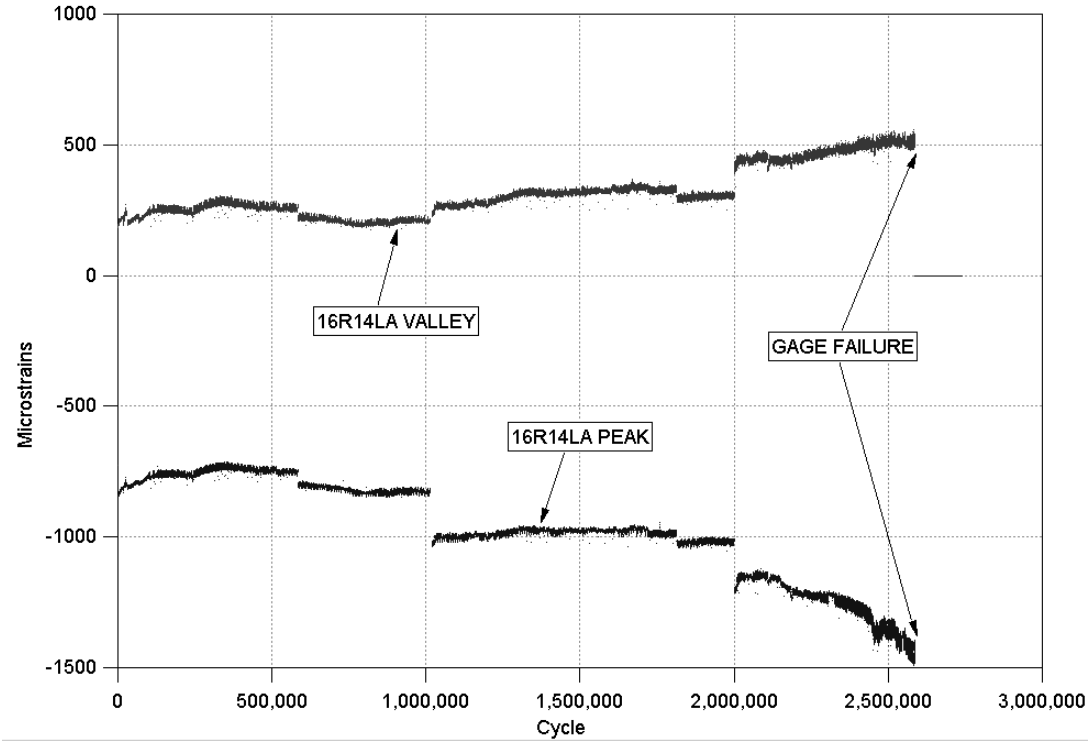

**Fig. C.6 - Gage 16R14LA peak/valley strain data**

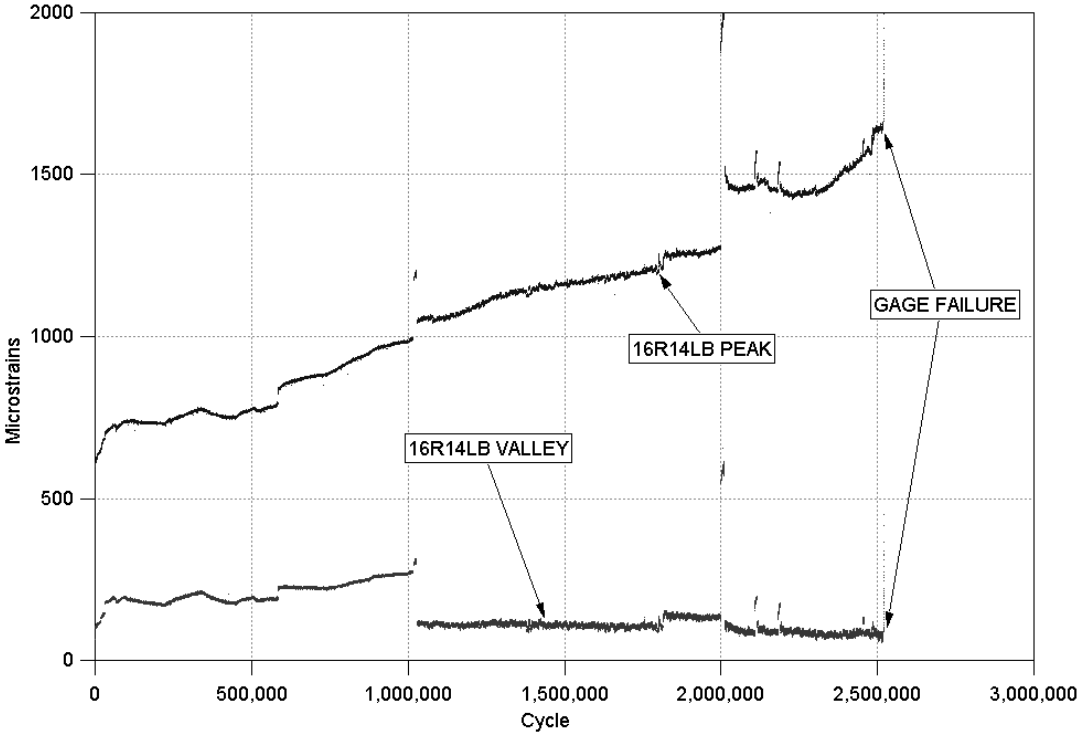


**Fig. C.7 - Gage 16R14LB peak/valley strain data**

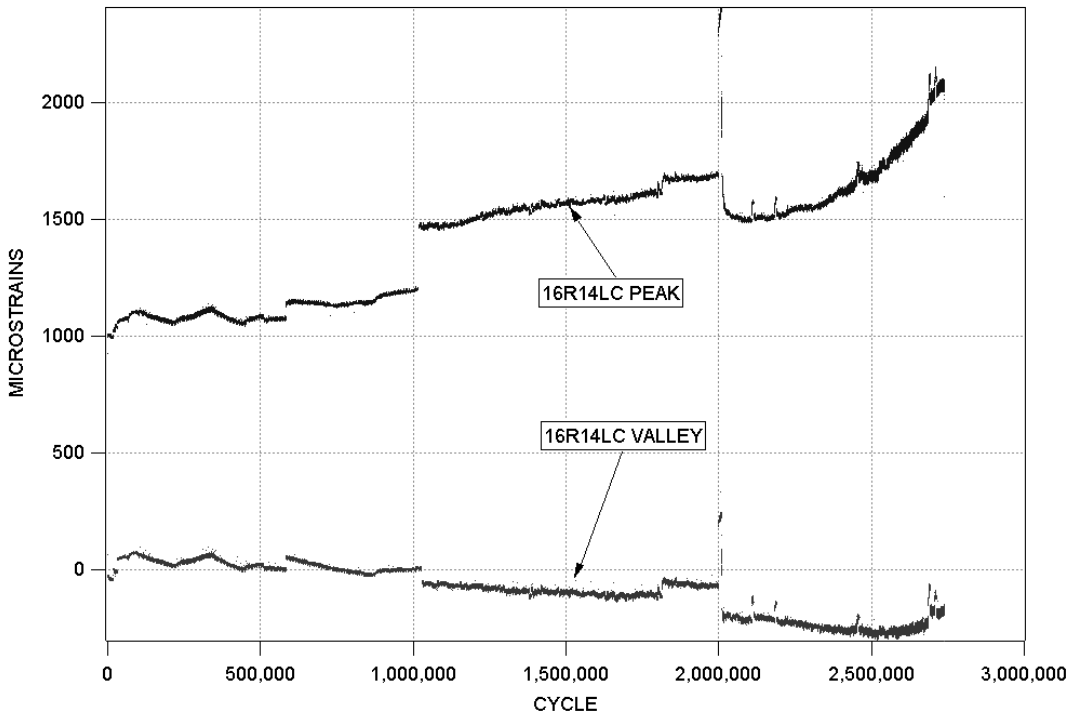

**Fig. C.8 - Gage 16R14LC peak/valley strain data**

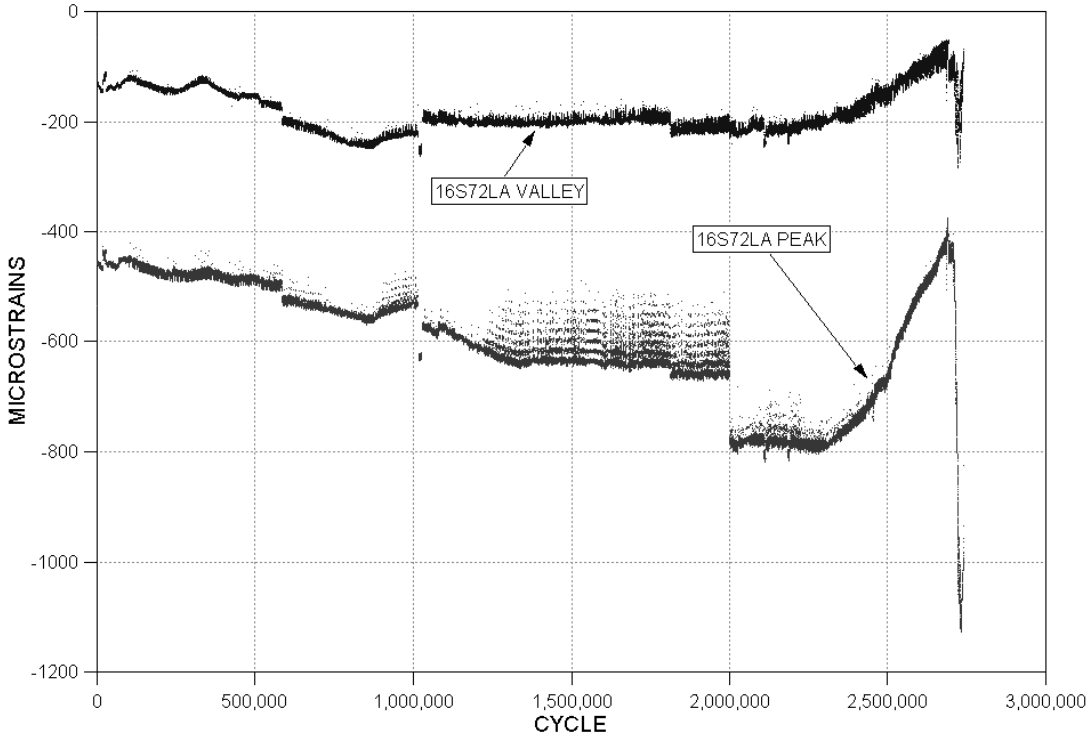


**Fig. C.9 - Gage 16S72LA peak/valley strain data**

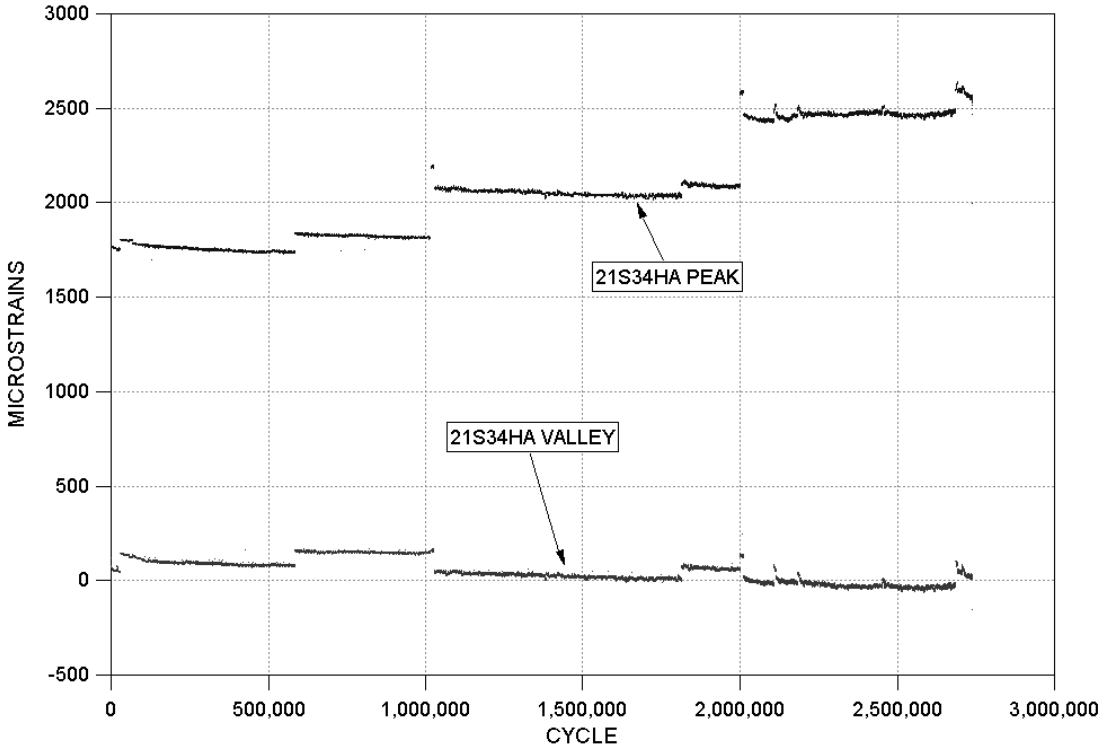


**Fig. C.10 - Gage 21S34HA peak/valley strain data**

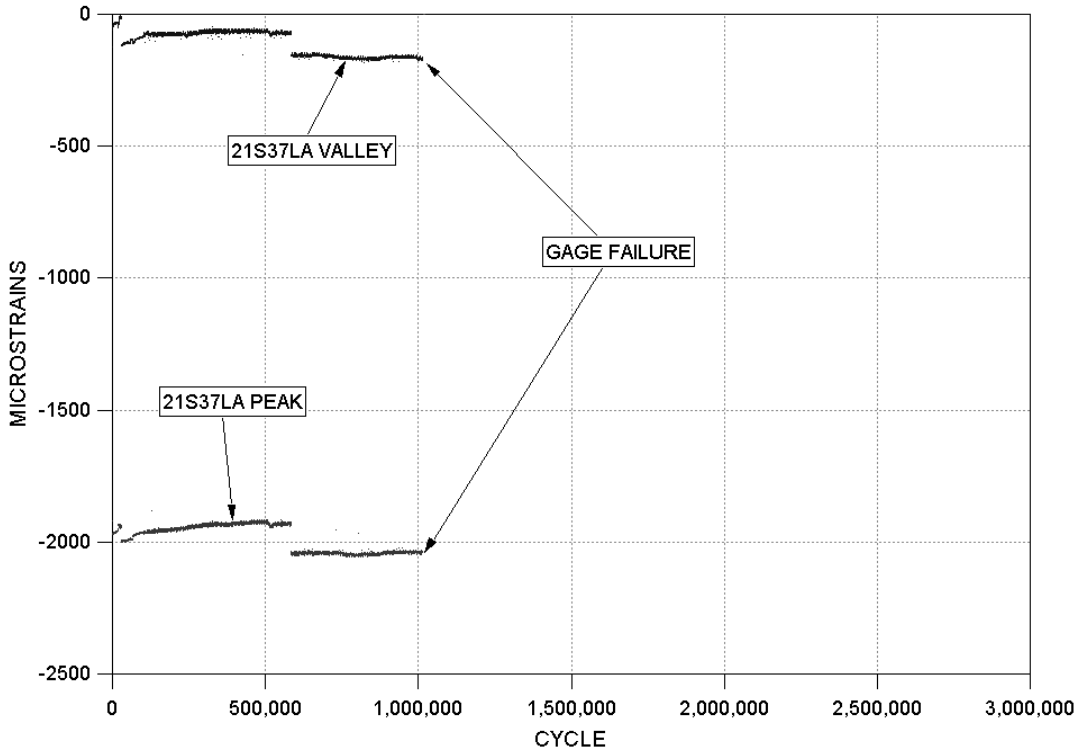


**Fig. C.11 - Gage 21S37LA peak/valley strain data**

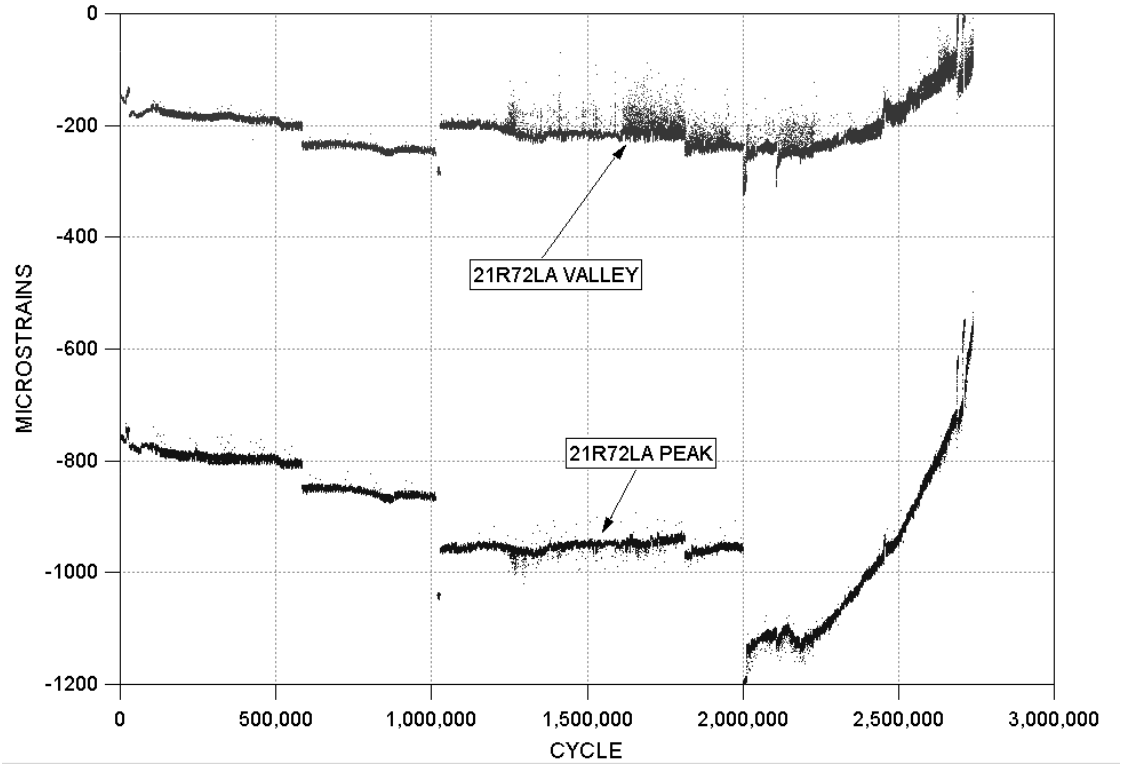


**Fig. C.12 - Gage 21R72LA peak/valley strain data**

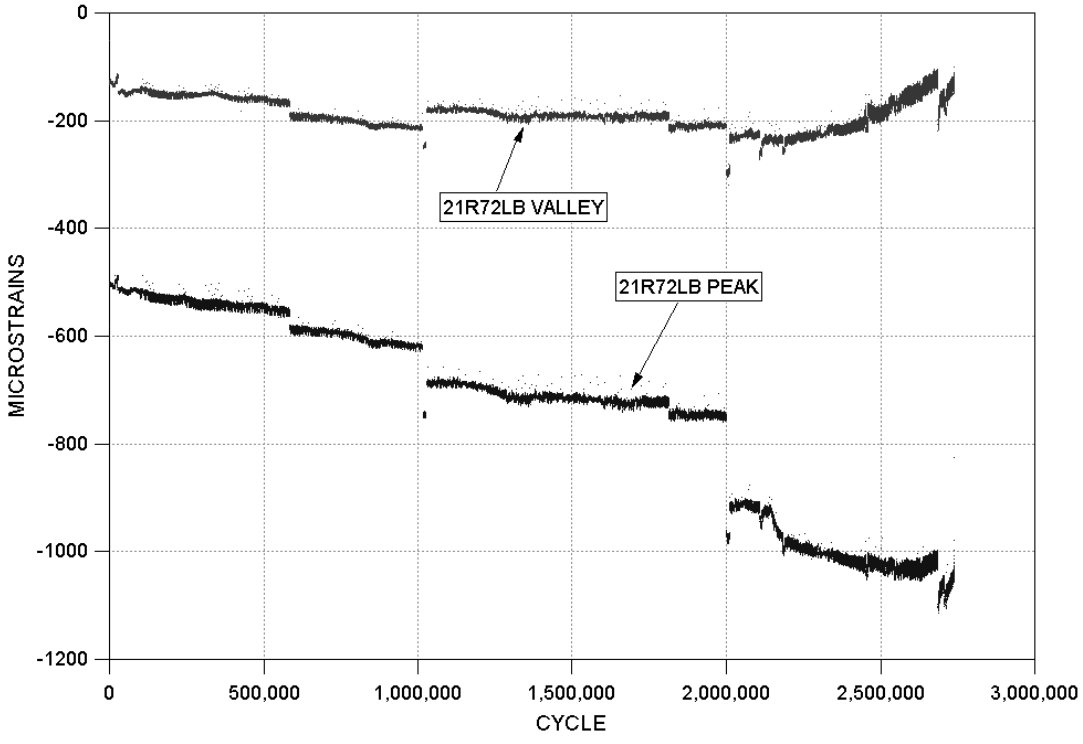


**Fig. C.13 - Gage 21R72LB peak/valley strain data**

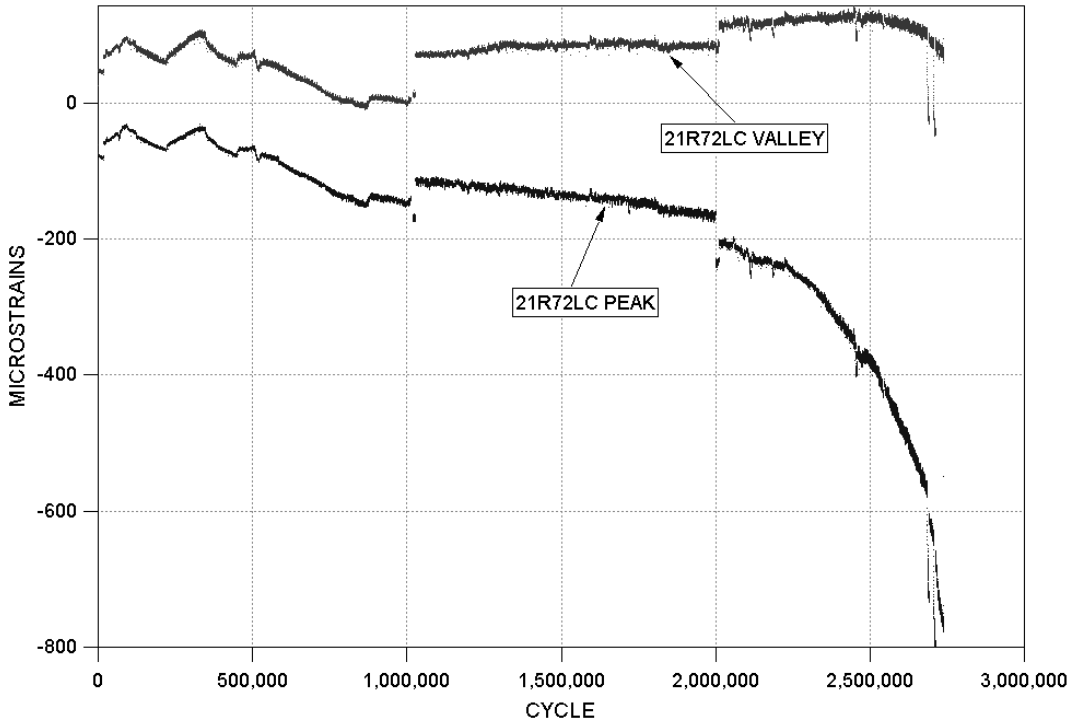


**Fig. C.14 - Gage 21R72LC peak/valley strain data**

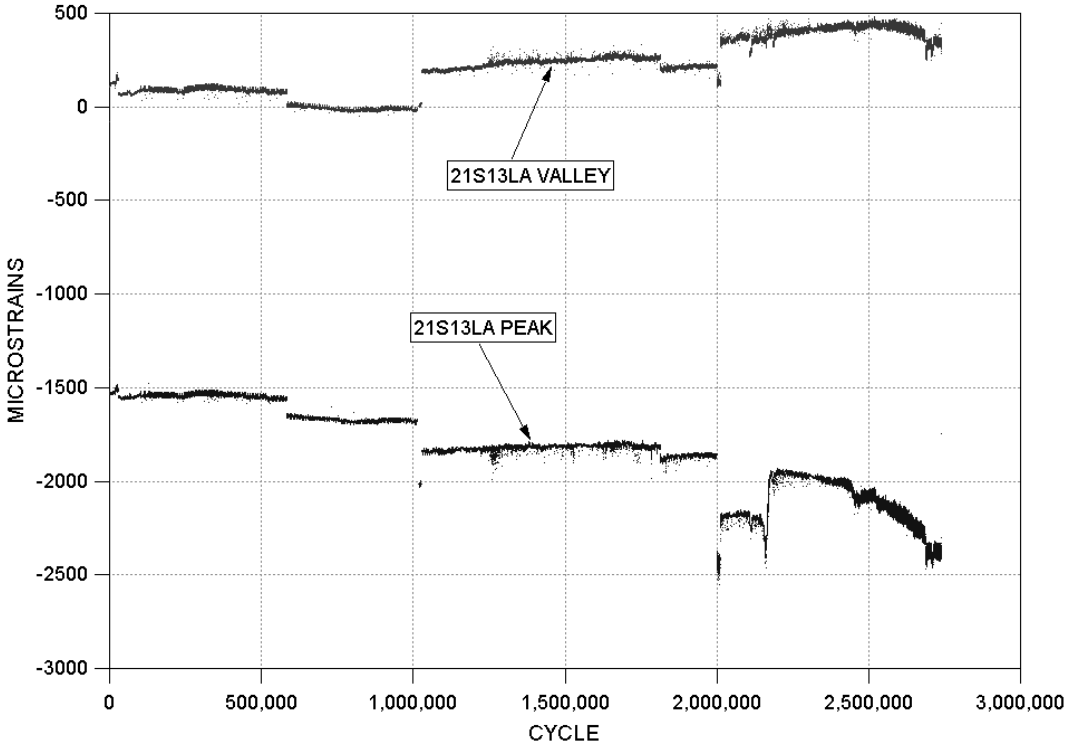

**Fig. C.15 - Gage 21S13LA peak/valley strain data**

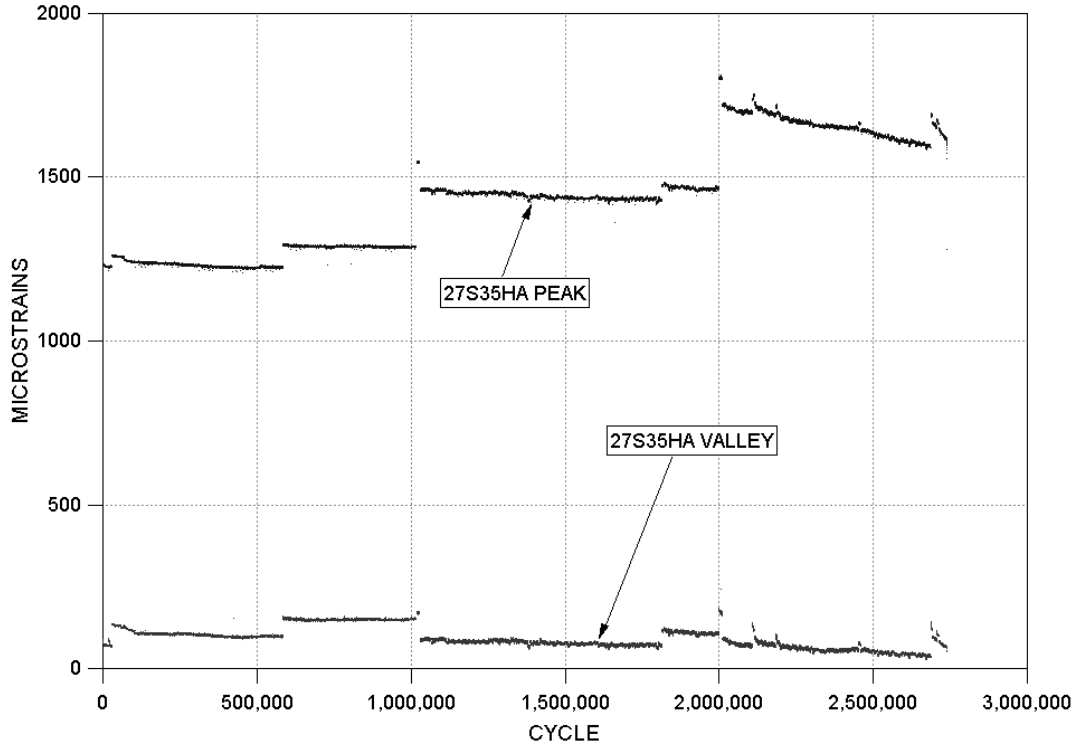


**Fig. C.16 - Gage 27S35HA peak/valley strain data**

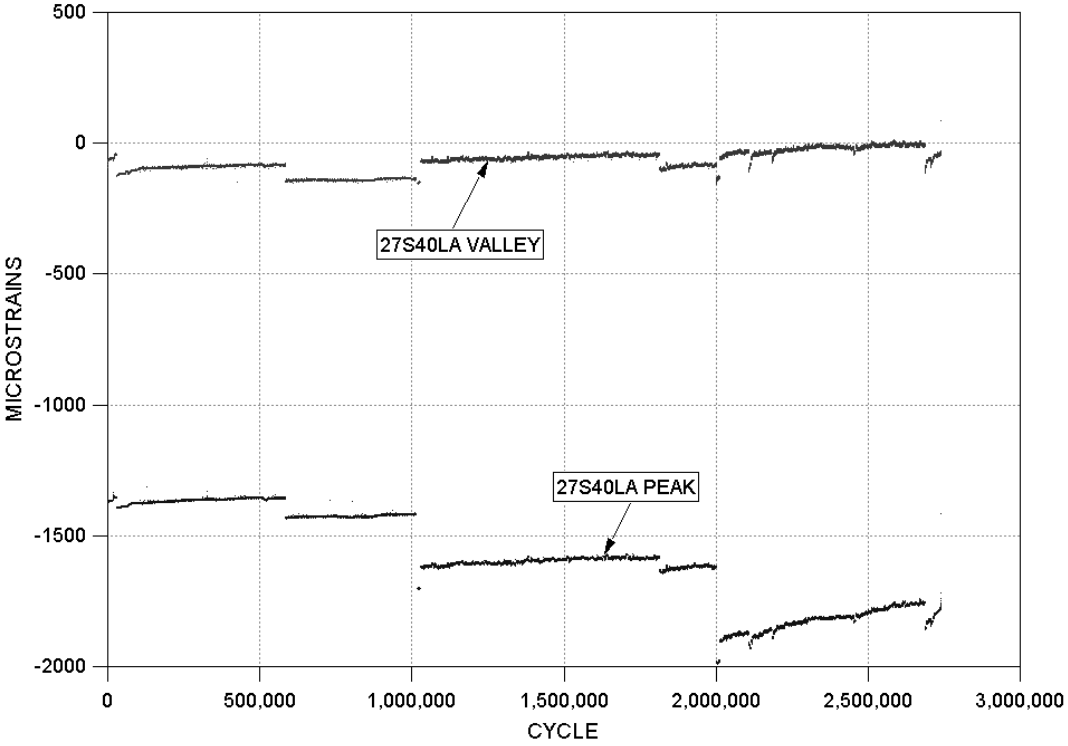

**Fig. C.17 - Gage 27S40LA peak/valley strain data**

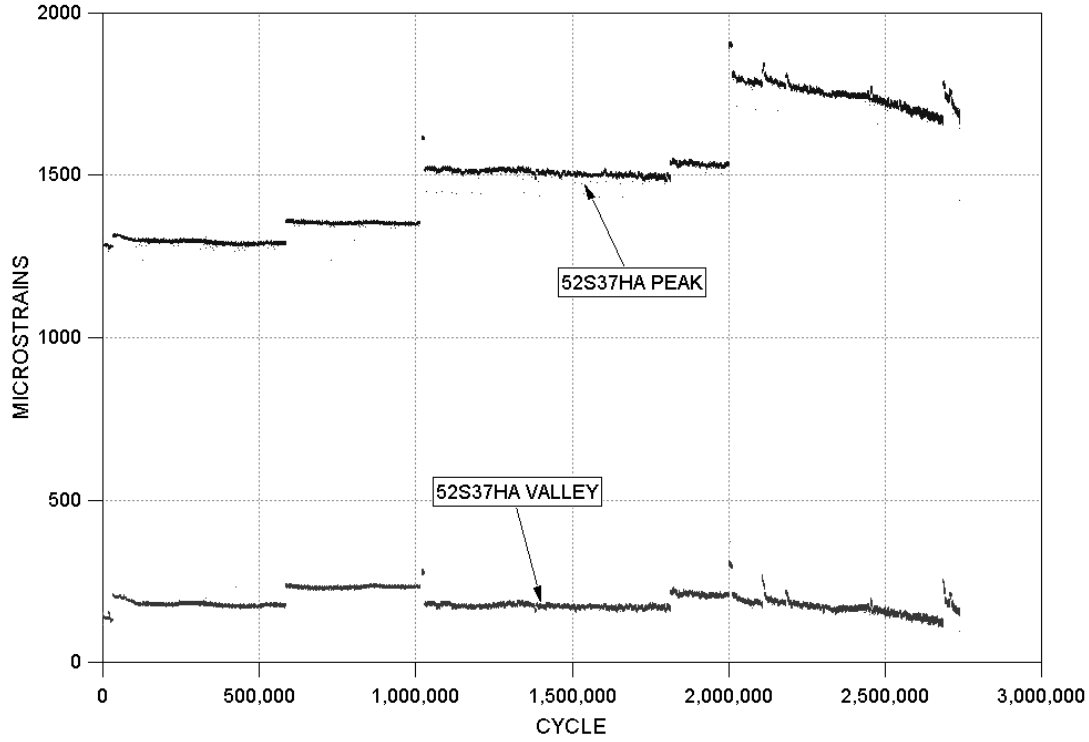


**Fig. C.18 - Gage 52S37HA peak/valley strain data**

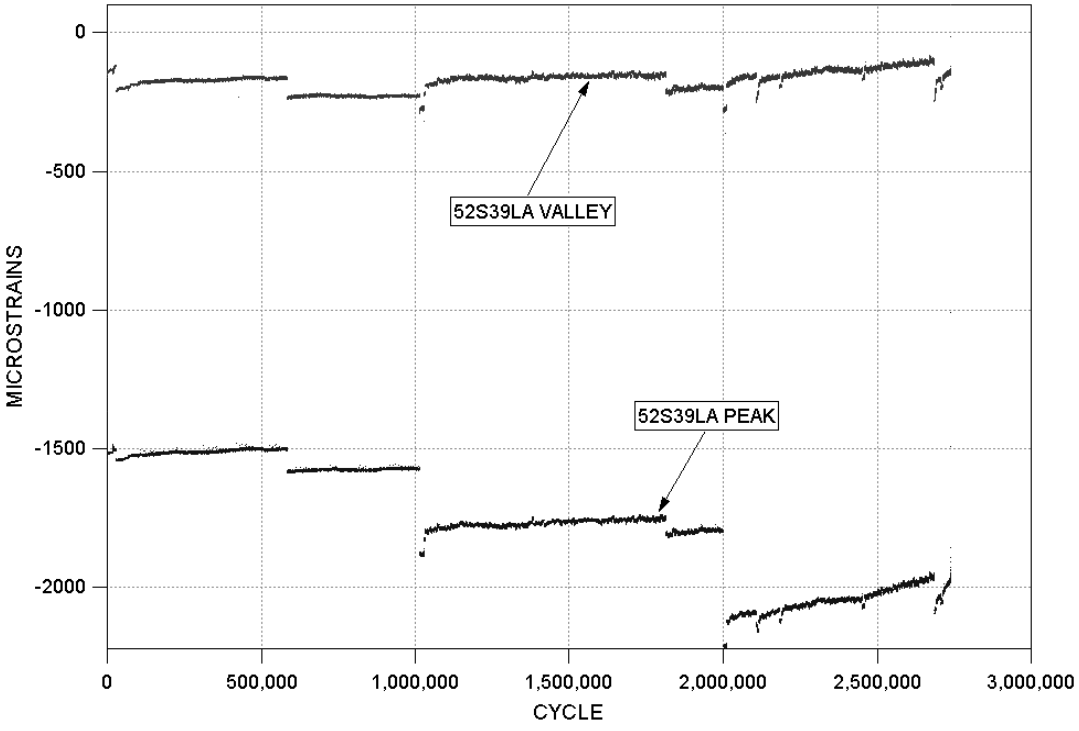

**Fig. C.19 - Gage 52S39LA peak/valley strain data**

# References


1. “Jacobs, Model 29-20 Wind Turbine, Technical Specifications," Brochure, Form 29-20-12/86, Wind Turbine Industries Corp., Prior Lake, MN.
2. E.E.S.I. engineering drawing, 1985.
3. Keble, P., Airfoils used on blade (airfoil names used to find coordinates), private communications, (612) 487-9222, Feb 1995.
4. Tangler, J.L. (NREL), Hybrid Jacobs turbine field test data taken Oct 1993 by Cam Anders, private communications, Dec 1994.
5. Lyon, C.A., Broeren, A.P., Giguère, P., Gopalarathnam, A., and Selig, M.S., Summary of Low-Speed Airfoil Data, Vol. 3, SoarTech Publications, Virginia Beach, VA, 1998, 418 pages.
6. Selig, M.S. and Tangler, J.L., "Development and Application of a Multipoint Inverse Design Method for Horizontal Axis Wind Turbines," Wind Engineering, Vol. 19, No. 2, 1995, pp. 91-105.
7. Turek, S., private communications, Wind Turbine Industries Corp, Prior Lake, MN, Oct 1998.
8. Selig, M.S., Guglielmo, J.J., Broeren, A.P., and Giguère, P., Summary of Low-Speed Airfoil Data, Vol. 1, SoarTech Publications, Virginia Beach, VA, 1995, 292 pages.
9. Selig, M.S., Lyon, C.A., Giguère, P. Ninham, C.N., and Guglielmo, J.J., Summary of Low-Speed Airfoil Data, Vol. 2, SoarTech Publications, Virginia Beach, VA, 1996, 252 pages.
10. Giguère, P. and Selig, M.S., "Design and Wind Tunnel Test Result for the SG6050 and SG6051 Airfoils," University of Illinois at Urbana-Champaign, Dept. of Aeronautical and Astronautical Engineering, AAE 98-04, UILU ENG 98-05-04, in preparation.
11. Althaus, D., "Niedrig-geschwindigkeits-profile," Friedr. Vieweg & Sohn Verlagsgesellschaft mbH (publisher) Braunschweig/Weisbaden, Germany, 1996, 591 pages. ISBN 3-528-03820-9.
12. Giguère, P. and Selig, M.S., "Design of a Tapered and Twisted Blade for the NREL Combined Experiment Rotor," University of Illinois at Urbana-Champaign, Dept. of Aeronautical and Astronautical Engineering, prepared under the National Renewable Energy Laboratory Subcontract No. XAF-4-14076-03, March 1998, 22 pages. Also, NREL/SR-500-26173, Golden, CO, April 1999.
13. Giguère, P. and Selig, M.S., "Aerodynamic Blade Design for the WindLite 8-kW Wind Turbine," University of Illinois at Urbana-Champaign, Dept. of Aeronautical and Astronautical Engineering, AAE 98-01, UILU ENG 98-05-01, prepared for WindLite Company, Inc, January 1998, 25 pages.
14. Willard Dill, Lalamilo Wind Farm, June 13, 2000.
15. Richard Santos and Harold F. Link, Document “LF24 991229 Test Plan Template,” Natl. Renewable Energy Laboratory, Golden, CO.
16. Seifert, H. and Hunter, R., “Volume 6, Mechanical Load Measurements,” European Wind Turbine Standards, Joule Programme, JOU2-CT93-0387, February, 1996.
17. International Energy Agency, “Recommended Practices for Wind Turbine Testing, 3. Fatigue Loads,” 2nd Edition, 1990.
18. Downing, S.D. and Socie, D.F., “Simple Rainflow Counting Algorithms,” *Int’l J. of Fatigue*, Vol. 4, No. 1, 1982.

19. Schluter, L.L. and Sutherland, H.J., “User’s Guide for LIFE2’s Rainflow Counting Algorithm,” Sandia Report SAND90-2259, Sandia Natl. Laboratories, Albuquerque, NM, 1991.

20. Kelley, N.D. and Sutherland, H.J., “Damage Estimates from Long-Term Structural Analysis of a Wind Turbine in a U.S. Wind Farm Environment,” NREL/CP-440-21672, Natl. Renewable Energy Laboratory, Golden, CO, 1996.

21. A 10-DOE/MSU Material Fatigue Database: Test Methods, Materials and Analysis, pg. 41, 60, 143, 146, 144 and 148.

22. Computational information was gleaned from SAND97-0032, DOE/MSU Material Fatigue Database: Test Methods, Materials and Analysis.

23. Steve Drouilhet (NREL), private communications, July 1998.

24. Selig, M.S., "Blade Design/Airfoil Trade-Off Study," part of the FMI Preliminary Design Report delivered to Sandia, Nov 1998.

25. Selig, M.S., "Baseline Jacobs 20 kW Modeling," part of FMI Preliminary Design Report delivered to Sandia, Nov 1998.

26. Richey, C., Private communications, Nov 23, 1998.

27. Bay Winds Wind Energy Systems, brochure 1997.

28. Jacobs Wind Energy Company, Minneapolis, MN; Brochure 1981

29. Enkalon International Estate, Antrim, Northern Ireland; Web site, galeforce.uk.com, May 12, 2001.

30. Ashlar, Inc., 12731 Research Blvd., Austin, TX 78759.

31. Solidworks Corp., 300 Baker Avenue, Concord, MA 01742.

32. Autodesk Inc., 111 McInnis Parkway, San Rafael, CA 94904.

33. Structural Research & Analysis Corp. 12121 Wilshire Blvd. Los Angeles, CA 90025.

34. Technology Publishing “Reference Book For Composites Technology”, edited by Stuart Lee, “Section 2, Epoxy Resins” by Ronald Bauer and L. Steven Corley, Copyright 1980.

35. IEC-88/98/FDIS, *Wind Turbine Generator Systems, Part 1: Safety Requirements.* 1999, International Electrotechnical Commission: Geneva.

36. IEC-88/84/CD, *Draft IEC 61400-23: Testing of Rotor Blades*. 1998, International Electrotechnical Commission.

37. *BSTRAIN Manual*. 1999, National Renewable Energy Laboratory: Golden, Colorado.

38. Musial, W.D., M.E. Clark, and T. Stensland, *Application of BSTRAIN software for Wind Turbine Blade Testing*, in *Windpower '96*. 1996, American Wind Energy Association: Denver, Colorado. p. 241-250.

39. Static Testing of the Foam Matrix BMI Blade. Test Plan. National Renewable Energy Laboratory. Walt Musial. June 6, 2000.

40. Internal NREL report, ‘FATIGUE TESTING OF THE FOAM MATRIX BMI BLADE’. Report ‘NWTC-ST-FMI-FAT-02-0201-FR’. July 2001.

41. Detailed Design Review. Blade Manufacturing Improvement Document ‘AX-2411’. Foam Matrix Inc. February 2, 1999.

42. NREL Report ‘NWTC-ST-FMI-STA-01-1000-FR’. “Static Testing of the Foam Matrix BMI Blade”. June 2001.

43. Musial, W.D., Allread, J. “Test Methodology and Control of Full-scale Fatigue Tests on Wind Turbine Blades.” Proc. ASME Wind Energy Symposium, 1993.